Hochschule für Angewandte Wissenschaften Hamburg
Hamburg University of Applied Sciences

Master Thesis

Department of Automotive and Aeronautical Engineering

Conceptual Design of a Medium Range Box Wing Aircraft

Daniel Schiktanz

5 July 2011

Hochschule für Angewandte Wissenschaften Hamburg
Fakultät Technik und Informatik
Department Fahrzeugtechnik und Flugzeugbau
Berliner Tor 9
20099 Hamburg

Verfasser: Dipl.-Ing. (FH) Daniel Schiktanz
Abgabedatum: 05.07.2011

1. Prüfer: Prof. Dr.-Ing. Dieter Scholz, MSME
2. Prüfer: Prof. Dr.-Ing. Martin Wagner

Abstract

This thesis covers the conceptual design of a box wing configuration, an unconventional non planar configuration comparable to a joint wing whose wings are connected on the tips by vertical winglets. In this way the wing configuration forms a rectangular box in the front view. The box wing configuration allows for savings in induced drag which results in reduced fuel consumption. Compared to conventional aircraft there are significant differences concerning aerodynamics, flight mechanics and the structural layout. These differences are elaborated and their consequences are applied to the design process. It is shown that the requirements according to longitudinal stability and controllability are a main design driver. The aircraft is very sensitive to shifts of its center of gravity. This issue is solved by a well balanced aircraft layout, comprising of a short fuselage not extending much more forward than the front wing and an engine position close to the center of gravity. For assessing the saving potentials of the box wing configuration a reference aircraft is chosen (the Airbus A320). The design mission and geometry constraints of the reference aircraft are applied to the box wing aircraft so that performance and operational characteristics of both aircraft can be compared. A shorter fuselage and cabin means more seats abreast, so this box wing aircraft becomes a wide body aircraft having two main aisles. This allows for a faster boarding /deboarding. The resulting increase of the cross sectional area of the fuselage permits the accommodation of standard LD3 containers. It is concluded that the designed box wing aircraft consumes 9 % less fuel and requires 2 % less take off thrust for the design mission. With reduced fuel burn the box wing configuration has also a potential of reduced emissions. The maximum take off weight of both aircraft is equal. Unlike other unconventional configurations (e.g. the blended wing body) the box wing is compatible to current airport facilities It is important to keep in mind that the presented conceptual design is based on simplifying assumptions as well as preliminary calculations and methods. The design has to be checked and confirmed in more detailed investigations. The designed box wing aircraft is not fully optimized yet. Hence it still leaves room for further performance improvements.

Hochschule für Angewandte Wissenschaften Hamburg
Hamburg University of Applied Sciences

DEPARTMENT OF AUTOMOTIVE AND AERONAUTICAL ENGINEERING

Conceptual Design of a Medium Range Box Wing Aircraft

Task for a Master Thesis according to university regulations

Background

Already in 1924 Ludwig Prandtl indicated that a wing system generating minimum induced drag consists of two wings whose tips are connected by vertical plates (**Prandtl 1924**). Today this configuration is mostly referred to as “box wing configuration”. Since a reduction of induced drag has positive effects on aircraft performance and weight, the box wing configuration has been subject of several studies (e.g. **Lockheed 1974**). However, only few of them contain a complete analysis of the overall design because of its unconventional nature and the lack of compatible methods. But with the growing availability of computational resources a complete design study becomes more feasible.

Because of its complexity, aircraft design often relies on statistical methods. These methods are applicable to new configurations only to a limited extent because most of them are based on conventional aircraft configurations. For this reason a reliable computational analysis of unknown configurations is mandatory, as well as experimental tests.

At the University of Applied Sciences Hamburg (HAW Hamburg) several tools are available for aircraft design. The tool PreSTo (Preliminary Sizing Tool) was developed within the Aero Research Group at HAW Hamburg, based on sizing calculations presented in the lecture “Aircraft Design” by Prof. D. Scholz (**Scholz 1999**). With its help a conventional aircraft can be sized in order to fulfill certain mission requirements. The generated data may be exported to other available tools for refining the design. One of these tools is the software suite CEASIOM (Computerized Environment for Aircraft Synthesis and Integrated Optimization Methods, URL: http://www.ceasiom.com). It was developed within the SimSAC project (Simulating Aircraft Stability and Control Characteristics for Use in Conceptual Design, URL: http://www.simsacdesign.eu) and enables the designer to analyze and optimize the design with the help of multidisciplinary methods.

Task

In this Master Thesis the conceptual design of a box wing aircraft shall be conducted with the help of the above mentioned methods and tools. Reference aircraft is the Airbus A320. In detail, the following tasks shall be performed:

1) Literature research
2) Discussion of essential parameters of the box wing configuration with regard to their special qualities compared to conventional aircraft
3) Preliminary sizing and conceptual design of the box wing aircraft equivalent with help of PreSTo
4) Multidisciplinary analysis of the box wing aircraft with help of CEASIOM
5) Comparison of the found box wing design with the reference aircraft in terms of weight and performance
6) Discussion of the results and the applicability of the used methods and software

For points 3) and 4) it has to be determined in which scope the software tools might be useful. Whenever needed, alternative methods have to be used and described.

The report has to be written in English based on German or international standards on report writing.

References

Lockheed 1974 LANGE, R.H. ; CAHILL, J.F. ; BRADLEY, E.S. ; et al.: *Feasibility Study of the Transonic Biplane Concept for Transport Aircraft Application*. Marietta : The Lockheed-Georgia Company, 1974. - Research report prepared under contract NAS1-12413 on behalf of the National Aero nautics and Space Administration

Prandtl 1924 PRANDTL, Ludwig: *Induced Drag of Multiplanes*. Langley : National Advisory Committee for Aeronautics, 1924. - NACA TN 182

Scholz 1999 SCHOLZ, Dieter: *Skript zur Vorlesung Flugzeugentwurf*, Hamburg, Fachhochschule Hamburg, FB Fahrzeugtechnik, Abt. Flugzeugbau, Vorlesungsskript, 1999

Declaration

Herewith I affirm that this master thesis is entirely my own work. Where use has been made of the work of others, it has been fully acknowledged and referenced.

Date Signature

Contents

List of Figures

List of Tables

Nomenclature

a	lift curve slope
A	aspect ratio
b	wing span
c	chord length
$\bar{c}$	mean aerodynamic chord
$\bar{c}'$	relative mean aerodynamic chord
d	diameter
D	drag
C	coefficient
e	span efficiency factor/Oswald efficiency factor
E	glide ratio, Young's modulus
FF	form factor
G	shear modulus
h	height, dimensionless distance between CG and LEMAC
h_0	dimensionless distance between AC and LEMAC
I	interference factor
K	factor influencing the lift curve slope of the whole aircraft
l	lever arm, length
l'	modified lever arm
L	lift
n	load factor
m	mass
M	moment, mission segment mass fraction
q	dynamic pressure, load per unit span
Q	interference factor
R	ratio
s	relative wing reference area
S	wing reference area, shear force
t	airfoil thickness, thickness
V	volume, tail volume
$\bar{V}'$	modified tail volume coefficient/modified aft wing volume coefficient
x	longitudinal position/distance
$\bar{x}$	longitudinal position of the mean aerodynamic chord
y	lateral position/distance
z	vertical position/distance

Greek Symbols

α	angle of attack, general angle
γ	shear strain
ε	downwash angle, normal strain
η	relative half span
λ	taper ratio, fuselage fineness ratio
ρ	density
σ	wing interference factor, normal stress
τ	airfoil thickness ratio (tip to root), shear stress
φ	sweep angle

Indices

0	zero lift, initial
25	25 % of the chord length
50	50 % of the chord length
B	body, beam
box	box wing aircraft
CG	center of gravity
CLB	climb
const	constant part
CR	cruise
D	drag
DES	descent
e	equivalent, exposed
eff	effective
ell	elliptical part
exp	exposed
f	skin friction
ff	fuel fraction
F	fuselage, fuel
i	induced, running number
L	lift, landing
LOI	loiter
M	moment
N	nose, nacelle
max	maximum
min	minimum

md	minimum drag
MTO	maximum take off
MZF	maximum zero fuel
OE	operating empty
r	wing root
ref	reference aircraft
RES	reserve
single	isolated wing of the box wing aircraft
t	wing tip
TO	take off
tot	total
ult	ultimate
v	vortex
V	vertical tail
W	wing
wet	wetted

List of Abbreviations

AC	aerodynamic center
CEASIOM	Computerized Environment for Aircraft Synthesis and Integrated Optimization Methods
CG	center of gravity
ISA	international standard atmosphere
LEMAC	leading edge of the mean aerodynamic chord
MAC	mean aerodynamic chord
SDSA	Simulation & Dynamic Stability Analysis

Terms and Definitions

Clean Configuration

The setting of an aircraft with all slats, flaps, control surfaces and the landing gear retracted is referred to as clean configuration.

CG Envelope

The CG envelope is the permissible region for the aircraft's center of gravity for all flight and ground operations.

CG Travel

The process of a change of the aircraft's CG position (e.g. because of loading or fuel burn) is referred to as CG travel.

Decalage

The difference in incidence angles of the forward and the aft wing is referred to as decalage.

Downwash

Downwash is the downward motion of air after having passed a lifting surface. It is responsible for the reduced angle of attack of tail surfaces.

h/*b* ratio

In the context of non planar aircraft the *h*/*b* ratio is the ratio of the vertical distance between the most upper and the most lower component of the wing configuration to the wing span. These components can be single wings but also winglets, for example. The *h*/*b* ratio is essential for assessing the interference between the single components.

Monoplane

A monoplane is an aircraft with only one wing. Hence all conventional aircraft are monoplanes.

Non Planar Configuration

This is a wing configuration where the wings are not situated in a single plane. Any single wing without dihedral is thus a planar wing configuration. Non planar configurations are, for example, wings with winglets or biplanes. Since a box wing configuration is a combination of a biplane and a tandem wing, it is a non planar configuration as well.

Reference Aircraft

For evaluating the performance of a box wing aircraft it is necessary to define a reference aircraft the box wing aircraft is based on. Both aircraft have the same design mission which allows for comparing their performance. For not confusing effects due to the better qualities of the box wing aircraft and indirectly optimizing the reference aircraft, certain geometry parameters of both aircraft are supposed to be equal. These are the total wing reference area and the wing span.

Zero Lift Line

The zero lift line is defined as the line built by the angle of attack of the total aircraft where the lift of the aircraft is zero.

1 Introduction

1.1 Motivation

As stated in Flightpath 2050 by **EU 2011**, civil aviation transport is facing challenges like globalisation, climate change and a cumulative scarcity of resources. To cope with these challenges, aircraft have to become more efficient, especially concerning energy and fuel consumption. With the latest aircraft emerging on the market, the inherent saving potentials of conventional configurations is almost exhausted. With these configurations progress in achieving the goals of Flightpath 2050 could only be made through better technologies and alternative fuels. This constitutes the need for new configurations having more inherent potential of reducing energy and fuel consumption compared to today's aircraft. One of these is the box wing configuration, a biplane with vertically and horizontally staggered wings whose tips are connected by extended winglets. The most recognized benefits of this configuration are its low induced drag and alleged structural superiority. This thesis serves to investigate the advantages of the box wing aircraft in detail and to deduce a possible medium range box wing aircraft.

The results of this thesis are supposed to be integrated into the research project *Efficient Airport 2030* (**Aiport 2030**) giving answers on how to reduce emissions in the airport environment and how to reduce costs for airlines with the help of an unconventional and more efficient aircraft.

1.2 Objectives

The aim of this thesis is to give an integral approach to the box wing configuration from the perspective of aircraft design. Therefore almost the whole process of the conceptual design of a medium range box wing aircraft is covered. Basis of this design is the reference aircraft (Airbus A320) whose design mission and geometric constraints are transferred to the box wing configuration.

In order to design the box wing aircraft theoretical foundations have to be built first, carving out essential differences compared to a conventional aircraft. The relating investigations mostly comprise the field of aerodynamics and flight mechanics and are based on published literature as well as own examinations. The findings from these fundamental investigations are introduced into the design process. Once a coherent box wing configuration is developed its performance will be compared with that of the reference aircraft.

Initially it was also planned to perform an additional multidisciplinary analysis of the developed box wing configuration with the help of the CEASIOM software suite. However, in the process of this thesis it became clear that a huge part is dedicated to fundamental investigations and their effects on the design which continuously had to be adapted to evolving knowledge. This is why a software-based multidisciplinary analysis has to be postponed to later studies.

1.3 Review of Literature

1.3.1 Aircraft Design Literature

The general design procedure is based on the lecture notes of Prof. Dieter Scholz (**Scholz 1999**) who teaches aircraft design at the Hamburg University of Applied Sciences. They give a comprehensive summary of all design steps and collect methods from basic aircraft design literature as **DATCOM 1978**, **Loftin 1980**, **Raymer 1992**, **Roskam 1985** or **Torenbeek 1982**. When needed, methods more dedicated to the current design tasks are taken from these books. Next to the lecture notes of Prof. Scholz supportive material provided by him via the internet is used (see references).

If not explicitly referenced different, all investigations in this thesis are based on the mentioned lecture notes. Occasionally the methods presented therein have to be modified so they can be adapted to the box wing configuration.

1.3.2 Box Wing Literature

Several studies concerning box wing aircraft have been conducted in the past. Their knowledge is an important basis for the design of a medium range box wing aircraft. Of course there is a lot more literature to be found about box wing configurations than mentioned in the following.

Initial examinations were already performed in the 20s of the 20th century by Ludwig Prandtl (**Prandtl 1924**) presenting a theory for assessing the induced drag of multiplanes. Further theoretical aspects of box wing aerodynamics were presented in **Durand 1935** which base on investigations conducted by Ludwig Prandtl, Theodore von Kármán and Max Munk. **DeYoung 1980** uses their findings to conduct a summary about the span efficiency factor of non planar wing configurations. **Cahill 1954** gives the results of wind tunnel tests with a simple box wing like configuration.

Next to these theoretical investigations some design studies have been performed as well. The first important to mention is **Lockheed 1974** which gives a good summary of the practical aspects of box wing aerodynamics as well as to stability and controllability, together with a description of the design synthesis of a long range aircraft. In this study it was found that box wing aircraft are very sensitive to flutter. This sensitivity seems to get stronger with an increasing h/b ratio.

For a huge part, more recent studies have been conducted at the University of Pisa under the supervision of Prof. Aldo Frediani (**Frediani 2005**, **Frediani 2007**, **Frediani 2009**). They give a survey of some of the design challenges and approaches of how to cope with them and contain examinations of medium and long range aircraft as well as ULM aircraft.

One of the starting points of the current thesis is **Khan 2010** which presents results of preliminary aerodynamic investigations of the box wing configuration conducted with the help of low fidelity CFD methods, as well as **Kroo 2005** elaborating the advantages of non planar configurations.

1.4 Structure of this Thesis

The chapters two to five describe the conducted investigations in order to gain a fundamental understanding of the box wing configuration. The chapters six to eleven focus on the conceptual design process and the assessment of the box wing configuration. The appendices contain additional material which was excluded from the main part for not interrupting the train of thoughts. In detail the distribution of chapters is as follows:

Chapter 2 gives a short introduction to non planar configurations in general and the box wing configuration in detail along with its geometry.

Chapter 3 presents the reference aircraft and its most important design parameters. They are the basis for the design of the box wing aircraft.

Chapter 4 deals with box wing aerodynamics. It describes essential relations concerning lift and drag and shows how to determine the induced drag of a box wing configuration and the resulting span efficiency.

Chapter 5 discusses aspects of aircraft performance and examines static longitudinal and static lateral stability and controllability of the box wing aircraft.

Chapter 6 focuses on the preliminary sizing of the box wing aircraft with the help of the preliminary sizing spreadsheet (**Scholz 2008**).

Chapter 7 goes into the details of the wing design. This comprises the design for transonic speeds, giving the final wing geometry, estimating the wing mass and the wing tank volume as well as a discussion of high lift and control surfaces.

Chapter 8 covers the design and integration of the other aircraft components, which are cabin and fuselage, empennage, engines and landing gear.

Chapter 9 presents the final aircraft layout with the help of a three view drawing.

Chapter 10 assesses the aircraft weight and balance together with the CG envelope based on cruise conditions.

Chapter 11 examines the performance of the final box wing configuration. This includes the determination of the zero lift drag coefficient and the payload-range diagram.

Chapter 12 gives a conclusion of this thesis, mentions possible shortcomings of the design study and outlines the future work to be done.

Appendix A defines the mean aerodynamic chord of a box wing configuration.

Appendix B presents detailed derivations whose results are used to describe box wing flight mechanics in chapter 5.

Appendix C gives the data used for the more precise estimation of the mass of the wing configuration.

Appendix D provides scaled drawings of the final box wing aircraft and also shows the evolution of intermediate versions.

Appendix E gives insight into the calculation of the tilting angle for lateral tilting stability of the landing gear.

Appendix F shows screenshots of the spreadsheets used for sizing and designing the box wing aircraft.

Appendix G presents the contents of the CD-ROM attached to this thesis.

2 The Box Wing Concept

2.1 Short Introduction to Non Planar Configurations

Non planar means that the wing of the aircraft is not situated within one single plane (the x-y-plane). Strictly speaking a wing with dihedral is not planar any more. A widespread application of non planar configurations are wings with winglets, which reduce the induced drag and thus increase the span efficiency factor.

Kroo 2005 gives a good summary concerning non planar configurations. There it is mentioned that the reduction of induced drag not only affects the fuel consumption during cruise, but rather all flight phases. The reason is that the aircraft has a significantly improved climb performance as well, because acc. to **Kroo 2005** the induced drag makes out 80 to 90 % of the total drag during take off and initial climb. This makes it possible to increase the maximum take off weight or to install engines with less thrust and fuel consumption. Additionally it is stated that one important advantage of non planar wings is the possibility of increasing the span efficiency without extending the wing span. This way it is possible to keep the structural weight within acceptable limits and to comply with current airport facilities.

Fig. 2.1 shows several non planar wing configurations and their theoretical span efficiency factors for a *h*/*b* ratio of 0,2. The *h*/*b* ratio is the relation of the vertical wing dimension to the wing span. The figure shows that the box wing configuration has the highest potential of drag decrease (e = 1,46). But it can be also seen that the C-Wing (e = 1,45) and large winglets (e = 1,41) also have huge potential.

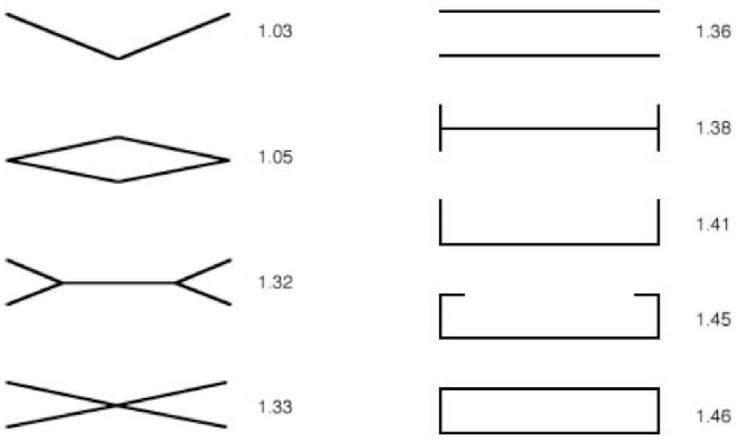

Figure 2.1 Span efficiency factors for optimally loaded non planar wings with *h*/*b* = 0,2 (**Kroo 2005**)

2.2 Box Wing Geometry

The main difference between a box wing and a conventional configuration is the wing while all other aircraft components are comparable to those of conventional aircraft (Fig. 2.2).

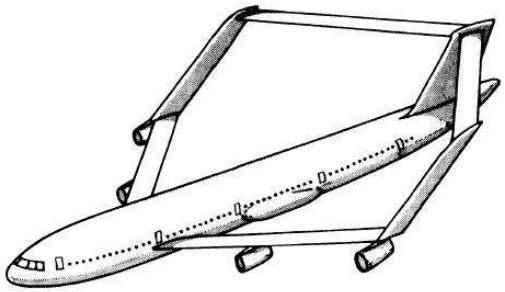

Figure 2.2 Example of a box wing configuration (**Lockheed 1974**)

In **Khan 2010** an overview of the wing geometry parameters of a box wing configuration is given (Fig. 2.3). Also note the conventions regarding the coordinate axes.

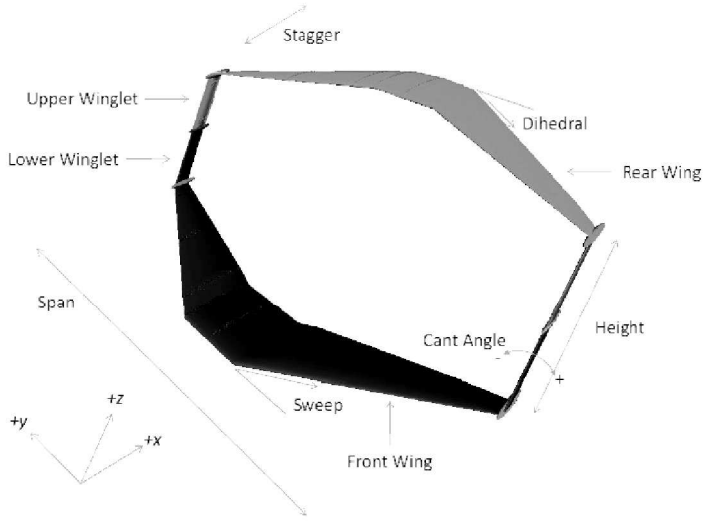

Figure 2.3 Wing geometry parameters of a box wing configuration (**Khan 2010**)

Most of these parameters are the same as for conventional configurations. But because of the presence of two wings some additional parameters need to be introduced. *Stagger* describes the horizontal position of the wings relative to each other. The accordant vertical position is the *height* of the wing configuration, which can be also referred to as *vertical stagger.* Hence the horizontal position would then be referred to as *horizontal stagger.* Another parameter is *decalage*, which describes the difference of incidence angles between both of the wings. These new parameters all originate from general biplane theory.

In the following paragraphs stagger (horizontal and vertical), the height to span ratio and the aspect ratio are discussed briefly.

2.2.1 Horizontal Stagger

There is a distinction between positive and negative horizontal stagger. It is positive when the upper wing is situated in front of the lower wing (Fig. 2.4).

Figure 2.4 Positive stagger of a biplane

With regard to the effect of horizontal stagger on the aerodynamic performance, Ludwig Prandtl wrote:

> *"Where there is a positive stagger, as is generally the case, the drag of the upper wing is diminished by the upward air currents produced by the lower wing; but, on the other hand, the drag of the lower wing is increased, to exactly the same extent, by the downward air current produced by the upper wing, so that the total drag is the same as in the case of an unstaggered biplane."*
> (**Prandtl 1924**)

This effect was described my Max Munk in detail and became generally known as Munk's stagger theorem. Thus the minimum induced drag of the box wing configuration does not depend on horizontal stagger. This means that the wing design can be optimised for transonic cruise by adding wing sweep and for higher stability (**Khan 2010**).

In almost every design study for box wing transport aircraft negative stagger is used. Here the integration of the wings is much easier and higher h/b ratios are possible, since the height of the aft wing is limited by the height of the vertical stabilizer and not by the fuselage height, as it would be the case for positive stagger.

2.2.2 Vertical Stagger and Height to Span Ratio

The vertical distance between the wings mostly affects their mutual interference. The more they are apart, the less interference exists which results in higher savings of induced drag. The effect of interference can be described with the help of the interference factor σ introduced in **Prandtl 1924** within the context of simple biplanes. The crucial parameter which σ depends on is the height to span ratio h/b of the wing configuration, which is the vertical stagger of both wings divided by the their average wing span (Fig. 2.5). In the present thesis only configurations with wings having the same span are discussed.

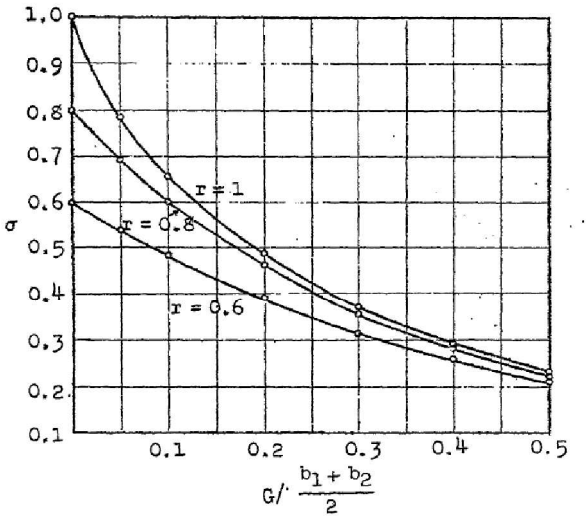

Figure 2.5 Wing interference factor of biplanes (**Prandtl 1924**, *G* means vertical gap, $r = b_2/b_1$)

2.2.3 Wing Area and Aspect Ratio

For biplanes, hence for box wings as well, it has to be differentiated between the geometry parameters of the individual wings and those of the whole wing configuration. The wing area S of the total configuration is the sum of both individual wing areas S_1 and S_2, so

$$S = S_1 + S_2 \quad . \tag{2.1}$$

The individual aspect ratios are defined by

$$A_i = \frac{b_i^2}{S_i} \quad ; \; i = 1 ; \; 2 \tag{2.2}$$

However, determining the aspect ratio of the whole configuration is not that clear. For the case where both wings have the same span **Khan 2010** proposes that

$$A = \frac{b^2}{S_1 + S_2} = \frac{b^2}{S} \quad . \tag{2.3}$$

If the wings have unequal spans, different approaches can be found in literature. As seen in Fig. 2.5 **Prandtl 1924** works with an average span of $(b_1 + b_2)/2$ for determining the wing interference factor.

Since in this thesis only configurations with equal spans are discussed, Eq. (2.3) is used for the determination of the aspect ratio. The total aspect ratio for configurations with unequal wing spans will not be investigated any further.

3 Design Requirements According to the Reference Aircraft

The reference aircraft for the present study is the Airbus A320. It is a short to medium range aircraft accommodating 150 passengers in a two-class layout. The data of the reference aircraft comes from published information and is also based on the data given in **Pester 2010a**. A three view drawing of the aircraft is shown in Fig. 3.1.

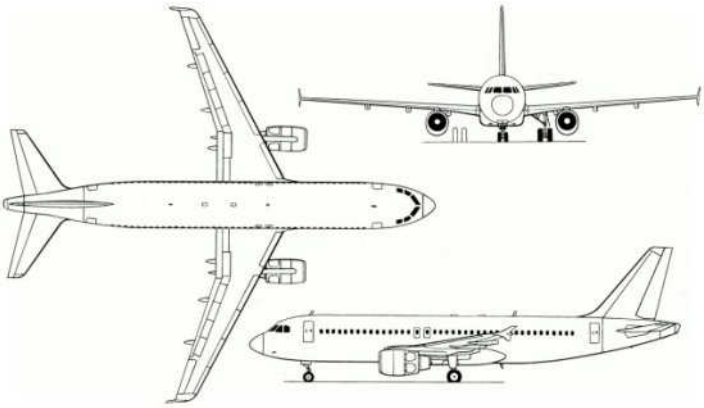

Figure 3.1 Three view drawing of the Airbus A320 (**Aerospaceweb 2011**)

3.1 Mission Requirements

The requirements according to the design mission are given in table 3.1. They are taken from **Pester 2011b**.

Table 3.1 Mission requirements of the reference aircraft

Design range	1550 nm
Maximum payload	20000 kg
Passengers	150 (2 class layout)
Cruise Mach number	0,76
Take off field length	2200 m
Landing field length	1700 m

These requirements are the basis of the box wing aircraft being studied in this thesis.

3.2 Additional Conditions

Next to the design mission there are other requirements and conditions which the box wing aircraft is supposed to fulfill. They contain geometric constraints and the engines.

3.2.1 Geometry

In order to have a valuable comparison between the box wing aircraft and the reference aircraft certain geometry parameters have to remain unchanged. They only concern the wing and are listed in table 3.2.

Table 3.2 Wing parameters to remain unchanged

Wing span	34,1 m
Total wing area	122,4 m²
Total aspect ratio	9,5

So the total wing area is distributed onto two wings which have the same span as the reference aircraft. This way the aspect ratio of one single wing will be about double the total aspect ratio.

3.2.2 Engines

The box wing aircraft is supposed to have the same engines as the reference aircraft. The engine parameters given according to **Pester 2010b** are summarized in table 3.3.

Table 3.3 Reference engine data

Bypass ratio	4,8
Specific fuel cons.	16,3 mg/(Ns)
Take off thrust	111 kN (m_{MTO})

3.3 Family Concept

An important aspect demanded by airlines and aircraft manufacturers is the possibility of building different versions of a basic aircraft. The common approach is to shorten or lengthen the fuselage by removing or adding certain sections of the cylindrical part of the fuselage while keeping the wing unchanged. This is the principle of the A320 family, for example.

The lack of this possibility most probably is a reason for an aircraft manufacturer to cancel any further studies of the affected aircraft. This is why the possibility of an aircraft family of the box wing configuration has to be existent.

For stretching a normal configuration two fuselage segments are inserted, one in front and one aft of the wing in order to keep the balance of the aircraft. Since the aft wing of the box wing aircraft is connected to the vertical stabiliser (see Fig. 3.2), this approach is not possible.

Consequently only one fuselage section is inserted, namely between the forward and the aft wing. This way the balance of the aircraft is kept and only small adjustments concerning the wing design have to be done. Since an additional fuselage section increases the distance between the forward and the aft wing, the sweep of the winglets has to be increased because the geometry of the horizontal wings is supposed to be unchanged. So for a new member of the box wing family a redesign of the vertical winglets is necessary.

Fig. 3.2 shows a comparison of the basic box wing configuration (continuous lines) and a possible stretched version (broken lines). Apart from the differences already mentioned engine integration is another important factor. As shown in Fig. 3.2 the engines are integrated on top of the fuselage. Strictly speaking two fuselage sections have to be added in order to have a well balanced aircraft, one in front and one aft of the engine. The feasibility of this option is part of further studies. Nevertheless it is also possible to insert only one fuselage section in front of the engines and assess the resulting changes concerning weight, balance and static longitudinal stability.

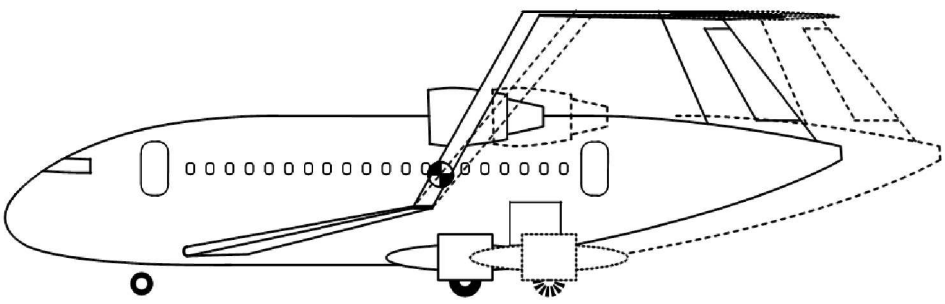

Figure 3.2 Comparison of the basic box wing configuration and a possible stretched version

4 Box Wing Aerodynamics

4.1 Lift

4.1.1 General Lift Distribution

From investigations in the past it is known that the lift distribution of a box wing aircraft has some special characteristics. Already in 1935 the distribution leading to minimum induced drag was shown to consist of an elliptical and a constant part for the horizontal wings and of a linear and butterfly shaped part for the vertical winglets (**Durand 1935**, Fig. 4.1). This fact was later confirmed by calculations of G. Montanari and A. Frediani (**Frediani 2009**).

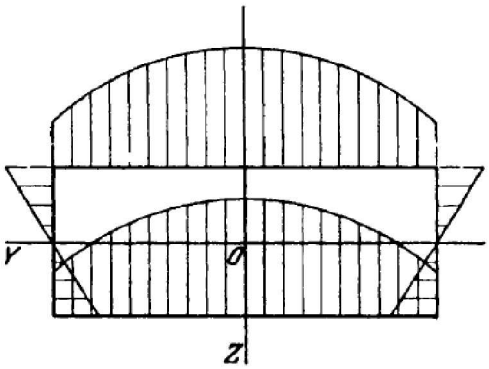

Figure 4.1 Lift distribution of a box wing aircraft (**Durand 1935**)

The lift distribution shown in Fig. 4.1 is based on the assumption that both wings generate the same amount of lift and have the optimum lift distribution. However, this is an ideal condition which is hard to realize in practice.

The total lift distribution may deviate from the optimum:

1) Both wings do not generate the same amount of lift
2) The distribution of one wing deviates from the optimum

These reasons could occur in combination but also separately. The first is mostly due to stability requirements which will be discussed in section 5.2. Its effect on the aerodynamic performance is part of section 4.6. The second reason does not necessarily mean that both wings generate a different amount of lift. It comprises two aspects:

2a) The ratio of the elliptical to the constant part is not optimal

2b) The span wise distribution is not optimal, e.g. because of wing twist or taper

Considering 2a) the ratio R_L is introduced by the author of this thesis, being:

$$R_L = \frac{\left(q_L\right)_{const}}{\left(q_L\right)_{ell,0}} \quad , \tag{4.1}$$

which shall represent the ratio of the constant part to the elliptical part of the lift distribution. In Eq. (4.1) q_L means lift per unit span. The meaning of R_L can be better understood with the help of Fig. 4.2.

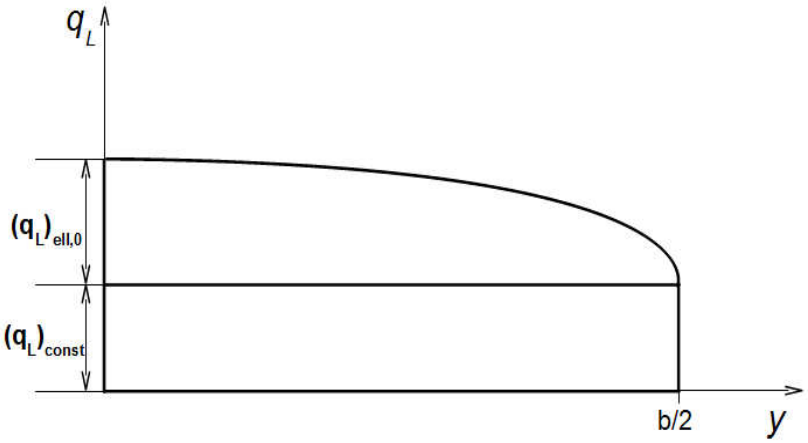

Figure 4.2 Lift distribution consisting of a constant and an elliptical part

In **Frediani 2009** it is stated that the circulation at the tip of one horizontal wing is transferred to the connected winglet. Since circulation is proportional to lift, this means that the value $(q_L)_{const}$ of the horizontal wing is, at the same time, the value of lift at the tip of the connected winglet. If $(q_L)_{const}$ is the same for the forward and the aft wing, the zero-crossing of the lift distribution of the winglet is at its symmetry axis (Fig. 4.1). Otherwise it will be shifted towards the wing with the smaller value for $(q_L)_{const}$ (Fig.4.3).

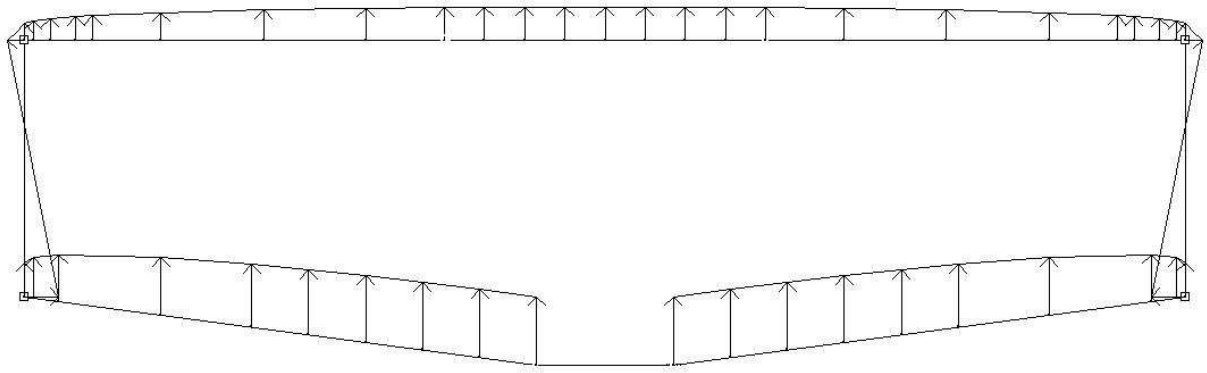

Figure 4.3 Lift distribution with different constant parts of both horizontal wings (modelled within *Framework* from **Wolsink 2011**)

From this consideration it becomes clear that the constant part of the lift distribution of the

horizontal wings determines the lift loading of the winglets. It is also obvious that a low value for the constant part decreases the loading on the wing tips of the horizontal wings, which leads to a lower wing root bending moment and lower values of the lift coefficient at the outer wing region. It is part of further aerodynamic investigations to determine the parameters which influence the ratio R_L. According to simple studies performed by F. Khan (**Khan 2011**) it seems that an increase of the h/b ratio leads to an increase of R_L, meaning the constant part becomes greater. This causes a higher wing bending moment and the risk of tip stall. Yet it has to be assessed which h/b ratios might become critical regarding tip stall and increase of root bending moment. Finally it is also not clear which value of R_L gives minimum induced drag.

4.1.2 Lift Coefficients

In this paragraph the correlations of the lift coefficients of the forward and aft wing as well as the total lift coefficient evolving from both individual lift coefficients are discussed. The purpose of this discussion is to sensitize to the special characteristics of the box wing configuration regarding the interaction of both wings in terms of lift.

The total lift coefficient of the aircraft comprises the individual lift coefficients of the lifting surfaces as well as effects generated by the fuselage. In the present investigation the fuselage effects are neglected for the sake of simplicity, so only the two lifting surfaces are of interest.

According to general aerodynamic theory the total lift coefficient of two lifting surfaces is calculated using their individual lift coefficients and areas, resulting in

$$C_L = \frac{C_{L,1} \cdot S_1 + C_{L,2} \cdot S_2}{S_1 + S_2} = C_{L,1} s_1 + C_{L,2} s_2 \quad . \tag{4.2}$$

Determining the individual lift coefficients requires special attention because of the downwash of the forward wing. Usually the lift coefficient is determined with the help of the angle of attack and the lift curve slope:

$$C_L = \frac{dC_L}{d\alpha} \cdot \alpha \tag{4.3}$$

with α being measured with regard to the zero lift line of the aircraft. Eq. (4.3) can be used for the total aircraft. It can be used for the forward wing without any problems, too, so

$$C_{L,1} = \frac{dC_{L,1}}{d\alpha} \cdot \alpha \quad . \tag{4.4}$$

However, for the aft wing the downwash of the forward wing has to be taken account of. Here the angle of attack is reduced by the downwash angle, which results in

$$C_{L,2} = \frac{dC_{L,2}}{d\alpha} \cdot (\alpha - \varepsilon) \tag{4.5}$$

The downwash angle depends on the downwash gradient and the angle of attack. Eq. (4.5) is then changed to

$$C_{L,2} = \frac{dC_{L,2}}{d\alpha} \cdot \left[\alpha - \left(\frac{d\varepsilon}{d\alpha} \cdot \alpha \right) \right] = \frac{dC_{L,2}}{d\alpha} \cdot \alpha \left(1 - \frac{d\varepsilon}{d\alpha} \right) \quad . \tag{4.6}$$

Combining Eqs. (4.2), (4.4) and (4.6) yields

$$C_L = \left[\frac{dC_{L,1}}{d\alpha} \cdot \alpha \right] s_1 + \left[\frac{dC_{L,2}}{d\alpha} \cdot \alpha \left(1 - \frac{d\varepsilon}{d\alpha} \right) \right] s_2 \tag{4.7}$$

As simplification the downwash gradient is assumed to be constant. Fig. 4.4 shows a possible lift polar for a configuration without decalage. It illustrates an anomaly of the box wing. It is supposed that, when isolated, both wings have the same lift curve slope ($dC_{L,1}/d\alpha = dC_{L,2}/d\alpha$). However, the resulting slopes are different because of the downwash of the forward wing.

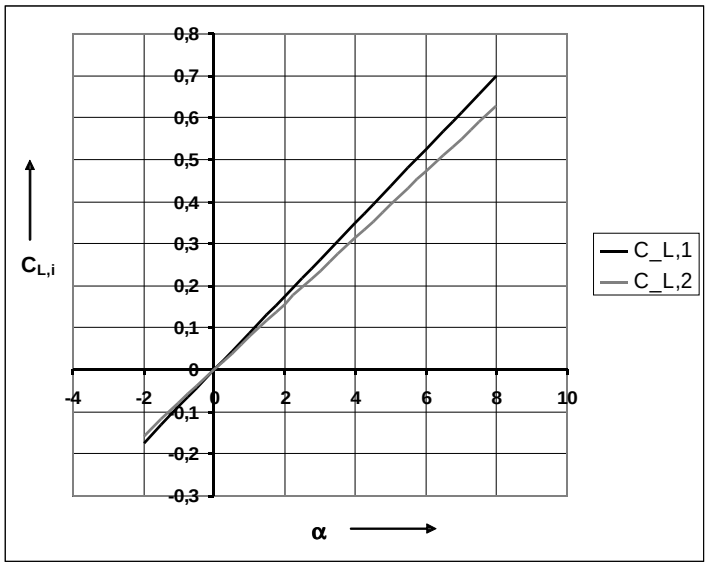

Figure 4.4 Generic lift polar of the individual wings of a box wing aircraft

Note that in this discussion the effect of upwash from the aft wing on the forward is not considered.

4.1.3 Lift Curve Slope

The lift curve slope describes the change of lift for a variation of the angle of attack. It is important for the determination of the incidence angles of the wings and for identifying the angle of attack where stall is to be expected as well as the required angle of attack for all flight phases (critical: approach/landing and take off rotation). The lift curve slope also influences the static margin and the reaction of the aircraft to gusts.

According to **Scholz 1999** the lift curve slope can be approximated for a first approach by

$$\frac{dC_L}{d\alpha} \approx \frac{2\cdot\pi\cdot A}{2+\sqrt{A^2\cdot\left(1+\tan^2\varphi_{50}-M^2\right)+4}} \quad . \tag{4.8}$$

With the help of this approximation the ratio of lift curve slopes of the box wing aircraft and the reference aircraft can easily be formulated. For this a single wing of the box wing aircraft is considered, which is assumed to have double the aspect ratio of the reference aircraft. Additionally both aircraft are supposed to have a wing sweep of 20° at half chord. Neglecting the effects of compressibility the following ratio is built:

$$\frac{\left(dC_L/d\alpha\right)_{box}}{\left(dC_L/d\alpha\right)_{ref}} = \frac{2\left(2+\sqrt{{A_{ref}}^2\cdot\left(1+\tan^2 20°\right)+4}\right)}{2+\sqrt{4\,{A_{ref}}^2\cdot\left(1+\tan^2 20°\right)+4}} = 1{,}103 \quad . \tag{4.9}$$

However, Eq. (4.9) does not take account of downwash effects of the forward wing on the aft wing. In **DATCOM 1978** these effects are considered within the scope of the lift curve slope of wing-body-tail combinations at angle of attack (DATCOM Section 4.5.1.1). If interferences with the body of the aircraft are neglected and the dynamic pressure is assumed to be the same at both wings, the general equation is[1]

$$\frac{dC_L}{d\alpha} = \frac{dC_{L,1}}{d\alpha}\cdot s_1 + \frac{dC_{L,2}}{d\alpha}\cdot s_2\cdot\left(1-\frac{d\varepsilon}{d\alpha}\right) \quad . \tag{4.10}$$

As a first approach $s_1 = s_2 = 0{,}5$. The lift curve slopes of the individual wings were determined in Eq. (4.8). Assessing Eq. (4.10) one recognizes that the downwash reduces the contribution of the aft wing to the overall lift curve slope. Supposing that the downwash gradient $d\varepsilon/d\alpha$ has a magnitude of about 0,1 the overall lift curve slope is reduced by 5 % compared to the lift curve slope of the individual wings. Keeping in mind the result of Eq. (4.9) this means that the lift curve slope of the box wing is about 1,048 times the lift curve slope of the reference aircraft, taking account of all simplifications.

[1] Eq. (4.10) can also be determined by differentiating Eq. (4.7) with respect to α.

Referring to the statements made at the beginning of this section, the box wing aircraft is consequently more sensitive to gusts than the reference aircraft. Additionally it is about to stall at lower angles of attack. But a higher lift curve slope also means lower pitch angles during landing and take off.

Strictly speaking Eq. (4.10) is only valid if the span of the aft surface is significantly smaller than that of the forward surface. However, this equation is suitable to show the general downwash effects. A detailed analysis taking account of equal spans is presented in section 5.2.2. From the results of section 5.2.2 it can be concluded that the lift curve slope is slightly overestimated when using the simple approach of Eq. (4.10).

4.2 Drag

4.2.1 Zero Lift Drag

Zero lift drag is the total drag of the aircraft in clean configuration minus the drag due to lift. The relating coefficient is $C_{D,0}$. According to **Loftin 1980** a good initial value for preliminary sizing is 0,02.

In the course of the conceptual design it becomes necessary to determine the zero lift drag more exactly with the help of more dedicated methods. In **Scholz 1999** two possibilities are presented.

The first is based on the equivalent skin friction coefficient C_{fe}, which in combination with the known aircraft geometry (more precise: its wetted area) results in the zero lift drag coefficient. The corresponding equation is

$$C_{D,0} = C_{fe} \cdot \frac{S_{wet}}{S_W} \tag{4.11}$$

with S_W being the wing reference area. This method contains some uncertainty because the equivalent skin friction coefficient is only know from statistics and experience.

The second method is summing up the drag of all aircraft components. This includes the determination of the individual skin friction drag, the pressure drag and the interference drag. The corresponding equation is

$$C_{D,0} = \sum_{i=1}^{n} C_{f,i} \cdot FF_i \cdot Q_i \cdot \frac{S_{wet,i}}{S_{ref}} \tag{4.12}$$

where $C_{f,i}$ are the individual skin friction drag coefficients, FF_i the form factors which take account of the pressure drag, Q_i the interference factors, $S_{wet,i}$ the wetted areas of the individual components and S_{ref} the reference area for the total zero lift drag coefficient.

It becomes clear that the latter method is more exact than the one based on the equivalent skin friction coefficient, but also much more labor intense. This is why the method used in this thesis is the one based on the equivalent skin friction coefficient, since it seems to be sufficient for preliminary performance calculations.

The determination of the zero lift drag coefficient of the final design is presented in section 11.1.

4.2.2 Induced Drag

Induced drag, or lift dependent drag, is the drag which results from the generation of lift. One of its causes is the formation of vortices on the wing tips, forming from the difference of pressure between the upper and the lower surface. These vortices induce a downward velocity (downwash) leading to a reduction of the effective angle of attack α_{eff}. The magnitude of reduction is specified by the induced angle of attack α_i. As it can be seen in Fig. 4.5 the lift vector, typically perpendicular to the free stream, is rotated through α_i, resulting in the formation of a drag component.

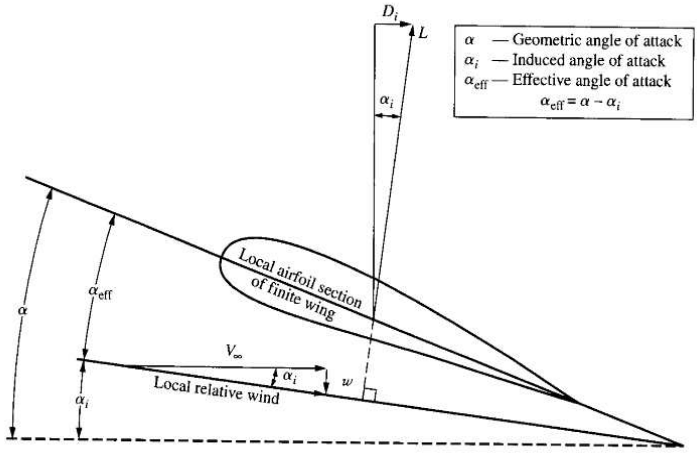

Figure 4.5 Effect of downwash on the local flow over a local airfoil section of a finite wing (**Anderson 2007**)

In dimensionless form the induced drag can be expressed by the following equation:

$$C_{D,i} = \frac{C_L^{\,2}}{\pi \cdot e \cdot A} \quad . \tag{4.13}$$

The crucial factor in Eq. (4.13) is the span efficiency factor *e*, whereas the lift coefficient C_L depends on the flight state and the aspect ratio *A* is defined by the geometry of the wing plan form.

A common interpretation of *e* is that it indicates the efficiency of the lift distribution along the wing. For planar wings a value of unity means the distribution is elliptical, thus generating minimum induced drag. However, this value can only be achieved in theory. In practice effects like viscous drag, pressure drag as well as interference drag reduce the efficiency resulting in values of *e* lower than unity, even if the distribution of lift is elliptical (**Kroo 2001**). According to **Kroo 2001** the conception of the span efficiency factor may sometimes be misleading. Considering wing twist, induced drag even occurs when $C_L = 0$. In this case one portion of the wing may produce positive lift, but another portion cancels this lift by producing a

downward force, resulting in no lift altogether. Nevertheless this arrangement causes wing tip vortices leading to induced drag.

With the following equation the absolute induced drag resulting from the accordant coefficient can be calculated:

$$D_i = C_{D,i} \cdot q_\infty \cdot S \tag{4.14}$$

As first approach it is assumed that a single wing of the box wing aircraft has half the area of the reference wing. The aspect ratio of a single wing of the box wing aircraft is supposed to be double the aspect ratio of the reference wing. The span efficiency factor of an isolated wing of the box wing aircraft is assumed to be the same as the span efficiency factor of the reference wing. With the help of these assumptions it is possible to calculate the induced drag of the box wing aircraft in relation to the induced drag of the reference aircraft.

Combining Eq. (4.13) and (4.14) gives

$$D_i = \frac{C_L^{\,2}}{\pi \cdot A \cdot e} \cdot q_\infty \cdot S \quad . \tag{4.15}$$

Building the ratio of the induced drag of one single wing of the box wing aircraft to the induced drag of the reference wing yields

$$\frac{D_{i,single}}{D_{i,ref}} = \frac{\frac{C_L^{\,2}}{\pi \cdot 2\,A_{ref} \cdot e} \cdot q_\infty \cdot 0{,}5\,S_{ref}}{\frac{C_L^{\,2}}{\pi \cdot A_{ref} \cdot e} \cdot q_\infty \cdot S_{ref}} = 0{,}25 \quad , \tag{4.16}$$

so the induced drag of a single wing of the box wing configuration is quarter the induced drag of the reference wing. Since the box wing consists of two wings, the total induced drag of the box wing configuration is half the induced drag of the reference aircraft. This consideration does not take account of the vertical winglets. In section 4.2.3 the effects of the additional winglets is shortly discussed.

In Eq. (4.16) no mutual wing interference is considered. It would increase the ratio of induced drag. The lower the *h*/*b* ratio, the higher the interference effects between both wings. The induced drag depending on the *h*/*b* ratio will be further discussed in sections 4.3 and 4.6, as well as the resulting span efficiency factor.

4.2.3 Wing Tip Vortices

Fig. 4.6 shows the lift distribution of the horizontal and the vertical wings separately as well as the resulting tip vortices. The vortices form because of the differential pressure between the upper and lower surfaces of the horizontal wings and between the inner and outer surfaces of the vertical wings. Since the air streams from high to low pressure the vortices are drawn so that they originate at the high pressure side. This way it can easily be seen that the vortices caused by the horizontal wings counteract the vortices caused by the vertical wings.

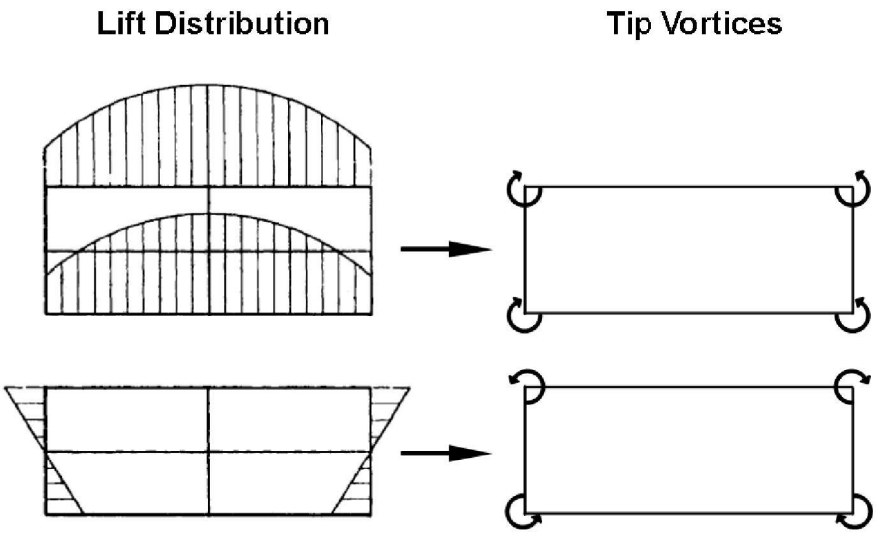

Figure 4.6 Counterrotating tip vortices of a box wing aircraft

In **Durand 1935** Theodore von Kármán writes:

> *„The forces on the vertical wings are necessary to reduce the vortices which would appear at the wingtips, if they were not united.“*

So apart from the savings because of the wing split, which reduces the induced drag to one half of that of the reference wing (theoretically!), the mutual damping of the tip vortices means further savings. This is why the ideal ratio of induced drag of the box wing aircraft to the reference aircraft is below 0,5. This is confirmed in literature for the most part. Section 4.3 will address this issue in detail.

4.3 Span Efficiency Factor

In literature several methods can be found for the determination of the span efficiency factor of a box wing. In this paragraph two of them are shown and in the end the most suitable method is chosen.

Method 1

In **DeYoung 1980** a method is given originally coming from **Durand 1935**. The calculation incorporates certain elliptic integrals and there exists no direct solution. However, results for the span efficiency factor depending on the *h*/*b* ratio are given in **DeYoung 1980**. The values for probable *h*/*b* ratios are given in table 4.1.

Table 4.1 Span efficiency factor of an ideally loaded rectangular box wing depending on *h*/*b* ratio (**DeYoung 1980**)

h/*b*	*e*
0	1
0,05	1,15178
0,1	1,26814
0,15	1,37327
0,2	1,47189
0,25	1,56610

Additionally **DeYoung 1980** shows that the rectangular box wing is generally the configuration with the highest span efficiency factor. Referring to section 4.2.3, where it was claimed that $D_{i,box}/D_{i,ref}$ is below 0,5 in the ideal case, the span efficiency factor goes to infinity for $h/b => \infty$ acc. to **DeYoung 1980**. For $h/b = 4$ it is about 7, which, acc. to Eq. (4.18) below, would be equivalent to a ratio $D_{i,BW}/D_{i,ref}$ of 0,143. This seems very unrealistic and indicates that the values proposed by **DeYoung 1980** can only be used for small *h*/*b* ratios.

Method 2

The second method for determining the span efficiency factor is based on the relation of the induced drag of a box wing configuration to that of a reference monoplane. The relation can be expressed with the following equation:

$$\frac{(C_{D,i})_{box}}{(C_{D,i})_{ref}} = \frac{\dfrac{C_L^{\,2}}{A_{box} \cdot e_{box}}}{\dfrac{C_L^{\,2}}{A_{ref} \cdot e_{ref}}} = \frac{A_{ref} \cdot e_{ref}}{A_{box} \cdot e_{box}} \tag{4.17}$$

As mentioned in section 3.2.1 the box wing aircraft should have the same total aspect ratio as the reference aircraft. With this assumption the span efficiency factor of a box wing aircraft in

relation to the equivalent monoplane is calculated with

$$\frac{e_{box}}{e_{ref}} = \frac{(C_{D,i})_{ref}}{(C_{D,i})_{box}} = \frac{1}{\kappa} \tag{4.18}$$

In **Prandtl 1924** κ is approximated for a box wing with

$$\kappa = \frac{1+0{,}45\,h/b}{1{,}04+2{,}81\,h/b} \;; \quad \frac{1}{15} < h/b < \frac{1}{2} \quad . \tag{4.19}$$

The limit value of κ is 0,16 , which is far below the value of 0,5 for a simple biplane.

In **Frediani 2009** an exact solution for the determination of κ is derived. The results are based on numerical calculations and therefore no simple correlation analogous to Eq. (4.19) could be formulated. Nevertheless, a plot of the results (see Fig. 4.7) shows that Prandtl's equation is well suited for height to span ratios up to 0,3 , which is the range coming into question for a box wing aircraft. However, in **Frediani 2005**, which refers to the calculations of **Frediani 2009**, it is claimed that for a box wing the limit value of κ is 0,5.

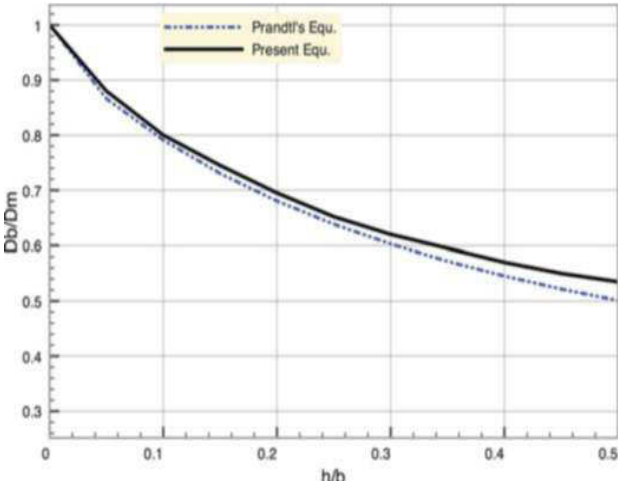

Figure 4.7 κ vs. *h*/*b* acc. to Prandtl and Frediani (**Frediani 2009**)

Rizzo 2007 derived an equation for κ coming from CFD analysis which generates values close to the plot from **Frediani 2009**. The accordant equation is

$$\kappa = \frac{0{,}44+0{,}9594\,h/b}{0{,}44+2{,}219\,h/b} \quad . \tag{4.20}$$

The limit value according to Eq. (4.20) is about 0,43.

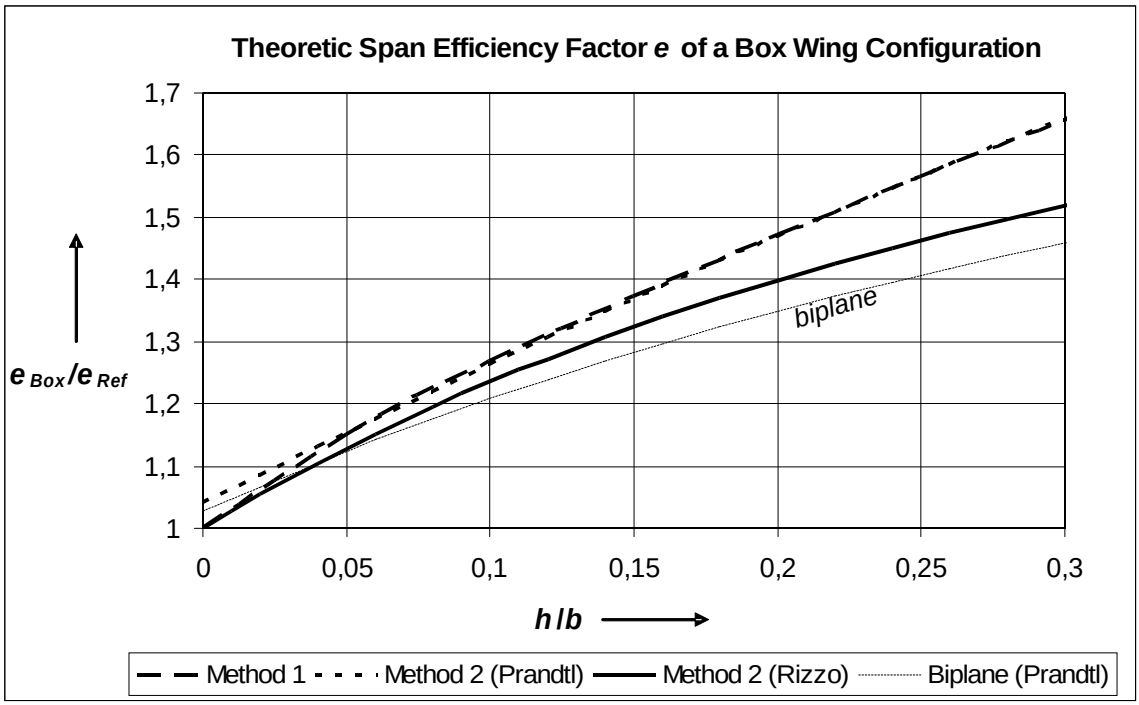

Figure 4.8 Theoretic span efficiency factor of a box wing configuration

Fig. 4.8 summarizes the results of the presented methods. It can be seen that Method 1 acc. to **DeYoung 1980** generates results similar to those by Method 2 (**Prandtl 1924**). As already mentioned they seem to be too optimistic, so the equation proposed by **Rizzo 2007** will be used for the following investigations.

According to Eq. (4.18) the span efficiency factor of the reference monoplane e_{ref} is needed in order to calculate its box wing counterpart e_{box}. In **Scholz 1999** the span efficiency factor of a monoplane is proposed to be 0,85 during cruise and 0,7 in landing configuration. Hence these values will be used in the forthcoming calculations.

One important point is how to determine the ratio h/b if both wings have different dihedral. In **Lockheed 1974** the conclusion is drawn that just the vertical distance between both wing tips is the crucial factor, hence the ratio h_{tip}/b. Therefore dihedral/anhedral also affects the span efficiency factor. This fact is also confirmed in **Kroo 2001**.

4.4 Mean Aerodynamic Chord

The mean aerodynamic chord (MAC) is a reference parameter for stability considerations and the travel of the center of gravity. Per se it is not a crucial factor influencing the design of the aircraft. However, its determination is based on physical principles which can be transferred to the box wing configuration.

There are two important parameters which are needed to describe the CG travel in terms of per cent MAC: The length of the MAC $\bar{c}$ and its longitudinal position/position along the x-axis $\bar{x}$. In this paragraph the equations for calculating these parameters are given, resulting from applying the mentioned physical principles. The detailed derivation can be found in Appendix A.

The length of the mean aerodynamic chord is given by

$$\bar{c} = s_1 \bar{c}_1 + s_2 \bar{c}_2 \tag{4.21}$$

with $\bar{c}_i$ being the length of the mean aerodynamic chords of the individual wings.

The longitudinal position is expressed in terms of the distance between the aerodynamic center of the total wing configuration, which is assumed to be at 25 % MAC, and the CG of the aircraft $(x_{CG\text{-}AC})_{tot}$ which is based on a derivation given in **Scholz 1999**. The final equation is

$$(x_{CG-AC})_{tot} = \frac{L_1 (x_{CG-AC})_1 + L_2 (x_{CG-AC})_2}{L_1 + L_2} \quad . \tag{4.22}$$

The definition of the parameters is given in Fig. 4.9.

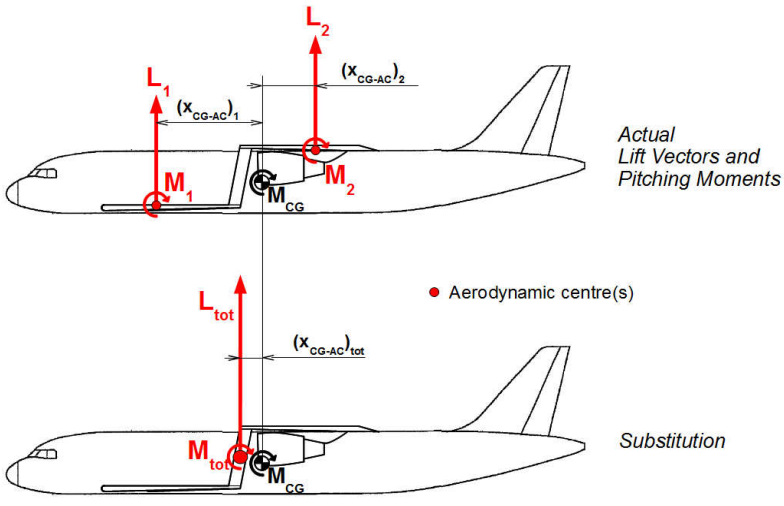

Figure 4.9 Parameters for the determination of the longitudinal position of the MAC

4.5 Effect of Low Reynolds Numbers

Because of the small chord lengths of the wings of the box wing aircraft the Reynolds numbers of the wings will only be about half as high as for the reference aircraft.

In general lower Reynolds numbers mean that a larger part of the airfoil has a laminar boundary layer. This leads to less skin friction drag. Usually the boundary layer on a transonic wing is almost entirely turbulent.

However, to assess the effects of lower Reynolds numbers detailed aerodynamic studies are necessary. Based on these, more exact conclusions concerning wing design, aerodynamics and performance of the aircraft can be made.

4.6 Effect of Unequal Lift Distributions between Both Wings

The minimum induced drag is reached when both wings generate the same lift. However, it is very unlikely that this state is present during the whole flight. Additionally, in chapter 5.2 it is shown that the requirements for minimum induced drag are in conflict with stability and controllability requirements. For these reasons the effect of an unequal lift division of both wings has to be investigated. The analysis will be limited to the assessment of the increase of induced drag.

4.6.1 Increase of Induced Drag

In **Lockheed 1974** a simple method for determining the increase of the induced drag depending on the lift ratio of both wings is presented. It is based on the biplane equations shown in **Prandtl 1924**. There a general equation for the induced drag of a biplane is given as well as an equation for the minimum induced drag of a biplane. Relating these two equations gives the factor of drag increase for given lift ratios. These equations can be used for a box wing aircraft without limitation, since the only factor that distinguishes a normal biplane from a box wing aircraft is the interference factor σ, at least according to Prandtl's theory. The interference factor is included in these equations.

During the investigation of the drag increase it was discovered that the resulting equation given in **Lockheed 1974** generates results which are four times higher than expected, which lead to the conclusion that the Lockheed equation contains a wrong factor. Strangely enough the relating plot in **Lockheed 1974** contains the expected results. This is why the derivation of the proper equation is shown in the following passage.

According to **Prandtl 1924** the equation for calculating the induced drag of a general biplane is

$$D_i = \frac{1}{\pi q}\left(\frac{{L_1}^2}{{b_1}^2} + 2\sigma\frac{L_1 L_2}{b_1 b_2} + \frac{{L_2}^2}{{b_2}^2}\right) \quad . \tag{4.23}$$

The determination of σ was discussed in chapter 4.3.

For the box wing aircraft investigated in this thesis both wings have the same wing span. For this special case the equation can be simplified as follows:

$$D_i = \frac{1}{\pi q b^2} \cdot \left(L_1{}^2 + 2\sigma L_1 L_2 + L_2{}^2 \right) \quad . \tag{4.24}$$

For minimum induced drag both wings have to produce the same amount of lift when their spans are equal (**Prandtl 1924**). This minimum is calculated with

$$D_{i,min} = \frac{1}{\pi q b^2} \cdot L^2 \cdot \left(\frac{1+\sigma}{2} \right) \quad . \tag{4.25}$$

Relating Eq. (4.24) to Eq. (4.25) gives

$$\frac{D_i}{D_{i,min}} = \frac{2\left(L_1{}^2 + L_2{}^2 + 2\sigma L_1 L_2 \right)}{L^2 \left(1+\sigma \right)} \quad . \tag{4.26}$$

Eq. (4.26) can be used to express the ratio of the actual induced drag to the minimum induced drag of a box wing. It is convenient to express this correlation depending on the lift ratio of both wings. So the following term is introduced:

$$x = \frac{L_1}{L_2} \quad . \tag{4.27}$$

According to Eq. (4.27) the lift of the forward wing can then be expressed with

$$L_1 = x \cdot L_2 \quad , \tag{4.28}$$

which is inserted in the numerator on the right hand side of Eq. (4.26).

The total lift is the sum of both the individual lift components L_1 and L_2. Using this correlation in combination with Eq. (4.28) gives

$$L = L_2 \left(x+1 \right) \quad , \tag{4.29}$$

which is used for the denominator on the right hand side of Eq. (4.26). With the just mentioned substitutions Eq. (4.26) becomes

$$\frac{D_i}{D_{i,min}} = \frac{2\left(L_2{}^2 x^2 + L_2{}^2 + 2\sigma L_2{}^2 x \right)}{L_2{}^2 \left(x+1 \right)^2 \left(1+\sigma \right)} \quad . \tag{4.30}$$

Eliminating L_2 finally yields

$$\frac{D_i}{D_{i,min}} = 2\frac{x^2+2\sigma x+1}{(\sigma+1)(x+1)^2}; \quad x = \frac{L_1}{L_2} \tag{4.31}$$

This correlation can also be expressed in terms of the individual lift coefficients. Assuming that both wings have the same reference area and that the dynamic pressure is the same on both wings, it can simply be written that

$$\frac{C_{D,i}}{(C_{D,i})_{min}} = 2\frac{x^2+2\sigma x+1}{(\sigma+1)(x+1)^2}; \quad x = \frac{C_{L,1}}{C_{L,2}};\ S_1 = S_2;\ q_1 = q_2 \tag{4.32}$$

The results of Eq. (4.31) are plotted in Fig. 4.10. The accordant determination of σ is based on the results for a box wing aircraft in **Rizzo 2007**. They were already shown in section 4.3 of this thesis.

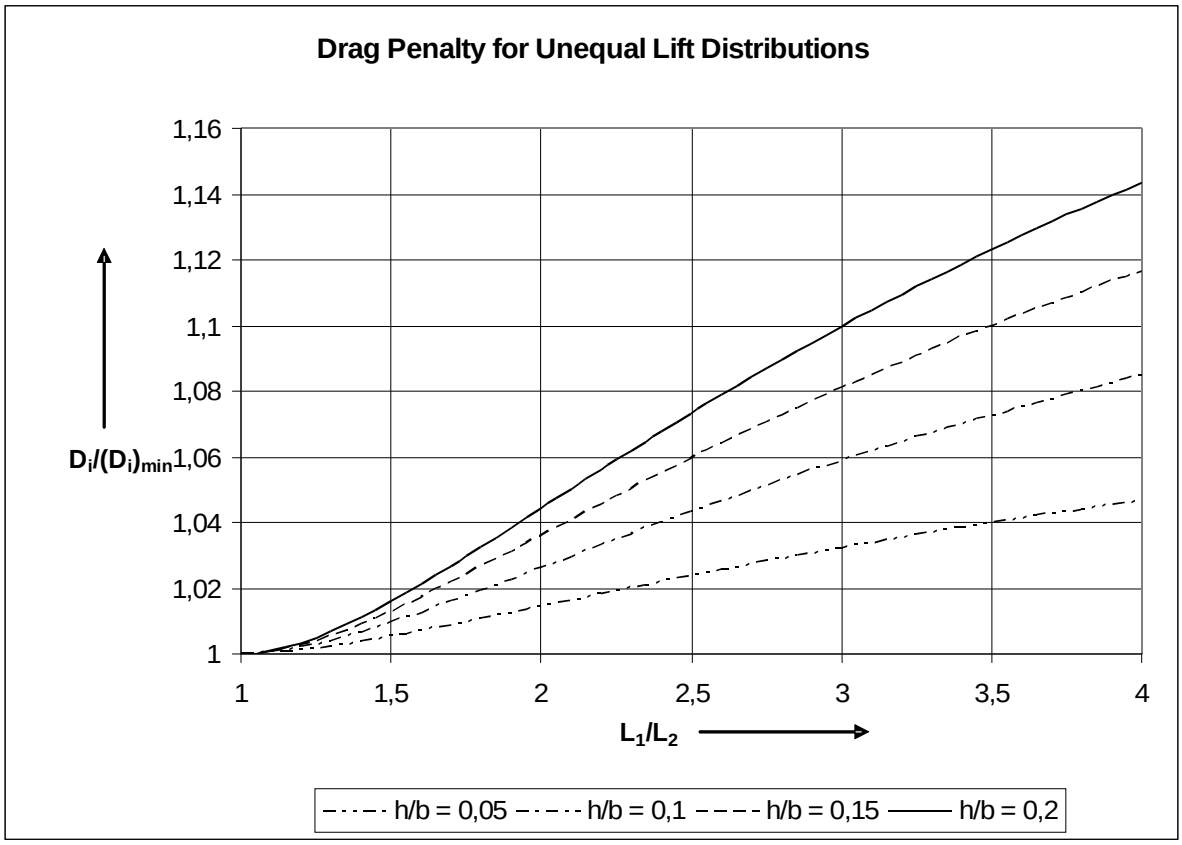

Figure 4.10 Induced drag penalty for unequal lift of both wings

4.6.2 Reduction of the Span Efficiency Factor

In chapter 4.3 the correlation of the induced drag and the span efficiency factor was shown. Concluding from the results of section 4.6.1 an unequal lift division of both wings leads to a reduction of the span efficiency factor. Deduced from Eq. (4.18) this reduction can be expressed with

$$\frac{e}{e_{min}} = \frac{D_{i,min}}{D_i} \tag{4.33}$$

It is possible to illustrate this reduction depending on the ratio L_1/L_2 by building the reciprocal of Eq. (4.31). The results are depicted in Fig. 4.11.

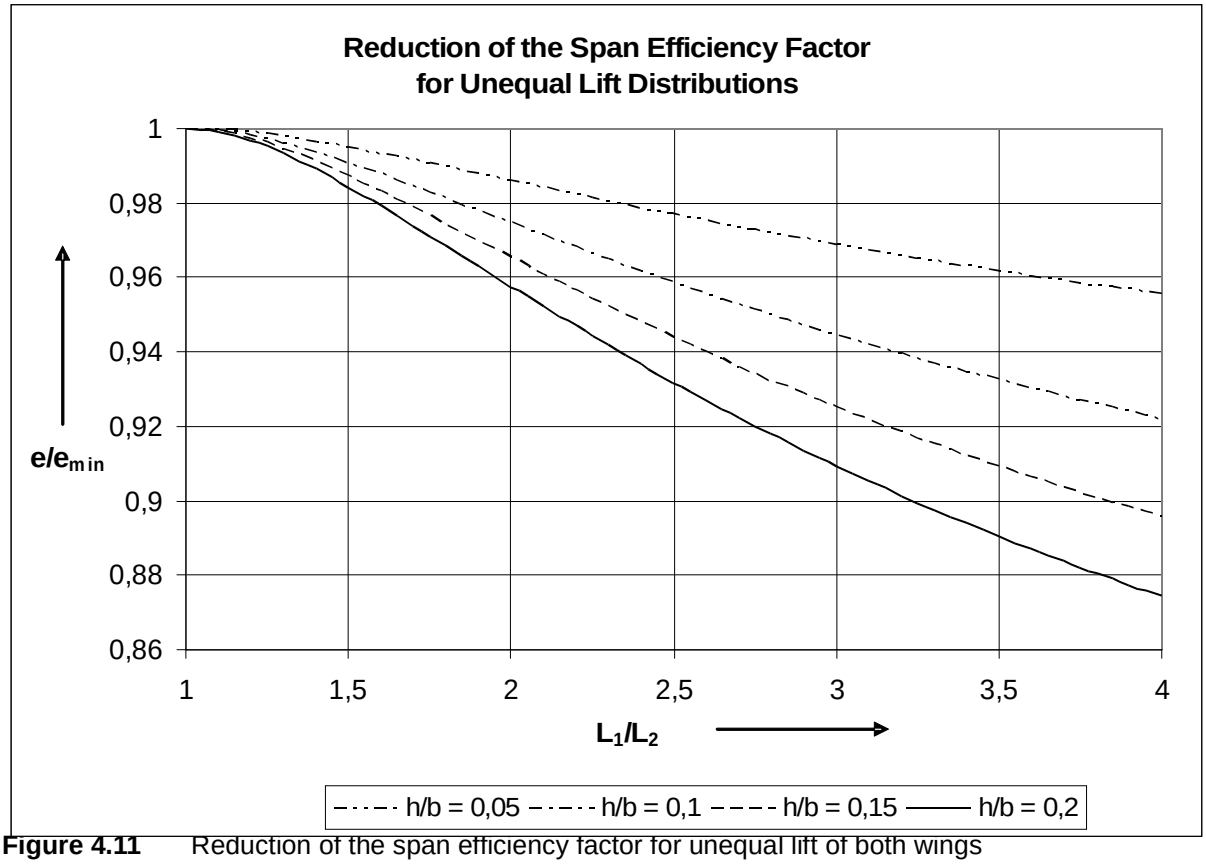

Figure 4.11 Reduction of the span efficiency factor for unequal lift of both wings

4.7 Stall Characteristics

The stall characteristics are important for an evaluation of the aircraft behaviour under extreme flight conditions. The stall characteristics of a box wing configuration are outlined in Fig. 4.12.

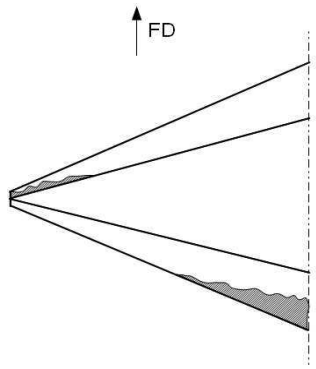

Figure 4.12 Stall characteristics of a box wing aircraft

The front wing is swept backwards and the aft wing is swept forwards. According to **Scholz 1999** backwards swept wings stall first near the tip region while forwards swept wings stall first near the root region. Since the areas of stall are aft of the aircraft's center of gravity for the most part, the risk of pitch up during stall is very high. Of course, this simple consideration does not take account of effects of mutual wing interference, downwash and the presence of the vertical wings, but the described issue needs to be investigated. Counteractive measures are adjustments of the wing design, e.g. wing twist, taper and incidence angles.

In contrast **Cahill 1954** concludes that there is a lack of pitch up for this type of wing configuration. There it is written that:

> *"The rear wing is, in general, in the downwash field of the front wing so that its angle of attack is generally less than that of the forward wing and, therefore, it would be expected to stall at a higher model angle of attack. The vortices shed from the forward wing also contribute a lateral component to the flow over the rear wing which opposes the spanwise flow in the boundary layer toward the root of the rear wing and, therefore, also tends to delay the premature stall usually encountered at the root of sweptforward wings."*

But it seems that no decalage was used for the tests performed within the scope of **Cahill 1954**. Additionally the *h*/*b* ratio was very small, the configuration rather resembled a tandem wing configuration. However, the described effects show that under certain design conditions it is possible to counteract the inherent pitch up tendency one would expect from the discussion at the beginning of this paragraph.

In general it is desired that the forward wing stalls first so that in this case the aircraft pitches down and flight speed increases to stabilize the aircraft.

4.8 Distinction of the Characteristics of the Individual Wings and the Whole Wing Configuration

It is important to differentiate between considerations concerning one single wing of the box wing configuration and those concerning the total wing configuration. Depending on the point of view, the reduction of induced drag can be justified by a higher span efficiency or an increased aspect ratio. However, it is important not to mix these two effects. In the following the peculiarities of each approach are briefly discussed.

Once again the general equation for calculating the coefficient of induced drag is given:

$$C_{D,i} = \frac{C_L^{\,2}}{\pi \cdot A \cdot e} \quad . \tag{4.34}$$

Additionally the equation for determining the absolute induced drag is given with

$$D_i = \frac{L^2}{q \cdot \pi \cdot b^2 \cdot e} \quad . \tag{4.35}$$

When looking at a single wing of the box wing configuration it becomes apparent that its aspect ratio is double the aspect ratio of the reference wing. The resulting reduction of induced drag of the whole wing configuration based on Eq. (4.34) was already expressed with the help of Eq. (4.16). So here the higher aspect ratio is the responsible parameter for the reduction. Consequently the span efficiency of a single wing of the box wing configuration is about the same as that of the reference wing.

On the other hand, when looking at the whole configuration the relations reverse. With the definition of section 2.2.3 and resulting from the geometry requirements given in section 3.2.1 the total aspect ratio of the box wing aircraft is the same as that of the reference aircraft. So here the span efficiency *e* is responsible for the reduction of the induced drag. This correlation was the basis for the investigations performed in section 4.3.

Using Eq. 4.35 also clarifies the distinction between the two approaches. Considering an individual wing of the box wing configuration means that the lift is half of that of the reference wing with all of the other parameters being constant. This results in an induced drag being 25% of that of the reference wing [compare Eq. (4.16)]. When considering the whole configuration it has to be referred to the different span efficiencies again, since all of the other parameters are constant. In contrast to Eq. (4.34) the aspect ratio is of no importance for Eq. (4.35), which simplifies the examination.

5 Box Wing Flight Mechanics

Flight Mechanics are a very broad subject. In this paragraph only aspects concerning performance and static stability are discussed. An assessment of flight dynamics, for example with the help of the SDSA module of CEASIOM, is part of further studies.

5.1 Performance

In this paragraph only general considerations concerning box wing performance are outlined. Final performance characteristics including zero lift drag, glide ratio and the payload-range diagram can be found in chapter 11.

5.1.1 Drag Polar

The drag polar is essential for assessing the performance of an aircraft. In all coming investigations the quadratic form of the drag polar is used. In its idealised form it is determined with

$$C_D = C_{D,0} + \frac{C_L^{\,2}}{\pi A e} \quad , \tag{5.1}$$

which applies to aircraft whose minimum drag coefficient is the zero lift drag coefficient. This is the case for aircraft with uncambered airfoils. However, this form is also often used for aircraft with cambered airfoils as first approximation. The actual polar of such aircraft is given with

$$C_D = C_{D,min} + \frac{\left[C_L - \left(C_L\right)_{C_{D,min}}\right]^2}{\pi A e} \tag{5.2}$$

(**Scholz 2000**)

Fig. 5.1 shows the difference between both polars.

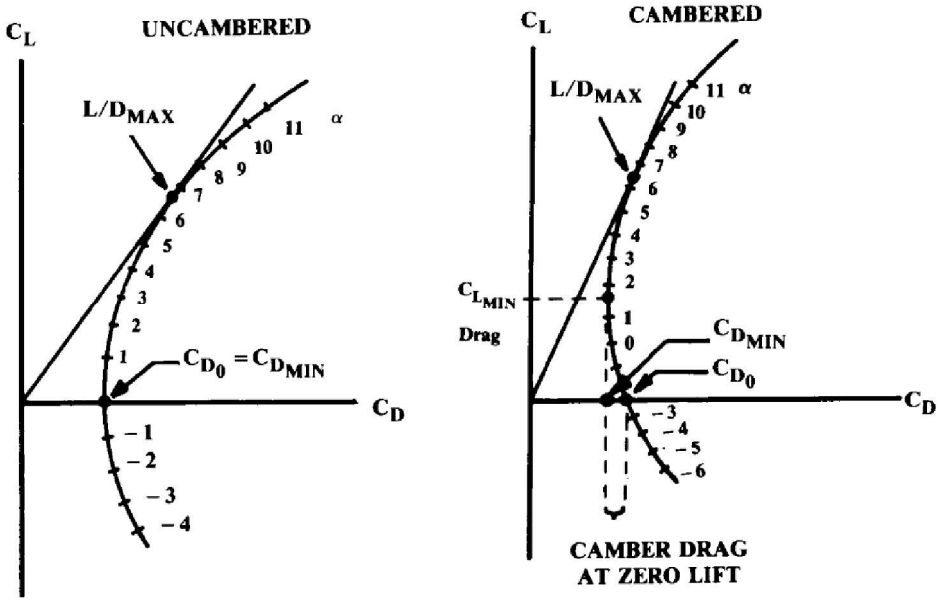

Figure 5.1 Idealised (left) and actual drag polars (**Raymer 1992**)

Fig. 5.1 reveals that there is a vertical shift between both of the polars. The minimum drag according to the actual polar is at lift coefficients higher than zero. This results in a higher maximum glide ratio, so using the actual drag polar is fundamental for more exact performance calculations. But also the zero lift coefficient seems to be higher according to the actual drag polar.

However, for preliminary studies it does not matter which kind of polar is used. As it will be shown in the coming sections 5.1.3 and 5.1.4, it is possible to build a ratio of glide ratios of the box wing and the reference aircraft with the help of the ratio of span efficiencies. So a drag polar is not required for a preliminary assessment of the performance of the box wing aircraft. Additionally it is difficult to determine $C_{L,min}$ for a cambered wing aircraft. Hence, when performing a more exact performance calculation of the final box wing configuration, the glide ratio is determined using a general equation based on the idealised drag polar (Eq. (5.10). The only input parameters which are needed are the zero lift drag coefficient and the span efficiency factor. Furthermore the determination of the glide ratio is performed within the preliminary sizing spreadsheet (**Scholz 2008**) as well.

The use of the actual drag polar also requires exact knowledge about the characteristics of the used airfoils. Since at this stage of the design study no definite airfoil choice is made, any further discussion of the actual drag polar is unnecessary.

5.1.2 Lift Coefficient for Minimum Drag Based on the Idealized Drag Polar

To prevent any confusion, the lift coefficient investigated here is the lift coefficient for minimum drag for cruise flight. Otherwise it could be argued that the minimum drag already occurs at zero lift (compare Fig. 5.1).

It is important to consider the lift coefficient for minimum drag because when operating at this lift coefficient the aircraft also operates at the highest glide ratio. Considering aerodynamics this is the most efficient state of flight. Acc. to **Young 2001** the lift coefficient for minimum drag can be calculated with

$$C_{L,md} = \sqrt{C_{D,0} \cdot \pi \cdot A \cdot e} \quad . \tag{5.3}$$

It needs to be kept in mind that Eq. (5.3) actually applies to aircraft with uncambered airfoils. The effects of using the actual drag polar are not considered in this paragraph. Referring to section 4.8, the approach of considering the configuration as a whole and not the individual wings is used.

Assuming that the reference aircraft has a zero lift drag coefficient of 0,02 and a span efficiency factor of 0,85, its lift coefficient for minimum drag is about 0,71.

For flying at E_{max} the following condition has to be met:

$$C_{D,i} = C_{D,0} \quad . \tag{5.4}$$

For preliminary considerations it can be assumed that the drag coefficient for zero lift is the same for both the box wing and the reference aircraft. This also means that the coefficient of induced drag is the same as well:

$$\left(C_{D,i}\right)_{md,box} = \left(C_{D,i}\right)_{md,ref} \tag{5.5}$$

The index *md* means that the coefficients are now referred to the minimum drag condition. Applying the standard formula for the induced drag coefficient [Eq. (4.13)] and rewriting yields:

$$\frac{\left(C_L\right)_{md,box}}{\left(C_L\right)_{md,ref}} = \sqrt{\frac{A_{box} \cdot e_{box}}{A_{ref} \cdot e_{ref}}} \tag{5.6}$$

This means that the lift coefficient for minimum drag of the box wing aircraft is higher than that of the reference aircraft, since the span efficiency factor of the box wing is also higher

than that of the reference aircraft, assuming that both have the same aspect ratio. This has the following consequences:

In the beginning it is assumed that the box wing and the reference aircraft should have the same cruise Mach number and wing area (see chapter 3). At first it is also guessed that their masses are equal. In other words, for flying with minimum drag both aircraft have to produce the same amount of lift at different lift coefficients. This can only be accomplished by varying the altitude. Fig. 5.2 clearly demonstrates this interrelationship. The shown graph was produced by assuming a lift coefficient for minimum drag of 0,71 for the reference aircraft (h/b = 0). The Mach number is 0,76 and the mass of the aircraft 73500 kg. The calculations which were performed in order to generate the graph shown in Fig. 5.2 can be found in Appendix B.1.

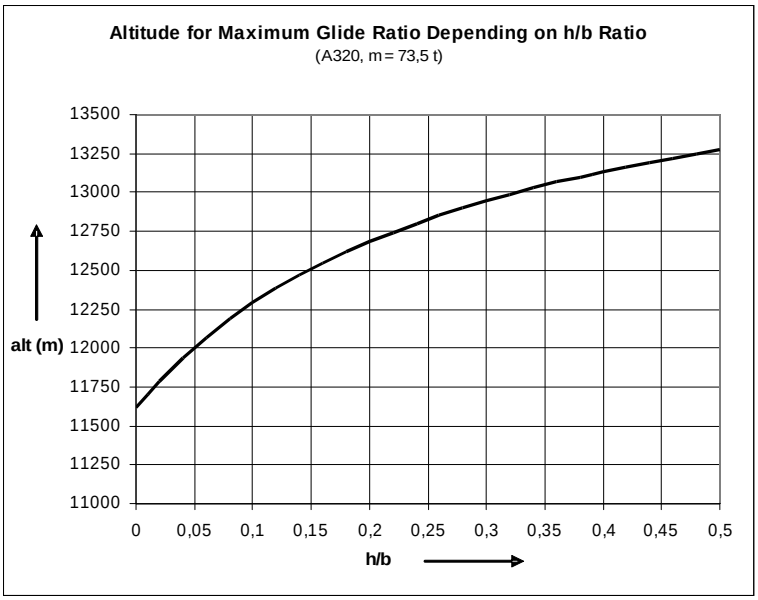

Figure 5.2 Altitude for maximum glide ratio depending on the h/b ratio under ISA conditions

The conclusion is that for flying at maximum glide ratio the box wing configuration needs to fly at higher altitudes compared to the reference aircraft. This results in a higher differential pressure for the cabin. For short range flights it might be unlikely that the altitude for the highest glide ratio is even attained. Higher altitudes also means that the flight mostly takes place in the stratosphere, which raises questions regarding ecological effects.

Another approach for attaining the maximum glide ratio could be the reduction of cruise speed, since lower speeds require higher lift coefficients. This way the possibility of a box wing prop arises.

5.1.3 Maximum Glide Ratio

The maximum glide ratio of an aircraft can be calculated with the help of the lift coefficient for minimum drag and the zero lift coefficient. In general the glide ratio is defined with

$$E = \frac{C_L}{C_D} \tag{5.7}$$

The lift coefficient for minimum drag is given by Eq. (5.3). Another condition for flight with maximum glide ratio is that the coefficient of induced drag is the same as the zero lift drag coefficient, so the total drag coefficient can be expressed as twice the zero lift drag coefficient. Consequently the maximum glide ratio is

$$E_{max} = \frac{\sqrt{C_{D,0} \cdot \pi \cdot A \cdot e}}{2 C_{D,0}} \quad . \tag{5.8}$$

Now the ratio of the maximum glide ratios of the box wing and the reference aircraft can be built. Assuming that both have the same zero lift drag coefficient and the same aspect ratio and that effects of transonic speeds are neglected, the ratio of maximum glide ratios can be written as

$$\frac{\left(E_{max}\right)_{box}}{\left(E_{max}\right)_{ref}} = \sqrt{\frac{e_{box}}{e_{ref}}} \quad . \tag{5.9}$$

The determination of e_{box}/e_{ref} depending on the h/b ratio was already discussed in section 4.3. Fig. 5.3 shows the possible increase of the maximum glide ratio of a box wing aircraft compared to the reference aircraft depending on the h/b ratio. As comparison the increase for a biplane is plotted as well. Note that the plot is only valid for the mentioned assumptions.

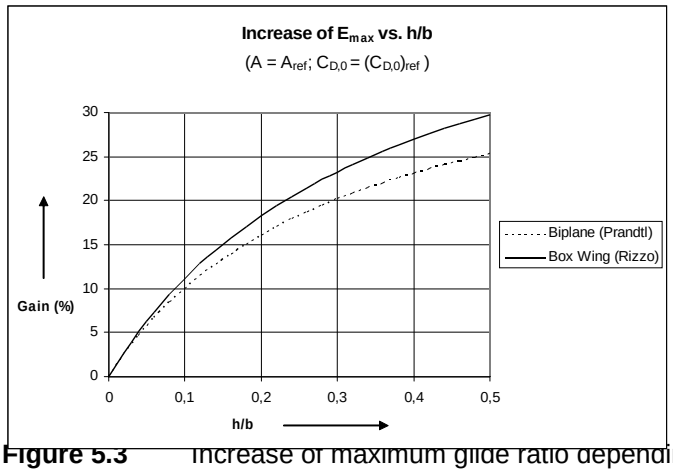

Figure 5.3 Increase of maximum glide ratio depending on the h/b ratio

5.1.4 Glide Ratio for Different Lift Coefficients

In this paragraph general investigations concerning the glide ratio are made. They help to understand the specific effects of a box wing configuration regarding aircraft performance during cruise. Based on the idealized drag polar the glide ratio can be calculated in general with

$$E = \frac{C_L}{C_{D,0} + \frac{C_L^{\,2}}{\pi A e}} \quad . \tag{5.10}$$

Making the same assumptions as in section 5.1.3 the span efficiency is the only parameter which affects the glide ratio, since all of the other parameters are the same for both the box wing and the reference aircraft.

With the help of Eq. (5.10) it is possible to show the trend of the glide ratio depending on the lift coefficient. This is important for assessing the aircraft performance for flight states requiring lift coefficients which deviate from the coefficient for minimum drag. The resulting graphs for different span efficiencies are shown in Fig. 5.4. The already mentioned trend for E_{max} moving to higher lift coefficients with increasing span efficiency is depicted as well.

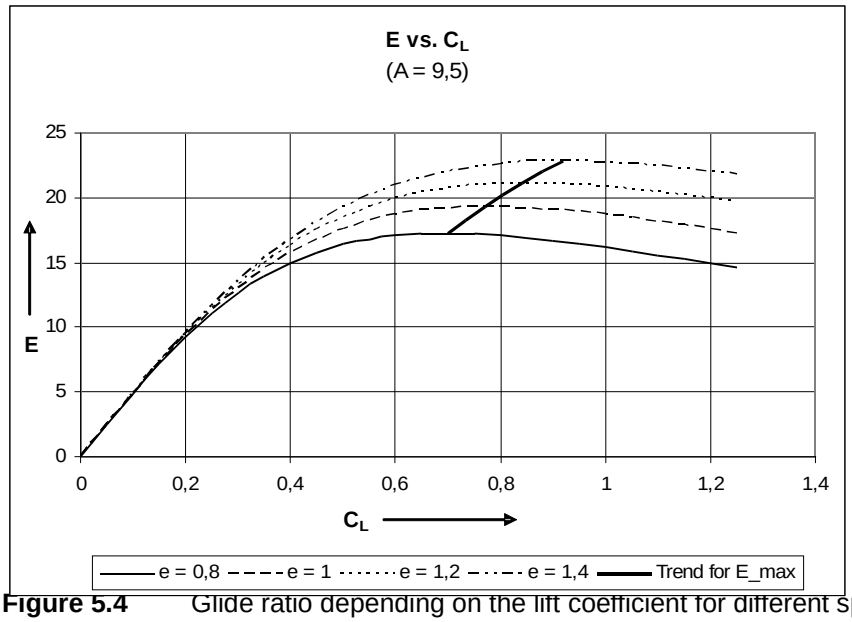

Figure 5.4 Glide ratio depending on the lift coefficient for different span efficiency factors

Fig. 5.4 illustrates that the region of lift coefficients close to the maximum glide ratio grows with higher span efficiencies. For example, if *e* is 1,4 the lift coefficients can range from 0,7 to 1,2 without significantly decreasing the glide ratio.

5.2 Static Longitudinal Stability and Controllability

Static longitudinal stability describes the behaviour of the aircraft when it is exposed to disturbances affecting the angle of attack. If, for example, the aircraft is hit by a vertical gust coming from below, the angle of attack is increased which leads to a higher lift coefficient and consequently to an increase of the pitch angle. The aircraft would be statically stable along the longitudinal axis if the angle of attack decreases again after the disturbance without any control input. Whether it decreases directly to the value from before or if there is an oscillation (convergent or divergent) around this value is not part of a static analysis.

Static longitudinal controllability comprises the controllability of the aircraft around the lateral axis (pitch attitude).

In **Raymer 1992** it is mentioned that:

> *"*(...) *to attain stability with a tandem-wing it is usually necessary to move the center of gravity somewhat forward of the location for an even weight split* (...)*."*

In top view (or along the longitudinal axis) a box wing aircraft can also be treated as a tandem wing. In other words Raymer states that for attaining stability the front wing of the aircraft has to generate more lift than the aft wing. However, for reaching minimum induced drag an equal division of lift between both wings is mandatory.

In this chapter it is examined whether it is possible to design a stable box wing having a 50/50 fragmentation of lift between both wings. The effects of unequal fragmentations are investigated as well. A possible elevator deflection is not taken account of (compare section 7.11 about control surfaces).

The method used is calculating the CG envelope which is limited by stability and controllability requirements, depending on geometric and aerodynamic parameters of the aircraft. The most forward CG position is determined by controllability requirements and the most aft position is determined by stability requirements.

A detailed derivation of the following relations can be found in Appendix B.2. In the present section only the results of important sub-steps are presented.

5.2.1 General Requirements

In general, **static longitudinal stability** comprises two conditions (**Young 2001**):

1) *Stability condition*
The slope of the pitching moment about the center of gravity is negative:

$$\frac{dC_{M,CG}}{dC_L} < 0 \quad . \tag{5.11}$$

2) *Trim condition*
The pitching moment about the center of gravity is positive at zero lift:

$$\left(C_{M,CG}\right)_{C_L=0} > 0 \quad . \tag{5.12}$$

The most aft position of the center of gravity before the aircraft becomes unstable can be calculated by formulating the equilibrium of moments about the aircraft's center of gravity and using the two conditions above. This CG position is referred to as neutral point. Here the aircraft is neutrally stable ($dC_{M,CG}/dC_L = 0$). If the center of gravity is shifted further rearwards, the aircraft would become unstable ($dC_{M,CG}/dC_L > 0$). For a stable aircraft ($dC_{M,CG}/dC_L < 0$) the CG position must be located in front of the neutral point. The plot of C_M vs. C_L for a stable aircraft is shown in Fig. 5.5.

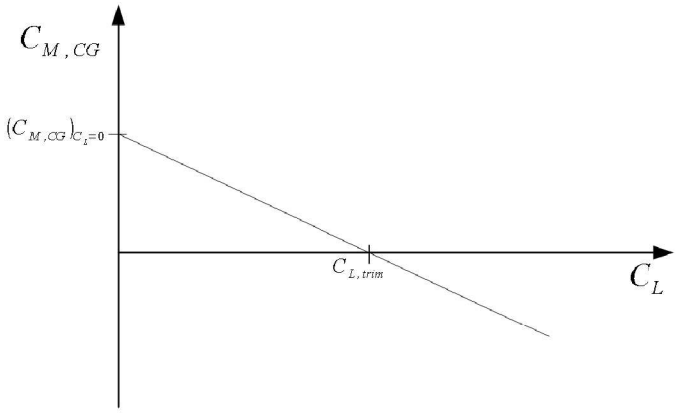

Figure 5.5 C_M over C_L for a stable aircraft

Static longitudinal controllability is achieved with the help of the elevators. For conventional tail aft configurations they are located at the horizontal tail. The elevators are also needed to trim the aircraft for horizontal flight ($C_{M,CG} = 0$). The required force to be generated by them in order to trim the aircraft depends on the CG position of the aircraft and the moment arm of the elevators. Additionally, the size of the elevator surfaces and their aerodynamic qualities limit the force they can generate.

When the CG position is shifted more forward for gaining static longitudinal stability, the elevators have to generate a higher force/moment in order to trim the aircraft. At a certain CG position the maximum force/moment which they can generate is reached. At this point the limit of control is attained since the whole impact of the elevators is needed for trimming the aircraft. This also means that the aircraft cannot produce a positive/nose up pitching moment any more.

Taking account of the previous argument, the condition of controllability for a stable aircraft can be expressed the following:

$$C_{M,CG} > 0 \quad . \tag{5.13}$$

With the Ineqs. (5.11) and (5.13) it is possible to express the envelope of the aircraft's center of gravity for attaining static longitudinal stability and controllability.

5.2.2 Derivation and Evaluation

The applied method is based on considerations for a conventional tail aft configuration which can be found in **Young 2001**. These considerations are now adapted to a box wing configuration.

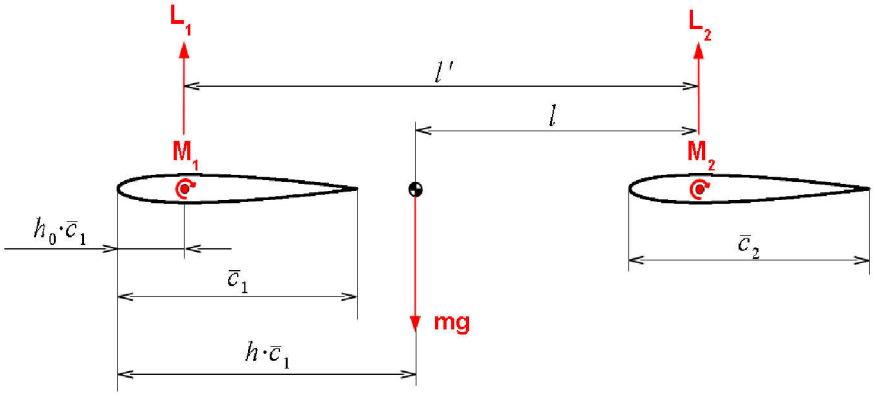

Figure 5.6 Forces and moments acting on a box wing aircraft

Fig. 5.6 depicts the forces and moments acting on a box wing. The CG position is shown in terms of the mean aerodynamic chord of the front wing $(h \cdot \bar{c}_1)$. Additionally the position of the aerodynamic center of the front wing is displayed in terms of its mean aerodynamic chord $(h_0 \cdot \bar{c}_1)$. The body of the aircraft is not shown, but its effects (interference with lifting surfaces) must not be neglected. Since horizontal forces like thrust or drag are not taken account of, the vertical distance between both surfaces is not of importance. The vertical connection of both surfaces at their tips is insigni- ficant for the analysis of static longitudinal stability and control.

According to Fig. 5.6 the equilibrium of moments about the center of gravity reads:

$$M_{CG} = L_1(h-h_0)\bar{c}_1 - L_2 l + M_1 + M_2 = 0 \quad . \tag{5.14}$$

By introducing the total lift *L*, rearranging Eq. (5.14) and dividing by $qS\bar{c}^{\,2}$ the coefficient form of the equilibrium can be formulated:

$$C_{M,CG} = C_L(h-h_0)\frac{\bar{c}_1}{\bar{c}} - C_{L_2}\bar{V}' + C_{M,1}\frac{\bar{c}_1 S_1}{\bar{c} S} + C_{M,2}\frac{\bar{c}_2 S_2}{\bar{c} S} = 0 \quad . \tag{5.15}$$

[2] The definition of the total mean aerodynamic chord was given in section 4.4.

As in section 4.1.2, the term S_1/S can also be expressed with s_1, S_2/S accordant. In the same manner the symbol $\bar{c}_1'$ is used instead of the term $\bar{c}_1/\bar{c}$ and $\bar{c}_2'$ instead of $\bar{c}_2/\bar{c}$. With these substitutions Eq. (5.15) can be written more simply:

$$C_{M,CG} = C_L\left(h-h_0\right)\bar{c}_1' - C_{L_2}\bar{V}' + C_{M,1}\bar{c}_1' s_1 + C_{M,2}\bar{c}_2' s_2 = 0 \quad . \tag{5.16}$$

Now the conditions from the Ineqs. (5.11), (5.12) and (5.13) are applied to Eq. (5.16) in order to determine the CG envelope which provides for static longitudinal stability and controllability. For static longitudinal stability the results are

$$h < h_0 + \frac{dC_{L,2}}{dC_L}\bar{V}' \cdot \frac{\bar{c}}{\bar{c}_1} \quad , \tag{5.17}$$

which means that the CG position needs to be in front of the neutral point expressed by the right hand side of the equation, and

$$C_{M,1}\bar{c}_1' s_1 + C_{M,2}\bar{c}_2' s_2 - \left(C_{L,2}\right)_{C_L=0}\bar{V}' > 0 \quad , \tag{5.18}$$

which is the condition to be met in order to have a trimmable aircraft. All terms except $C_{L,2}$ are assumed to be constant with regard to the lift coefficient. The value of $C_{L,2}$ for a total lift coefficient of zero can be determined with the help of the gradient $dC_{L,2}/dC_L$ which is also needed for solving Ineq. (5.17):

$$\left(C_{L,2}\right)_{C_L=0} = C_{L,2} - \frac{dC_{L,2}}{dC_L}\cdot C_L \tag{5.19}$$

The condition for static longitudinal controllability reads

$$h > h_0 + \frac{C_{L,2}}{C_L}\cdot\frac{\bar{V}'}{\bar{c}_1'} + \frac{C_{M,1}}{C_L}s_1 + \frac{C_{M,2}}{C_L}s_2\frac{\bar{c}_2}{\bar{c}_1} \quad , \tag{5.20}$$

meaning that the center of gravity needs to be aft of a defined position in order to provide for static longitudinal controllability.

In the Ineqs. (5.18) and (5.20) almost all parameters are given by known aerodynamic or geometric characteristics. However, the term $dC_{L,2}/dC_L$ in Ineq. (5.17) and Eq. (5.19) cannot be determined as easily and further considerations are needed. According to **Young 2001** it is possible to expand the term for making its calculation possible:

$$\frac{dC_{L,2}}{dC_L} = \frac{dC_{L,2}}{d\alpha_2} \cdot \frac{d\alpha_2}{d\alpha} \cdot \frac{d\alpha}{dC_L} \quad . \tag{5.21}$$

The first term on the right hand side of Eq. (5.21) is the lift curve slope of the aft wing, which shall be referred to as a_2. It can be determined with the following equation, taken from **DATCOM 1978** in **Scholz 1999**:

$$a_2 = \frac{dC_{L,2}}{dC_L} = \frac{2\pi \cdot A_2}{2 + \sqrt{A_2^{\,2}\left(1 + \tan^2 \varphi_{50,2} - M^2\right) + 4}} \tag{5.22}$$

The second term on the right hand side of Eq. (5.21) is the change of the angle of attack at the aft wing depending on the change of the angle of attack of the whole aircraft.[3] This derivative can be calculated with the help of the downwash induced by the front wing acting on the aft wing (**Young 2001**):

$$\frac{d\alpha_2}{d\alpha} = 1 - \frac{d\varepsilon}{d\alpha} \tag{5.23}$$

The term $d\varepsilon/d\alpha$ is the downwash gradient. According to **DATCOM 1978** in **Scholz 1999** it can be calculated with

$$\frac{d\varepsilon}{d\alpha} = 4{,}44 \cdot \left(k_{A,1} \cdot k_{\lambda,1} \cdot k_H \cdot \sqrt{\cos \varphi_{25,1}}\right)^{1,19} \cdot \frac{\left(C_{L,\alpha}\right)_{1,M}}{\left(C_{L,\alpha}\right)_{1,M=0}} \tag{5.24}$$

where

$$k_{A,1} = \frac{1}{A_1} - \frac{1}{1 + A_1^{\,1,7}} \quad , \tag{5.25}$$

$$k_{\lambda,1} = \frac{10 - 3\lambda_1}{7} \tag{5.26}$$

and

$$k_H = \frac{1 - \left|\frac{z}{b_1}\right|}{\sqrt[3]{\frac{2l'}{b_1}}} \tag{5.27}$$

with z as the vertical distance between the chord lines of the forward and aft wing. $(C_{L,\alpha})_{1,M}$ is

[3] For the total aircraft, the angle of attack is measured with regard to its zero lift line. The same method is applied for the aft wing.

the lift curve slope of the forward wing including compressibility effects, $(C_{L,\alpha})_{1,M=0}$ is the lift curve slope of the forward wing without any compressibility effects.

The last term on the right hand side of Eq. (5.21) is the inverse of the lift curve slope of the total aircraft. This lift curve slope shall be referred to as *a*. Its determination is based on the methods presented in Section 4.5.1.1 in **DATCOM 1978**. It takes account of interference effects between the body and the lifting surfaces, the downwash of the front wing as well as the effect of the wing tip vortices on the aft wing, which are induced by the front wing. Because of all of these circumstances, it is impossible to use Eq. (5.22) for the whole aircraft.

In the following the method for determining the lift curve slope of the whole aircraft is described briefly. A detailed description can be found in Appendix B.2.2. In section 4.1.3 a simple equation was presented for the determination of the lift curve slope of the whole aircraft [Eq. (4.10)], but it was already stated that there are some deviations between this simple equation and the more extensive approach presented in the present section.

Acc. to **DATCOM 1978** the equation for calculating the lift curve slope of an aircraft having two lifting surfaces of equal span is

$$\begin{aligned} a = \left(\frac{dC_L}{d\alpha}\right) = s_1\left(\frac{dC_L}{d\alpha}\right)_1 \cdot \left(K_N + K_{W(B)} + K_{B(W)}\right)_1 \cdot \frac{S_{e,1}}{S_1} \\ + s_2\left(\frac{dC_L}{d\alpha}\right)_2 \cdot \left(K_{W(B)} + K_{B(W)}\right)_2 \cdot \frac{q_2}{q_\infty} \cdot \frac{S_2}{S_1} \cdot \frac{S_{e,2}}{S_2} + \left(\frac{dC_L}{d\alpha}\right)_{W_2(v)} \end{aligned} \quad , \qquad (5.28)$$

where

$$\left(\frac{dC_L}{d\alpha}\right)_{W_2(v)} = \frac{\left(\frac{dC_L}{d\alpha}\right)_1 \cdot \frac{S_{e,1}}{S_1} \cdot \left(\frac{dC_L}{d\alpha}\right)_2 \cdot \frac{q_2}{q_\infty} \cdot K_{W(B),1} \cdot I_{V_{W,1(W,2)}} \cdot \left(\frac{b_2}{2} - \frac{d_2}{2}\right)}{2\pi \cdot A_2 \cdot \left(\frac{b_1}{2} - \frac{d_1}{2}\right)} \quad , \qquad (5.29)$$

which accounts for the effects of the vortices induced by the front wing.

In the Eqs. (5.28) and (5.29) some assumptions and modifications are already incorporated, as well as in the forthcoming equations. For not interrupting the train of thoughts in this section, they are further explicated in Appendix B.2.2.

The terms $(dC_L/d\alpha)_1$ and $(dC_L/d\alpha)_2$ are the lift curve slopes of the individual lifting surfaces, which can be calculated according to Eq. (5.22).

The *K*-factors include additional lift effects generated by the aircraft nose (*N*) as well as by the mutual interferences of wing and body [*W*(*B*) and *B*(*W*)]. Their calculation is as follows:[4]

$$K_N = \frac{\pi \cdot d^2}{2\left(\frac{dC_L}{d\alpha}\right)_1 \cdot S_{e,1}} \tag{5.30}$$

with *d* being the fuselage diameter and S_e the exposed wing area.

Furthermore the sum of $K_{W(B)}$ and $K_{B(W)}$ can be expressed by

$$K_{W(B)i} + K_{B(W)i} = \left(\frac{d}{b} + 1\right)^2 \tag{5.31}$$

and $K_{W(B)}$ by

$$K_{W(B)i} = 0{,}8\frac{d}{b} + 1 \quad . \tag{5.32}$$

The ratios of the exposed to the reference surfaces $(S_e/S)_i$ are roughly estimated according to the aircraft geometry, which is sufficient for the present investigation. The dynamic pressure ratio q_2/q_∞ of the aft wing is commonly assumed to be 0,9 for conventional tail aft configurations (**Scholz 1999**). This value may also be used for a box wing. A more exact calculation is not needed at this stage of analysis.

All parameters for Eq. (5.29) were already included in the previous discussion, except for $I_{V_{W,1(W,2)}}$, the so called vortex interference factor, which considers the effect of the trailing vortices of the front wing regarding the total lift of the aircraft (**DATCOM 1978**). It depends on the geometry of the wing system. For the current investigation its values are determined assuming that $b_1 = b_2 = b$; $d/b \sim 0{,}2$; $\lambda \sim 0{,}5$ and $\alpha = \alpha_{cruise}$. These parameters do not reflect the exact geometry of the aircraft being studied in this thesis. However, because of the lack of appropriate DATCOM charts, these values are used because a chart with these very values exists and they come closest to the geometry of the aircraft being investigated in this thesis. With these assumptions the vortex interference factor only depends on the *h*/*b* ratio. Table 5.1 shows the correlation between these two parameters. The exact derivation can be retraced in Appendix B.2.2.

[4] Eqs. (5.29) and (5.30) are from DATCOM 1978, Section 4.3.1.2, par. A, Method 1. Eq. (5.32) cannot directly be found in DATCOM 1978. Its derivation is shown in Appendix B.2.2.

Table 5.1 Vortex interference factor depending on the *h*/*b* ratio

h/*b*	$I_{V_{W,1(W,2)}}$
0	-2,6
0,05	-2,3
0,1	-2,0
0,15	-1,75
0,2	-1,5
0,25	-1,35

Now all terms on the right hand side of Eq. (5.21) are known. Finally, with the introduced symbols a and a_1 Eq. (5.21) can be written more simply:

$$\frac{dC_{L,2}}{dC_L} = \frac{a_2}{a}\left(1-\frac{d\,\varepsilon}{d\,\alpha}\right) \quad . \tag{5.33}$$

The calculation for the CG envelope was implemented into a spreadsheet for a quick analysis of different geometric and aerodynamic configurations (Appendix F.2.1). The results are presented in chapter 5.2.3.

At last it needs to be pointed out that the gradient $dC_{L,2}/dC_L$ is assumed to be independent of the angle of attack in this analysis. Strictly speaking this is not true since at higher angles of attack the vertical distance between the forward and the aft wing, measured perpendicularly to the free stream, becomes smaller. However, for the current examination the chosen approach is sufficient.

5.2.3 Results and Conclusion

Detailed results with screenshots from the calculation spreadsheet can be found in Appendix F.2.1.

When both wings have the same lift coefficient, it is impossible to attain longitudinal stability and controllability. At this condition the control limit for the center of gravity is situated aft of the stability limit, which means that for having a controllable aircraft, it needs to be statically unstable. However, an inherently unstable aircraft cannot be certified for commercial transport (CS 25.173, **EASA 2010**).

The main reason for this issue is the absence of a control surface which generates a positive pitching moment counteracting the negative pitching moment generated by the wings.[5] For a conventional tail aft configuration the positive moment is provided by the horizontal stabilizer. However, as it will be shown in section 7.11 the inner control surfaces of both wings of the box wing aircraft might be used as elevators which could provide an additional positive pitching moment. But in this context the resulting effects on the lift distribution of both wings have to be studied carefully.

For a box wing configuration the main contributors to the zero lift pitching moment are the wings, the fuselage and probably the engines if they are positioned significantly above or below the aircraft's center of gravity. So by modifying the wings or the fuselage it could be possible to provide for a positive zero lift pitching moment.

There are several ways of reducing the value of negative pitching moment of wing sections. Some of them are presented in **Barger 1975**. It is even possible for sections to have a positive pitching moment which is mostly achieved by modifying the camber in the region of the trailing edge (see Fig. 5.7). However, the qualities of such reflexed wing sections in the transonic flight regime is a topic of its own and part of more detailed aerodynamic studies.

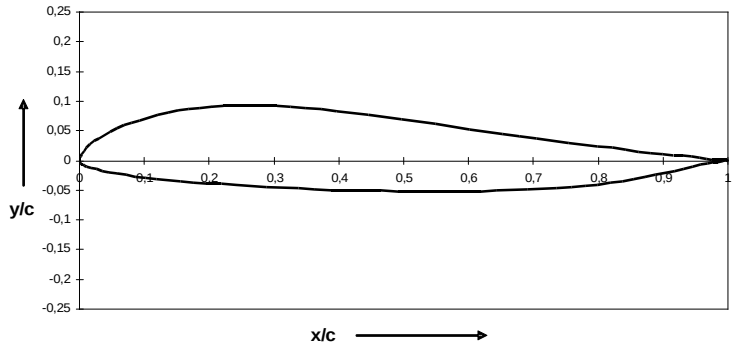

Figure 5.7 Eppler 340 airfoil as an example for a reflexed wing section

[5] The same problem occurs with a flying wing or a blended wing body, where there also is no horizontal stabilizer which produces an additional positive pitching moment.

Another possibility referring to wing modifications is adjusting the wing twist in connection with a swept wing. This way parts of the wing should produce more lift the more they are forward of the aircraft's center of gravity. This method is often applied in conjunction with flying wings or blended wing bodies, where the tips of the swept wing are twisted in a way so that they produce little lift (or even negative lift) and thus a positive pitching moment.

The fuselage may also have a shape similar to a reflexed airfoil (see Fig. 5.8) so that it generates an additional positive pitching moment. But the drag of such a shape may be huge at high subsonic Mach numbers.

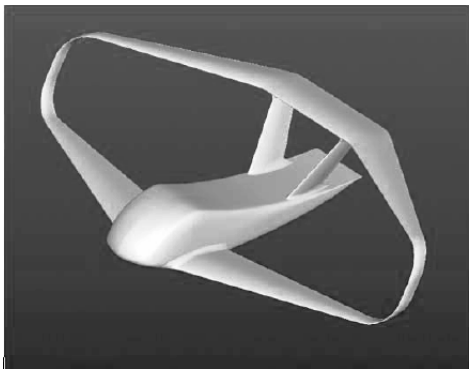

Figure 5.8 Box wing aircraft with a reflexed fuselage (**Frediani 2007**)

Since the aerodynamic performance of the mentioned modifications is questionable and the accordant investigations are part of further studies, these modifications will no longer be part of the current discussion. In the following, possibilities are described how to avoid the necessity of a positive zero lift pitching moment of the wings or the fuselage. This approach is used for the design of the studied box wing configuration.

When examining the Ineqs. (5.17) and (5.20) which localize the CG position for attaining static stability and controllability, it becomes evident that the only variable parameters are the individual lift coefficients and the gradient $dC_{L,2}/dC_L$. All of the other parameters are either aerodynamic constants or given by aircraft geometry. In order to expand the CG envelope it is required to either move the stability limit more aft (meaning that the value of the right hand side of Ineq. (5.17) increases) or to move the control limit more forward (meaning that the value of the right hand side of Ineq. (5.20) decreases). A combination of both would be the optimum solution.

Concluding from the explanation in the last passage, a **forward shift of the control limit** can be achieved by decreasing the ratio $C_{L,2}/C_L$ and also by increasing the total lift coefficient [compare Ineq. (5.20)].

The total lift coefficient depends on the aircraft weight, flight speed and altitude. Preferably it

should be in the region of the lift coefficient for minimum drag (see section 5.1.2). For this reason the total lift coefficient cannot be chosen arbitrarily just for shifting the control limit.

The ratio $C_{L,2}/C_L$ can be manipulated by changing the lift coefficient of the aft wing. So for shifting the control limit more forward, the value of $C_{L,2}$ needs to be decreased while keeping the total lift coefficient constant. The result is an increase of the ratio $C_{L,1}/C_{L,2}$. However, this also means that the induced drag increases when both wings have the same reference area, as it was shown in section 4.6.1.

Acc. to Ineq. (5.17) an **aft shift of the stability limit** is possible by increasing the gradient $dC_{L,2}/dC_L$. In chapter 5.2.2 it was shown that this gradient mostly depends on the geometry of the aircraft. The affecting parameters are the wing sweep which has a great influence on the lift curve slope of the wings, as well as the height to span ratio, the ratio of the exposed wing area to the wing reference area and the average ratio of fuselage diameter to wing span at the wing root. The sweep and the height to span ratio are the only parameters that can be arbitrarily chosen, disregarding aerodynamic and aeroelastic considerations. The other parameters result from fuselage layout and wing integration.

With the help of the spreadsheet it was determined that an increase of the ratio of $C_{L,1}/C_{L,2}$ is the most effective way of expanding the CG envelope. It is important to pay attention to the consequences, e.g. airfoil choice and stall characteristics. Depending on the aircraft geometry, a value of 1,5 to 3 for the $C_{L,1}/C_{L,2}$ ratio is probable.

A general increase of the CG envelope can also be achieved by placing the wings further apart longitudinally. This way the the parameter $\bar{V}$ is increased which makes it also possible to decrease the ratio $C_{L,1}/C_{L,2}$ for a given CG envelope.

An adjustment of the wing sweep can be treated as a supporting measure. Here requirements relating to transonic aerodynamics and to stall characteristics have to be considered. For increasing the CG envelope the sweep of the forward wing has to be as high as possible, while the sweep of the aft wing has to be as low as possible.

It needs to be pointed out once more that the above methods result from the assumption that the zero lift pitching moment of the wings and the fuselage remain negative, which compares to conventional tail aft configurations. A deflection of elevators was not taken account of.

The choice of the final wing configuration considering the requirements coming from aerodynamic considerations as well as the analysis of stability and controllability will be discussed in chapter 7.

5.3 Static Lateral Stability and Controllability

Capturing the characteristics of static lateral stability in detail is an extensive job. Since in the present thesis the focus is rather set on static longitudinal stability only trends based on general correlations and statements are described in the present section.

Generally lateral stability includes the rolling and the yawing motions of the aircraft. Comparable to longitudinal stability (section 5.2) an aircraft is laterally stable if it tends to the initial attitude after a disturbance (e.g. gusts) without pilot input. For example, if a gust leads to an unsymmetric loading between the left and the right wing the aircraft will roll towards the side of the lower loading. Provided that the rolling angle does not become too high, the aircraft should level out without any pilot input.

According to **Scholz 1999** wing design is important for lateral stability. Increasing dihedral and wing sweep will also increase lateral stability, whereas anhedral and a forward swept wing are reductive. Another point is the wing interaction with the fuselage. Shoulder wing aircraft have an increased lateral stability while low wing aircraft have reduced stability. With the help of these three design parameters the wing design of the box wing aircraft can be adjusted for lateral stability.

In **Scholz 1999** some simple correlations are given. Accordingly 10° of wing sweep have the same effect regarding lateral stability as 1° of dihedral. Additionally “switching” from a middle wing to a shoulder wing or from a low wing to a middle wing will increase lateral stability as much as 3,5° more dihedral. Furthermore **Raymer 1992** states that a low wing aircraft requires about 5° of dihedral to become neutrally stable.

Usually wing sweep is dominated by transonic aerodynamics. So this parameter is already given. For the box wing configuration it is also defined that the forward wing is a low wing. According to the final configuration (see chapter 9) the aft wing is connected to the vertical stabilizer, thus there are no significant interference effects between the fuselage and the aft wing. Consequently the only parameter to be adjusted for lateral stability is the dihedral.

For finding the proper dihedral of the individual wings a simple method is used. The degree of lateral stability of the reference aircraft is assessed in terms of a necessary dihedral angle. The results are given in table 5.2. Accordingly the reference aircraft has an excess of 3,5° of dihedral, which means that with a dihedral which is 3,5° lower the aircraft would be neutrally stable. Supplementary it has to be mentioned that here the final dihedral angle rather results from requirements according to sufficient engine clearance to the ground.

Table 5.2 Degree of lateral stability of the reference aircraft in terms of dihedral angle

Wing parameter	Value	Equivalent to dihedral of
Vertical position	low	-5°
Sweep	25°	2,5°
Dihedral	6°	6°
	Σ	**3,5°**

It is assumed that the degree of lateral stability of the box wing configuration is supposed to be in the same region, or probably a bit lower. For its determination the same method as in table 5.2 is applied, now for the forward and the aft wing separately (see table 5.3).

Table 5.3 Degree of lateral stability of the box wing aircraft in terms of dihedral angle

Wing	Wing parameter	Value	Equivalent to dihedral of
forward	Vertical position	low	-5°
	Sweep	ca. 30°	3°
aft	Vertical position	no effect	0°
	Sweep	ca. -30°	-3
		Σ	**-5°**

From table 5.3 it can be concluded at first that the opposite swept wings neutralize their individual effect on lateral stability. Furthermore the aft wing is situated above the fuselage and hence does not affect the degree of lateral stability as well. The only factor which requires dihedral in terms of lateral stability is the low position of the forward wing.

An important constraint for the choice of proper dihedral is that the aft wing is not integrated into the fuselage. This might cause structural problems. Therefore it is chosen that the aft wing is supposed to have no dihedral at all, since a kink because of dihedral might additionally weaken the wing structure. Consequently the forward wing has to have a dihedral of at least 5°. To prevent any risk caused by the simple approach used here, the final dihedral is increased to 6°. A drawing of the resulting wing configuration is shown in section 7.5.3. Note that the dihedral decreases the h/b ratio at the tips, which decreases the span efficiency (compare section 4.3).

The contribution of the vertical winglets has been neglected in the present analysis. It is supposed to be part of more dedicated studies concerning lateral stability of box wing aircraft. However, the winglets will be loaded because of the chosen dihedral. Since only the forward wing has dihedral it will be the only wing who tends to level out the aircraft. This means that during a rolling maneuver the lower side of the front wing moves up while the relating side of the aft wing tends to stay in the current position. This causes additional compression stresses within the winglet.

6 Preliminary Sizing

The preliminary sizing of the box wing aircraft is performed with the preliminary sizing spreadsheet (**Scholz 2008**). In order to size the aircraft a number of parameters have to be determined in advance, next to the ones already given by the design requirements (see chapter 3). These parameters and their respective values are listed in table 6.1. Next to each parameter a short comment is inserted in order to understand where its value is coming from.

Table 6.1 Parameters used for preliminary sizing

parameter	Value	Comment
k_{App}	1,7 $(m/s^2)^{1/2}$	standard value
k_L	0,107 kg/m³	derives from k_{App}
$C_{L,max}$ (take off)	2,92	adjusted for getting S_W = 122 m²
$C_{L,max}$ (landing)	2,1	a little higher than for A320
$C_{D,0}$	0,021	see section 11.1
$C_{D,P}$ (landing)	0,066	derives from standard settings
$C_{D,P}$ (take off)	0,046	derives from standard settings
$C_{f,eqv}$	0,003	standard value
S_{wet}/S	7,0	see explanation below and section 11.1.6
e (landing)	0,964	determination is described in section 6.1
e (clean)	1,17	determination is described in section 6.1
m_L/m_{TO}	0,889	see explanation below
m_{OE}/m_{TO}	0,565	iterated with mass estimation (see chapter 10)
$M_{ff,engine}$	0,999	same as for A320 (Pester 2010b)
$M_{ff,taxi}$	0,996	same as for A320 (Pester 2010b)
$M_{ff,TO}$	0,995	same as for A320 (Pester 2010b)
$M_{ff,CLB}$	0,995	same as for A320 (Pester 2010b)
$M_{ff,DES}$	0,992	same as for A320 (Pester 2010b)
$M_{ff,L}$	0,992	same as for A320 (Pester 2010b)

For the reference aircraft the ratio m_L/m_{TO} is 0,878. Because the glide ratio of the box wing configuration is assumed to be higher than that of the reference aircraft it will consume less fuel. On the other hand this results in a slightly lower maximum take of mass. Now it can be assumed that because of the same design mission and a similar structural layout the maximum landing mass of both aircraft is the same. Hence the ratio m_L/m_{TO} can be adjusted accordingly. The minimum allowed value is 0,889.

Concerning the relative wetted area S_{wet}/S standard values are between 6 and 6,2. For the box wing a ratio of 7,0 is determined (see section 11.1.6) because of the huge winglets and stabilizers as well as the fact that the root of the rear wing does not disappear inside the fuselage but is exposed to the free steam.

The matching chart resulting from the preliminary sizing is depicted in Fig. 6.1.

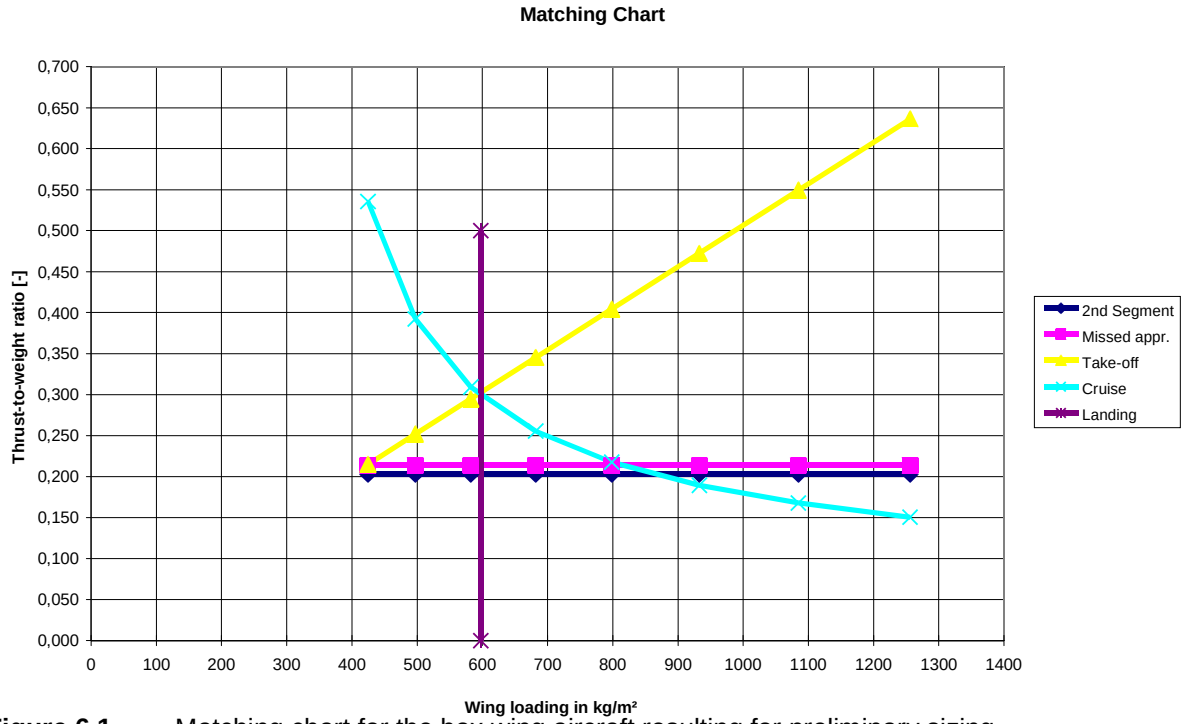

Figure 6.1 Matching chart for the box wing aircraft resulting for preliminary sizing

Further results are given in table 6.2 and compared with the data of the reference aircraft. The whole preliminary sizing spreadsheet is shown in Appendix F.1.

Table 6.2 Further results from the preliminary sizing

parameter	Box Wing	Reference	Difference	
			absolute	percentage
m_{MTO}/S_W (kg/m²)	597	601	-4	-0,67
$T_{TO}/(m_{MTO}*g)$	0,303	0,309	-0,004	-1,94
h_{cruise} (m)	12893	12326	567	4,6
$C_{L,m}$	0,86	0,71	0,15	21,13
m_{MTO} (kg)	73245	73500	-255	-0,35
m_{ML} (kg)	65115	64500	615	0,95
m_{OE} (kg)	41383	40500	883	2,18
m_{MZF} (kg)	61383	60500	883	1,46
$m_{F,req}$ (kg)	12168	13400	-1232	-9,19
S_W (m²)	122,6	122,4	0,2	0,16
T_{TO} (kN)	217,4	222,0	-4,6	-2,07

The most important result is a reduction of the required fuel mass by 9 % because of the high-

er glide ratio of the aircraft. This leads to a slightly reduced maximum take off mass (-0,4 %), which on the other hand decreases the required thrust for take off by 1,9%. It is apparent that all of the other masses match quite well to those of the reference aircraft. After some iterations the resulting operating empty mass is very close to the one coming from a more precise mass estimation, which is presented in section 10.2. As predicted in section 5.1.2 the lift coefficient for minimum drag increases because of the higher span efficiency factor. This results in a higher cruise altitude.

6.1 Determination of the Final Span Efficiency Factor

In section 4.3 the determination of the span efficiency factor depending on the h/b ratio was shown. The method proposed to be used gives the ratio e_{box}/e_{ref} as function of the h/b ratio. Once the span efficiency factor of the reference aircraft is known, the box wing counterpart can be determined. It was already assumed that $e_{ref,clean}$ = 0,85 and $e_{ref,land}$ = 0,7. The h/b ratio derives from the geometry of the box wing aircraft. At this point the final geometry needs to be anticipated from section 7.5.3. There the vertical distance between both wing tips is 7,5 m, resulting in a h/b ratio of 0,22.

However, the requirements according to static longitudinal stability have to be considered as well (compare section 5.2.3). As consequence the lift coefficient of the forward wing is higher than that of the aft wing, which reduces the span efficiency. The amount of reduction is determined with the help of Eq. (4.31), since $C_{D,i}/(C_{D,i})_{min} = e_{max}/e$, where e_{max} is the span efficiency for equal lift of both wings.

With the help of a separate sizing spreadsheet (Appendix F.2) which includes the requirements according to static longitudinal stability, the resulting loss of aerodynamic efficiency as well as the more detailed mass estimation, it was found that the span efficiency decreases by 3,4 % because of stability requirements. The spreadsheet including the data of the final box wing configuration can also be found on the CD attached to this thesis.

Results
The ratio e_{box}/e_{ref} is 1,426 for a h/b ratio of 0,22 [compare Fig. 4.8, Rizzo graph, evolving from Eq. (4.20)]. This ratio is reduced by 3,4 %, which results in 1,377. This is the factor the span efficiencies for the clean and landing configuration of the reference aircraft have to be multiplied with. Finally we get

$e_{box,clean}$ = 1,17 and
$e_{box,land}$ = 0,964.

7 Wing Design

As already stated the wing configuration is the characteristic feature that distinguishes the box wing from the reference aircraft. Since the reference wing is literally split into two separate wings the design space is enlarged and the relating set of parameters is extended. This allows for more flexibility in design but also makes it more challenging. For limiting the design space it is decided that both wings are supposed to have the same reference area. This might not lead to an optimum configuration but helps to adjust the other wing parameters for a first design.

In this paragraph the most important aspects of wing design are discussed. This includes the design for transonic speeds and an optimum lift distribution, the choice of airfoils and characteristics concerning fuel volume and structural weight.

7.1 Design for Transonic Speeds

The parameters which influence the transonic characteristics of the wing are mainly sweep and the thickness to chord ratio. Wing twist is also used to decrease the lift coefficient at certain span stations for lowering the probability of shock waves. However, wing twist is excluded from the present discussion.

7.1.1 Wing Sweep

At first it is important to be aware that the wing sweep does not only affect the transonic characteristics but also the qualities with regard to static longitudinal stability and controllability. As concluded in section 5.2.3 it is desired that the amount of sweep of the forward wing is higher than that of the aft wing in order to increase the CG envelope for stability and controllability. Ideally the aft wing should not be swept at all, which of course contradicts transonic requirements. For simplifying the design process it was decided that both wings have the same amount of sweep. With this constraint the other parameters like cruise lift coefficients of the individual wings and the longitudinal distance between the wings were adjusted so that the CG envelope suits the CG position resulting from weight and balance (section 10.2).

The wing sweep of the reference aircraft is 25° (¼ chord length). Since both the reference and the box wing configuration have a cruise Mach number of 0,76, this wing sweep was the initial value for the box wing configuration.

Another aspect influencing the amount of sweep is the integration of the wing configuration with regard to the fuselage and the sweep of the winglets as well. Taking account of the mutual impact of all of these parameters the final wing sweep is chosen to be about 28,5° for the forward and -28° for the aft wing. Further information discussing and justifying this choice is given in section 7.5 .

7.1.2 Thickness to Chord Ratio

According to **Torenbeek 1982** the thickness to chord ratio results from the wing sweep, the design lift coefficient and the drag divergence Mach number. The accordant equation is

$$\frac{t}{c} = 0{,}3 \cdot \cos\varphi_{25} \cdot \left(\left[1 - \left(\frac{5 + M_{DD,eff}^{\ 2}}{5 + (k_M - 0{,}25\, C_L)^2} \right)^{3{,}5} \right] \cdot \frac{\sqrt{1 - M_{DD,eff}^{\ 2}}}{M_{DD,eff}^{\ 2}} \right)^{2/3} \quad . \tag{7.1}$$

This ratio is the maximum allowed thickness to chord ratio of the airfoil resulting from cutting the wing parallelly to the aircraft's symmetry axis. For getting the thickness to chord ratio of the actual airfoil the following transformation has to be performed according to **Dubs 1987** in **Scholz 1999** (compare Fig. 7.1):

$$\left(\frac{t}{c} \right)_{eff} = \frac{t}{c} \cdot \frac{1}{\cos\varphi_{25}} \tag{7.2}$$

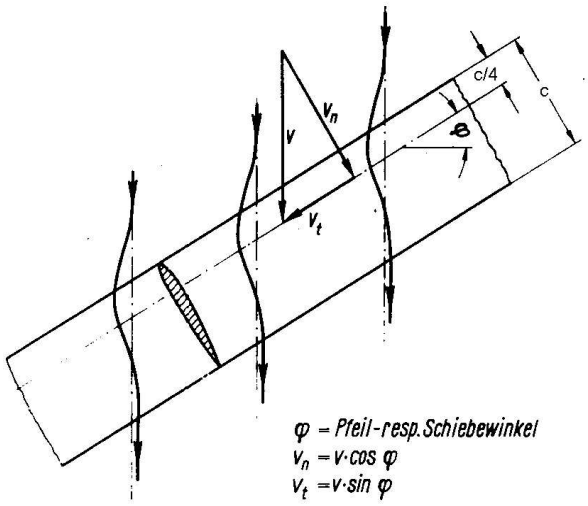

Figure 7.1 Decomposition of the free stream vector into a normal and a tangential component (**Dubs 1987** in **Scholz 1999**)

The effective drag divergence Mach number results from the actual Mach number and the wing sweep. **Torenbeek 1982** proposes

$$M_{DD,eff} = M_{DD} \cdot \sqrt{\cos \varphi_{25}} \quad . \tag{7.3}$$

According to **Scholz 1999** there are several ways of defining the drag divergence Mach number. Depending on the approach it ranges from the cruise Mach number to M_{Cr} + 0,1. As compromise the drag divergence Mach number used here is supposed to be M_{Cr} + 0,05, giving 0,81. The design lift coefficient is supposed to be the lift coefficient for minimum drag. According to the preliminary sizing (chapter 6) it is 0,84. The factor k_M in Eq. (7.1) takes account of the airfoil type. For modern supercritical airfoils it is assumed to be 1,2.

Considering a wing sweep of 28° (compare section 7.1.1) the final value for the maximum thickness to chord ratio according to Eq. (7.1) is 0,103. Transforming this value to the thickness to chord ratio of the actual airfoil finally gives 0,116 as maximum. According to **Böttger 2010** this value applies for the relative wing span ranging from 0,4 to 1. For the region closer to the wing root the thickness to chord ratio is usually higher.

7.2 Taper Ratio

Taper ratio is commonly used to change the spanwise lift distribution so that it comes close to the optimum. For minimum induced drag the optimum taper ratio can be determined depending on the wing sweep (**Torenbeek 1982**):

$$\lambda_{opt} = 0{,}45 \cdot e^{-0{,}036\varphi_{25}} \quad , \tag{7.4}$$

which applies to conventional wings. Although the composition of the lift distribution of the box wing aircraft is different (additional constant part) Eq. (7.4) is used to determine the optimum taper. Note that the sweep angle has to be inserted in degrees. The results are given in table 7.1.

Table 7.1 Optimum taper for both wings

	sweep	**taper**
fwd wing	28°	0,16
aft wing	-28,5°	1,26

It becomes clear that the optimum taper ratios are quite utopic. For the forward wing 0,16 is too low. Because of the low chord lengths this taper would not allow for enough room for the integration of flap and aileron mechanisms. For the aft wing a taper ratio of 1,26 means that the wing's center of gravity would be shifted in the direction of the wing tips, creating a huge root bending moment and increasing wing mass. Consequently the chosen taper ratios are different. The taper ratio of the reference wing is 0,24, so this value is used for the forward wing as well. The integration of flap and aileron mechanisms taking account of the small chord lengths is yet to be investigated. For the aft wing a taper ratio of 0,8 is chosen, which should be a good compromise between the requirement according to Eq. (7.4) and an acceptable wing mass.

7.3 Decalage

According to the box wing sizing spreadsheet (Appendix F.2) the lift coefficient of the aft wing is -0,136 for zero total lift. Since both wings have the same reference area (as defined in the beginning of chapter 7) this means that the forward wing has a lift coefficient of 0,136 for zero total lift. So the difference in lift coefficients of both wings is 0,272 for zero lift. The plot of the individual lift coefficients depending on the total lift coefficient is shown in Fig. 7.2. It results from sizing the box wing configuration according to requirements of static longitudinal stability and controllability based on cruise conditions.

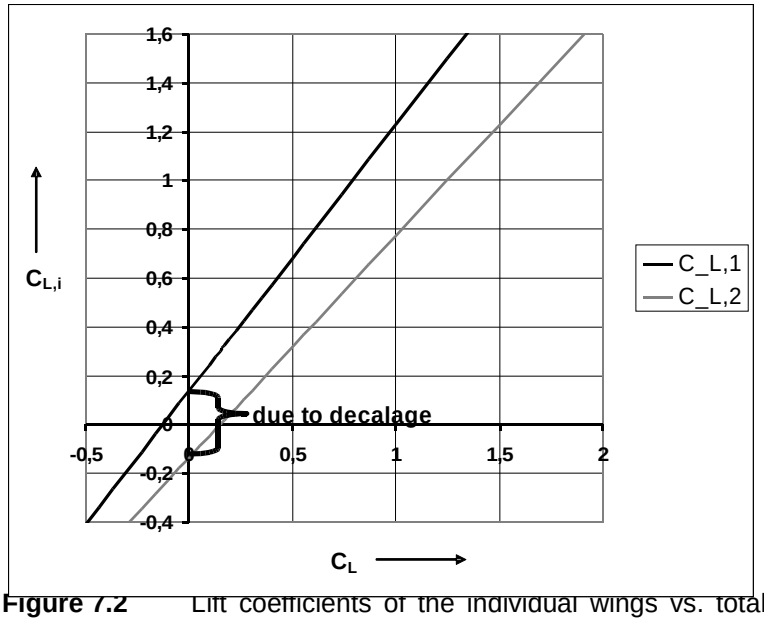

Figure 7.2 Lift coefficients of the individual wings vs. total lift coefficient for the final box wing configuration

With the help of the lift curve slope of the individual wings, which is determined according to Eq. (4.8), the decalage (the difference of incidence angles) can be calculated, provided that the small amount of downwash is negligible. The lift curve slope for both individual wings is approximately 5,05 rad^{-1}. Dividing the difference of lift coefficients by this number gives a decalage of 0,054 rad or 3,1°.

Note that this decalage is based on stability and controllability requirements concerning cruise conditions. For other flight states the individual lift coefficients are different which might lead to other lift coefficients for zero lift, resulting in a different decalage. The effects of deflecting flaps and control surfaces have to be investigated as well. In the current phase of the design study the stability of the aircraft for flight states other than cruise is not known. Therefore no final statement concerning individual incidence angles and the resulting decalage can be made.

7.4 Torenbeek Mass Estimation

The dimensions of a single wing are only about half of those of the reference wing, except for the span. This makes it necessary to investigate the mass of the wing more thoroughly. As a first approximation a simple formula given in **Torenbeek 1982** can be used:

$$\frac{m_W}{m_{MZF}} = 6{,}67 \cdot 10^{-3} \cdot b_s^{\,0{,}75} \cdot \left(1 + \sqrt{\frac{b_{ref}}{b_s}}\right) \cdot n_{ult}^{\,0{,}55} \cdot \left(\frac{b_s / t_r}{m_{MZF} / S_W}\right)^{0{,}3} \tag{7.5}$$

where

$$b_S = \frac{b}{\cos \varphi_{50}} \tag{7.6}$$

being the structural wing span and

$$b_{ref} = 1{,}905 \text{ m} \tag{7.7}$$

as reference span. Eq. (7.5) was derived for configurations with a conventional wing. To use it for a box wing it is assumed that both of its wings can be combined to one conventional wing. This way the result is a wing of equal area , wing loading m_{MZF}/S_W and span as the reference wing. Only the airfoil thickness at the wing root is half the value of that of the reference wing. Supposing that both the reference wing and the box wing possess the same structural span because of identical wing spans and wing sweeps leads to the elimination of the factor

$$\sqrt{\frac{b_{ref}}{b_s}} \quad .$$

Of course the ultimate load factor is the same for both aircraft as well. Eliminating all equal parameters leads to the relation

$$\frac{\left(\frac{m_W}{m_{MZF}}\right)_{box}}{\left(\frac{m_W}{m_{MZF}}\right)_{ref}} = \left(\frac{t_{r,ref}}{t_{r,box}}\right)^{0{,}3} = 1{,}23 \quad .$$

Of course this relation is based on very simple considerations and additionally neglects any possible brace support of the winglets, but it shows that the wing structure of the box wing is heavier than that of the reference aircraft. The main reason is the wing geometry, where one single wing has an aspect ratio of about 19. The total airfoil thickness, and thus the height of the wing box, is only half as much as that of the reference wing.

It can be seen that for lowering the weight of the wings the thickness to chord ratio of the airfoils should be as high as possible. However, this is in conflict with requirements according to transonic flight.

For getting a deeper insight into the structural aspect of the wings, an analysis of wing internal loads is conducted in section 7.6. For doing so, the exact wing geometry is needed, which is discussed in the next section.

7.5 Design Integration and Resulting Wing Geometry

In order to conduct further investigation concerning the wings their exact geometry is needed. This is why the wing integration and the resulting wing geometry is already discussed at this point. Although the fuselage layout was not defined yet, its geometry is anticipated from section 8.1 in order to have the constraints for wing integration.

In this section the longitudinal and vertical dimensions of the wing configuration are defined. They derive from the given wing sweep (section 7.1.1), taper (section 7.2) and dihedral (section 5.3). In order to have a high reduction of induced drag the *h*/*b* ratio shall be as high as possible. This is why it is chosen to attach the aft wing on top of the vertical stabilizer. At this point it is necessary to anticipate the stabilizer geometry as well. It is a V-tail whose design is derived later in section 8.2.

After discussing the most important aspects of finding the longitudinal and vertical wing positions, the final wing geometry is presented in section 7.5.3.

7.5.1 Longitudinal Positions

For high static longitudinal stability it is desired that the longitudinal distance between both wings is as high as possible. However, this distance is limited by certain factors which can be easily described with the help of Fig. 7.3.

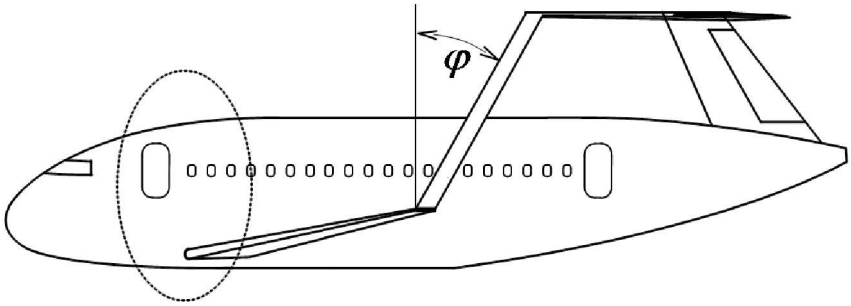

Figure 7.3 Limiting factors for the longitudinal distance between both wings

The forward wing can only be moved as much to the front as long as there is enough clearance to the forward exit. The position of the aft wing has to comply with the position and geometry of the stabilizers. Since the sweep of the horizontal wings is already defined, the winglet sweep automatically results from the longitudinal positions of the horizontal wing. In order to have an acceptable winglet sweep the longitudinal distance between both horizontal wings cannot become too high.

Finally the wings have to be positioned so that the CG envelope resulting from longitudinal

stability requirements (section 5.2) coincides with the actual CG positions coming from weight and balance (section 10.2).

The whole process of finding the proper longitudinal wing position is iterative. It has to be repeated after every change of the aircraft geometry, its weight and balance or the lift division between both horizontal wings.

7.5.2 Vertical Positions

Since it is desired to have a high *h*/*b* ratio the forward wing shall be positioned as low as possible. This means that a conventional integration of the engines under this wing is not possible because there is not enough room. The height of the aft wing is defined by the height of the stabilizers.

Because of the low position of the forward wing it is possible to have a continuous cargo compartment. However, the accommodation of additional fuel tanks in the fuselage (see sections 10.2 and 11.4.4) might split the cargo compartment.

7.5.3 Resulting Geometry

Table 7.2 summarizes the final wing geometry. Further dimensions are given in Figs. 7.4, 7.5 and 7.6.

Table 7.2 Geometry parameters of the final wing configuration

Parameter	Forward Wing	Aft Wing
Reference area (m²)	61	61
Span (m)	34,1	34,1
MAC (m)	2,02	1,81
Root chord (m)	2,9	2
Tip chord (m)	0,7	1,6
Taper ratio	0,24	0,8
Sweep (1/4 chord)	28,5°	-28°
Dihedral	6°	0°
h_{tip}/b	0,22	

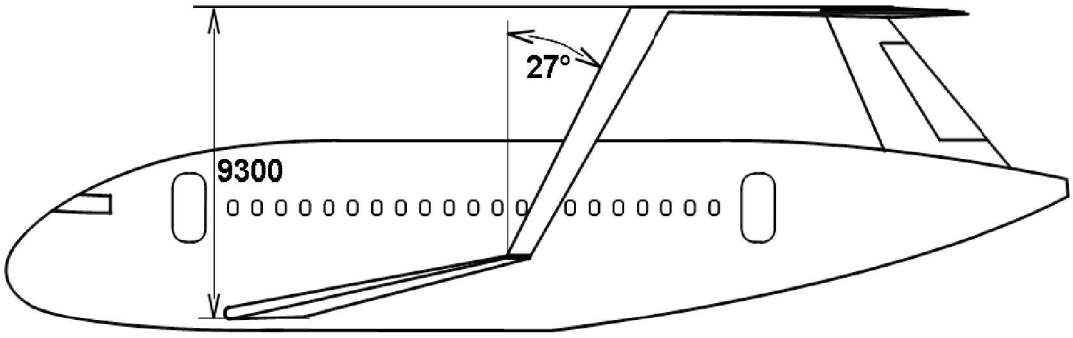

Figure 7.4 Wing dimensions, side view

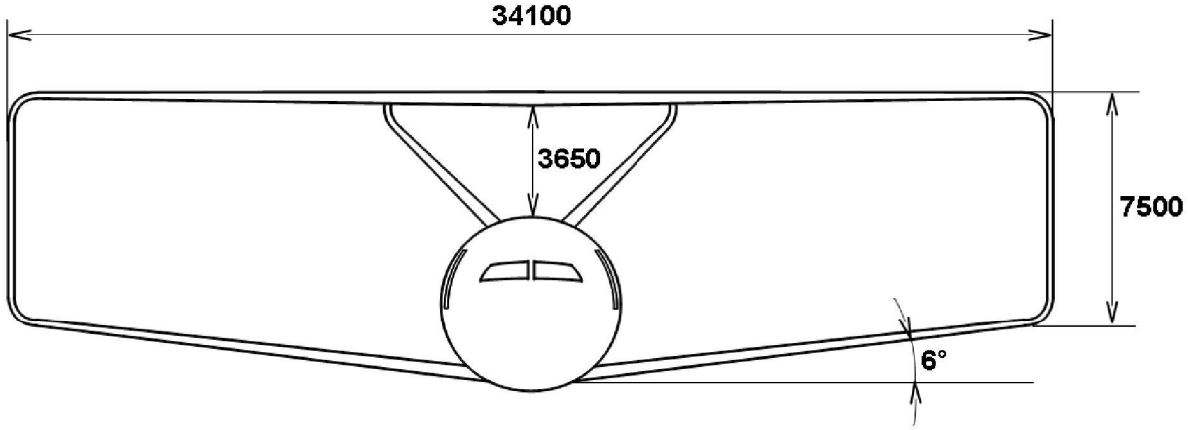

Figure 7.5 Wing dimensions, front view

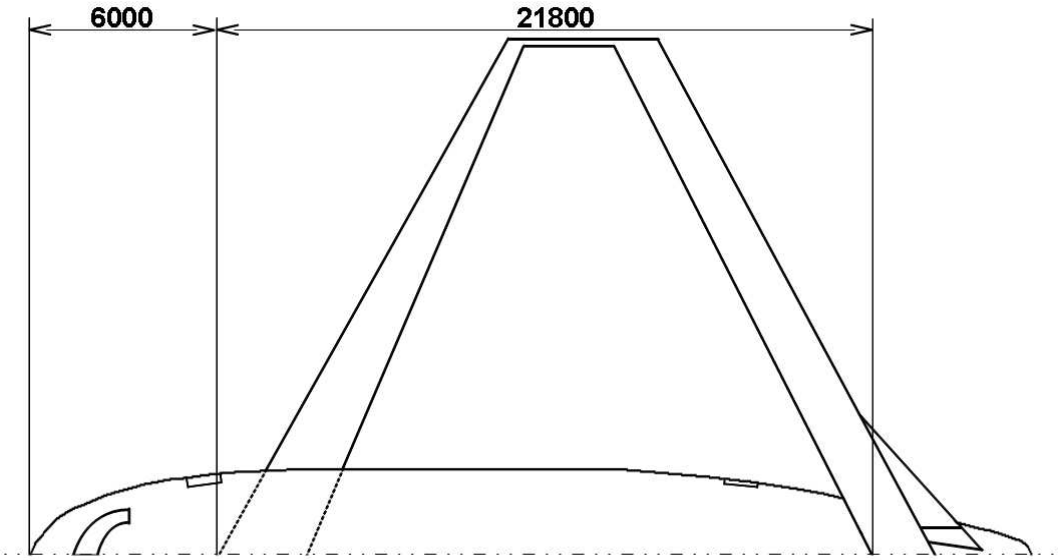

Figure 7.6 Wing dimensions, top view

7.6 More Precise Mass Estimation

The method used in paragraph 7.4 was originally derived for conventional aircraft configurations. That is why the results for the wing mass of the box wing configuration determined with the help of this method imply some uncertainties. In order to eliminate them for the most part a more precise method is applied in this paragraph.

The approach is to estimate the wing mass depending on the actual loads the wing is exposed to. In the present thesis a simple method presented in **Oyama 2000** is used and slightly adapted (see section 7.6.1).

To use this method it is necessary to determine the internal loads along the wing span. For this the wing configuration is assumed to be a 2-dimensional framework. The calculation of the internal loads is done with the help of the freeware *Framework* programmed by Gerrit Wolsink (**Wolsink 2011**).

For the beginning the internal loads along the vertical winglets and their resulting mass is not part of the mass estimation. The winglet structure will be taken account of in further studies. At the moment their mass is assumed to be 1 t for both winglets combined.

7.6.1 Method

A simple approach is presented in **Oyama 2000**. Here the wing is modelled as a so called box-beam (see Fig. 7.7).

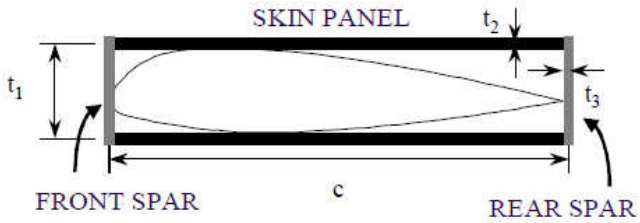

Figure 7.7 Box-beam modelling for wing mass estimation acc. to **Oyama 2000 (Oyama 2000)**

However, test calculations for estimating the wing mass of the A320 (which is given according to **Pester 2010a**) have shown that the modelling in Fig. 7.7 generates very low values. It is possible to produce values close to the real wing mass of the A320 by adjusting the dimensions of the box-beam so that it has approximately the size of the real wing box (Fig. 7.8) and by neglecting stress relieve due to the mass of the wing, fuel and engines.

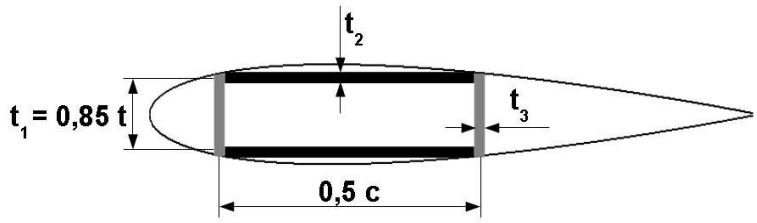

Figure 7.8 Adjusted box-beam modelling for wing mass estimation

The chord length c and and the spar height t_1 (Fig. 7.8) are given by the airfoil geometry. The skin thickness t_2 and the spar thickness t_3 are determined depending on the present internal loads. It is assumed that the wing bending moment is only absorbed by the skin panels which carry the resulting normal forces. Shear forces are solely absorbed by the front and the rear spar. When the corresponding thickness t_2 and t_3 are determined, it is possible to calculate the mass of the box-beam and thus of the so modelled wing.

Acc. to **Oyama 2000** and considering the geometry given in Fig. 7.8 the thickness t_2 of the skin panel at a certain span station is given by

$$t_2 = \frac{2M}{\sigma_{allowed} \cdot c \cdot t_1} = \frac{2M}{\varepsilon_{allowed} \cdot E \cdot c \cdot t_1} \tag{7.8}$$

and the thickness t_3 of the spars at the same span station by

$$t_3 = \frac{L}{2 \cdot \tau_{allowed} \cdot t_1} = \frac{L}{2 \cdot \gamma_{allowed} \cdot G \cdot t_1} \quad . \tag{7.9}$$

Eqs. (7.8) and (7.9) can also be understood using the derivations given in **Seibel 2005**.

The applied load factor (n = 3,75) is taken account of in the determination of M and L. It has to be noted that M is the wing bending moment about the longitudinal axis. The torsional moment about the lateral axis is neglected in this analysis. Since the value of torsional moment usually is about 10% of that of the bending moment, this simplification is reasonable for a first mass estimation. As seen in Eq. (7.9) only the lift L is considered as shear force. However, it seems to be more reasonable to consider the reaction shear forces due to lift than the lift itself. This is why the lift L in Eq. (7.9) is replaced by the shear force S_L due to lift. Stress relief due to wing and fuel weight as well as the weight of the engines is not considered. Validating the presented approach by estimating the wing mass of the A320 has shown good results (deviation of -0,8 %, see section 7.6.4).

The wing mass can be calculated with the help of the determined skin and spar thickness. Using the approach in **Oyama 2000** and considering the geometry shown in Fig. 7.8, the mass of the skin panels per unit span is calculated at the given span station with

$$m'_{skin} = 2 \cdot \rho \cdot t_2 \cdot 0{,}5\, c = \rho \cdot t_2 \cdot c \tag{7.10}$$

and the mass of the spars with

$$m'_{spar} = 2 \cdot \rho \cdot t_3 \cdot t_1 \quad . \tag{7.11}$$

The intention of this paragraph is to estimate the wing mass depending on the span wise internal loads. These internal loads may be determined at any span station which makes it possible to calculate the wing mass of the relating wing segment. The mass of the whole wing is then calculated by summing up the masses of the analyzed segments. If the internal loads are given as a function of the wing span, being $M = M(y)$ and $S = S(y)$, it would be possible to analytically assess the total wing mass by integrating the mass distribution along the wing span. For doing so it is necessary to alter Eq. (7.10) the following:

$$m'_{skin}(y) = \rho \cdot t_2(y) \cdot c(y) \quad , \tag{7.12}$$

and Eq. (7.11) to

$$m'_{spar}(y) = 2 \cdot \rho \cdot t_3(y) \cdot t_1(y) \tag{7.13}$$

The total wing mass is then determined with

$$m_{wing} = 2 \cdot \int_0^{b/2} \left[m'_{skin}(y) + m'_{spar}(y) \right] dy \tag{7.14}$$

For evaluating the integral it is necessary to calculate the functions of the skin and spar thickness. By changing Eq. (7.8) the skin thickness now is

$$t_2(y) = \frac{2}{\varepsilon_{allowed} \cdot E} \cdot \frac{M(y)}{c(y) \cdot t_1(y)} \quad . \tag{7.15}$$

The chord function $c(y)$ is given by wing geometry. The spar height $t_1(y)$ is calculated by

$$t_1(y) = 0{,}85 \cdot \frac{t}{c}(y) \cdot c(y) \quad , \tag{7.16}$$

based on the assumption that the height of the wing box is 85% of the absolute airfoil thickness. The distribution of the thickness to chord ratio is assumed to decline linearly from its value at the wing root to a given value at 35% of the half span. For all following span stations up to the wing tip the thickness to chord ratio is proposed to be constant having the value which is present at 35% of the half span. This distribution is similar to the one shown in **Böttger 2010** (Fig. 7.9).

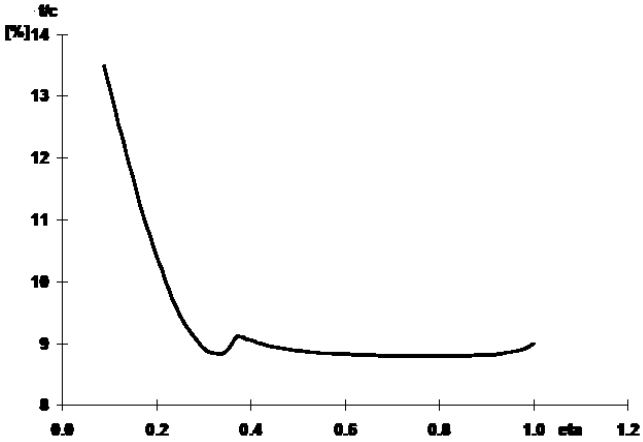

Figure 7.9 Span wise distribution of thickness to chord ratio for a jet transport aircraft (acc. to **Böttger 2010**)

According to Eq. (7.9) and taking account of the replacement of L by S_L, the spar thickness now is

$$t_3(y) = \frac{1}{2 \cdot \gamma_{allowed} \cdot G} \cdot \frac{S_L(y)}{t_1(y)} \tag{7.17}$$

Combining the just derived correlations finally gives the total wing mass as

$$m_{wing} = 4\rho \left(\frac{1}{0{,}85\,\varepsilon_{allowed}\,E} \cdot \int_0^{b/2} \frac{M(y)}{\frac{t}{c}(y) \cdot c(y)} dy + \frac{1}{2\gamma_{allowed} G} \int_0^{b/2} S_L(y)\, dy \right) \quad . \tag{7.18}$$

The wing is assumed to be made of aluminium, thus the material parameters are:

ρ = 2,7 kg/m³
E = 70000 MPa,
G = 28000 MPa.

All deformations shall not exceed the elastic range, thus:

$\varepsilon_{allowed} = \gamma_{allowed} = 0{,}003$.

Within the mass estimation no distinction is made between tensile and compression stresses. This is why buckling is not considered as well.

7.6.2 Lift Loads

For the present analysis only lift loads are considered. Their span wise distribution has to be determined in order to evaluate the distribution of internal loads. Lift can be written as a distributed load q_L whose value depends on the span station y. For a box wing the lift distribution is assumed to consist of a constant and an elliptical part (see Fig. 7.10). This is the ideal distribution according to aerodynamic requirements. It does not take account of additional structural requirements, otherwise the optimum distribution would deviate from the one which is assumed here. The equation for the span wise distribution can be formulated as

$$q_L(y) = \left(q_L\right)_{const} + \left(q_L\right)_{ell,o}\sqrt{1-\left(\frac{2y}{b}\right)^2} \quad . \tag{7.19}$$

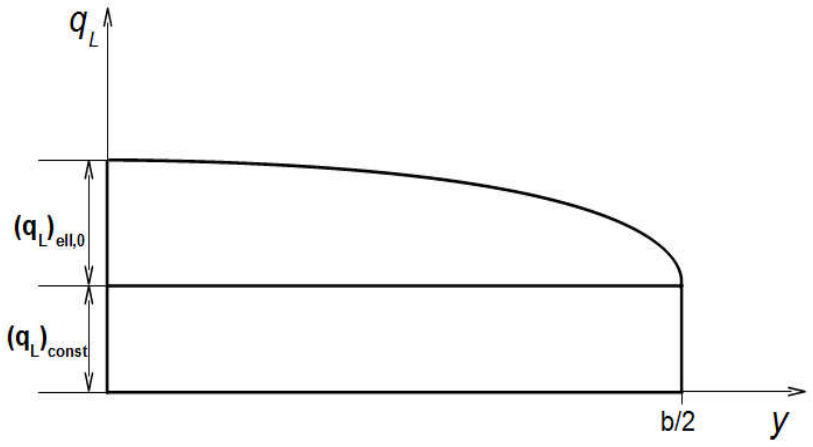

Figure 7.10 Lift distribution consisting of a constant and an elliptical part

The total lift generated along the wing half span is calculated by integrating the lift distribution along the half span:

$$L/2 = \int_0^{b/2} q_L(y)\,dy \quad , \tag{7.20}$$

with L being the lift generated by the whole wing. The integral of Eq. (7.20) is equal to the area of the rectangle with the edge lengths $(q_L)_{const}$ and $b/2$ plus the area of the quarter ellipse with $(q_L)_{ell,0}$ as semi-minor axis and $b/2$ as semi-major axis. So Eq. (7.20) can also be written as

$$L/2 = b/2\left[\left(q_L\right)_{const} + \left(q_L\right)_{ell,0}\cdot\frac{\pi}{4}\right] \quad . \tag{7.21}$$

Let R_L be the ratio of the elliptical to the constant part at the wing root. If R_L is given with

$$R_L = \frac{\left(q_L\right)_{const}}{\left(q_L\right)_{ell,0}} \tag{7.22}$$

then both parts can be determined with the help of this ratio and the total lift, in other words by combining Eqs. (7.21) and (7.22), which gives

$$\left(q_L\right)_{ell,0} = \frac{L}{b\left(R_L + \pi/4\right)} \tag{7.23}$$

and

$$\left(q_L\right)_{const} = \frac{R_L \cdot L}{b\left(R_L + \pi/4\right)} \tag{7.24}$$

Now the span wise lift distribution is known acc. to Eq. (7.19). For the current study the ratio R_L is assumed to be unity.

7.6.3 Effect of Wing Sweep

Since the wing is modelled as a 2-D-framework, effects of wing sweep have to be taken account of separately. In **Seibel 2005** it is shown that for the determination of the internal loads of a swept wing it is possible to assume an unswept reference wing with the same wing span. The span wise load distribution is the same as for the real wing. The internal loads are calculated for the unswept reference wing and then transposed to the geometry of the real wing:

1) All shear loads are unchanged, so

$$S_\varphi = S_{\varphi=0} \quad . \tag{7.25}$$

2) The bending moment about the longitudinal axis is transformed with

$$M_\varphi = \frac{1}{\cos\varphi} \cdot M_{\varphi=0} \quad . \tag{7.26}$$

Wing sweep does not effect the distribution of the thickness of the spars and the skin, so it also does not have any additional effects on the wing mass except the higher bending moment. This is because the sweep does not change the wing area for a given distribution of chord lengths, provided that the chord length is measured parallelly to the aircraft's symmetry axis. It is assumed that an unchanged wing area also means that the wing weight remains un-

changed.

Note that the internal loads displayed in the coming paragraphs do not consider wing sweep because they are the results coming directly from the 2D-analyis. The derived values considering sweep used for the mass estimation can be found in Appendix C.2.

7.6.4 Validation of the Method with A320 Wing Mass

For assessing the significance of the used method it is tested by estimating the known wing mass of the reference aircraft A320. The wing is modelled within the freeware *Framework.* The lift distribution is assumed to be elliptical and is approximated with the help of ten span stations along the half span. The values of lift per unit span were determined by applying the method described in paragraph 7.6.2 with the condition that $(q_L)_{const} = 0$ and assuming that the aircraft has the maximum take off mass. The modelled wing geometry and lift distribution can be seen in Fig. 7.11. The exact values of the lift distribution and the internal loads are given in Appendix C.

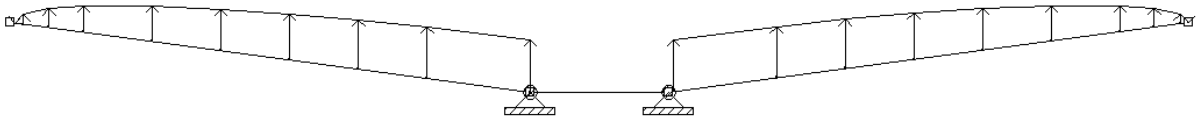

Figure 7.11 A320 wing geometry and lift distribution modelled in Framework

Note the indicated hinge supports in Fig. 7.11. Of course the modelled beams could not be carried by hinge supports. That is why the constraint is added that there is no rotation at the supports, which is possible within *Framework.* This constraint is applied to all hinge supports which will be shown in the coming figures and leads to a transfer of internal bending moment.

With the help of *Framework* it is possible to extract the values of internal loads at an arbitrary number of equidistant span stations. This number is chosen to be 50 per beam element. This way the function of internal loads does not need to be determined analytically but is approximated with the help of these span stations. Thus the integrals of Eq. (7.18) can be evaluated numerically. This is done with the help of the trapezoidal rule, where the value of an integral is the sum of the areas of all trapezes which the area under the relating function is split into (Fig. 7.12). The general equation for approximating the integral with the help of *i* arbitrary points is

$$\int_a^b f(x)\,dx \approx \sum_{i=1}^{n-1} 0{,}5\left(y_{i+1}+y_i\right)\left(x_{i+1}-x_i\right) \quad . \tag{7.27}$$

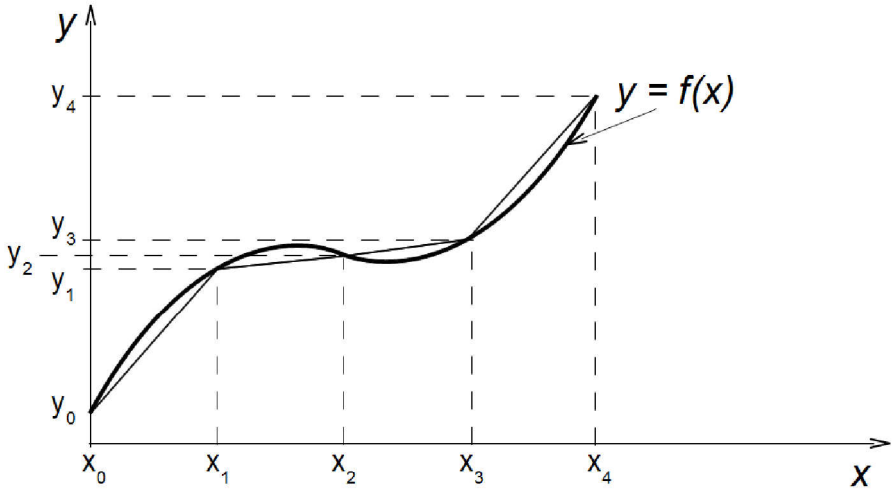

Figure 7.12 Trapezoidal rule for evaluating an integral

The more points are used, the closer the approximated value comes to the actual value of the integral.

The wing is modelled to be a simple trapeze having three partitions (Fig. 7.13). Their geometry is summarized in table 7.3.

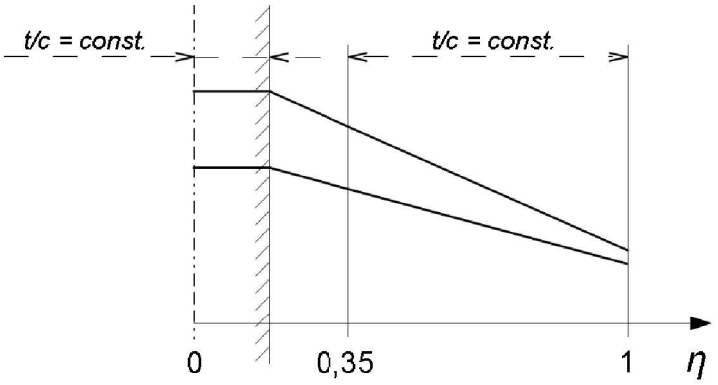

Figure 7.13 A320 wing model for wing mass estimation

Table 7.3 Wing geometry data for A320 wing mass estimation

Partition	Description	η_o	y_o [m]	$(t/c)_i$	$(t/c)_o$	c_i [m]	c_o [m]
1	Center wing box	0,118	2	0,15	0,15	5,8	5,8
2	Outer wing 1	0,35	5,95	0,15	0,09	5,8	4,461
3	Outer wing 2	1	17	0,09	0,09	4,461	1

The internal loads determined with *Framework* are shown in Figs. 7.14 and 7.15. Shear loads are shown in kN and bending moments in kNm. It can be seen that there are small asymmetries between both sides of the wing, although geometry and lift were modelled symmetrically. For the mass estimation the higher values on the right side are used. Note that these values do not yet consider wing sweep. Unfortunately the load factor was confused for the Framework

calculation (n = 3 was used instead of n = 3,75). However, this mistake was corrected afterwards within the spreadsheet used for calculating the wing mass. All internal loads were simply multiplied by the factor 1,25.

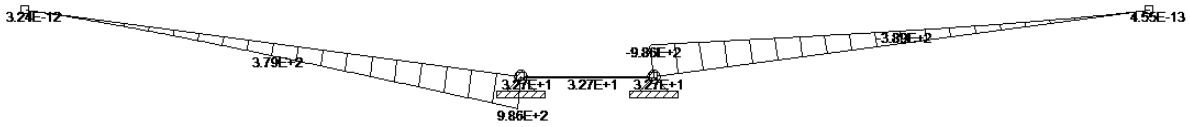

Figure 7.14 Distribution of shear load along A320 wing due to lift (values in kN)

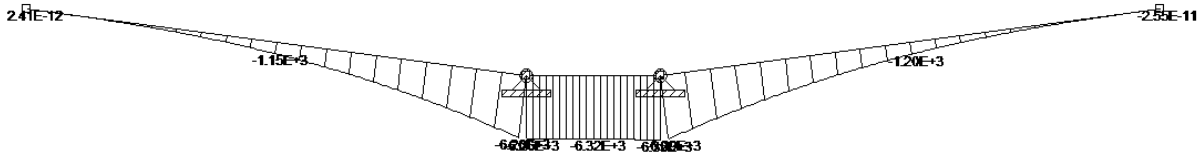

Figure 7.15 Distribution of bending moment along A320 wing due to lift (values in kNm)

The internal loads were extracted to a spreadsheet and were converted according to section 7.6.3 for taking account of wing sweep. This sheet contains the wing geometry data and the lift data as well and with its help the integrals of Eq. (7.18) are evaluated numerically using the trapezoidal rule (Eq. (7.27). This evaluation is done for each wing partition which gives the mass of each partition. The results are presented in table 7.4. The relating spreadsheet can be found on the CD-ROM attached to this thesis.

Table 7.4 A320 wing mass according to more precise estimation method

Partition	m_{skin} [kg]	m_{spar} [kg]	m_{tot} [kg]
1	659	0	659
2	2393	260	2653
3	2673	243	2916
Σ	5725	503	**6228**

In **Pester 2010a** the A320 wing mass is given. Although the present method of mass estimation does not consider wing ribs and system ribs for engine and main gear integration, it produces very good results, deviating by -0,8 % from the actual mass. It seems that neglecting the aspects of lightweight construction, which is a result of the simple box-beam model, as well as ignoring stress relief due to wing, fuel and engine weight, counteracts the missing mass of the ribs.

The conclusion is that the present method for estimating the wing mass is also suitable for a box wing configuration.

7.6.5 Wing Mass Estimation of the Box Wing Configuration

Here all connections and joints are assumed to be totally rigid, since this results in the lowest wing mass. The influence of flexible joints is discussed in section 7.7.

The wing geometry parameters derive from the numbers given in chapter 7. For the mass estimation each wing is modelled to have three partitions (Figs. 7.16 and 7.17). Their geometry data is given in tables 7.5 and 7.6.

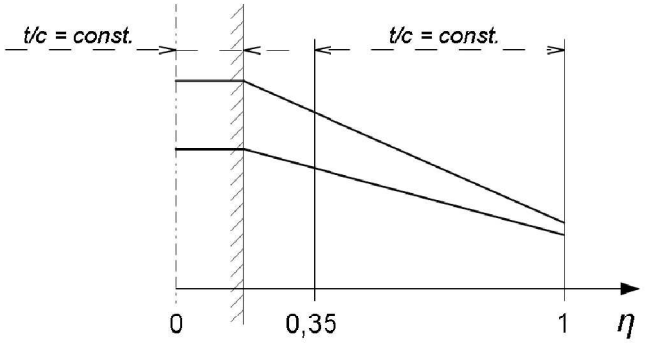

Figure 7.16 Model of the forward wing for wing mass estimation

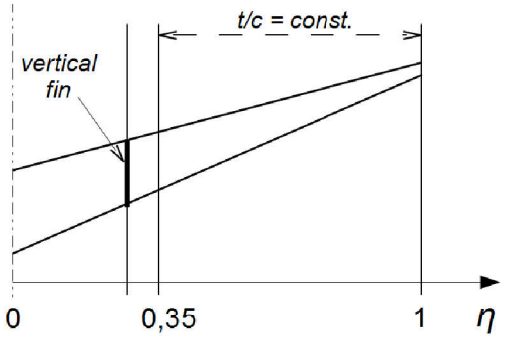

Figure 7.17 Model of the aft wing for wing mass estimation

Table 7.5 Geometry data of the forward wing

Partition	Description	η_o	y_o [m]	$(t/c)_i$	$(t/c)_o$	c_i [m]	c_o [m]
1	Center wing box	0,118	2	0,15	0,15	2,6	2,6
2	Outer wing 1	0,35	5,95	0,15	0,11	2,6	2,1
3	Outer wing 2	1	17	0,11	0,11	2,1	0,7

Table 7.6 Geometry data of the aft wing

Partition	Description	η_o	y_o [m]	$(t/c)_i$	$(t/c)_o$	c_i [m]	c_o [m]
1	Section until fin	0,276	4,7	0,15	0,118	2	1,89
2	Outer wing 1	0,35	5,95	0,118	0,11	1,89	1,86
3	Outer wing 2	1	17	0,11	0,11	1,86	1,6

The wing geometry is implemented into *Framework* as a 2-D framework and the lift distribution is determined applying the method shown in section 7.6.2. The division of total lift between the forward and aft wing was determined according to the requirements of static longitudinal stability and controllability discussed in section 5.2. The total aircraft mass was found with the help of PreSTo (**PreSTo 2011**) and independent and additional weight estimations (see section 10.2). With the help of the precise wing mass estimation only a small number of iterations was necessary to find a consistent aircraft mass which is the origin for the lift distribution. The distribution along the winglets is linear with the constraint that its extreme values coincide with the constant value $(q_L)_{const}$ of the adjacent horizontal wings. The wing geometry and the resulting lift distribution is shown in Fig. 7.18. Exact values can be found in Appendix C.

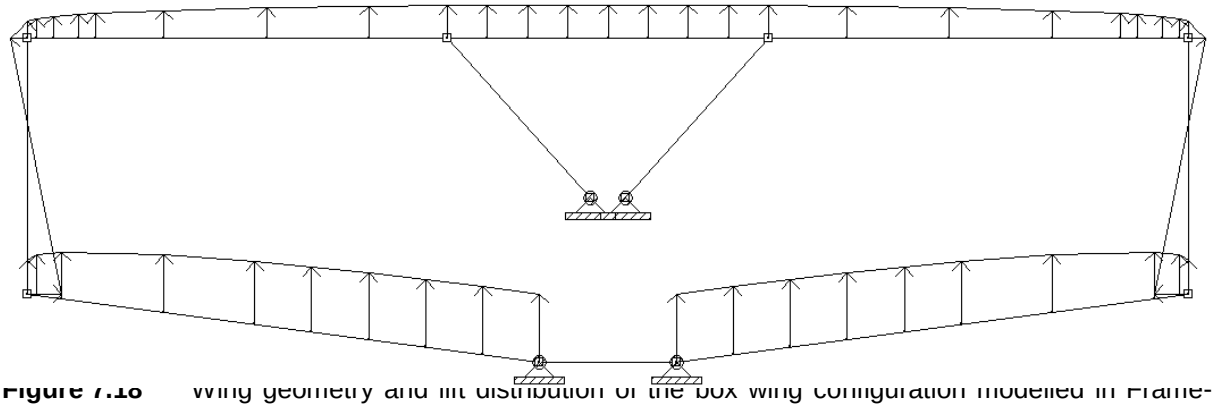

Figure 7.18 Wing geometry and lift distribution of the box wing configuration modelled in Framework

Remember that the depicted hinge supports do not allow any rotation and thus transfer the internal bending moment.

The resulting internal loads are presented in Figs. 7.19 and 7.20 (no sweep considered and wrong load factor, all corrected within spreadsheet). Their values used within the spreadsheet can be found in Appendix C.2.1.

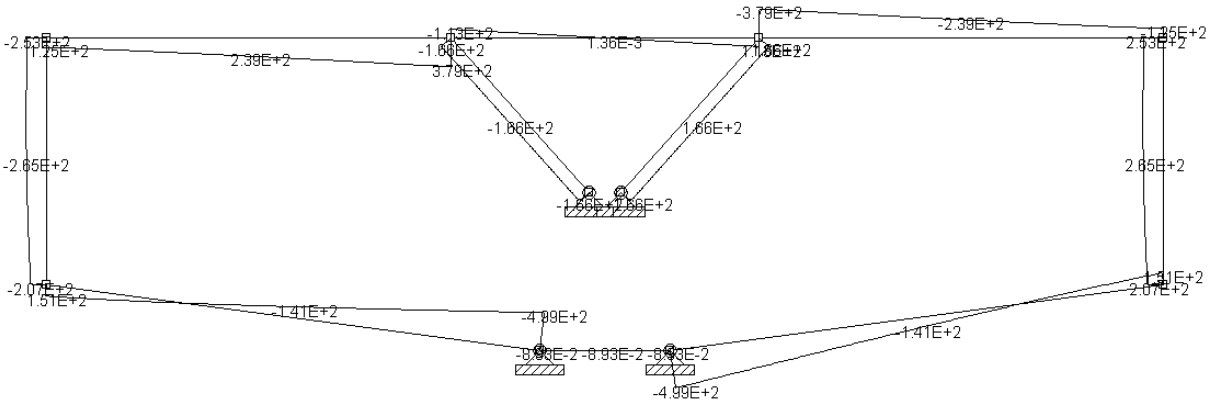

Figure 7.19 Distribution of shear load due to lift along wings of the box wing configuration (values in kN)

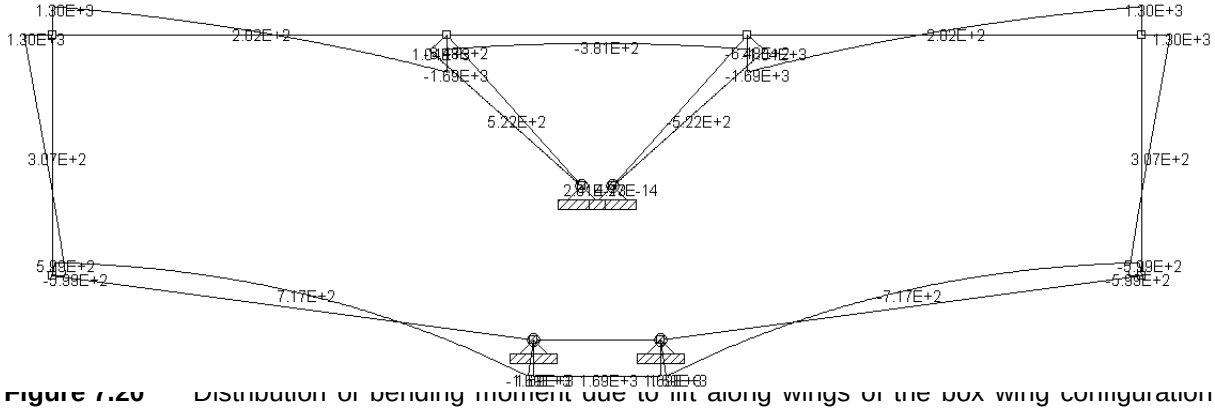

Figure 7.20 Distribution of bending moment due to lift along wings of the box wing configuration (values in kNm)

As for the A320 wing the internal loads are extracted to a spreadsheet and the wing mass is determined by numerically evaluating Eq. (7.18). The results are presented in table 7.7.

Table 7.7 Wing mass of the box wing configuration according to the more precise estimation

Forward Wing				Aft Wing			
Partition	m_{skin} **[kg]**	m_{spar} **[kg]**	m_{tot} **[kg]**	**Partition**	m_{skin} **[kg]**	m_{spar} **[kg]**	m_{tot} **[kg]**
1	524	0	524	1	721	21	742
2	860	128	988	2	701	36	737
3	5080	112	5192	3	3326	204	3530
Σ	6464	240	**6704**		4748	261	**5009**
Total	**11713 kg**						

7.6.6 Discussion of Results

As shown in section 7.6.4 the used method produces good results for the wing mass of the A320. Applying this method for the box wing configuration gives a wing mass of 11421 kg, which is almost twice as much as the weight of the reference wing (factor 1,865). According to the Torenbeek mass estimation this factor is only about 1,23. In terms of total mass, this difference means a deviation of about 4 t, which cannot be neglected.

The question is if the used method can be adapted to the box wing configuration of this thesis. The wing of the A320 is used for the integration of the main gear and the engines, which requires heavy system ribs carrying the accordant loads, which increases the wing mass. Since the mass estimated in section 7.6.4 is very close to the actual mass of the A320 wing, these systems ribs can be assumed to be included within the estimation. However, the main gear and the engines of the present box wing configuration are not integrated into the wings, so for this heavy system ribs are not necessary. On the other hand, the absence of the engines means less stress relief in the real case, but this stress relief exists on the A320.

The conclusion can be drawn that for the box wing configuration the effects of missing system ribs and missing stress relief neutralize each other and so the estimated mass of 11713 kg is a realistic value under the given circumstances.

A different aspect is the lift distribution of the box wing aircraft concerning its composition (constant plus elliptical part). The higher the constant part of the distribution, the more the lift centroid is shifted towards the wing tip which increases the mass of the wing. So it is possible to reduce the mass by increasing the elliptical part. For the A320 an elliptical distribution is assumed, which is not the optimum in terms of structural weight. Overall, the lift distributions used for the mass estimation generate some uncertainty.

7.7 Influence of Joint Types on Wing Structure

For the estimation of the wing mass of the box wing aircraft it was assumed that all joints are totally rigid. The joints connect the horizontal and the vertical wings as well as the aft wing and the vertical fins. It was claimed that rigid joints lead to the lowest wing weight. For supporting this claim the effects of the joint type on the wing structure are shown in this section, based on the evaluation of the corresponding internal loads as well as the corresponding wing mass according to the more precise estimation method of section 7.6.

Two cases are examined:

1) all joints are flexible
2) all joints are rigid

For both cases the lift loads and the wing geometry is the same as in the initial wing estimation shown in section 7.6.5. In the following a comparison of the two cases is done with regard to the internal loads (shear force and bending moment), the displacements (only qualitative) and the wing mass.

7.7.1 Shear Forces

From table 7.7 it becomes apparent that the contribution of shear forces to the wing mass are almost negligible. Table 7.8 shows that the joint type does not play an important role with regard to shear loads. However, rigid joints tend to increase the value of shear forces. It is striking that the winglets are loaded about six times as much as with flexible joints.

Table 7.8 Wing shear forces depending on the joint type (n = 3)

Lifting Surface	Station/Value	1) all flexible (kN)	2) all rigid (kN)
Forward wing	Wing root	564	499
	Wing tip	-86	-207
Aft wing	Wing root	347	379
	Wing tip	93	125
Winglet	Maximum	46	268

7.7.2 Bending Moment

The distribution of bending moment is essential for estimating the wing mass because most of the wing structure has to carry normal stresses caused by the bending moment. The distribution of bending moment is depicted for flexible joints (Fig. 7.21) and rigid joints (Fig. 7.22) as it results from the *Framework* calculation.

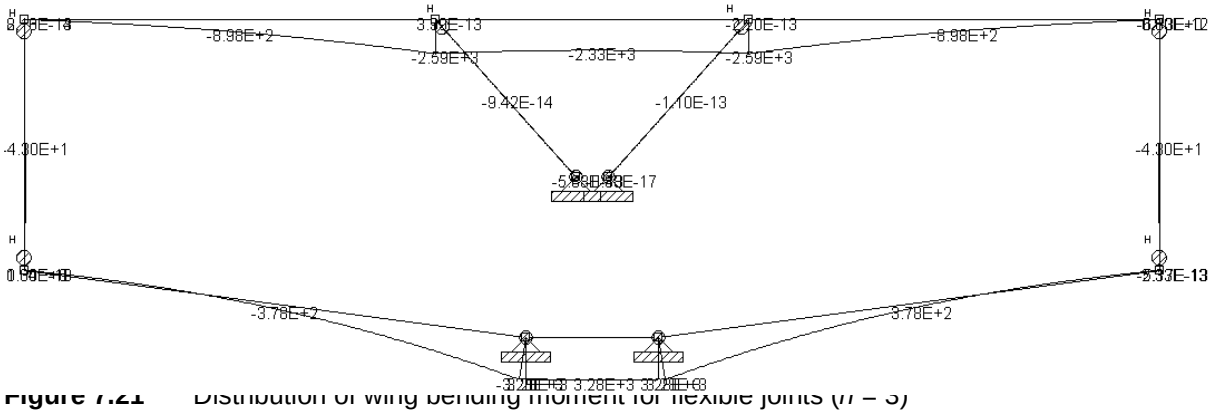

Figure 7.21 Distribution of wing bending moment for flexible joints (n = 3)

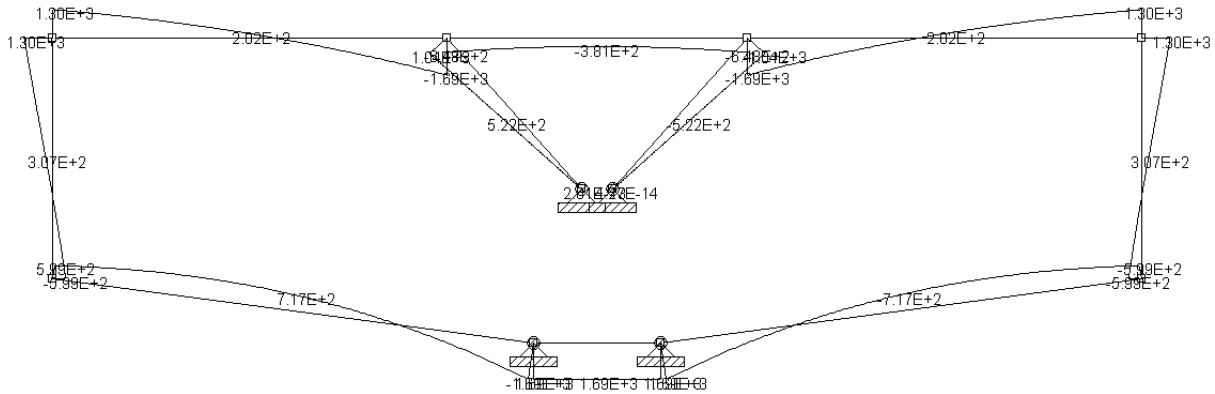

Figure 7.22 Distribution of wing bending moment for rigid joints (n = 3)

Table 7.9 Wing bending moment depending on the joint type (n = 3)

Lifting Surface	Station/Value	1) all flexible (kNm)	2) all rigid (kNm)
Forward wing	Wing root	3280	1690
	Wing tip	0	-599
Aft wing	Wing root	2590	1690
	Wing tip	0	-1300
Winglet	Maximum	43	1300

Table 7.9 shows the most important values of the internal bending moments. It becomes evident that rigid joints significantly reduce the wing root bending moment and the bending moment between the fins. However, the region near the wing tips and the winglets are remarkably loaded, as well as the joints themselves. Because of the rigid connection to the

fins, they also have to withstand a considerable bending moment. In case of rigid joints, it has to be assessed thoroughly if the structural design is feasible.

Flexible connections generate a distribution of bending moment common for conventional wings and unload the fins and winglets. So in this case the horizontal wings are indeed heavier but the mass of the vertical fins and the winglets is lower. It needs to be further investigated if these effects might neutralize each other.

7.7.3 Displacements

The displacements shown in Figs. 7.23 and 7.24 are only qualitative since the cross sections of the beams were not implemented into *Framework* according to the actual wing geometry. Nevertheless a simple comparison can be made, because for both configurations the modelled cross sections are the same.

It can be seen that rigid joints significantly decrease the amount of displacement. Although a quantitative assessment cannot be made, it is possible to conclude that the joint type is important regarding aeroelastic phenomena.

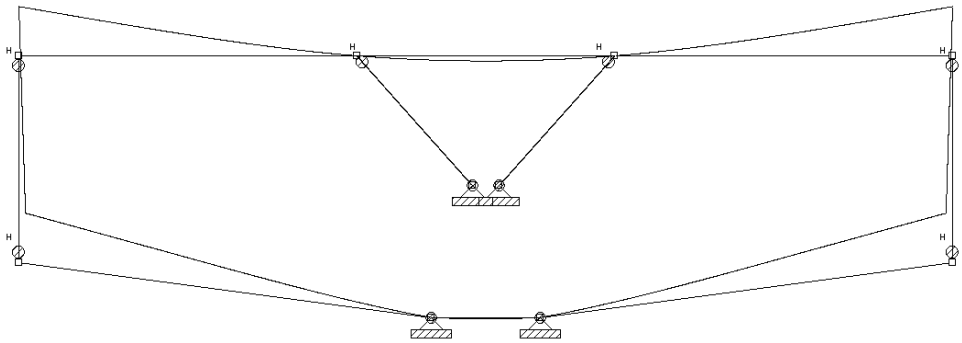

Figure 7.23 Qualitative displacements for flexible joints

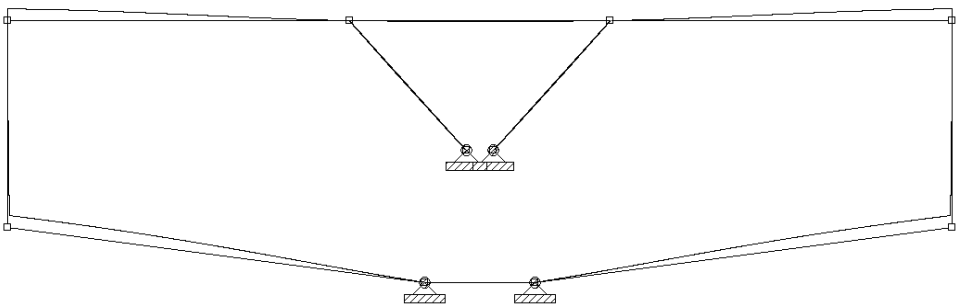

Figure 7.24 Qualitative displacements for rigid joints

7.7.4 Wing Mass

Based on the distribution of internal loads the wing mass was estimated for both joint types. The results are presented in table 7.10. The division of mass between the forward and aft wing is shown in Fig. 7.25

Table 7.10 Wing mass estimation for flexible and rigid joints (n = 3,75)

joint type	total mass	forward wing	aft wing	fwd wing percentage	aft wing percentage
flexible	14762	5591	9171	37,9	62,1
rigid	11713	6704	5009	57,2	42,8

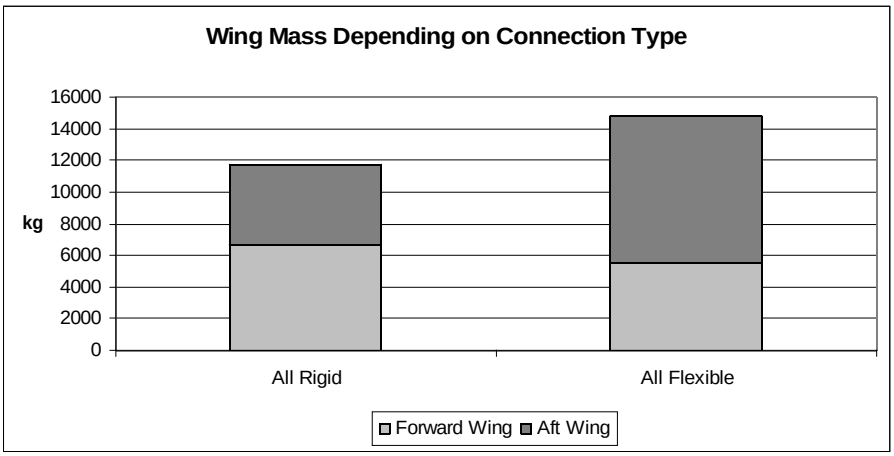

Figure 7.25 Division of wing mass for rigid and flexible joints

It is remarkable that the mass of the aft wing almost is two thirds of the total wing mass for flexible joints. This is because of the missing effect of unloading due to the fins, which is present for a rigid connection.

For rigid joints the mass of the forward wing is higher than its mass for flexible joints. The reason is that the forward wing is highly tapered, which means that near the wing tips the height of the wing box is quite small. This leads to a huge skin thickness and thus a mass increase due to the significant bending moment near the wing tips for rigid joints.

Overall rigid joints lead to a reduction of 21 % in wing weight compared to flexible joints. However, the structural design of the joints and their resulting weight is an open issue, since the joints have to carry a significant load.

7.8 Fuel Volume

The smaller wing dimensions with respect to the chord lengths and airfoil thickness affect the fuel volume which the wings can accommodate. The resulting volume of the wing tanks is determined in this paragraph.

According to **Torenbeek 1982** the volume of a wing tank is calculated with

$$V_{tank} = 0{,}54 \cdot \left(S_W\right)^{1{,}5} \cdot \left(\frac{t}{c}\right)_r \cdot \frac{1}{\sqrt{A}} \cdot \frac{1+\lambda\cdot\sqrt{\tau}+\lambda^2\cdot\tau}{\left(1+\lambda\right)^2} \tag{7.28}$$

where

$$\tau = \frac{\left(t/c\right)_t}{\left(t/c\right)_r} \quad . \tag{7.29}$$

which implies a linear decline of the thickness to chord ratio from root to tip. As indicated in section 7.6.5 and tables 7.5 and 7.6 respectively the *t*/*c* distribution however consists of two parts. The first goes from the wing root to approximately 35 % of the half span. Here the *t*/*c* ratio declines linearly from 0,15 to 0,11. From 35 % of the half span to the wing tip the *t*/*c* ratio is constant, having a value of 0,11. For getting proper estimations of the wing tank volume this *t*/*c* distribution has to be taken account of. As consequence Eq. (7.28) is applied separately for the inner and the outer wings.

Considering that the forward and the aft wing both have a trapezoidal planform the following tank capacities result (tables 7.11 and 7.12), assuming a fuel density of 785 kg/m³. Additionally all necessary geometry parameters for evaluating Eq. (7.28) are given.

Table 7.11 Tank capacity of the forward wing

Part	S_W (m²)	$(t/c)_r$	τ	A	λ		V_{tank} (m³)	m_{tank} (t)
Inner wing	29,9	0,15	0,733	4,73	0,74		4,11	3,22
Outer wing	31,2	0,11	1	15,61	0,33		2,14	1,68
						Σ	**6,25**	**4,90**

Table 7.12 Tank capacity of the aft wing

Part	S_W (m²)	$(t/c)_r$	τ	A	λ		V_{tank} (m³)	m_{tank} (t)
Inner wing	23,0	0,15	0,733	6,17	0,93		2,34	1,84
Outer wing	38,2	0,11	1	12,77	0,86		2,95	2,32
						Σ	**5,29**	**4,16**

Consequently the total capacity of the wing tanks is 9,1 t while that of the reference wing tanks is 18,6 t.

7.9 Airfoils

According to **Khan 2010** airfoils have to be chosen thouroughly in order to have adequate transonic characteristics. Although choosing the right airfoils requires detailed aerodynamic studies some key points can already be stated:

1) Lower Reynolds numbers because of the small chord lengths have to be considered.
2) For an adequate wing tank capacity and structural strength of the wing box the effective thickness to chord ratio should not be lower than 0,11.
3) For static longitudinal stability and controllability the zero lift pitching moment of the airfoils should preferrably be around zero or even positive. However, supercritical airfoils usually have a huge negative pitching moment.
4) The winglets have to provide a certain lift distribution (see Fig. 7.18), so their airfoils also have to be chosen taking account of the above three points. Here the transition from one wing to the winglet has to be designed with care to avoid high wave drag (**Khan 2010**).

By far these are not all points to be considered for the airfoil choice, but those who are different compared to the airfoil choice for a conventional transonic wing.

7.10 High Lift Devices and Maximum Lift Coefficient

For preliminary sizing the maximum lift coefficients were assumed to be 2,95 for landing and 2,1 for take off. These numbers are composed by the lift coefficients of the individual wings. According to the requirements coming from static longitudinal stability and controllability the ratio $C_{L,1}/C_{L,2}$ needs to reach a certain value higher than 1. This means that the lift coefficient of the forward wing has to be higher than the total lift coefficient of the aircraft while the lift coefficient of the aft wing is lower.

Regarding a total lift coefficient of 2,95 this seems very challenging. If the ratio $C_{L,1}/C_{L,2}$ for cruise is taken, which is 1,74, this would mean that the forward maximum lift coefficient has a value of 3,75! However, the actual value for $C_{L,1}/C_{L,2}$ under landing conditions still has to be investigated. Nevertheless it can be seen that the layout of the high lift devices is a very difficult task. Probably the total wing area needs to be increased so that the required lift coefficient for landing decreases. On the other hand the areas of the individual wings may be chosen to be different, so that the forward wing has a higher area which decreases its lift coefficient. Additionally the zero lift pitching moment of the aircraft could be adjusted with the help of other measures than setting the ratio $C_{L,1}/C_{L,2}$ to a certain value (wing twist, contribution of the fuselage).

Another approach could be an adaptation of the mission requirements (**Scholz 2011**). By setting the take off field length to 2200 m, which is the same as the landing field length, a maximum lift coefficient of 2,25 is required. This means a lift coefficient of 2,86 for the forward wing. All other design parameters remain unchanged.

Iezzi 2006 conducted a study concerning the preliminary aerodynamic layout of the high lift devices of a box wing aircraft. There further aspects are mentioned to be considered for the design of the high lift devices. The most important ones are:

- The interaction between both lifting surfaces has to be carefully watched.
- The difference in the term ($C_{L,max} - C_L$) of both wings has to be kept to a minimum. Otherwise one wing would begin to stall while the other has not yet exhausted its full lifting capacities. This means that the high lift devices of this wing are oversized.
- Increasing the lift of the front wing could be counterproductive because of the huge downwash on the aft wing.

(acc. to **Iezzi 2006**)

Consequently the aircraft performance at low speeds is a very critical point, as is the design of the high lift devices. As **Iezzi 2006** concludes very few studies have been made on this topic, so there is a high demand for further investigations.

7.11 Control Surfaces

Because of the presence of two wings which have the common types of control surfaces a whole new set of possible combinations of control surface deflection arises. Fig. 7.26 shows an example of possible control surfaces on the wings of a box wing configuration, based on the study performed in **Iezzi 2006**.

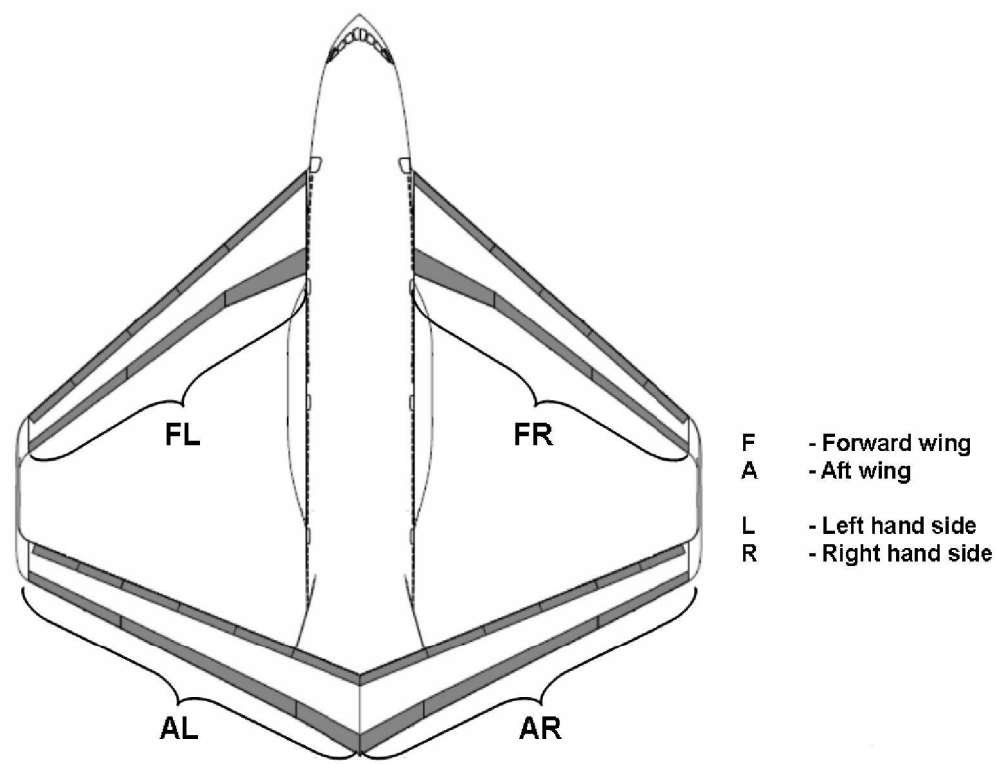

Figure 7.26 Control surfaces and high lift devices on a box wing aircraft (acc. to **Iezzi 2006**)

In Fig. 7.26 only control surfaces are emphasized, no high lift devices. For the sake of simplicity there is no deviation between inner, center and outer surfaces. The control surfaces of one side of one wing are treated as one surface. **Siuru 1987** gives a short introduction to the possibilities of maneuvers for aircraft with two wings and the accordant control surfaces. The mentioned maneuvers depending on the combination of surface deflections are summarized in Table 7.13. Note that not every possible combination is taken account of.

Table 7.13 Maneuvers depending on the combinations of control surface deflection

Maneuver	Control surface deflection			
	fwd left	**fwd right**	**aft left**	**aft right**
fast pitch down	up	up	down	down
fast pitch up	down	down	up	up
left turn	up	down	up	down
right turn	down	up	down	up
sideways left	up	down	down	up
sideways right	down	up	up	down

The most striking possibility is a controlled flight sideways, shown in the last two lines of table 7.13. Of course it is also possible to reduce the rotational moments during the maneuvers by only using one surface (inner, center or outer) per wing, e.g. for low and high speed flight with the accordant ailerons. Depending on the design philosophy an option could also be to allocate all ailerons to the forward wing and all elevators to the aft wing. As shown in **Iezzi 2006** ailerons could also be allocated to the all outer surfaces while all inner surfaces serve as elevators.

From this little excursus concerning control surfaces it becomes obvious that there is a vast amount of options for the design of the control system. Taking account of the small chord lengths limiting the room where mechanical components of the control surfaces can be integrated, the many possibilities of allocating the control surfaces may mitigate this problem.

8 Design and Integration of Other Aircraft Components

8.1 Cabin and Fuselage

At first it was intended to keep the original fuselage of the reference aircraft, so that the aircraft shown in Fig. 8.1 could have been a possible box wing configuration. But as the investigations concerning static longitudinal stability have shown the aircraft is very sensitive with regard to a huge shift of the CG position. Because of this it was decided to design the cabin as compact as possible so that the CG travel for different loading scenarios is as small as possible. This can be accomplished by decreasing the cabin length, which on the other hand means that more seats abreast are needed.

The resulting new design of the cabin and the fuselage is performed with the help of PreSTo Cabin (**PreSTo 2011**) and is presented in the next paragraph.

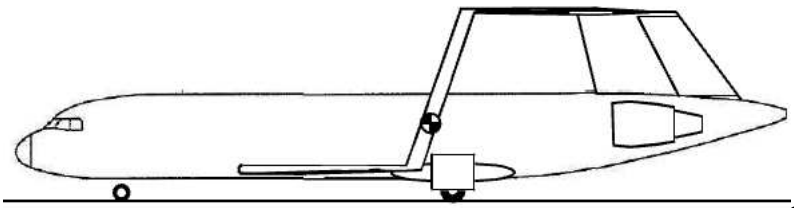

Figure 8.1 Possible box wing configuration with fuselage of the reference aircraft

8.1.1 Layout with PreSTo Cabin

Other than for the reference aircraft the fuselage cross section is supposed to be circular. The reference cabin accommodates 150 passengers in a two-class-layout with 12 passengers in business class (four seats abreast) and 138 passengers in economy class (six seats abreast). For the box wing aircraft the numbers of seats abreast were chosen to be six and eight, so the cabin accommodates 148 passengers (12 in business class and 136 in economy class). The overall number of seat rows is reduced by six compared to the reference cabin.

Figure 8.2 shows the fuselage cross section for economy class (left) and business class (right).

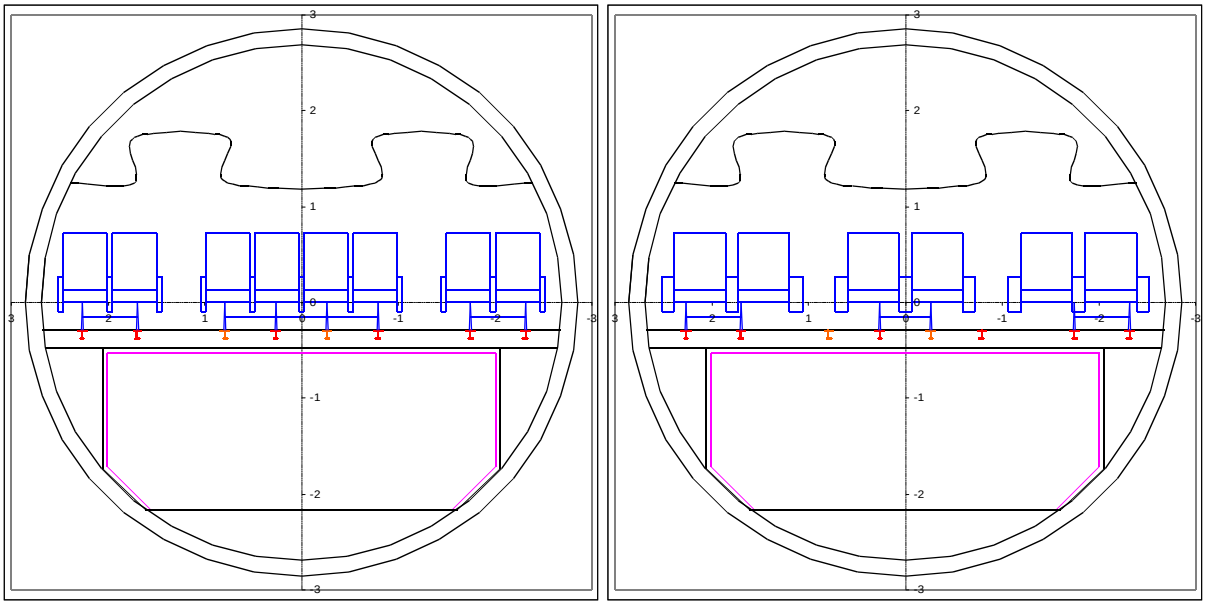

Figure 8.2 Fuselage cross section for economy class and business class (modelled with PreSTo Cabin)

It can be seen that there are two aisles. They only have the minimum required width of 20 inches (**EASA 2010**) which means a reduction in cabin comfort compared to current cabin layouts. However, for a short range aircraft having two aisles this seems to be sufficient. The presence of a second aisle should also lead to lower boarding and de-boarding times. Because of the higher fuselage diameter the cargo compartment can accommodate standard LD3 containers, so transshipping containers from long range aircraft is no problem. The huge cross-sectional area also arises the possibility of designing the aircraft as a dedicated freighter.

In Figure 8.3 the cabin floor plan is illustrated.

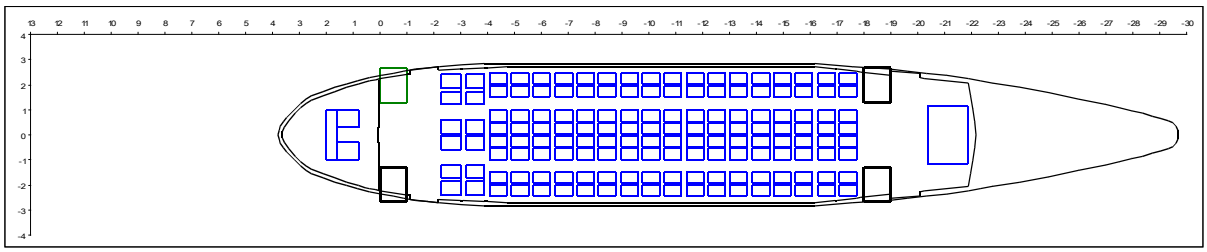

Figure 8.3 Cabin floor plan of the box wing aircraft (modelled with PreSTo Cabin)

Behind the cockpit wall there is a galley on the right hand side and a lavatory on the left hand side. These two are supposed to be used by business class passengers. At the end of the cabin there are two lavatories in front of the aft exit and one big galley aft of the aft exit. Both exits are Type A exits. The conformity of the cabin layout with certification requirements was positively checked by PreSTo Cabin. The nose and the tail were shaped so that they correspond to the values proposed by **Schmidt 1998** given in **Scholz 1999**.

The resulting geometry of the cabin and the fuselage is summarized in section 8.1.2.

8.1.2 Final Geometry

Figure 8.4 shows the exit positions and the total fuselage lengths. A summary of the fuselage and cabin parameters is given in table 8.1.

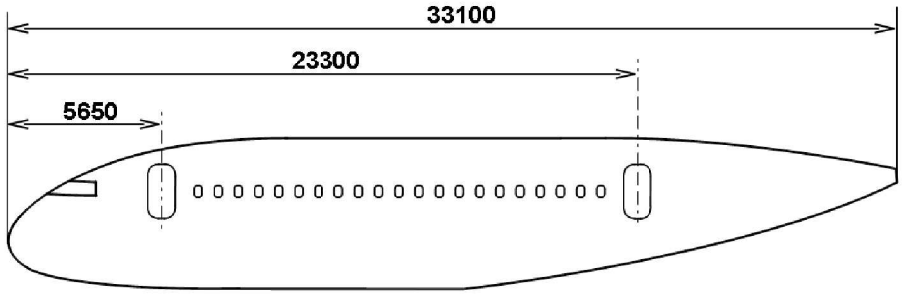

Figure 8.4 Exit positions of the box wing aircraft

Table 8.1 Parameters for fuselage and cabin layout

fuselage length	33,1 m
fuselage diameter	5,7 m
fuselage fineness ratio (*l*/*d*)	5,8
cargo volume	43 m³ (12 LD3 containers)
cabin length	21,9 m
cabin floor height (above fuselage bottom edge)	2,57 m
B/C	12 pax 2-2-2 36“ seat pitch
Y/C	138 pax 2-4-2 32“ seat pitch

Compared to the reference aircraft the cabin and the fuselage could be shortened by 5,6 m and 4,5 m respectively, which reduces the difference in CG positions for different loading scenarios. In combination with the engine position (see section 8.3) the aircraft is well balanced and should be insensitive to the CG positions resulting from all possible loading scenarios. A detailed study has yet to be performed for confirmation.

8.2 Empennage

The empennage is designed as a V-tail so that the stabilizers serve as struts for the aft wing to increase its stability (see Fig. 8.5). The dihedral of the stabilizers is 45°. As discussed in section 7.11 the inner surfaces of the wings may be used as elevators, so there is no need for a separate horizontal stabilizer. This is why the surfaces of the V-tail are supposed to function as vertical stabilizers for the most part which defines their sizing. Nevertheless the tail surfaces may also be used as additional horizontal stabilizers.

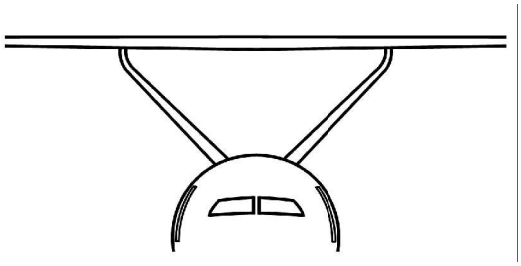

Figure 8.5 Front view of the V-tail

Usually the vertical stabilizer is sized depending on requirements regarding stability and controllability. In most cases an engine failure and the resulting yawing moment is the sizing case for the vertical stabilizer and the rudder. However, in this paragraph a more simple approach is chosen for a rough and fast sizing. The approach is based on the vertical tail volume which can be an indicator if the size of the vertical tail is sufficient. The volume is given with

$$V_V = S_V \cdot l_V \tag{8.1}$$

where S_V is the area of the vertical tail and l_V the distance between the neutral points of the wing and the vertical tail. The stabilizers of the box wing aircraft are sized in order to get the same vertical tail volume as for the reference aircraft. This way it is assumed that the size of the box wing stabilizers is sufficient. Strictly speaking this approach is conservative, because the engines of the box wing aircraft are very close to the fuselage (which will be shown in section 8.3) which causes less yawing moment in the case of a single engine failure in comparison with the reference aircraft.

With the given geometry of the reference aircraft its vertical tail volume is determined to be about 300 m³ (S_V ca. 19,5 m², l_V ca. 15,5 m). For the box wing aircraft the distance between the wing neutral point and the neutral point of the vertical tail has to be determined. Here it is necessary to know the final geometry of the aircraft. It is anticipated from chapter 9. The neutral point is determined with the help of the box wing sizing sheet where it results from the investigations regarding static longitudinal stability. With this information the distance l_V is about 12 m. Solving Eq. (8.1) for S_V and inserting 300 m³ for V_V together with the known l_V, the required tail surface is 25 m². Note that this area is the projected area since the tail consists of angular surfaces (V-tail).

The V-tail consists of two surfaces which means that the projected area of one surface is about 12,5 m². Here possible interferences between both surfaces reducing their efficiency are neglected. In combination with the conservative approach neglecting the engines being close to the fuselage this approach is justifiable.

Now the geometry has to be determined so that the required projected area is the result. One geometrical constraint is the connection of the tail surfaces to the wing, where both are required to have the same chord length. At the connection point the chord length is about 1,9 m. The other geometry parameters can be determined with the help of the equation for calculating the projected area which reads

$$S_V = 0{,}5 \cdot \left(c_{r,V} + c_{t,V} \right) \cdot h_V \quad . \tag{8.2}$$

The parameters to be determined are the stabilizer height h_V and the chord length at the stabilizer root. The height is chosen so that the resulting h/b ratio of the wing configuration does not significantly exceed a value of 0,2, since for higher values aeroelastic problems were discovered (**Lockheed 1974**). Additionally the projected aspect ratio of one vertical stabilizer shall be in the region proposed by **Roskam 1985a**, which ranges from 0,7 to 2. The chosen height is 3,4 m resulting in h/b = 0,22 and $A_{V,proj}$ = 1,5. Solving Eq. (8.2) for $c_{r,V}$ and inserting all defined parameters gives a root chord length of 3,8 m. This gives a taper ratio of 0,5, which is in the range proposed by **Roskam 1985a** (0,26 to 0,73).

The last parameter which has to be set is the sweep of the stabilizers. According to **Roskam 1985a** it should be between 33° and 53° for jet transport aircraft. For the box wing aircraft the sweep also is influenced by the longitudinal position of the aft wing and the length of the fuselage. As shown in Fig. 8.6 the stabilizers are swept forward which allows for a sufficient lever arm. The chosen sweep angle is -30°. The rudders are indicated to make out 35 to 40 % of the chord length.

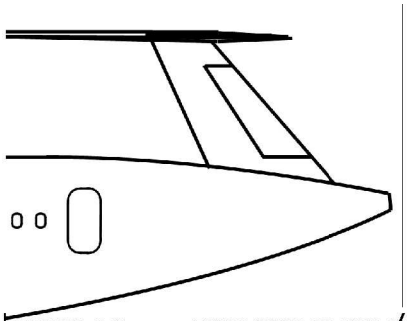

Figure 8.6 Side view of the V-tail

Table 8.2 gives a summary of the basic geometry parameters of the V-tail.

Table 8.2 Geometry parameters of the V-tail sized as vertical stabilizer

$S_{V,proj}$ (single stabilizer)	12,25 m²
h_V	4,3 m
$A_{V,proj}$ (single stabilizer)	1,51
$c_{t,V}$	1,9
$c_{r,V}$	3,8
λ_V	0,5
$\varphi_{25,V}$	-30°
l_V	12 m
V_V	294 m³

8.3 Engines

The box wing aircraft is supposed to have the same engines as the reference aircraft, although the required take off thrust is a bit lower (3,4 %). Of the two possible engine options the CFM 56-5 engine is chosen. An integration of engines with higher bypass ratios, as it is done with the current NEO project of the reference aircraft, shall also be possible.

The driving factor for the engine position is the fact that the aircraft has to be well balanced because of stability requirements. Consequently the engine has to be positioned close to the aircraft's center of gravity so that the shift of the center of gravity during boarding is minimal. Having a look at Fig. 8.7 two options are identified:

1) Engines at the tips of the forward wing or on the winglets
2) Engines at the center fuselage

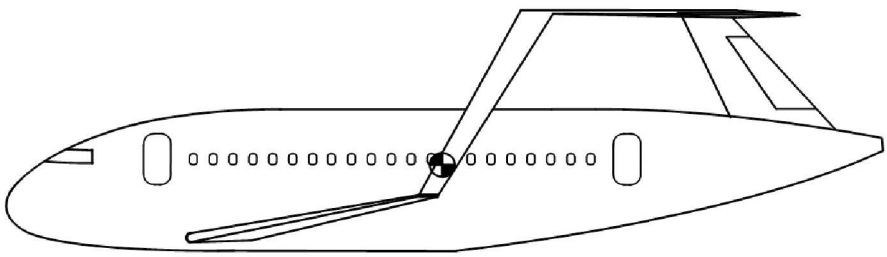

Figure 8.7 Box wing aircraft without engines

Option 1 is very unrealistic because of the thin wing structure at the tips or the winglet. Furthermore an integration into the wings could enforce aeroelastic problems.

For option 2 there are two possibilities. At first it was intended to have strengthened landing gear beams for integrating the engines as well. But this would mean that the engines are positioned quite low and directly in the downwash of the forward wing. The other possibility is the integration directly into the fuselage. For not limiting the passenger view and because of noise the engines cannot be positioned on the side of the fuselage. Consequently they have to be on top (see Fig. 8.8).

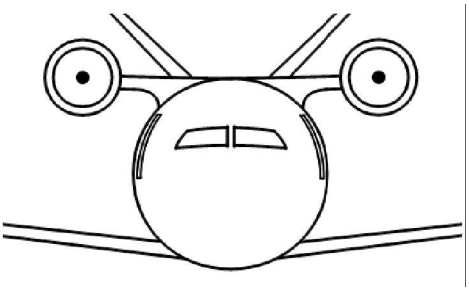

Figure 8.8 Front view of the engine integration

It can be seen that the engines are carried by a beam integrated into the fuselage. At this point it has to be decided whether the beam runs through the cabin (similar to the wing of the Avro RJ) or not (similar to the wing of the ATR 42/72). For the current study the first option was chosen because of expected aerodynamic advantages. However an additional trade study opposing additional drag to more cabin room for overhead bins might be necessary. In general the aerodynamic design of the beam still needs to be specified in detail. The span of the beam was chosen so that engines with higher bypass ratios, and consequently with a higher diameter, can be integrated. If necessary the span of the beam can be still increased.

8.4 Landing Gear

For conventional configurations with low wings the main landing gear is integrated into the wing. However, as it can be seen from Fig. 8.7, the CG position of the box wing aircraft makes it impossible to integrate the main landing gear into the lower wing. For this reason the main landing gear has to be integrated into the fuselage as it is done for the Avro RJ. Such a type of integration means that the fuselage is close to the ground during taxiing, take off and landing.

Concerning the number of wheels the same number as for the reference aircraft is chosen because both aircraft have a similar maximum take off and landing weight. In this study no specific statements concerning the mechanical design of the landing gear are made. The following investigations are limited to the rough positioning of the main landing gear for sufficient clearance and tilting stability.

8.4.1 Ground Clearance and Longitudinal Tip Over Stability

The landing gear has to be designed in order for the aircraft to have enough clearance during take off and landing. For take off the aircraft has to reach the necessary pitch angle without the tail striking the ground. If there are gusty winds it could be possible that the aircraft performs unexpected rolling maneuvers. In this case there has to be enough clearance so that the wing tips or wing mounted engines do not strike the ground.

According to **Trahmer 2004** the pitch angle before the tail strikes the ground should be around 8° to 13° and the angle between the bottom of the wing or engine and the ground around 6° to 8° (see Fig. 8.9).

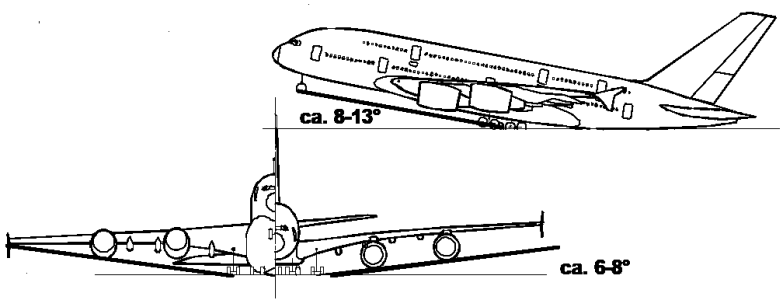

Figure 8.9 Landing gear layout for sufficient ground clearance (acc. to **Trahmer 2004**)

The chosen position of the landing gear for the box wing aircraft is depicted in Figs. 8.10 and 8.11.

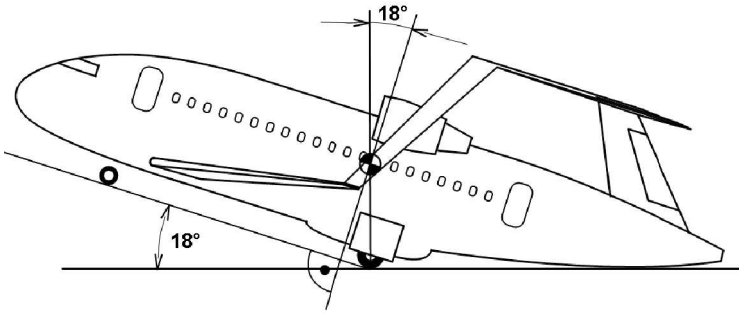

Figure 8.10 Pitch angle at tail strike

Note the longitudinal position of the main landing gear relative to the center of gravity. In Fig. 8.10 the accordant angle is specified with 18°. According to **Roskam 1985b** its minimum value should be 15° so that a sufficient nose down moment is induced during the landing impact. **Roskam 1985b** also shows that this angle has to have at least the value of the angle to tail strike which assures that there is no risk of tip over (sufficient longitudinal tip over stability). As Fig. 8.10 illustrates the main landing gear meets this requirement as well. However, it has to be mentioned that the drawn CG position applies to the conditions according to maximum payload and that its vertical position is only guessed.

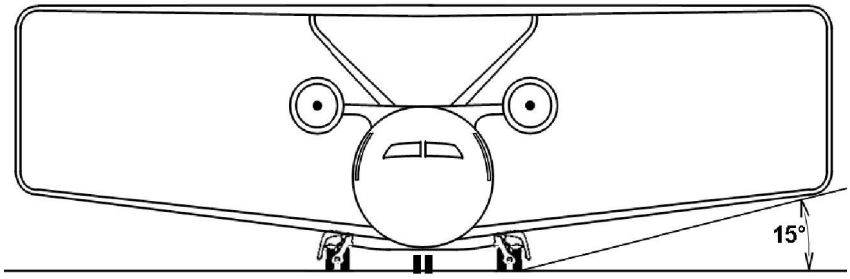

Figure 8.11 Wing clearance to ground

Fig. 8.11 indicates that the clearance of the wings to the ground is more than sufficient.

The detailed manner of main gear integration and the resulting fairings are not discussed at this point of the study. The dimensions of the fairing are indicated in the drawings.

8.4.2 Lateral Tip Over Stability

Lateral tip over stability is necessary in order to ensure safe maneuvering on ground and to compensate yawing moments due to an engine failure during take off (**Trahmer 2004**). For assessing the lateral tip over stability of an aircraft its tilting angle in relation to the line between nose gear and the left or right main landing gear has to be determined (see Fig. 8.12). The requirement for assuring sufficient stability is a tilting angle of less than 55°.

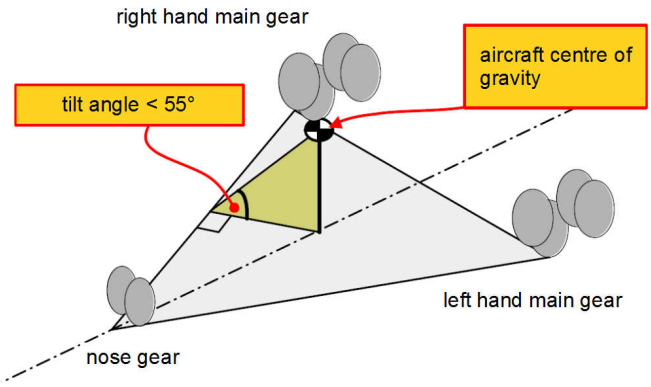

Figure 8.12 Tilting angle for assessing lateral tip over stability (acc. to **Trahmer 2004**)

For determining the tilting angle it is necessary to know the coordinates of the center of gravity. Its longitudinal position was already determined for maximum payload. However, its vertical position is only guessed for this investigation. If the real vertical position is higher than guessed here, the tilting angle will increase. Additionally the positions of the nose and main landing gear are required.

When all these positions are determined it is possible to calculate the tilting angle with the help of analytical geometry. The developed calculation method can be understood in Appendix E. It was implemented into a spreadsheet which can be found on the CD attached to this thesis. In table 8.3 the input geometry and the resulting tilting angle are given. It shows that with the current geometry of the landing gear the lateral tip over stability is sufficient.

Table 8.3 Input parameters and result of tilting angle calculation

	Coordinates (m)		
	x	**y**	**z**
Center of Gravity	16,4	0	4,7
Nose Gear	5,2	0	0
Main Gear (right)	17,7	4	0
Tilting Angle	**54°**		

9 Final Aircraft Layout

The final box wing configuration evolved from all of the investigations presented in this thesis. The main drivers for the final design are the requirements for static longitudinal stability and controllability. The layout of the individual aircraft components can be justified with the descriptions in the chapters 7 and 8. Within these paragraphs alternative designs of the components were discussed as well, together with a justification of their refusal.

At this point it can be argued if all combinations off possible layouts should be collected within a morphological matrix. By doing so alternative box wing configurations can be found and assessed more systematically. However, regarding the required effort it was decided to abandon such an approach for this initial design study. Since in this thesis a huge part is dedicated to building foundations of box wing design and to understanding and interpreting the new aspects a systematic assessment of alternative box wing versions is postponed to later studies.

Of course finding the final layout is an iterative process which produces many intermediate versions which are continuously improved and adapted to newly developed knowledge. The evolution of box wing versions can be found in Appendix D.2. Their development can be understood for the most part with the help of the section 5.2.3 as well as the chapters 7 and 8. In this section only the final configuration is presented (Fig. 9.1). Scaled and bigger drawings of the final configuration can be found in Appendix D.1.

However, it can already be foreseen that the shown configuration will also just be intermediate. There is enough evidence that several components might be changed in order to have a feasible design. Chapter 12 gives a conclusive discussion about this topic.

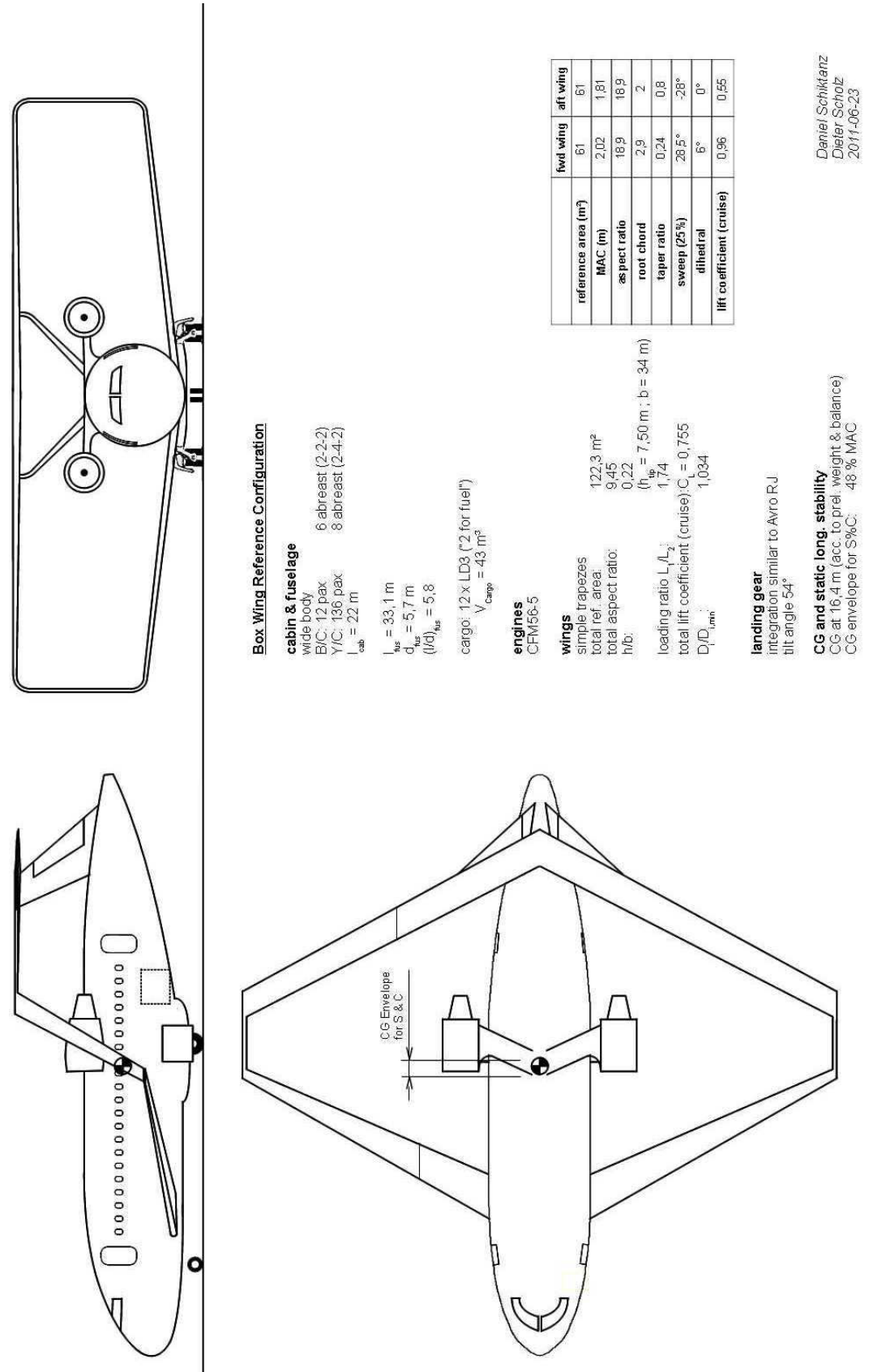

Figure 9.1 Three view drawing and data of the final box wing configuration

10 Weight and Balance

After having found the final configuration its mass has to be estimated to see if it agrees with the mass predicted in the preliminary sizing. When the masses of the individual aircraft components are known, the aircraft's center of gravity can be determined to check if it lies within the limits coming from the requirements according to static longitudinal stability and controllability. Of course this process is iterative and the data for mass and center of gravity were matched according to all requirements for every design change.

10.1 Loading Chart

The loading chart displays the travel of the aircraft's center of gravity for different loading scenarios. With its help critical loading conditions can be examined, where the CG might exceed the allowable range.

As already discussed it was emphasized that the overall configuration should be well balanced because of the stability requirements. This means that the loading chart of the aircraft would resemble Fig. 10.1. It can be seen that passengers and cargo do not significantly change the longitudinal position of the center of gravity. Because of the existence of a forward and an aft wing it could even be possible to have vertical lines for the CG travel between the maximum take of mass and the maximum zero fuel weight. This means that the CG would not change when the aircraft burns fuel, because fuel is taken from both wings in an accordant fashion. But it has to be noted that the permissible CG travel is small compared to conventional aircraft. This fact is further discussed in section 10.2.1.

A detailed loading chart of the final box wing configuration is part of further studies.

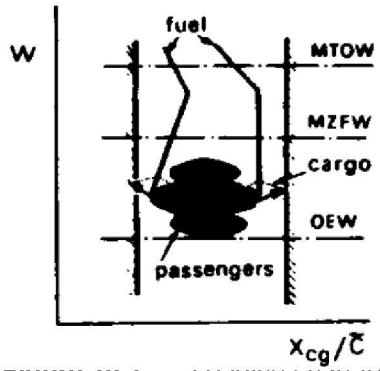

Figure 10.1 Loading chart for a balanced aircraft (**Torenbeek 1982**)

10.2 Component Masses and Center of Gravity

The component masses are mostly estimated with methods coming from **Torenbeek 1982** which are collected in **Scholz 1999**. The results are presented in table 10.1, together with the individual CG positions. Detailed information regarding the results, input parameters, calculation methods and assumptions can be found in Appendix F.2.2.

Table 10.1 Component masses and center of gravity positions

			Component	Sub-component	Mass (kg)	x_{CG} (m) from nose
m_{MTO}	m_{MZF}	m_{OE}	Wings	Fwd wing	6704	11,3
				Aft wing	5009	24,8
				Winglets	1000	17,9
			Tail surfaces		2197	27,7
			Fuselage		7800	14,9
			Landing gear	Nose gear	433	5,2
				Main gear	2450	18
			Engines (incl. nacelles)		6500	17,7
			Systems + op. items		9240	14,9
			Payload	Pax	13950	14,6
				Cargo	6050	16
			Fuel	Fwd wing tank	4905	11,3
				Aft wing tank	4157	24,8
				Fuselage tank	2106	12,2
				Tail/trim tank	1000	27,7

Table 10.2 gives a comparison of the masses resulting from the preliminary sizing and those coming from the estimation shown in table 10.1.

Table 10.2 Comparison of masses according to preliminary sizing and mass estimation

Mass	Preliminary sizing (kg)	Mass estimation (kg)	deviation (%)	Reference Aircraft (kg)	Deviation of box wing from reference (%)
m_{OE}	41383	41333	-0,12	40500	2,23
m_{MZF}	61383	61333	-0,08	60500	1,38
m_{MTO}	73245	73501	0,35	73500	0

Table 10.2 shows that a sufficient number of iterations was performed for a mass agreement of both methods. Now the maximum take off mass of the box wing aircraft is practically equal to that of the reference aircraft. The operating empty mass is 833 kg higher according to the

weight estimation of this paragraph. However, these numbers do not consider the constructive design of the tail and the wing-winglet-connections. Concluding from section 7.6.6 it could be possible that the operating empty mass increases once the detail design has been done.

With the help of table 10.1 the overall CG position of the aircraft can be determined. The general equation is

$$x_{CG} = \frac{\sum_{i}^{n} m_i \cdot x_{CG,i}}{\sum_{i}^{n} m_i} \quad . \tag{10.1}$$

According to the given data in table 10.1, the longitudinal CG position is at 16,4 m, which is within the permissible CG range coming from stability requirements (compare section 10.2.1).

The CG data are based on the maximum take off weight and cruise flight. It is indispensable to investigate the CG position and the permissible CG range for other flight conditions and loading scenarios. This however has to be done in forthcoming studies.

10.2.1 Permissible CG Travel

The method for the determination of the permissible CG travel according to requirements of static longitudinal stability and controllability was discussed in section 5.2.2. The result was a forward and an aft limit of the CG position. The distance between these two limits is commonly expressed in percent of the mean aerodynamic chord, whose calculation was shown in section 4.4. Because of the special wing characteristics of the box wing aircraft, the mean aerodynamic has only about half the length of that of the reference aircraft.

Usually the permissible CG travel is desired to be 20-25% MAC for passenger transport aircraft (**Torenbeek 1982**). This percentage is only valid for aircraft with a conventional wing. Transferring the requirement to the box wing aircraft, this would mean that the CG travel is desired to be about 40-50% MAC.

For cruise the following data (table 10.3) were determined with the help of the sizing spreadsheet. The individual lift coefficients are given in the table because they strongly influence the permissible CG travel. The data of the spreadsheet are given in Appendix F.2.

Table 10.3 Permissible CG travel in cruise condition with m_{MTO}

MAC (m)	$C_{L,1}$	$C_{L,2}$	$x_{CG,fwd}$ (m)	$x_{CG,aft}$ (m)	Δx_{CG} (% MAC)
1,92	0,96	0,55	15,9	16,8	48

It needs to be mentioned again that these data are only valid for cruise flight with maximum take off weight. The CG envelope for other flight and loading conditions is yet to be investigated. Furthermore the total lift coefficient was chosen to be about 0,75, which is about 0,1 lower than the lift coefficient for minimum drag. Due to the amount of iterations to find the final maximum take off weight the total lift which the stability calculations refer to is about 1,5 % lower than required for carrying the final maximum take off weight.

10.3 Mass Decomposition

In this paragraph the composition of the maximum take off mass and the operating empty mass of both the box wing and the reference aircraft are compared. This is useful to illustrate the effect of the higher glide ratio of the box wing configuration as well as the higher wing mass. The type of visualization is based on **SAWE 2011**. The resulting chart is presented in Fig. 10.2.

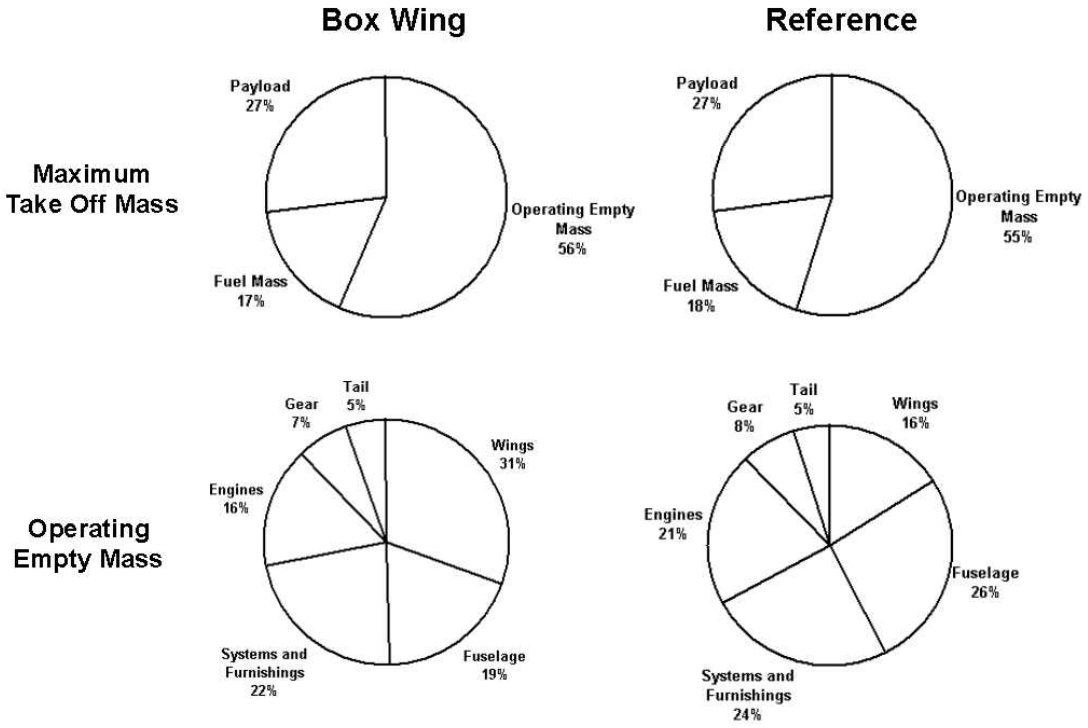

Figure 10.2 Decomposition of the maximum take off and the operating empty mass

At first it needs to be mentioned that parts of the operating empty mass of the reference aircraft originate from manufacturer data, others were estimated with the help of the methods used in section 10.2. So the shown percentages might slightly deviate from the actual ones.

The differences in the decomposition of the maximum take off mass are relatively small. They occur because of the lower fuel consumption of the box wing aircraft. When looking at the operating empty mass it can clearly be seen that the wings of the box wing configuration account for a huge part of the operating empty mass. The wing and the fuselage normally make out about 50% of the operating empty mass (**SAWE 2011**). This ratio applies to the box wing configuration. For the reference aircraft only 40% account for wings and fuselage, so they seem to be constructed in a very good way.

11 Performance of the Final Configuration

In this paragraph performance investigations are conducted based on cruise conditions. Considerations for other flight phases have to be part of forthcoming investigations.

11.1 Final Zero Lift Drag

As discussed in section 4.2.1 the zero lift drag coefficient is estimated by using the method based on the equivalent skin friction coefficient presented in **Scholz 1999**. The accordant equation is

$$C_{D,0} = C_{fe} \cdot \frac{S_{wet}}{S_W} \quad . \tag{11.1}$$

The wing area is known from the aircraft geometry and the equivalent skin friction coefficient can be estimated from statistics. The only parameter to be determined is the total wetted area of the aircraft. It is composed of the wetted areas of the individual components. These components are the fuselage, wings and winglets, stabilizers, engine nacelles and the beams supporting the engines. So the equation for calculating the total wetted area is

$$S_{wet} = S_{wet,F} + S_{wet,W} + 2 \cdot S_{wet,Stab} + 2 \cdot S_{wet,N} + 2 \cdot S_{wet,B} \quad . \tag{11.2}$$

The individual wetted areas are determined in the following paragraphs with the help of the methods collected in **Scholz 1999**. The geometry parameters needed for the calculation are taken from the drawings in Appendix D.1.

11.1.1 Wetted Area of the Fuselage

The fuselage is a conventional one with a cylindrical center part (compare drawings in chapter 9). According to **Torenbeek 1982** its wetted area is calculated with

$$S_{wet,F} = \pi \cdot d_F \cdot l_F \cdot \left(1 - \frac{2}{\lambda_F}\right)^{2/3} \cdot \left(1 + \frac{1}{\lambda_F^{\,2}}\right) \tag{11.3}$$

where λ_F is the fuselage fineness ratio which is simply the ratio l_F/d_F. According to section 8.1.2 the fuselage diameter is 5,7 m and its length 33,1 m. With these values the wetted area of the fuselage is 460,6 m².

11.1.2 Wetted Area of Wings and Winglets

According to **Torenbeek 1982** the wetted area of a wing is determined with

$$S_{wet,W} = 2 \cdot S_{exp} \cdot \left(1 + 0{,}25 \left(\frac{t}{c} \right)_r \cdot \frac{1 + \tau \cdot \lambda}{1 + \lambda} \right) \tag{11.4}$$

where $\tau = (t/c)_t/(t/c)_r$ and λ is the taper ratio. The parameters needed for the calculation and the results are given in table 11.1.

Table 11.1 Wing parameters for calculating the wetted area of the wings

Parameter	Forward wing	Aft wing	Winglet
S_{exp} (m²)	50	61	8,6
$(t/c)_r$	0,15	0,15	0,11
τ	0,733	0,733	1
λ	0,24	0,8	0,44
S_{wet} (m²)	103,6	126,0	17,67

The total wetted area of all wings is then calculated with

$$S_{wet,W} = \left(S_{wet,W} \right)_{fwd} + \left(S_{wet,W} \right)_{aft} + 2 \cdot S_{wet,winglet} \tag{11.5}$$

which results in $S_{wet,W} = 265{,}0$ m².

11.1.3 Wetted Area of the Stabilizers

The two stabilizers are treated as wings whose wetted area is determined according to Eq. (11.4). The real half span $b_{Stab}/2$ of one stabilizer is calculated with the help of its projected half span $b_{Stab,proj}/2$ and its projected height $h_{Stab,proj}$. Both can be taken from the three view drawings in Appendix D.1. The accordant equation reads

$$\frac{b_{Stab}}{2} = \sqrt{\left(\frac{b_{Stab\,,proj}}{2}\right)^2 + h_{Stab\,,proj}{}^2} \quad . \tag{11.6}$$

Both the projected half span and the projected height are 4,2 m, so the real half span of one stabilizer is 5,94 m. The thickness to chord ratio at the root is assumed to be 0,15. The root chord length is about 3,6 m, the tip chord length is about 1,8 m, so the taper ratio is 0,5. With these numbers the exposed area is determined to be 16,0 m². The ratio τ is assumed to be unity. According to Eq. (11.4) the wetted area of one stabilizer consequently is 33,3 m².

11.1.4 Wetted Area of the Nacelle

Since the contribution of the nacelles to the total wetted area is quite small, the equation proposed by **Torenbeek 1982** seems to be too detailed for the purposes of the current investigation. Instead the nacelles are regarded as simple cylinders whose wetted area is calculated with

$$S_{wet\,,N} = 2\pi \cdot r \cdot l \quad . \tag{11.7}$$

The length of one nacelle is estimated to be 4,5 m and its average radius to be 0,9 m. According to these numbers and Eq. (11.7) the wetted are of one nacelle is 25,4 m².

11.1.5 Wetted Area of the Engine Beam

In section 8.3 it can be seen that the engine beams resemble small wings having a huge thickness to chord ratio. Of course this comparison is only made with regard to the geometry, not to the function. This is why Eq. (11.4) can be used to determine the wetted area of the engine beams. One beam has a half span of about 2,8 m, a taper ratio of 1, a chord length of 1,4 m and a thickness to chord ratio of about 0,27. Consequently τ = 1 and S_{exp} = 3,9 m² and finally the wetted area of one beam is 8,3 m².

11.1.6 Total Wetted Area and Zero Lift Drag Coefficient

The calculated wetted areas of the individual components and the total wetted area of the box wing aircraft according to Eq. (11.2) are summarized in table 11.2.

Table 11.2 Wetted areas of aircraft components and total wetted area

Component	Wetted Area (m²)
Fuselage	460,6
Wings	265,0
Stabilizers	66,6
Nacelles	50,8
Engine Beam	16,6
Total Wetted Area	**859,6**

With a wing reference area of 122 m² the ratio $\boldsymbol{S_{wet}/S}$ **becomes 7,0**. This is quite a high value compared to values of 6 to 6,2 for conventional transport aircraft.

For the reference aircraft the skin friction coefficient is assumed to be 0,003, so this value is used for the box wing aircraft as well. Hence, with the help of Eq. (11.1) **the zero lift drag coefficient is 0,021**, which is a bit higher than the value initially assumed.

11.2 Final Glide Ratio

11.2.1 Maximum Glide Ratio

The maximum glide ratio is determined with the help of the preliminary sizing spreadsheet (**Scholz 2008**). Based on a span efficiency factor of 1,17, an equivalent skin friction coefficient of 0,003 and a relative wetted area of 7,0 the maximum glide ratio is 20,39. The one of the reference aircraft is given with 17,88, which means an **increase of 14 %**. According to Eq. (5.9) an increase of 17,3 % is expected. The difference occurs because of the zero lift drag of the box wing aircraft determined in section 11.1 which is higher than that of the reference aircraft.

11.2.2 Glide Ratio vs. Cruise Lift Coefficient

With the help of Eq. (5.3) the lift coefficient for minimum drag is defined to be 0,86. It will not be possible to keep this lift coefficient during cruise during usual flight operations because of traffic restrictions. But as it was mentioned before, because of the high span efficiency factor the range of lift coefficients for high glide ratios is relatively wide. As figure 11.1 illustrates the aircraft will still have glide ratio above 20 (2 % loss of efficiency) for lift coefficients from about 0,7 to 1,05. If we assume the same loss of efficiency for the reference aircraft (see dotted line in Fig. 11.1), the range of accordant lift coefficients would be from about 0,6 to 0,85. However, it is not certain yet if the lift coefficients mentioned for the box wing aircraft are attainable with regard to static longitudinal stability.

Note that these considerations neglect pressure drag due to separation at high lift coefficients and wave drag.

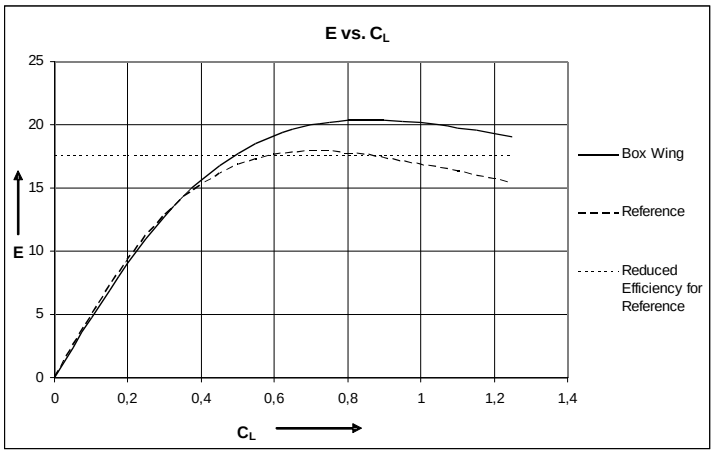

Figure 11.1 Glide ratio depending on the lift coefficient during cruise

11.3 Final Idealized Drag Polar

The idealized drag polars of the box wing and the reference aircraft (Fig. 11.2) are shown just to illustrate the better performance of the box wing aircraft and its higher zero lift drag. The polar is not needed for further calculations, since the determined glide ratio is the reference value for aircraft performance.

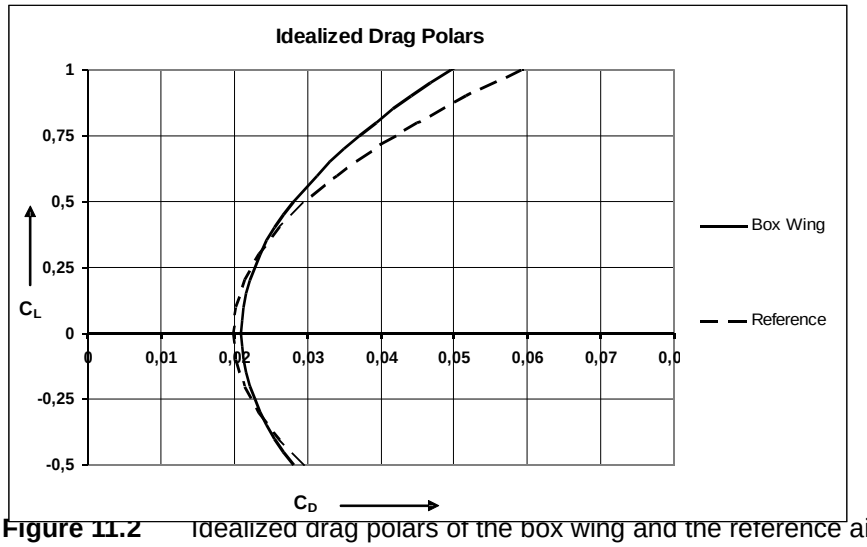

Figure 11.2 Idealized drag polars of the box wing and the reference aircraft

11.4 Payload-Range Diagram

The payload-range diagram shows the range of the aircraft depending on different loading scenarios. The determination of the payload-range diagram of the final box wing configuration is presented in the following sections.

11.4.1 Basics

The general composition of the payload-range diagram is shown in Fig. 11.3.

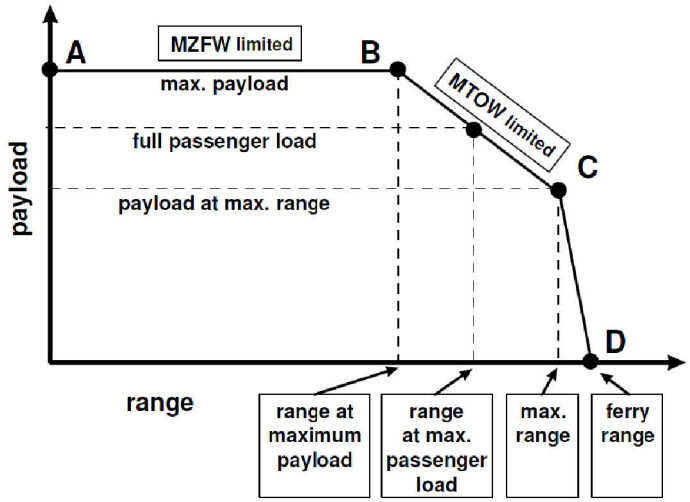

Figure 11.3 General composition of the payload-range diagram (**Scholz 1999**)

It is composed of three straight lines. The line from point A to point B gives the range for maximum payload, the line from point B to point C gives the range depending on the payload which is limited by the maximum take off mass. For a longer range the payload is reduced and replaced by additional fuel. This is limited by the maximum fuel capacity of the aircraft which is reached at point C. Point D results from flying with maximum fuel and no payload, which gives the ferry range.

The range for each scenario is calculated with the help of the Breguet range equation. Its derivation and application is summarized in **Scholz 1999**. A short description with assumptions and the required input parameters are given in section 11.4.2.

11.4.2 Breguet Range Calculation

In general the range is calculated according to the following equation:

$$R = -B_R \cdot \ln \frac{m_1}{m_0} \quad , \tag{11.8}$$

where B_R is the Breguet range factor. m_0 and m_1 are the masses of the aircraft at the beginning and at the end of the investigated flight segment. The difference between these two masses is the burned mass of fuel, so:

$$m_1 = m_0 - m_F \quad . \tag{11.9}$$

For cruise the Breguet range factor is given with

$$B_R = \frac{L/D \cdot v}{SFC_T \cdot g} \quad . \tag{11.10}$$

Here it is assumed that the glide ratio, the cruise speed and the specific fuel consumption remain constant which is a reasonable assumption within the scope of this thesis. According to the preliminary sizing spreadsheet (Appendix F.1.1) the chosen cruise speed is the speed for minimum drag, so cruise takes places at the maximum glide ratio of 20,39. The cruise speed is 224,3 m/s, the specific fuel consumption is 16,3 mg/(Ns).

With these numbers the resulting Breguet range factor for cruise is $2{,}859 \cdot 10^7$ m. This factor is assumed to be constant. Actually this means that the aircraft slowly climbs during cruise and constantly adjusts the cruise Mach number so that the cruise speed remains constant.

11.4.3 Range and Mission Segment Mass Fractions for Maximum Payload

The data for maximum payload have already been determined during the preliminary sizing. Actually the accordant range calculation was used within the preliminary sizing spreadsheet to size the aircraft. The calculations shown in this paragraph are based on this spreadsheet and the relating documentation (**Scholz 2007**) and are presented in order to provide a basis for the range determination for the other loading scenarios (sections 11.4.4 and 11.4.5).

According to Eq. (11.8) the mass ratio m_1/m_0 is required for calculating the total flight distance, which is the ratio of masses at the end and at the beginning of the flight. Note that the resulting flight distance is different from the range shown in the payload-range diagram. The ratio m_1/m_0 can be determined with the help of the mission segment mass fractions of all flight phases. The relating equation is

$$\frac{m_1}{m_0} = \frac{m_L}{m_{T0}} = M_{ff,std} \cdot M_{ff,res} \tag{11.11}$$

with

$$M_{ff,std} = M_{ff,T0} \cdot M_{ff,CLB} \cdot M_{ff,CR} \cdot M_{ff,DES} \cdot M_{ff,L} \tag{11.12}$$

and

$$M_{ff,res} = M_{ff,CLB} \cdot M_{ff,RES} \cdot M_{ff,LOI} \cdot M_{ff,DES} \tag{11.13}$$

$M_{ff,std}$ is the fuel fraction for a standard flight. The design range is taken account of by the cruise mass fraction $M_{ff,CR}$. $M_{ff,res}$ is the fuel fraction because of required reserve fuel for reaching an alternate airport and loiter time. It is emphasized that acc. to Eq. (11.11) the aircraft also uses all reserve fuel for the flight. This fact is important for the calculations in sections 11.4.4 and 11.4.5. The mission segment mass fractions for the phases take off, climb, descent and landing are given in table 11.3. The cruise mass fraction is determined with the help of the defined design range of R = 2870 km. Solving equation (11.8) for the mass ratio gives

$$\frac{m_1}{m_0} = e^{-R/B_R} \quad . \tag{11.14}$$

Inserting the design range and the already determined Breguet range factor results in a cruise mass fraction of 0,904. The same method is applied to calculate the mass fraction for the extra flight distance to an alternate airport including reserves. According to **Scholz 2007** this distance is given with 657,5 km. Using Eq. (11.14) the relating mass fraction $M_{ff,RES}$ is 0,977.

The loiter requirement is that the aircraft shall perform a loiter of at least 1800 s. The mass fraction for this time of flight can be determined with the Breguet endurance equation. It reads

$$t = -B_t \cdot \ln \frac{m_1}{m_0} \quad , \tag{11.15}$$

where B_t is the Breguet endurance factor, which can be calculated with

$$B_t = \frac{B_R}{v} \quad . \tag{11.16}$$

So for the given cruise conditions the Breguet endurance factor is $1{,}275 \cdot 10^5$ s. Solving Eq. (11.15) for the mass ratio yields

$$\frac{m_1}{m_0} = e^{-t/B_t} \quad . \tag{11.17}$$

Loiter time is 1800 s, so the mass fraction for loiter $M_{ff,LOI}$ is 0,986.

Now all required mission segment mass fractions have been determined. They are summarized in table 11.3.

Table 11.3 Mission segment mass fractions for flight with maximum payload

$M_{ff,engine}$	0,999
$M_{ff,taxi}$	0,996
$M_{ff,TO}$	0,995
$M_{ff,CLB}$	0,995
$M_{ff,CR}$	0,904
$M_{ff,DES}$	0,992
$M_{ff,L}$	0,992
$M_{ff,LOI}$	0,986
$M_{ff,RES}$	0,977

Acc. to Eq. (11.11) the resulting mass ratio for the total flight is 0,838.

11.4.4 Range for Maximum Take Off Mass and Maximum Fuel

This scenario equals point C in Fig. 11.3. At first the fuel capacity of the aircraft needs to be known. With the help of Eq. (7.5) the fuel capacity of the forward wing was estimated to be 4905 kg and that of the aft wing to be 4157 kg. Additionally a trim tank accommodating 1000 kg of fuel is assumed. For having enough fuel in order to fulfil the design mission, it is necessary to integrate additional tanks into the fuselage. Their volume is supposed to be equivalent to two LD3 containers, resulting in 6700 kg extra fuel.

Consequently the total fuel capacity is 16762 kg. The permissible payload is determined with

$$m_{PL} = m_{MTO} - m_{OE} - m_F \tag{11.18}$$

According to the weight estimation of table 10.2 the resulting payload is 15406 kg. The total mass at the the end of the flight is

$$m_L = m_{PL} + m_{OE} \tag{11.19}$$

which is 56739 kg. As mentioned in section 11.4.3 it is assumed that the aircraft also uses all fuel reserves for the flight [compare Eq. (11.11)]. This is why the landing mass does not include any fuel.

The take off weight of the aircraft is the maximum take off weight (73501 kg). The ratio m_L/m_{TO} then gives 0,772. Compared to the value of 0,838 for flight with maximum payload the trend of an increased range can already be made out.

As stated in section 11.4.3 the range of the aircraft depends on the cruise mass fraction. Since all other mission segment mass fractions remain constant and the total mass fraction m_L/m_{TO} is known, the cruise mass fraction can be calculated by solving Eq. (11.11) for $M_{ff,CR}$. This yields

$$M_{ff,CR} = \frac{m_L}{m_{T0} \cdot M_{ff,res} \cdot M_{ff,T0} \cdot M_{ff,CLB} \cdot M_{ff,DES} \cdot M_{ff,L}} \quad , \tag{11.20}$$

giving a cruise mass fraction of 0,832. According to Eq. (11.8) this equals a range of 5247 km.

11.4.5 Ferry Range

The ferry range is determined by assuming that the tanks are completely filled and no payload is transported. Here the take off mass is lower than the maximum take off mass, since now

$$m_{T0} = m_{OE} + m_F \tag{11.21}$$

which gives a take off mass of 58038 kg. According to Eq. (11.19) the mass m_L at the end of the flight is the operating empty mass of 41333 kg. This results in a ratio m_L/m_{TO} of 0,711. Corresponding to Eq. (11.20) the cruise mass fraction consequently is 0,767. With Eq. (11.8) the ferry range is calculated, resulting in 7580 km.

11.4.6 Results

The resulting data are summarized in table 11.4. The relating payload-range diagrams are presented in Fig. 11.4. For comparison the payload-range diagram has been determined for the reference aircraft as well using the same methods as for the box wing aircraft. The calculations were performed with the help of a little spreadsheet (Appendix F.3). It also contains the data of the reference aircraft used for determining its payload-range diagram.

Table 11.4 Results of the payload-range calculations

Scenario	**Box Wing**		**Reference**	
	Payload (t)	Range (km)	Payload (t)	Range (km)
Max Payload	20	2870	20	2870
Max Fuel	15,4	5247	14,4	5313
Ferry Range	0	7580	0	7480

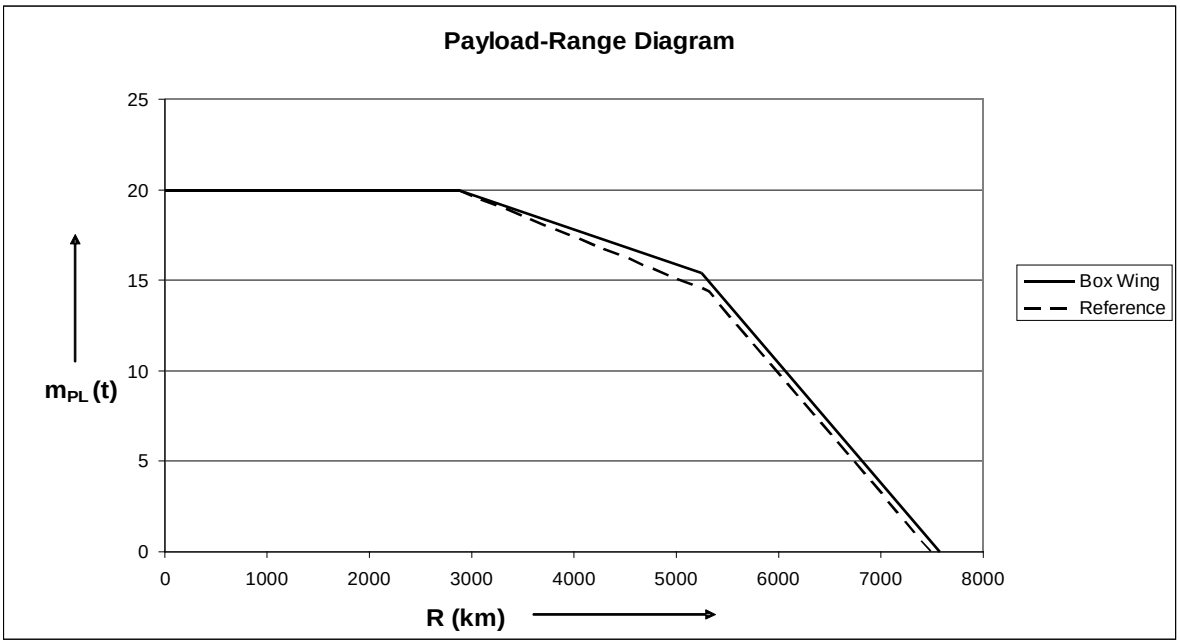

Figure 11.4 Payload-range diagram

As intended both aircraft have the same range when flying with maximum payload. For flight with maximum fuel and maximum take off mass the range of the box wing aircraft is insignificantly lower than that of the reference aircraft. What is more important in this segment of the chart is that the box wing aircraft is able to carry a higher payload (1 t more). This is because of its higher glide ratio and the circumstance that its tanks have less capacity than those of the reference aircraft. This means that the box wing aircraft carries more payload when its tanks are completely full, taking account of the fact that the maximum take off mass of both aircraft is the same. A further reduction of payload results in the box wing aircraft having a slightly higher range. It can be concluded that the lower fuel capacity of the box wing aircraft is more than just compensated by its higher glide ratio.

12 Conclusion and Outlook

The conceptual design of a medium range box wing aircraft was performed and its performance was compared with a reference aircraft with the help of simple methods. For this the box wing and the reference aircraft were chosen to have the same design mission. As expected savings in fuel consumption could be confirmed, which have a magnitude of 9 %.

The approach of the study was to apply the methods of aircraft design to the unconventional configuration, starting at mission requirements and ending with an assessment of aircraft performance. In order to do so it was necessary to check these methods with regard to their applicability. This is why the special characteristics of the configuration regarding aerodynamics, flight mechanics, structural layout and design synthesis were investigated in detail.

Considering aerodynamics it was shown why the box wing configuration allows for significantly reducing the induced drag. Since one wing carries only about half of the total lift, each of the two wings produces only quarter the induced drag of a comparable and conventional reference wing. Here it is important not to confuse the aerodynamic characteristics of the individual wings with those of the whole aircraft. The lift distribution of the winglets further decreases the amount of induced drag. A method was presented how to determine the induced drag as well as the span efficiency of the wing configuration. Additionally it was examined how much the induced drag increases when both wings do not generate the same amount of lift. Next to these investigations it was shown that the lift curve slope of the whole aircraft is slightly higher than that of the reference aircraft. In this context the downwash of the forward wing plays an important role. Additionally a controversial discussion about the stall characteristics was performed, leading to the conclusion that the effects due to downwash and vorticity complicate an assessment. A definition of the mean aerodynamic chord was given as well which showed that it has only about half the value of conventional wing configurations with comparable geometry.

As observed in literature the requirements for attaining static longitudinal stability and controllability are hard to achieve. It was found out that the positive zero lift pitching moment necessary for having a stable aircraft is difficult to obtain because initially it was assumed that balancing the pitch attitude is done only by both of the wings. This is why a horizontal stabilizer was not considered in the analysis which provides the positive zero lift pitching moment for conventional configurations. The solution is a difference in lift coefficients of both of the wings, meaning that the forward wing has a higher coefficient than the aft wing. This way it is not necessary to manipulate the zero lift pitching moment of the wings or the fuselage. Another conclusion from the performed analysis of static longitudinal stability and controllability is that the permissible CG travel is smaller compared to conventional aircraft which demands for a well-balanced layout.

From a general examination of the cruise lift coefficient for minimum drag it was reasoned that due to the higher span efficiency the box wing aircraft has to fly at very high altitudes for maximum glide ratio (ca. 13 km).

The preliminary sizing of the aircraft was based on parameters coming from the reference aircraft and those who were determined according to the conclusions from aerodynamic investigations. The required zero lift drag was determined with the help of the relative wetted area, which was evaluated based on the final aircraft geometry. At this point the iterative nature of the design process becomes apparent. The relative wetted area is about 7,0. Normally a value from 6,0 to 6,2 is assumed. The increase is mostly because of the V-tail, the engine beams and the winglets. The span efficiency during cruise was determined to be 1,17, that for landing 0,96. The resulting maximum glide ratio is 20,39, which means an increase of 14 % compared to the reference aircraft. The mass ratios needed for preliminary sizing were adjusted so that the resulting masses comply with the masses coming from a more detailed mass estimation. This way it was found that the aircraft has the same maximum take off mass as the reference aircraft while the needed fuel mass is decreased by 10 %. The lower fuel mass is compensated by a higher operating empty mass, for the most part because of a significantly heavier wing configuration.

A whole chapter was dedicated to the design of the wing configuration. It was stated that the requirements for transonic design are in conflict with those for structural design, since transonic wings demand for low thickness to chord ratios while higher ratios allow for a lower wing mass and for a higher wing tank capacity as well. The small chord lengths of the wings intensify these issues. Consequently the wings only have a tank capacity of 9,1 t which is more than 50 % less than that of the reference wing. This is why additional fuselage tanks having the volume of two LD3 containers are integrated into the fuselage. The software *Framework* was used to assess the wing internal loads. This allowed a more precise estimation of the wing mass which resulted in a mass significantly higher than that according to the Torenbeek estimation. A discussion of control surfaces revealed the many possibilities of maneuvering the aircraft. However, the small wing dimensions make the integration of the accordant mechanical components very challenging. This applies for the high lift devices as well. The final wing configuration comprises symmetrically swept wings (28°/-28°) and taper ratios roughly adjusted for optimal lift distribution (λ_1 = 0,24, λ_2 = 0,8). The lower wing has a dihedral of 6° for providing sufficient lateral stability.

The fuselage was designed in order to comply with the sensitivity of the aircraft towards CG travel. The cabin is 4,5 m shorter than the reference cabin. For accommodating the same amount of passengers as the reference aircraft the cabin was widened in order to have 8 seats abreast. This demands for a second main aisle. Consequently the fuselage is 5,7 wide, which allows for the cargo compartment to accommodate standard LD3 containers. Overall the cargo capacity is assumed to be 43 m³ while that of the reference aircraft is 37 m³.

The empennage is a V-tail which is supposed to carry the aft wing. For the most part it functions as a vertical stabilizer, but it could also be used as additional horizontal stabilizer. However, because of the angular surfaces a huge stabilizer area is needed. The engines are integrated in the middle of the fuselage, close to the center of gravity, on order to attain a well balanced aircraft. The landing gear is integrated into the fuselage because the positions of the wings do not allow an integration into the wings. Hence the fuselage is close to the ground which might facilitate the process of loading cargo.

All in all the box wing configuration can be further optimized. For example an equal division of lift between both wings would make the maximum glide ratio about 17 % higher than that of the reference aircraft (currently 14 %).

It has to be emphasized that the results of this study are based on methods and assumptions which have to be checked and confirmed with the help of more dedicated investigations. The field of future research is very wide. In the following the topics to be examined more detailed are listed.

- Effect of the ratio of the constant to the elliptical part of the lift distribution on aerodynamic performance
- Examination of the effects of upwash, downwash and wing tip vortices
- Confirmation of the determined span efficiencies/glide ratios and their dependency on dihedral and unequal lift distributions between both wings
- Drag for cruise speed, esp. wave drag
- Inclusion of thrust effects and the horizontal stabilizer in the analysis of static longitudinal stability
- General investigations concerning static longitudinal stability for other flight phases than cruise
- Static lateral stability in detail
- Flight Dynamics
- Exact positions of the center of gravity, incl. vertical position
- Aircraft performance and CG margins for other flight phases than cruise
- Load and trim chart
- Further validation/improvement of the method for wing mass estimation
- Structural analysis of the wings including joints and connection to vertical fins
- Aeroelastic phenomena
- Systems layout and integration
- Direct operating costs
- Ground handling
- Investigation of stretched/shrunk versions
- Systematic assessment of alternative box wing versions

References

Adams 1959 ADAMS, Frank D., NATIONAL AERONAUTICS AND SPACE ADMINISTRATION (Ed.): *Aeronautical Dictionary.* Washington : United States Government Printing Office, 1959. - NASA-TM-101286, URL: http://ntrs.nasa.gov/archive/nasa/casi.ntrs.nasa.gov/19900066158_1990066158.pdf (2011-06-28)

Aerospaceweb 2011 URL: http://www.aerospaceweb.org (2011-06-10)

Anderson 2005 ANDERSON, JR., John D.: *Introduction to Flight*. International Edition. New York : McGraw-Hill, 2005. - ISBN 007-123818-2

Anderson 2007 ANDERSON, JR., John D.: *Fundamentals of Aerodynamics*. 4th Edition. New York : McGraw-Hill, 2007. - ISBN 007-125408-0

Barger 1975 BARGER, Raymond L., NATIONAL AERONAUTICS AND SPACE ADMINISTRATION (Ed.): *Procedures for the Design of Low-Pitching Moment Airfoils*. Springfield (VA) : National Technical Information Service 1975.- NASA TN D-7982. - URL: http://ntrs.nasa.gov/archive/nasa/casi.ntrs.nasa.gov/19750019932_1975019932.pdf (2011-06-28)

Böttger 2010 BÖTTGER, Ole: *Flügelentwurf* : *Auslegung der Hauptparameter.* Hamburg, University of Applied Sciences Hamburg, Department of Automotive and Aeronautical Engineering, Lecture Notes, 2010.

Cahill 1954 CAHILL, Jones F.; STEAD, Dexter H.; NATIONAL ADVISORY COMMITTEE FOR AERONAUTICS: *Preliminary Investigation at Subsonic and Transonic Speeds of the Aerodynamic Characteristics of a Biplane Composed of a Sweptback and a Sweptforward Wing Joined at the Tips. Washington* : NACA, 1954. - RM L53L24b, URL: http://ntrs.nasa.gov/archive/nasa/casi.ntrs.nasa.gov/19930090477_1993090477.pdf (2011-06-28)

DATCOM 1978 FINCK, R. D.: *USAF Stability and Control Datcom*. Long Beach (CA) : McDonnell Douglas Corporation, Douglas Aircraft Division, 1978. - Report prepared under contract F33615-76-C-3061 on behalf of the Air Force Wright Aeronautical Laboratories, Flight Dynamics Laboratory, Wright-Patterson AFB (OH)

DeYoung 1980 DEYOUNG, John: *Induced Drag Ideal Efficiency Factor of Arbitrary Lateral-Vertical Wing Forms*. Virginia : Kentron International, Inc., 1980. - Research report prepared under contract NAS1-16000 on behalf of the National Aeronautics and Space Administration. - NASA Contractor Report 3357, URL: http://ntrs.nasa.gov/archive/nasa/casi.ntrs.nasa.gov/19810003514_1981003514.pdf (2010-06-28)

Durand 1935 DURAND, William F. (Ed.); VON KÁRMÁN, Theodore; BURGERS, J.M.: *Aerodynamic Theory Vol. 2 : General Aerodynamic Theory – Perfect Fluids.* Berlin : Julius Springer, 1935

EASA 2010 EUROPEAN AVIATION SAFETY AGENCY: *Certification Specifications for Large Aeroplanes* : *CS-25*. Amendment 10. Cologne : EASA, 2010.- http://www.easa.europa.eu (2011-03-29)

EU 2011 EUROPEAN UNION : *Flighpath 2050 : Europe's Vision for Aviation.* Brussels : European Union, 2011.- ISBN: 978-92-79-19724-6, URL: http://www.acare4europe.com/docs/Flightpath2050_Final.pdf (2011-06-27)

Frediani 2005 FREDIANI, Aldo : The Prandtl Wing. In: VON KÁRMAN INSTITUTE FOR FLUID DYNAMICS: *VKI Lecture Series* : *Innovative Configurations and Advanced Concepts for Future Civil Transport Aircraft.* Rhode St-Genèse: Von Kárman Institute for Fluid Dynamics, 2005. - URL: http://www.engbrasil.eng.br/index_arquivos/art95.pdf (2011-06-28)

Frediani 2007 FREDIANI, A., RIZZO, E.; CIPOLLA, V.; et. al.: Development of ULM Prandtlplane Aircraft and Flight Tests on Scaled Models. In: AIDAA: *XIX Congresso Nazionale AIDAA* (*Forlí 2007*). Forlí : AIDAA, 2007.- URL: http://www.prandtlplane.it/temp/Development%20of%20ULM%20PrandtlPlane.pdf (2011-06-28)

Frediani 2009 FREDIANI, Aldo; MONTANARI, Guido: Best Wing System: An Exact Solution of the Prandtl's Problem. In: BUTTAZZO, Giuseppe (Ed.); FREDIANI, Aldo (Ed.): *Variational Analysis and Aerospace Engineering.* Dordrecht, Heidelberg, London, New York : Springer, 2009, p. 183-211.- ISSN 1931-6828, ISBN 978-0-387-95856-9, e-ISBN 978-0-387-95857-6

HAW 2011 HAW HAMBURG: *AP 4.1* : *Entwurf, Analyse und Bewertung von für Bodenprozesse optimierten Flugzeugkonfigurationen für das Szenario 2015*. Hamburg, 2011. - URL: http://www.fzt.haw-hamburg.de/pers/Scholz/Airport2030.html (2011-06-27)

Iezzi 2006 IEZZI, Giuseppe: *PrandtlPlane High Lift System Preliminary Aerodynamic Design*. Pisa, Università di Pisa, Dipartimento di Ingegneria Aerospaziale “Lucio Lazzarino”, Thesis, 2006. - URL: http://etd.adm.unipi.it/theses/available/etd-09222006-113301/unrestricted/tesi_iezzi.pdf (2011-06-28)

Khan 2010 KHAN, Fahad Aman; KRAMMER, Philip; SCHOLZ, Dieter: Preliminary Aerodynamic Investigation of Box-Wing Configurations Using Low Fidelity Codes. In: DGLR: *Deutscher Luft- und Raumfahrtkongress 2010 : Tagungsband - Manuskripte* (DLRK, Hamburg, 31. August - 02. September 2010). - ISBN: 978-3-932182-68-5. DocumentID: 161308. URL: http://Airport2030.ProfScholz.de (2011-06-27)

Khan 2011 KHAN, Fahad Aman: Box Wing Longitudinal Stability and Controllability : e-mail. 2011-04-07

Kroo 2001 KROO, Ilan: Drag due to Lift : Concepts for Prediction and Reduction. In: *Annual Review of Fluid Mechanics Vol. 33* (2001), p. 587-617. - URL: http://www.annualreviews.org/doi/abs/10.1146/annurev.fluid.33.1.587 (2011-06-28)

Kroo 2005 KROO, Ilan : Nonplanar Wing Concepts for Increased Aircraft Efficiency. In: VON KÁRMAN INSTITUTE FOR FLUID DYNAMICS: *VKI Lecture Series* : *Innovative Configurations and Advanced Concepts for Future Civil Transport Aircraft.* Rhode St-Genèse: Von Kárman Institute for Fluid Dynamics, 2005. - URL: http://aero.stanford.edu/Reports/VKI_nonplanar_Kroo.pdf (2011-06-28)

Lockheed 1974 LANGE, R.H. ; CAHILL, J.F. ; BRADLEY, E.S. ; et al.: *Feasibility Study of the Transonic Biplane Concept for Transport Aircraft Application*. Marietta : The Lockheed-Georgia Company, 1974. - Research report prepared under contract NAS1-12413 on behalf of the National Aeronautics and Space Administration, URL: http://ntrs.nasa.gov/archive/nasa/casi.ntrs.nasa.gov/19740026364_1974026364.pdf (2011-06-28)

Loftin 1980 LOFTIN, JR, Laurence K.; NASA : *Subsonic Aircraft: Evolution and Matching of Size to Performance*. Washington, D.C. : National Aeronautics and Space Administration, 1980. - NASA Reference Publication 1060. - URL: http://www.ultraligero.net/Cursos/varios/aviones_subsonicos.pdf **(**2011-06-28)

NACA 1954 NATIONAL ADVISORY COMMITTEE FOR AERONAUTICS: *Manual of the ICAO Standard Atmosphere* : *Calculations by the NACA*. Washington : National Advisory Committee for Aeronautics, 1954. - NACA TN 3182, URL: http://aerade.cranfield.ac.uk/ara/1954/naca-tn-3182.pdf (2011-06-28)

Oyama 2000 OYAMA, Akira: Multidisciplinary Optimization of Transonic Wing Design Based on Evolutionary Algorithms Coupled With CFD Solver. In: *European Congress on Computational Methods in Applied Sciences and Engineering*. Barcelona : ECCOMAS, 2000. - URL: http://citeseerx.ist.psu.edu/viewdoc/download?doi=10.1.1.24.378&rep=rep1&type=pdf (2011-06-28)

Pester 2010a PESTER, Maria: *Multi-Disciplinary Conceptual Aircraft Design Using CEASIOM*. Hamburg, HAW Hamburg, Department Fahrzeugtechnik und Flugzeugbau, Master Thesis, 2010. - URL: http://www.fzt.haw-hamburg.de/pers/Scholz/arbeiten/TextPester.pdf (2011-06-28)

Pester 2010b PESTER, Maria: A-C_Preliminary_SizingA320.xls. Excel-File, 2010

Prandtl 1924 PRANDTL, Ludwig: *Induced Drag of Multiplanes*. Langley : National Advisory Committee for Aeronautics, 1924. - NACA TN 182, URL: http://naca.central.cranfield.ac.uk/report.php?NID=505 (2011-06-28)

PreSTo 2011 URL: http://www.fzt.haw-hamburg.de/pers/Scholz/PreSTo.html (2011-06-27)

Raymer 1992 RAYMER, Daniel P.: *Aircraft Design : A Conceptual Approach*. 2nd Edition. Washington : AIAA, 1992. - ISBN 0-930403-51-7

Rizzo 2007 RIZZO, Emanuele: *Optimization Methods Applied to the Preliminary Design of Innovative, Non Conventional Aircraft Configurations*. Edizioni ETS. Pisa, 2007.- ISBN 978-884672458-8, http://books.google.it/books?id=bSCv_8FIOFMC&printsec=frontcover&hl=de#v=onepage&q&f=false (2011-03-31)

Roskam 1985a ROSKAM, Jan: *Airplane Design* : *Part II: Preliminary Configuration Design and Integration of the Propulsion System*. Kansas : Roskam Aviation and Engineering Corporation, 1985

Roskam 1985b ROSKAM, Jan: *Airplane Design* : *Part IV: Layout Design of Landing Gear and Systems*. Kansas : Roskam Aviation and Engineering Corporation, 1985

SAWE 2011 SOCIETY OF ALLIED WEIGHT ENGINEERS: *OWE and Structure Decomposition*, 1997. - URL: http://central-europe.sawe.org/tecinfo/ac%20weight%20break/owedecompo.html (2011-06-28)

Scholz 1999 SCHOLZ, Dieter: *Skript zur Vorlesung Flugzeugentwurf*, Hamburg, Fachhochschule Hamburg, FB Fahrzeugtechnik, Abt. Flugzeugbau, Aircraft Design Lecture Notes, 1999

Scholz 2000 SCHOLZ, Dieter: *Actual Drag Polars*, 2000. - URL: http://www.fzt.haw-hamburg.de/pers/Scholz/MaterialFM1.html (2011-06-28)

Scholz 2007 SCHOLZ, Dieter: *AC-Dimensionierung*, 2007. - URL: http://www.fzt.haw-hamburg.de/pers/Scholz/Flugzeugentwurf.html#Zusatzmaterial (2011-06-28)

Scholz 2008 SCHOLZ, Dieter: A-C_Preliminary_Sizing.xls, Excel-File, 2008 http://www.fzt.haw-hamburg.de/pers/Scholz/Flugzeugentwurf.html#Zusatzmaterial (2011-06-28)

Scholz 2011 SCHOLZ, Dieter: High Lift of the Box Wing Configuration : Phone Call. 2011-06-30

Seibel 2005 SEIBEL, Michael; FLÜH, Hans J.: *Strukturkonstruktion* : *Eine Vorlesung zur Gestaltung und Auslegung von Flugzeugzellen*. Hamburg, HAW Hamburg, Fachbereich Fahrzeugtechnik und Flugzeugbau, Lecture Notes, 2005

Siuru 1987 SIURU, Bill; BUSICK, John D.: *Future Flight* : *The Next Generation of Aircraft Technology*. Blue Ridge Summit : Tab Books, 1987. - ISBN: 0-8306-7415-2

Stagliano 2008 STAGLIANO, Florian: *Konzeptentwurf für einen senkrechtstartenden Regionaljet*. München, Technische Universität München, Lehrstuhl für Luftfahrttechnik, Diplomarbeit, 2008. - LT-DA 08/05-Ex

Torenbeek 1982 TORENBEEK, Egbert: *Synthesis of Subsonic Airplane Design*. Delft : Delft University Press, 1982. - ISBN 90-247-2724-3

Trahmer 2004 TRAHMER, Bernd: *Fahrwerk / Undercarriage / Landing Gear : Fahrwerksintegration in den Gesamtentwurf*. Hamburg, University of Applied Sciences Hamburg, Department of Automotive and Aeronautical Engineering, Lecture Notes, 2004

Wolsink 2011 http://members.ziggo.nl/wolsink/ (2011-06-28)

Young 2001 YOUNG, Trevor: *Flight Mechanics*. Limerick, University of Limerick, Department of Mechanical & Aeronautical Engineering, Lecture Notes, 2001

Acknowledgements

I would like to thank those people who contributed to the development of this thesis.

First of all I want to thank Prof. Dr.-Ing. Dieter Scholz, MSME for his support. Our discussions about many of the new aspects of a box wing configuration were very motivating and helped to understand the aircraft as a whole. I also would like to thank him for patiently explaining several details regarding aircraft design. Furthermore I thank Dipl.-Ing. Philip Krammer for his engagement in initiating this thesis. I am also grateful for the support of Fahad Khan, MSc who it was inspiring to exchange thoughts with about different aspects of box wing aerodynamics and stability.

Next to these people more or less associated with the University of Applied Sciences Hamburg there was also support from people outside of the university. I would like to express my gratitude to Dieter Schulz-Hoos for giving some important impulses regarding the investigation of stability. I also thank Prof. Aldo Frediani and Dr. Emanuele Rizzo for clarifying my confusion about different charts regarding the aerodynamic efficiency of box wing aircraft.

Finally I want to thank my parents for their support during my studies and Thomas for believing in me and supporting me.

Appendix A

Definition of the Mean Aerodynamic Chord

The following definition will be used for further considerations:

Adams 1959 (Aeronautical Dictionary)

> *"The chord of an **imaginary rectangular airfoil** that would have **pitching moments** throughout the flight range the same as those of an actual airfoil or combination of airfoils under consideration, calculated to make equations of aerodynamic forces applicable."*

This definition is interpreted this way:

The mean aerodynamic chord is the chord of a rectangular wing generating the same pitching moment as the original wing configuration.

A.1 Length of the Mean Aerodynamic Chord

The length of the mean aerodynamic chord $\bar{c}$ depends on the definition used for the calculation. In the following two methods are presented.

Method 1
Calculation with the standard formula

At first the equation for calculating the mean aerodynamic chord of a conventional double trapeze wing is derived. The approach of this derivation is then applied to a box wing configuration.

The general equation for determining the length of the mean aerodynamic chord reads

$$\bar{c} = \frac{2}{S} \int_0^{b/2} c(y)^2 \, dy \quad . \tag{A.1}$$

(**Scholz 1999**)

Conventional configuration

A conventional double trapeze wing is shown in Fig. A.1. The inner wing having the area S_i and the outer wing having the area S_o are separated by the kink.

The total wing area is

$$S_{tot} = S_i + S_o \quad . \tag{A.2}$$

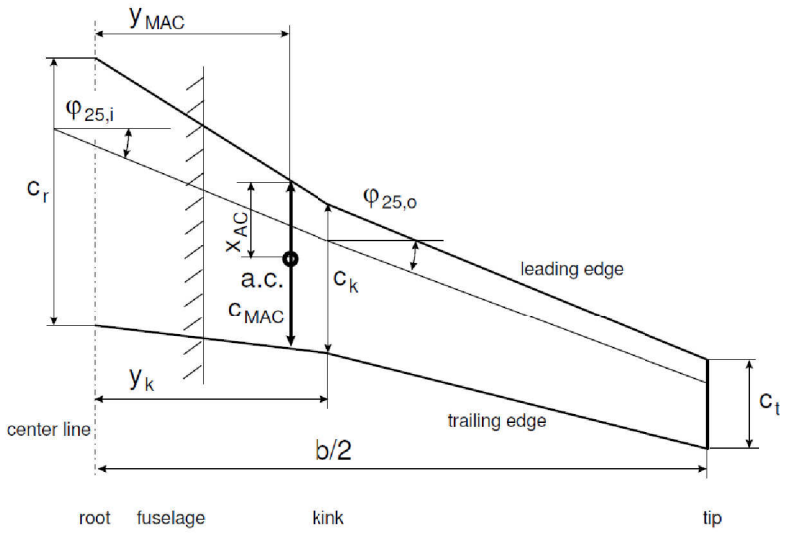

Figure A.1 Conventional double trapeze wing (**Scholz 1999**)

Additionally each partial wing has its individual function of chord length *c(y)*. So we have $c_i(y)$ and $c_o(y)$, where *y* is the span position. In order to calculate the total MAC of the whole wing it is at first necessary to determine the individual MAC of each partial wing.

Using Eq. (A.1) we get

$$\bar{c}_i = \frac{2}{S_i} \int_0^{y_k} c_i(y)^2 \, dy \tag{A.3}$$

and

$$\bar{c}_o = \frac{2}{S_o} \int_{y_k}^{b/2} c_o(y)^2 \, dy \quad . \tag{A.4}$$

Since $c_i(y)$ and $c_o(y)$ are known, $\bar{c}_i$ and $\bar{c}_o$ can be determined easily. Note that per definition the mean aerodynamic chord refers to the chord length of an imaginary rectangular wing having the same qualities as the original wing. So the following considerations base on these rectangular wings having the constant chord lengths $\bar{c}_i$ and $\bar{c}_o$ (see Fig. A.2).

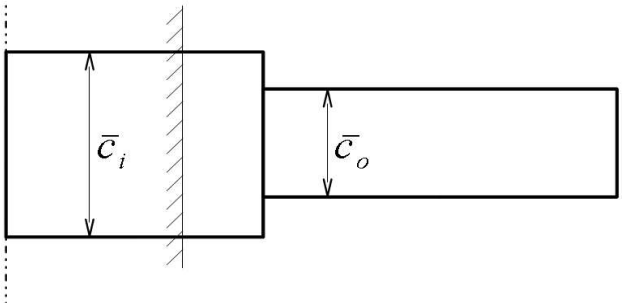

Figure A.2 Imaginary rectangular wings substituting the original inner and outer wing

Now the equation for the total MAC can be formulated acc. to Eq. (A.1):

$$\bar{c} = \frac{2}{S_i + S_o} \cdot \left[\int_0^{y_k} c_i(y)^2 \, dy + \int_{y_k}^{b/2} c_o(y)^2 \, dy \right] \tag{A.5}$$

with

$$c_i(y) = \bar{c}_i = const. \tag{A.6}$$

and

$$c_o(y) = \bar{c}_o = const. \quad . \tag{A.7}$$

So Eq. (A.5) simplifies to

$$\bar{c} = \frac{2}{S_i + S_o} \cdot \left[\bar{c}_i^2 \cdot y_k + \bar{c}_o^{\,2} \cdot \left(\frac{b}{2} - y_k \right) \right] \quad . \tag{A.8}$$

Introducing the areas

$$S_i = 2 \cdot \bar{c}_i \cdot y_k \tag{A.9}$$

and

$$S_o = 2 \cdot \bar{c}_o \left(\frac{b}{2} - y_k \right) \tag{A.10}$$

leads to the equation

$$\bar{c} = \frac{S_i \cdot \bar{c}_i + S_o \cdot \bar{c}_o}{S_i + S_o} \quad . \tag{A.11}$$

Box Wing Configuration

For the conventional configuration a double trapeze wing was considered. These are in fact two wings arranged next to each other. For a box wing configuration still two wings are present, but now arranged one after another (see Fig. A.3).

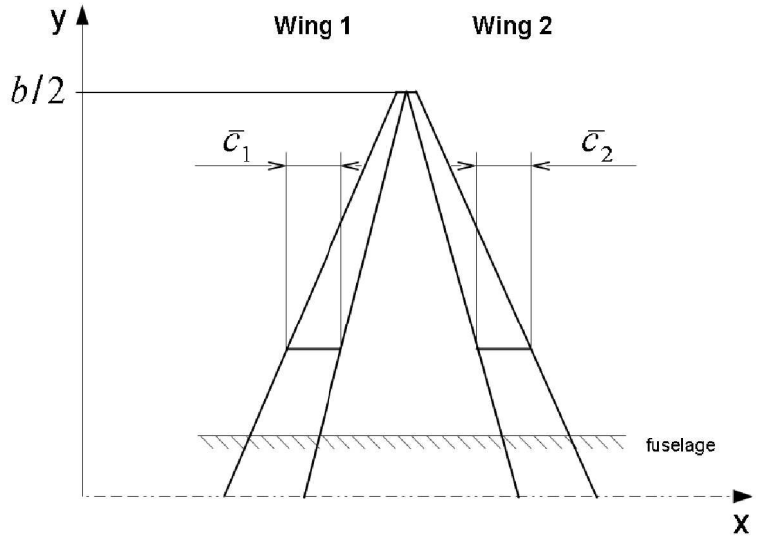

Figure A.3 Box wing consisting of two trapezoidal wings

As it was shown for the conventional wing, the MAC of each individual wing needs to be calculated first:

$$\bar{c}_1 = \frac{2}{S_1}\int_0^{b/2} c_1(y)^2\,dy \quad , \tag{A.12}$$

$$\bar{c}_2 = \frac{2}{S_2}\int_0^{b/2} c_2(y)^2\,dy \quad . \tag{A.13}$$

Now the original box wing configuration can be substituted by two rectangular wings having the individual constant chord lengths $\bar{c}_1$ and $\bar{c}_2$ (see Fig. A.4). The equation for the total MAC reads

$$\bar{c} = \frac{2}{S}\int_0^{b/2} [\bar{c}_1(y)^2 + \bar{c}_2(y)^2]\,dy \tag{A.14}$$

with

$$S = S_1 + S_2 \quad . \tag{A.15}$$

Eq. (A.14) can be written as follows:

$$\bar{c} = \frac{2}{S_1 + S_2}\left(\frac{b}{2}\cdot \bar{c}_1^{\,2} + \frac{b}{2}\cdot \bar{c}_2^{\,2}\right) \quad . \tag{A.16}$$

By introducing the individual wing areas

$$S_1 = b\cdot \bar{c}_1 \tag{A.17}$$

and

$$S_2 = b\cdot \bar{c}_2 \tag{A.18}$$

we get

$$\bar{c} = \frac{S_1 \bar{c}_1 + S_2 \bar{c}_2}{S_1 + S_2} \quad , \tag{A.19}$$

which is exactly the same correlation as for the conventional configuration.

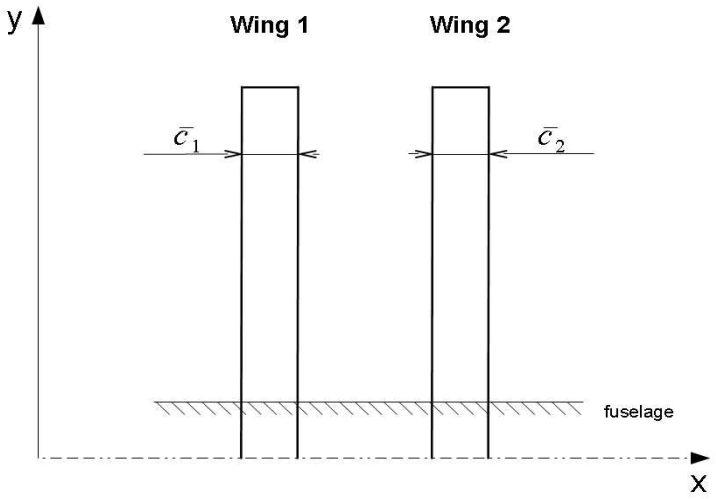

Figure A.4 Imaginary rectangular wings substituting the original forward and aft wing

Method 2
Calculation based on the consideration of pitching moments (compare **Adams 1959**)

The general equation of the pitching moment of a wing is

$$M = q_\infty \cdot C_M \cdot S \cdot \bar{c} \quad . \tag{A.20}$$

For a box wing aircraft the total wing pitching moment is the sum of the respective pitching moments induced by each wing. It is assumed that for both wings the coefficient of pitching moment is the same, so the total pitching moment reads:

$$M_{tot} = q_\infty C_M (S_1 \bar{c}_1 + S_2 \bar{c}_2) \quad . \tag{A.21}$$

According to the definition in **Adams 1959** the total pitching moment shall also be generated by an imaginary rectangular wing having the chord length $\bar{c}$, thus:

$$M_{tot} = q_\infty C_M S_{tot} \bar{c} = q_\infty C_M (S_1 + S_2) \bar{c} \quad . \tag{A.22}$$

Equating the two latter equations and substituting for $\bar{c}$ results in Eq. (A.19) shown above.

Conclusion

Both methods lead to the same result. Thus in this thesis the length of the mean aerodynamic chord of a box wing aircraft is calculated acc. to Eq. (A.19):

$$\bar{c} = \frac{S_1 \bar{c}_1 + S_2 \bar{c}_2}{S_1 + S_2} \tag{A.19}$$

A.2 Longitudinal Position of the Mean Aerodynamic Chord

For purposes of weight and balance as well as for stability considerations it is necessary to determine the longitudinal position $\bar{x}$ of the mean aerodynamic chord, which derives from the position of the total aerodynamic center of the wing configuration. The method presented below is based on an analysis of the pitching moment of the aircraft about its center of gravity. For the examination of $\bar{x}$ it is sufficient to take account of the pitching moment induced by the wings. Moments generated by the engines or the fuselage for example can be neglected. This simplification can be justified with the fact that the mean aerodynamic chord of a box wing aircraft is the chord length of an imaginary rectangular wing which substitutes both actual wings in terms of forces and moments. Due to this substitution the influence of the engines and the fuselage remains unchanged.

Fig. A.5 illustrates the considered forces and moments, as well as their substitution. The displayed relations are described in the following.

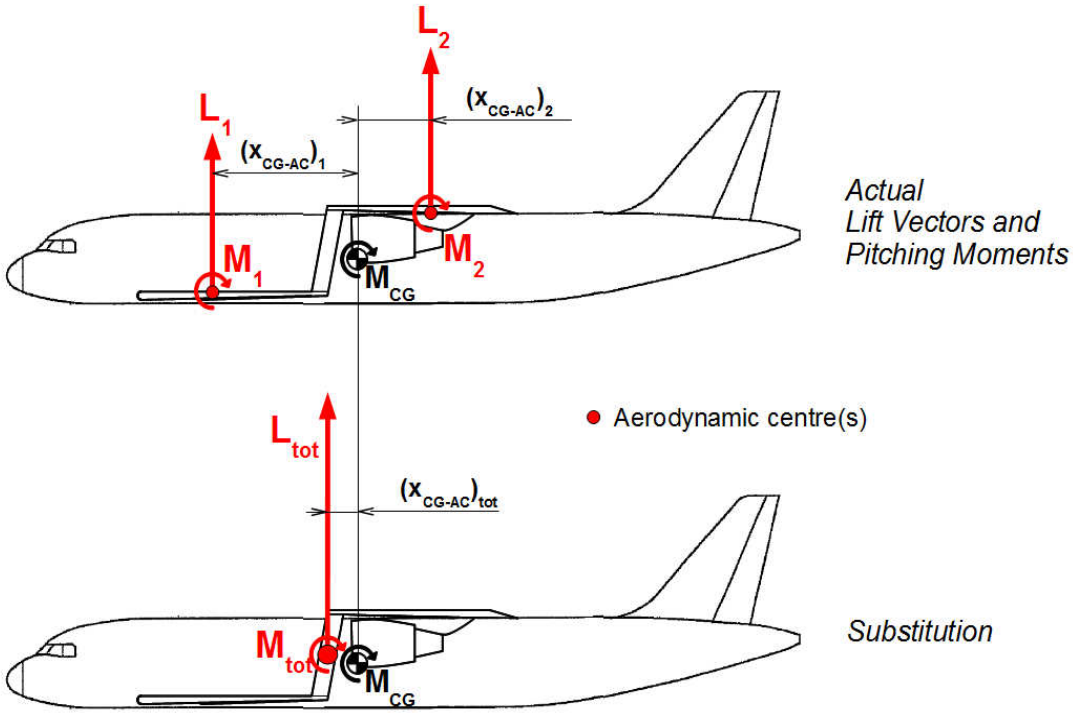

Figure A.5 Actual forces and moments acting on the box wing aircraft and their substitution

In reality there are two lift vectors and two pitching moments induced by both wings. They act on the aerodynamic center (AC) of each wing, which is assumed to be at 25% MAC of each wing. The longitudinal position of each AC is represented by the variable $(x_{CG\text{-}AC})_i$. Formulating the equilibrium of moments about the center of gravity yields

$$M_{CG} = M_1 + L_1 (x_{CG-AC})_1 + M_2 + L_2 (x_{CG-AC})_2 \quad . \tag{A.23}$$

Now all induced forces and moments are combined to one substitute force and one substitute pitching moment which both act at the total aerodynamic center of the whole wing configuration. The longitudinal position of the total aerodynamic center is assumed to equal 25% of the total mean aerodynamic chord. The equilibrium of moments based on the substitution reads

$$M_{CG} = M_{tot} + L_{tot}(x_{CG-AC})_{tot} \quad . \tag{A.24}$$

Evidently the total pitching moment M_{tot} induced by the substitute wing is a superposition of the two pitching moments M_1 and M_2 induced by the two actual wings, thus:

$$M_{tot} = M_1 + M_2 \quad . \tag{A.25}$$

Considering this condition, combining Eqs. (A.23) and (A.24) and substituting for $(x_{CG-AC})_{tot}$ finally yields:

$$(x_{CG-AC})_{tot} = \frac{L_1(x_{CG-AC})_1 + L_2(x_{CG-AC})_2}{L_1 + L_2} \quad . \tag{A.26}$$

Now the longitudinal position of the total mean aerodynamic chord can be calculated depending on the lengths and the longitudinal positions of the individual mean aerodynamic chords.

Appendix B

Flight Mechanics

B.1 Altitude for Maximum Glide Ratio as Function of the Height to Span Ratio

For understanding the consequences of high span efficiency factors regarding the maximum glide ratio a graph was shown in section 5.1.2 depicting the cruise altitude for E_{max} depending on the h/b ratio (Fig. 5.2).[6]

The reference aircraft has a mass of 73500 kg and a cruise Mach number of 0,76. Its lift coefficient for minimum induced drag is assumed to be 0,71. Since this flight condition can only be reached at altitudes in the stratosphere, the speed of sound is constant.

The speed of sound is calculated with

$$a = \sqrt{\kappa \cdot R \cdot T} \tag{B.1}$$

where κ_R = 401,8812 J/(kgK) for air. Acc. to **Anderson 2005** the temperature in the stratosphere under ISA conditions is 216,66 K, so the accordant speed of sound is 295,07 m/s.

With these data the required air density for cruise flight at maximum glide ratio can be calculated. The lift equation for this condition reads

$$L = mg = C_{L,md} \cdot \frac{\rho}{2} \cdot \left(a \cdot M\right)^2 \cdot S \quad . \tag{B.2}$$

Solving for the density gives

$$\rho = \frac{2\,mg}{C_{L,md} \cdot \left(a \cdot M\right)^2 \cdot S} \quad . \tag{B.3}$$

[6] As shown in Fig. 4.8 the span efficiency factor depends on the h/b ratio.

With the help of Eq. (5.6) $C_{L,md}$ can be calculated for any span efficiency factor, and thus for any h/b ratio. The required air density is given by Eq. (B.3). For attaining the accordant altitude the equations given in the definition of the standard atmosphere have to be used. In **Anderson 2005** the air density depending on the altitude in isothermal layers[7] of the atmosphere is given with

$$\frac{\rho}{\rho_1} = e^{-\frac{g_0}{RT}(h-h_1)} \tag{B.4}$$

where the values with the index 1 are base values given at a certain geopotential altitude. In the current case these are the values present at the tropopause ($h = h_1 = 11000$ m). Solving Eq. (B.4) for the altitude h gives

$$h(\rho) = -\frac{RT}{g_0} \cdot \ln\frac{\rho}{\rho_1} + h_1 \tag{B.5}$$

According to **NACA 1954** the values of the constants are given with

$\rho_1 = 0{,}36392$ kg/m^3,
$g_0 = 9{,}80665$ m/s,
$R = 287{,}04$ J/(kgK) and
$T = T(h = 11000\text{ m}) = 216{,}66$ K.

Now the altitude can be calculated depending on the air density.

[7] The stratosphere is an isothermal layer of the atmosphere.

B.2 Equations for Assessing Static Longitudinal Stability and Control

B.2.1 Equilibrium of Moments

The applied method is based on considerations for a conventional tail aft configuration which can be found in **Young 2001**. These considerations are now adapted to a box wing configuration.

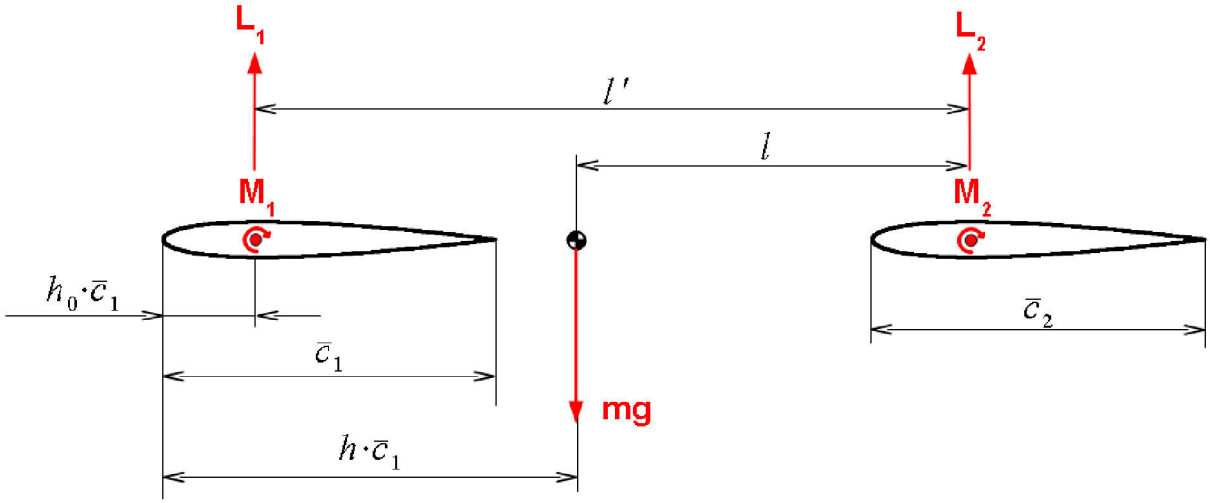

Figure B.1 Forces and moments acting on a box wing aircraft

With the assumptions made in section 5.2.2 and according to Fig. B.1, the equilibrium of moments about the aircraft's center of gravity reads

$$M_{CG} = L_1(h-h_0)\bar{c}_1 - L_2 l + M_1 + M_2 = 0 \quad . \tag{B.6}$$

From the equilibrium of vertical forces and since $mg = L$, it can be concluded that

$$L_1 = L - L_2 \quad . \tag{B.7}$$

Substituting Eq. (B.7) into Eq. (B.6) and rearranging yields

$$L(h-h_0)\bar{c}_1 - L_2\left[(h-h_0)\bar{c}_1 + l\right] + M_1 + M_2 = 0 \quad . \tag{B.8}$$

In Fig. B.1 it can be seen that

$$(h-h_0)\bar{c}_1 + l = l' \tag{B.9}$$

with *l'* being the modified lever arm. By using this simplification and deviding by $qS\bar{c}$, we get

$$C_L(h-h_0)\frac{\bar{c}_1}{\bar{c}}-C_{L,2}\frac{l'S_2}{\bar{c}S}+C_{M,1}\frac{\bar{c}_1 S_1}{\bar{c}S}+C_{M,2}\frac{\bar{c}_2 S_2}{\bar{c}S} \quad . \tag{B.10}$$

Finally the following simplifications are introduced:

$$\frac{l'S_2}{\bar{c}S}=\bar{V}' \quad , \tag{B.11}$$

$$\frac{\bar{c}_i}{\bar{c}}=\bar{c}_i' \tag{B.12}$$

and

$$\frac{S_i}{S}=s_i \quad . \tag{B.13}$$

For conventional tail aft configurations $\bar{V}'$ is referred to as the modified tail volume coefficent. For a box wing configuration this term cannot be applied any more. In the current case $\bar{V}'$ shall be called the modified volume coefficient of the aft lifting surface. With the above simplifications the final equation reads

$$C_L(h-h_0)\bar{c}_1'-C_{L,2}\bar{V}'+C_{M,1}\bar{c}_1' s_1+C_{M,2}\bar{c}_2' s_2 \quad . \tag{B.14}$$

B.2.2 Lift Curve Slope of the Whole Aircraft

The original equation for an aircraft having two surfaces of equal span, taken from **DATCOM 1978**, Section 4.5.1.1, par. A, Method 2, reads:

$$\frac{dC_L}{d\alpha} = \left(\frac{dC_L}{d\alpha}\right)_{e,1} \left[K_N + K_{W(B)} + K_{B(W)}\right]_1 \frac{S_{e,1}}{S_1} + \left(\frac{dC_L}{d\alpha}\right)_{e,2} \left[K_{W(B)} + K_{B(W)}\right]_2 \frac{q_2}{q_\infty} \frac{S_2}{S_1} \frac{S_{e,2}}{S_2} + \left(\frac{dC_L}{d\alpha}\right)_{W_2(v)} \quad . \tag{B.15}$$

where

$$\left(\frac{dC_L}{d\alpha}\right)_{W_2(v)} = \frac{\left(\frac{dC_L}{d\alpha}\right)_{e,1} \cdot \frac{S_{e,1}}{S_1} \cdot \left(\frac{dC_L}{d\alpha}\right)_{e,2} \cdot \frac{q_2}{q_\infty} \cdot K_{W(B),1} \cdot I_{V_{W,1(W,2)}} \cdot \left(\frac{b_2}{2} - \frac{d_2}{2}\right)}{2\pi \cdot A_{e,2} \cdot \left(\frac{b_1}{2} - \frac{d_1}{2}\right)} \quad . \tag{B.16}$$

At first it is assumed that the lift curve slope is the same for the exposed and the reference wing area, so it can be written that:

$$\left(\frac{dC_L}{d\alpha}\right)_{e,i} = \left(\frac{dC_L}{d\alpha}\right)_i \quad . \tag{B.17}$$

It is also assumed that for a wing the exposed aspect ratio is the same as the aspect ratio based on the reference area:

$$A_{e,i} = A_i \quad . \tag{B.18}$$

Next it will be shown that Eq. (B.15) in its apparent form cannot be used for a box wing aircraft. All aerodynamic coefficients of the total box wing aircraft are based on the total wing area. However, in Eq. (B.15) these coefficients are based on the front wing area. This statement can be proved by the following simple considerations:

The lift coefficient in the linear region of the lift curve slope is calculated by

$$C_L = \frac{dC_L}{d\alpha} \cdot \alpha \tag{B.19}$$

with α being measured in relation to the zero lift line.

When there are two lifting surfaces, the total lift coefficient is calculated by

$$C_L = \frac{C_{L,1} S_1 + C_{L,2} S_2}{S_{ref}} \quad , \tag{B.20}$$

as it was shown in section 4.1.2.

Applying Eq. (B.19) for two lifting surfaces and neglecting any downwash yields

$$C_L = \frac{\left(\frac{dC_L}{d\alpha}\right)_1 \alpha_1 S_1 + \left(\frac{dC_L}{d\alpha}\right)_2 \alpha_2 S_2}{S_{ref}} \tag{B.21}$$

Assuming that $\alpha_1 = \alpha_2 = \alpha$ and differentiating Eq. (5.31) with regard to α yields

$$\frac{dC_L}{d\alpha} = \frac{\left(\frac{dC_L}{d\alpha}\right)_1 S_1 + \left(\frac{dC_L}{d\alpha}\right)_2 S_2}{S_{ref}} \quad . \tag{B.22}$$

If the area of the forward wing S_1 is taken as reference area, the area weighting factors are *one* for the forward wing and S_2/S_1 for the aft wing. This weighting is used in the DATCOM equation [Eq. (B.15)]. If the reference area is the sum of both the individual wing areas, as it is the case for a box wing configuration, the weighting factors are S_1/S and S_2/S, which can also be expressed with s_1 and s_2.

So finally Eq. (B.15) is adapted as follows.

$$\begin{aligned}\left(\frac{dC_L}{d\alpha}\right) = {} & s_1 \left(\frac{dC_L}{d\alpha}\right)_1 \cdot \left(K_N + K_{W(B)} + K_{B(W)}\right)_1 \cdot \frac{S_{e,1}}{S_1} \\ & + s_2 \left(\frac{dC_L}{d\alpha}\right)_2 \cdot \left(K_{W(B)} + K_{B(W)}\right)_2 \cdot \frac{q_2}{q_\infty} \cdot \frac{S_{e,2}}{S_2} + \left(\frac{dC_L}{d\alpha}\right)_{W_2(v)}\end{aligned} \tag{B.23}$$

Next it is shown how Eq. (5.32) is determined for calculating the factor $K_{W(B)}$ considering additional lift effects due to wing body interferences.

The individual values of the factors $K_{W(B)}$ and $K_{B(W)}$ can be taken from the chart given in **DATCOM 1978**, page 4.3.1.2-10. This chart is shown in Fig. B.2. It is illustrated that the *K*-factors only depend on the ratio *d*/*b* (fuselage diameter to wing span). Their values can be approximated by linear functions for *d*/*b* ratios of up to 0,2. The ratio of the for the box wing aircraft is about 0,12 , so this approximation is feasible. For evaluating Eq. (5.29)/(B.16) only the factor $K_{W(B)}$ is needed. It can be approximated by

$$K_{W(B)}\left(\frac{d}{b}\right) = 0{,}8\frac{d}{b}+1\,; \qquad 0 \leqslant \frac{d}{b} < 0{,}2 \quad . \tag{B.24}$$

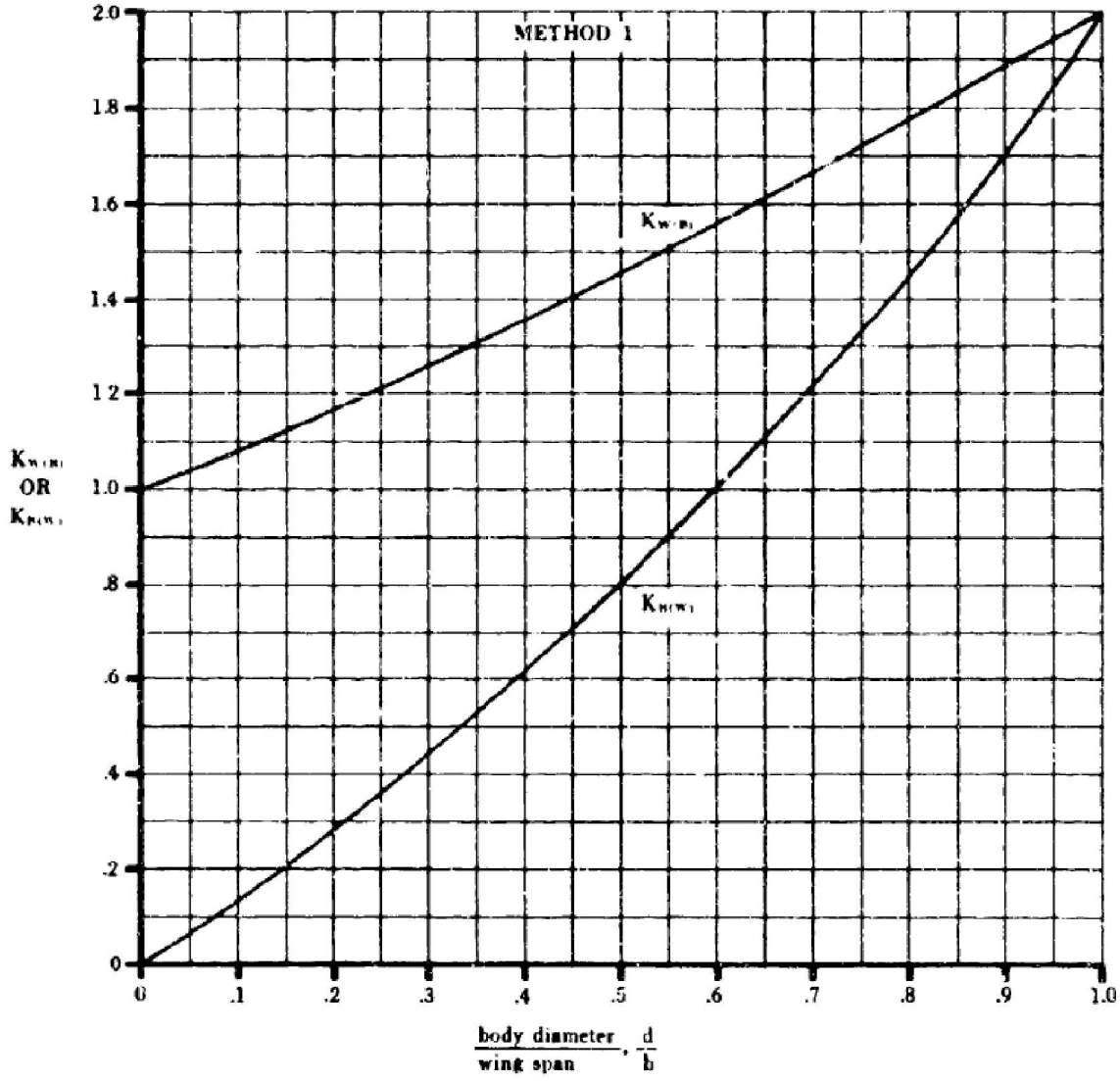

Figure B.2 *K*-factors for considering lift effects due to wing body interferences (**DATCOM 1978**)

Finally the determination of the vortex interference factor $I_{V_{W,1(W,2)}}$ will be discussed.

The used method is taken from **DATCOM 1978**, Section 4.4.1, par. A, Method 3. There, on page 4.4.1-8 it can be read:

> *"For configurations in which the span of the forward surface is approximately equal to or less than that of the aft surface, the following method* (…) *is recommended.*
>
> *Step 1.*
> *The spatial position of the trailing vortices is first determined relative to the aft surface. The lateral spacing is determined from Figure 4.4.1-71 as a function of the exposed forward-surface planform geometry. This spacing is invariant with longitudinal distance and angle of attack. The vertical position is determined by assuming that the vortex springs from the trailing edge at the previously determined lateral position and trails in the free-stream direction. The pertinent vertical dimension is the distance between the quarter-chord point of the MAC of the aft surface and the vortex as determined above.*
>
> *Step 2.*
> *The vortex interference factor* (…) *is obtained* (...) *as a function of the lateral and vertical vortex positions, determined in Step I above, and the geometry of the aft panel.* (...)
>
> *Step 3.*
> *The vortex interference factor so determined is used in Sections 4.5.1.1 and 4.5.1.2 to obtain the lift generated on the aft surface for complete wing-body-tail combinations."*

Step 1

At first the lateral position of the trailing vortices needs to be determined. Fig. B.3 shows the related chart, taken from DATCOM Figure 4.4.1-71. Assuming that the taper ratio will be about 0,5 or a bit lower it can be concluded that the factor $(b_V'/2 - d'/2)/(b'/2 - d'/2)$ is about 0,75 , independently from the effective aspect ratio and the wing sweep.

The vertical distance between the forward wing trailing vortices and the aft wing is assumed to be the same as the vertical distance between these two wings. This can be justified with the vortices trailing in the free stream direction assuming that the angle between the center line of the aircraft and the free stream is zero.

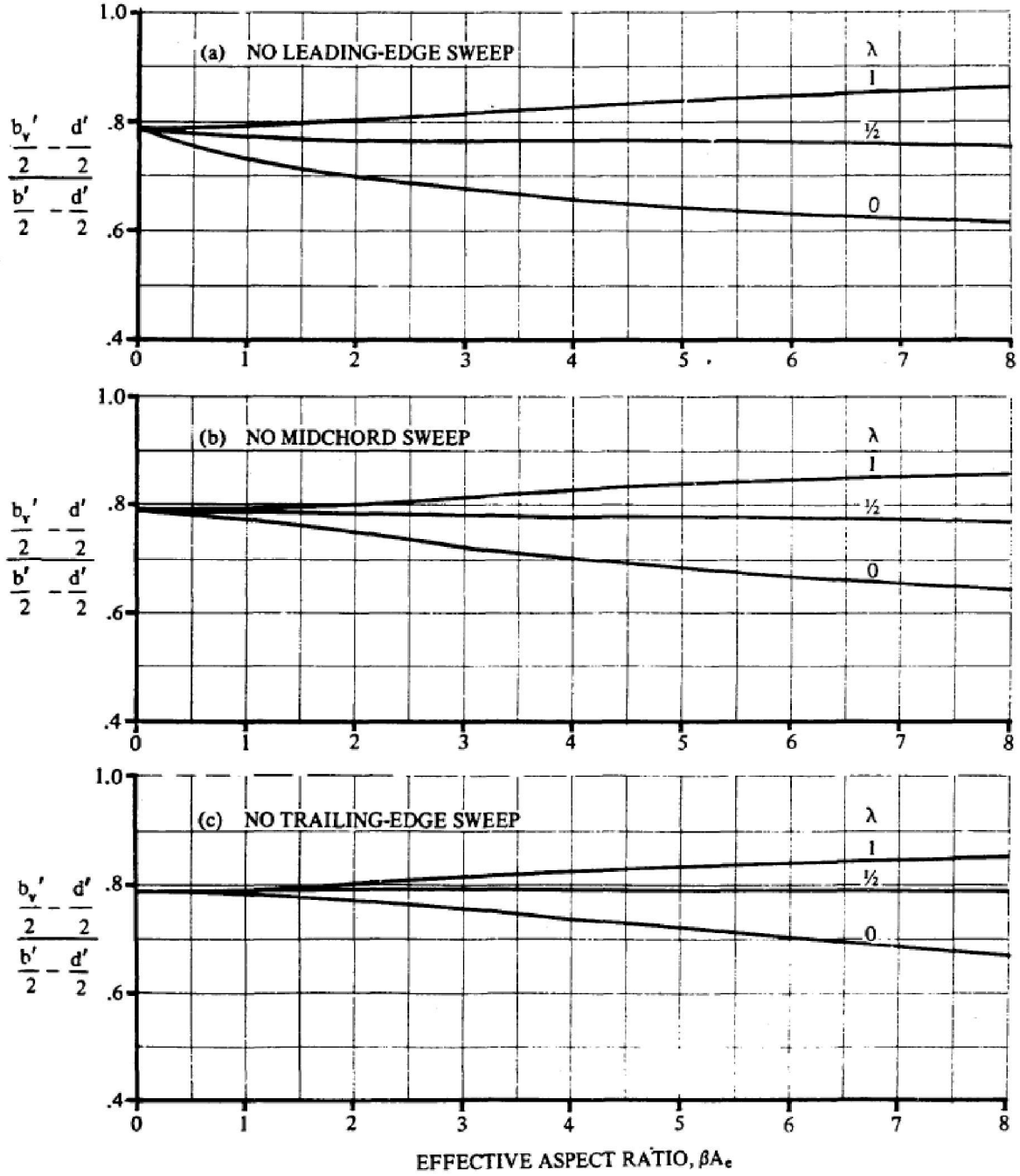

Figure B.3 Lateral vortex position depending on effective aspect ratio and wing and body geometry (**DATCOM 1978**)

Step 2

Once the position of the trailing vortices is known, the vortex interference factor can be determined with the help of the charts from pages 4.3.1.3-7 to 4.3.1.3-12 in **DATCOM 1978**. There the vortex interference factor is shown depending on the vortex position, the taper ratio of the wing and the ratio of fuselage diameter to half of the wing span. As already described in chapter 5.2.2 there are no charts for the exact geometric parameters of the box wing aircraft. So a chart is used where these parameters come closest to the parameters of the box wing aircraft (λ = 0,5; $r/0{,}5b_W$ = 0,2; see Fig. B.4).

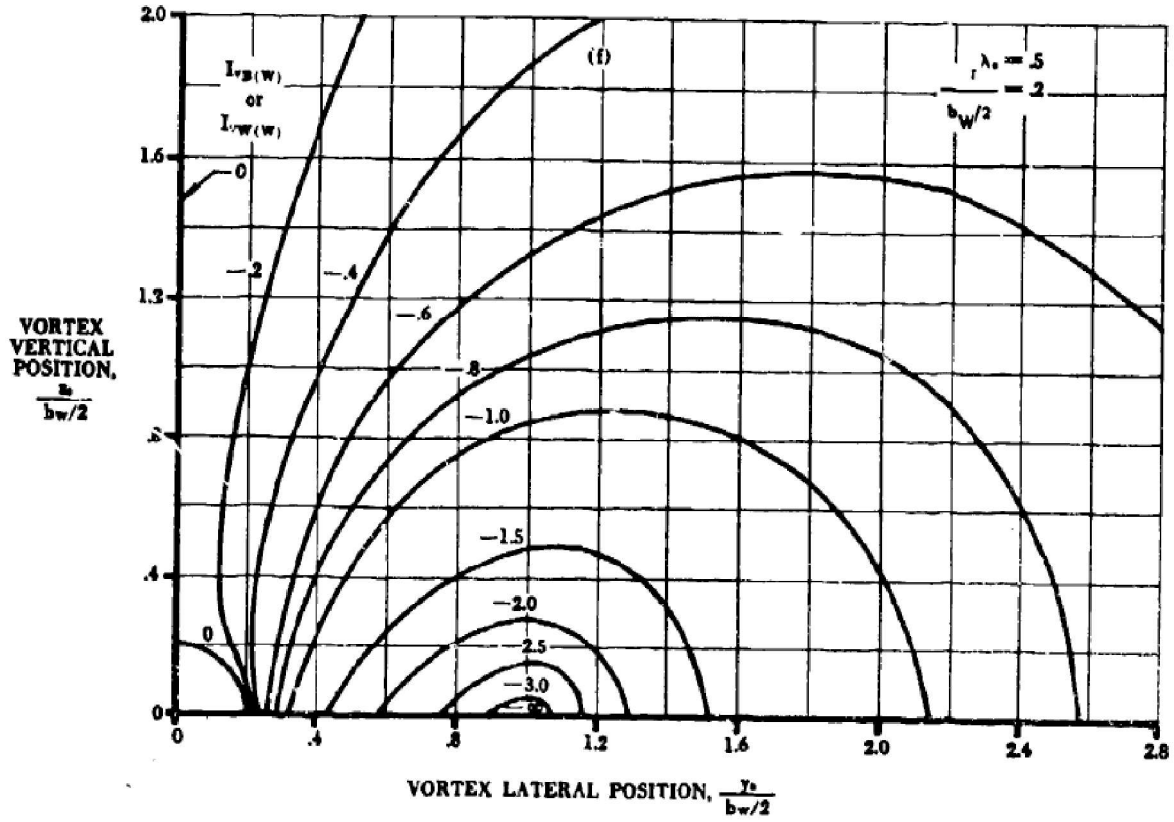

Figure B.4 Vortex interference factor depending on vortex position, wing and fuselage geometry (**DATCOM 1978**)

The lateral vortex position is expressed by $y_0/0{,}5b_W$ in Fig. B.4. However, in Fig. B.3 this position has been referenced as $(b_V'/2 - d'/2)/(b'/2 - d'/2)$. So at first it has to be converted.

Acc. to Fig. B.3 it was concluded that

$$\frac{\frac{b_{V,1}}{2} - \frac{d_1}{2}}{\frac{b_1}{2} - \frac{d_1}{2}} = 0{,}75 \quad . \tag{B.25}$$

The ratio d_1/b_1 is 0,2 acc. to Fig. B.4, so $d_1 = 0{,}2b_1$. Introducing this condition to Eq. (B.25) and rearranging yields

$$\frac{b_{V,1}}{b_1} = 0{,}8 \quad , \tag{B.26}$$

which is the same as $y_0/0{,}5b_W$ in Fig. B.4, since $y_0 = 0{,}5b_V$ and $b_1 = b_W$.

The vertical vortex position is expressed as $z_0/0{,}5b_W$ in Fig. B.4, which is the same as $2h/b$, meaning double the h/b ratio of the box wing.

Now it is possible to get the vortex interference factor depending on the h/b ratio from Fig. B.4 with the value 0,8 for the abscissa. The results for probable h/b ratios were summarized in table 5.1 in chapter 5.2.2.

Appendix C

Wing Design Data

C.1 Span Wise Lift Distribution

In this section the values of lift distribution per unit span are given for the span stations the lift distribution is approximated with for the determination of the internal loads of the wing structure. The lift distribution was modelled so that it is the optimum distribution with regard to aerodynamics. The values were determined according to the method presented in section 7.6.2 and with the help of the box wing sizing sheet (see Appendix F.2).

C.1.1 Box Wing Configuration

Table C.1 Span wise lift distribution of forward wing

Span Station No.	y (m)	$q_{L,ell}$ (kN/m)	$q_{L,const}$ (kN/m)	$q_{L,tot}$ (kN/m)
1	0	0,000	0,000	0,000
2	0,5	0,000	0,000	0,000
3	1	8,280	8,299	16,579
4	1,5	8,294	8,299	16,593
5	2	8,299	8,299	16,597
6	3,67	8,247	8,299	16,546
7	5,34	8,090	8,299	16,389
8	7,01	7,822	8,299	16,121
9	8,68	7,430	8,299	15,729
10	10,35	6,894	8,299	15,193
11	13	5,642	8,299	13,941
12	16	2,979	8,299	11,278
13	16,75	1,509	8,299	9,807
14	17	0,000	8,299	8,299

Table C.2 Span wise lift distribution of aft wing

Span Station No.	y (m)	$q_{L,ell}$ (kN/m)	$q_{L,const}$ (kN/m)	$q_{L,tot}$ (kN/m)
1	0	4,200	4,200	8,400
2	1,175	4,190	4,200	8,389
3	2,35	4,159	4,200	8,359
4	3,525	4,108	4,200	8,308
5	4,7	4,036	4,200	8,236
6	7	3,827	4,200	8,027
7	10	3,396	4,200	7,596
8	13	2,706	4,200	6,906
9	15	1,976	4,200	6,176
10	15,5	1,725	4,200	5,925
11	16,25	1,234	4,200	5,433
12	16,75	0,718	4,200	4,917
13	17	0,000	4,200	4,200

The lift distribution of the winglets is linear. The values on the edges are the values of the connected wing tips, which are 8,299 kN/m for the forward wing and 4,2 kN/m for the aft wing.

C.1.2 Reference Configuration

Table C.3 Span wise lift distribution of reference wing

Span Station No.	y (m)	q_L (kN/m)
1	0	0,000
2	0,5	0,000
3	1	28,234
4	1,5	28,282
5	2	28,297
6	5	27,726
7	7	26,679
8	9	25,027
9	11	22,638
10	13	19,238
11	15	14,117
12	16	10,159
13	16,75	5,145
14	17	0,000

C.2 Internal Loads for Wing Mass Estimation

In the following tables the absolute values of the internal wing loads are given for the wing mass estimation. Whether bending moments are positive or negative is not of importance because no distinction is made between tensile and compression stresses. The algebraic sign of the shear forces is unimportant for a the wing mass estimation anyway. Normal forces are not given because they were neglected in the analysis. All loads apply for a load factor of 3,75.

C.2.1 Box Wing Configuration with Rigid Joints

Table C.4 shows the absolute values of the internal loads of the forward wing except for the center wing box. So the origin of the y-coordinates is not the wing root but the point where the wing intersects the fuselage. In the center wing box shear forces are assumed to be zero and the bending moment has the value of the point where the wing intersects the fuselage.

Tables C.5 and C.6 give the absolute values of the internal loads of the aft wing. It is divided into two parts. The inner part goes from the wing root to the connection with the vertical stabilizer (y = 4,7 m), the outer part from the connection with the vertical stabilizer to the wing tip.

Table C.4 Absolute values of the internal loads of the forward wing (rigid joints)

Span Station (m)	Shear Force (kN)	Bending Moment (kNm)
0,00E+00	6,23E+02	2,40E+03
3,03E-01	6,05E+02	2,19E+03
6,05E-01	5,87E+02	1,99E+03
9,08E-01	5,69E+02	1,79E+03
1,21E+00	5,50E+02	1,59E+03
1,51E+00	5,32E+02	1,41E+03
1,82E+00	5,14E+02	1,23E+03
2,12E+00	4,96E+02	1,05E+03
2,42E+00	4,78E+02	8,86E+02
2,72E+00	4,59E+02	7,25E+02
3,03E+00	4,41E+02	5,70E+02
3,33E+00	4,23E+02	4,21E+02
3,63E+00	4,05E+02	2,78E+02
3,94E+00	3,87E+02	1,42E+02
4,24E+00	3,69E+02	1,14E+01
4,54E+00	3,51E+02	1,13E+02
4,84E+00	3,34E+02	2,31E+02
5,15E+00	3,16E+02	3,43E+02
5,45E+00	2,98E+02	4,48E+02
5,75E+00	2,81E+02	5,48E+02
6,05E+00	2,63E+02	6,41E+02
6,36E+00	2,46E+02	7,29E+02
6,66E+00	2,28E+02	8,10E+02
6,96E+00	2,11E+02	8,86E+02
7,26E+00	1,94E+02	9,56E+02
7,57E+00	1,77E+02	1,02E+03
7,87E+00	1,60E+02	1,08E+03
8,17E+00	1,43E+02	1,13E+03
8,47E+00	1,26E+02	1,18E+03
8,78E+00	1,09E+02	1,22E+03
9,08E+00	9,28E+01	1,25E+03
9,38E+00	7,65E+01	1,28E+03
9,69E+00	6,03E+01	1,30E+03
9,99E+00	4,43E+01	1,32E+03
1,03E+01	2,84E+01	1,33E+03
1,06E+01	1,28E+01	1,34E+03
1,09E+01	2,79E+00	1,34E+03
1,12E+01	1,82E+01	1,34E+03
1,15E+01	3,33E+01	1,33E+03
1,18E+01	4,81E+01	1,32E+03
1,21E+01	6,26E+01	1,30E+03
1,24E+01	7,69E+01	1,27E+03
1,27E+01	9,08E+01	1,24E+03
1,30E+01	1,04E+02	1,21E+03
1,33E+01	1,18E+02	1,17E+03
1,36E+01	1,31E+02	1,13E+03
1,39E+01	1,44E+02	1,08E+03
1,42E+01	1,56E+02	1,03E+03
1,45E+01	1,68E+02	9,75E+02
1,48E+01	1,79E+02	9,15E+02
1,51E+01	1,89E+02	8,52E+02

Table C.5 Absolute values of the internal loads of the aft wing, inner part (rigid joints)

Span Station (m)	Shear Force (kN)	Bending Moment (kNm)
0,00E+00	1,70E-03	5,26E+02
1,88E-01	5,70E+00	5,26E+02
3,76E-01	1,14E+01	5,28E+02
5,64E-01	1,71E+01	5,31E+02
7,52E-01	2,28E+01	5,35E+02
9,40E-01	2,85E+01	5,41E+02
1,13E+00	3,42E+01	5,47E+02
1,32E+00	3,99E+01	5,55E+02
1,50E+00	4,56E+01	5,64E+02
1,69E+00	5,13E+01	5,74E+02
1,88E+00	5,70E+01	5,85E+02
2,07E+00	6,27E+01	5,97E+02
2,26E+00	6,84E+01	6,11E+02
2,44E+00	7,40E+01	6,26E+02
2,63E+00	7,97E+01	6,42E+02
2,82E+00	8,54E+01	6,59E+02
3,01E+00	9,10E+01	6,77E+02
3,20E+00	9,67E+01	6,97E+02
3,38E+00	1,02E+02	7,17E+02
3,57E+00	1,08E+02	7,39E+02
3,76E+00	1,14E+02	7,62E+02
3,95E+00	1,19E+02	7,86E+02
4,14E+00	1,25E+02	8,11E+02
4,32E+00	1,31E+02	8,38E+02
4,51E+00	1,36E+02	8,65E+02
4,70E+00	1,42E+02	8,94E+02

Table C.6 Absolute values of the internal loads of the aft wing, outer part (rigid joints)

Span Station (m)	Shear Force (kN)	Bending Moment (kNm)
0,00E+00	4,74E+02	2,34E+03
2,46E-01	4,67E+02	2,21E+03
4,92E-01	4,60E+02	2,08E+03
7,38E-01	4,53E+02	1,96E+03
9,84E-01	4,45E+02	1,84E+03
1,23E+00	4,38E+02	1,72E+03
1,48E+00	4,31E+02	1,60E+03
1,72E+00	4,24E+02	1,48E+03
1,97E+00	4,16E+02	1,37E+03
2,21E+00	4,09E+02	1,26E+03
2,46E+00	4,02E+02	1,15E+03
2,71E+00	3,95E+02	1,04E+03
2,95E+00	3,88E+02	9,31E+02
3,20E+00	3,81E+02	8,27E+02
3,44E+00	3,74E+02	7,25E+02
3,69E+00	3,67E+02	6,24E+02
3,94E+00	3,60E+02	5,25E+02
4,18E+00	3,53E+02	4,29E+02
4,43E+00	3,46E+02	3,34E+02
4,67E+00	3,39E+02	2,41E+02
4,92E+00	3,33E+02	1,50E+02
5,17E+00	3,26E+02	6,01E+01
5,41E+00	3,19E+02	2,74E+01
5,66E+00	3,12E+02	1,13E+02
5,90E+00	3,06E+02	1,97E+02
6,15E+00	2,99E+02	2,79E+02
6,40E+00	2,93E+02	3,59E+02
6,64E+00	2,86E+02	4,38E+02
6,89E+00	2,80E+02	5,14E+02
7,13E+00	2,73E+02	5,89E+02
7,38E+00	2,67E+02	6,63E+02
7,63E+00	2,61E+02	7,34E+02
7,87E+00	2,54E+02	8,04E+02
8,12E+00	2,48E+02	8,72E+02
8,36E+00	2,42E+02	9,39E+02
8,61E+00	2,36E+02	1,00E+03
8,86E+00	2,30E+02	1,07E+03
9,10E+00	2,24E+02	1,13E+03
9,35E+00	2,18E+02	1,19E+03
9,59E+00	2,12E+02	1,25E+03
9,84E+00	2,07E+02	1,30E+03
1,01E+01	2,01E+02	1,36E+03
1,03E+01	1,96E+02	1,41E+03
1,06E+01	1,90E+02	1,46E+03
1,08E+01	1,85E+02	1,52E+03
1,11E+01	1,80E+02	1,57E+03
1,13E+01	1,75E+02	1,61E+03
1,16E+01	1,70E+02	1,66E+03
1,18E+01	1,65E+02	1,70E+03
1,21E+01	1,60E+02	1,75E+03
1,23E+01	1,56E+02	1,79E+03

C.2.2 Box Wing Configuration with Flexible Joints

The tables in this section are distributed the same way as in Appendix C.2.1.

Table C.7 Absolute values of the internal loads of the forward wing (flexible joints)

Span Station	Shear Force (kN)	Bending Moment (kNm)
0,00E+00	7,05E+02	4,66E+03
3,03E-01	6,87E+02	4,42E+03
6,05E-01	6,69E+02	4,19E+03
9,08E-01	6,51E+02	3,96E+03
1,21E+00	6,32E+02	3,74E+03
1,51E+00	6,14E+02	3,53E+03
1,82E+00	5,96E+02	3,32E+03
2,12E+00	5,78E+02	3,12E+03
2,42E+00	5,59E+02	2,92E+03
2,72E+00	5,41E+02	2,73E+03
3,03E+00	5,23E+02	2,55E+03
3,33E+00	5,05E+02	2,37E+03
3,63E+00	4,87E+02	2,20E+03
3,94E+00	4,69E+02	2,04E+03
4,24E+00	4,51E+02	1,88E+03
4,54E+00	4,33E+02	1,73E+03
4,84E+00	4,16E+02	1,58E+03
5,15E+00	3,98E+02	1,44E+03
5,45E+00	3,80E+02	1,31E+03
5,75E+00	3,62E+02	1,18E+03
6,05E+00	3,45E+02	1,06E+03
6,36E+00	3,27E+02	9,41E+02
6,66E+00	3,10E+02	8,31E+02
6,96E+00	2,93E+02	7,27E+02
7,26E+00	2,76E+02	6,29E+02
7,57E+00	2,58E+02	5,38E+02
7,87E+00	2,42E+02	4,51E+02
8,17E+00	2,25E+02	3,71E+02
8,47E+00	2,08E+02	2,97E+02
8,78E+00	1,91E+02	2,28E+02
9,08E+00	1,75E+02	1,65E+02
9,38E+00	1,58E+02	1,08E+02
9,69E+00	1,42E+02	5,59E+01
9,99E+00	1,26E+02	9,70E+00
1,03E+01	1,10E+02	3,10E+01
1,06E+01	9,47E+01	6,63E+01
1,09E+01	7,91E+01	9,63E+01
1,12E+01	6,38E+01	1,21E+02
1,15E+01	4,86E+01	1,40E+02
1,18E+01	3,38E+01	1,54E+02
1,21E+01	1,93E+01	1,64E+02
1,24E+01	5,06E+00	1,68E+02
1,27E+01	8,88E+00	1,67E+02
1,30E+01	2,25E+01	1,62E+02
1,33E+01	3,59E+01	1,51E+02
1,36E+01	4,89E+01	1,37E+02
1,39E+01	6,17E+01	1,18E+02
1,42E+01	7,42E+01	9,45E+01
1,45E+01	8,60E+01	6,69E+01
1,48E+01	9,73E+01	3,53E+01
1,51E+01	1,07E+02	7,35E-13

Table C.8 Absolute values of the internal loads of the aft wing, inner part (flexible joints)

Span Station	Shear Force (kN)	Bending Moment (kNm)
0,00E+00	8,17E-13	3,21E+03
1,88E-01	5,71E+00	3,21E+03
3,76E-01	1,14E+01	3,21E+03
5,64E-01	1,71E+01	3,21E+03
7,52E-01	2,28E+01	3,22E+03
9,40E-01	2,85E+01	3,22E+03
1,13E+00	3,42E+01	3,23E+03
1,32E+00	3,99E+01	3,24E+03
1,50E+00	4,56E+01	3,25E+03
1,69E+00	5,13E+01	3,26E+03
1,88E+00	5,70E+01	3,27E+03
2,07E+00	6,27E+01	3,28E+03
2,26E+00	6,84E+01	3,29E+03
2,44E+00	7,40E+01	3,31E+03
2,63E+00	7,97E+01	3,33E+03
2,82E+00	8,54E+01	3,34E+03
3,01E+00	9,10E+01	3,36E+03
3,20E+00	9,67E+01	3,38E+03
3,38E+00	1,02E+02	3,40E+03
3,57E+00	1,08E+02	3,42E+03
3,76E+00	1,14E+02	3,45E+03
3,95E+00	1,19E+02	3,47E+03
4,14E+00	1,25E+02	3,49E+03
4,32E+00	1,31E+02	3,52E+03
4,51E+00	1,36E+02	3,55E+03
4,70E+00	1,42E+02	3,58E+03

Table C.9 Absolute values of the internal loads of the aft wing, outer part (flexible joints)

Span Station	Shear Force (kN)	Bending Moment (kNm)
0,00E+00	4,34E+02	3,58E+03
2,46E-01	4,27E+02	3,46E+03
4,92E-01	4,19E+02	3,35E+03
7,38E-01	4,12E+02	3,23E+03
9,84E-01	4,05E+02	3,12E+03
1,23E+00	3,98E+02	3,01E+03
1,48E+00	3,90E+02	2,91E+03
1,72E+00	3,83E+02	2,80E+03
1,97E+00	3,76E+02	2,70E+03
2,21E+00	3,69E+02	2,60E+03
2,46E+00	3,62E+02	2,50E+03
2,71E+00	3,55E+02	2,40E+03
2,95E+00	3,48E+02	2,31E+03
3,20E+00	3,41E+02	2,21E+03
3,44E+00	3,34E+02	2,12E+03
3,69E+00	3,27E+02	2,03E+03
3,94E+00	3,20E+02	1,94E+03
4,18E+00	3,13E+02	1,86E+03
4,43E+00	3,06E+02	1,78E+03
4,67E+00	2,99E+02	1,69E+03
4,92E+00	2,92E+02	1,61E+03
5,17E+00	2,85E+02	1,53E+03
5,41E+00	2,79E+02	1,46E+03
5,66E+00	2,72E+02	1,38E+03
5,90E+00	2,65E+02	1,31E+03
6,15E+00	2,59E+02	1,24E+03
6,40E+00	2,52E+02	1,17E+03
6,64E+00	2,46E+02	1,10E+03
6,89E+00	2,39E+02	1,04E+03
7,13E+00	2,33E+02	9,72E+02
7,38E+00	2,26E+02	9,10E+02
7,63E+00	2,20E+02	8,50E+02
7,87E+00	2,14E+02	7,91E+02
8,12E+00	2,08E+02	7,34E+02
8,36E+00	2,01E+02	6,78E+02
8,61E+00	1,95E+02	6,24E+02
8,86E+00	1,89E+02	5,72E+02
9,10E+00	1,83E+02	5,21E+02
9,35E+00	1,78E+02	4,73E+02
9,59E+00	1,72E+02	4,25E+02
9,84E+00	1,66E+02	3,79E+02
1,01E+01	1,61E+02	3,35E+02
1,03E+01	1,55E+02	2,92E+02
1,06E+01	1,50E+02	2,51E+02
1,08E+01	1,44E+02	2,11E+02
1,11E+01	1,39E+02	1,72E+02
1,13E+01	1,34E+02	1,35E+02
1,16E+01	1,29E+02	9,96E+01
1,18E+01	1,24E+02	6,52E+01
1,21E+01	1,20E+02	3,20E+01
1,23E+01	1,16E+02	1,13E-12

C.2.3 Reference Configuration

As for the forward wing of the box wing configuration the values for the center wing box are not given, so the origin for the y-coordinates is the intersection of wing and fuselage. For the center wing box shear loads are assumed to be zero and the bending moment has the value of the wing-fuselage-intersection.

Table C.10 Absolute values of the internal loads of the reference wing

Span Station (m)	Shear Force (kN)	Bending Moment (kNm)
0,00E+00	1,23E+03	8,63E+03
3,03E-01	1,20E+03	8,23E+03
6,05E-01	1,17E+03	7,83E+03
9,08E-01	1,14E+03	7,45E+03
1,21E+00	1,11E+03	7,07E+03
1,51E+00	1,07E+03	6,71E+03
1,82E+00	1,04E+03	6,35E+03
2,12E+00	1,01E+03	6,01E+03
2,42E+00	9,80E+02	5,68E+03
2,72E+00	9,49E+02	5,36E+03
3,03E+00	9,17E+02	5,04E+03
3,33E+00	8,86E+02	4,74E+03
3,63E+00	8,55E+02	4,45E+03
3,94E+00	8,25E+02	4,17E+03
4,24E+00	7,94E+02	3,90E+03
4,54E+00	7,64E+02	3,64E+03
4,84E+00	7,34E+02	3,39E+03
5,15E+00	7,04E+02	3,15E+03
5,45E+00	6,74E+02	2,92E+03
5,75E+00	6,44E+02	2,70E+03
6,05E+00	6,15E+02	2,49E+03
6,36E+00	5,86E+02	2,29E+03
6,66E+00	5,58E+02	2,10E+03
6,96E+00	5,29E+02	1,92E+03
7,26E+00	5,01E+02	1,75E+03
7,57E+00	4,74E+02	1,58E+03
7,87E+00	4,47E+02	1,43E+03
8,17E+00	4,20E+02	1,28E+03
8,47E+00	3,93E+02	1,15E+03
8,78E+00	3,67E+02	1,02E+03
9,08E+00	3,42E+02	9,04E+02
9,38E+00	3,17E+02	7,94E+02
9,69E+00	2,92E+02	6,92E+02
9,99E+00	2,69E+02	5,99E+02
1,03E+01	2,45E+02	5,13E+02
1,06E+01	2,23E+02	4,35E+02
1,09E+01	2,00E+02	3,64E+02
1,12E+01	1,79E+02	3,01E+02
1,15E+01	1,58E+02	2,45E+02
1,18E+01	1,39E+02	1,95E+02
1,21E+01	1,20E+02	1,52E+02
1,24E+01	1,02E+02	1,15E+02
1,27E+01	8,44E+01	8,41E+01
1,30E+01	6,81E+01	5,87E+01
1,33E+01	5,30E+01	3,85E+01
1,36E+01	3,92E+01	2,32E+01
1,39E+01	2,67E+01	1,22E+01
1,42E+01	1,59E+01	5,18E+00
1,45E+01	7,26E+00	1,38E+00
1,48E+01	1,10E+00	6,90E-02
1,51E+01	4,05E-12	3,32E-12

Appendix D

Configuration Drawings

D.1 Final Box Wing Configuration, Scaled Drawings

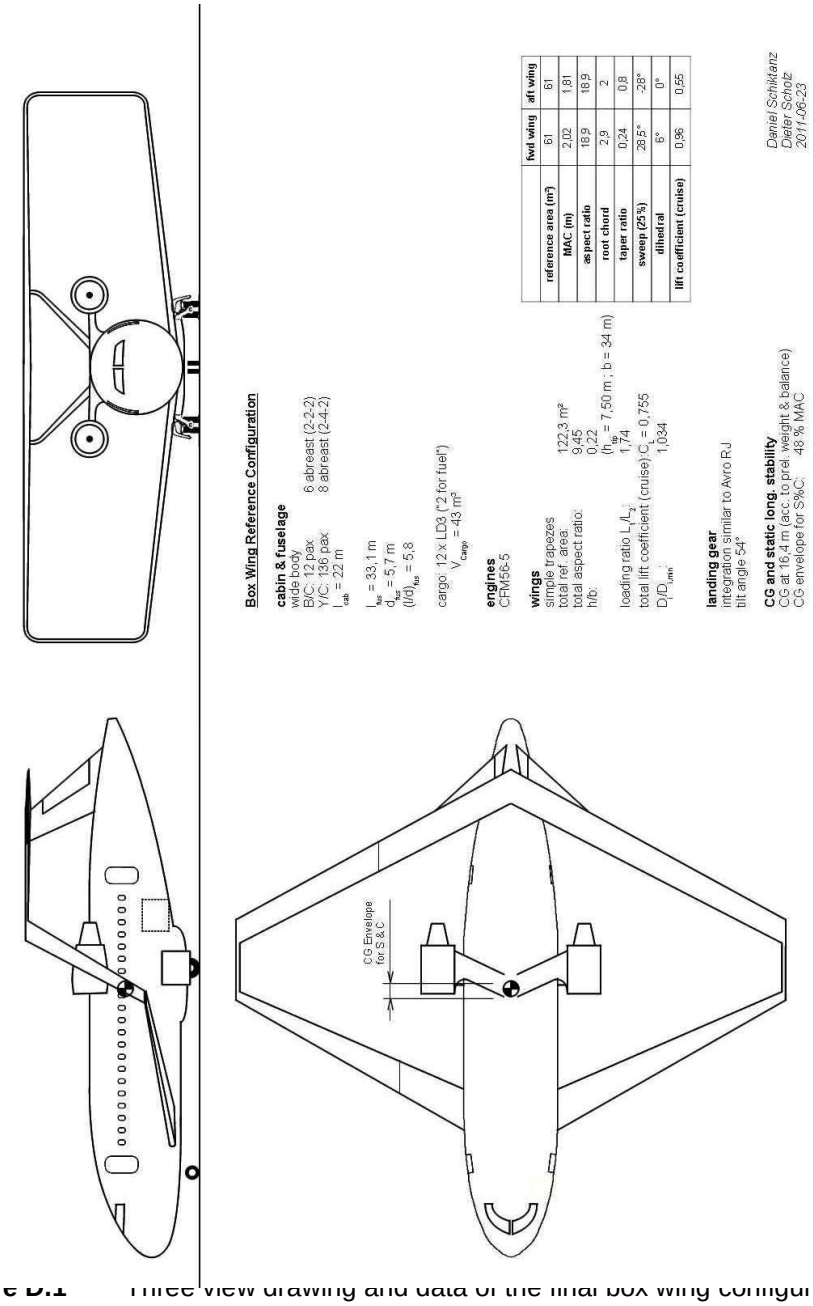

Figure D.1 Three view drawing and data of the final box wing configuration

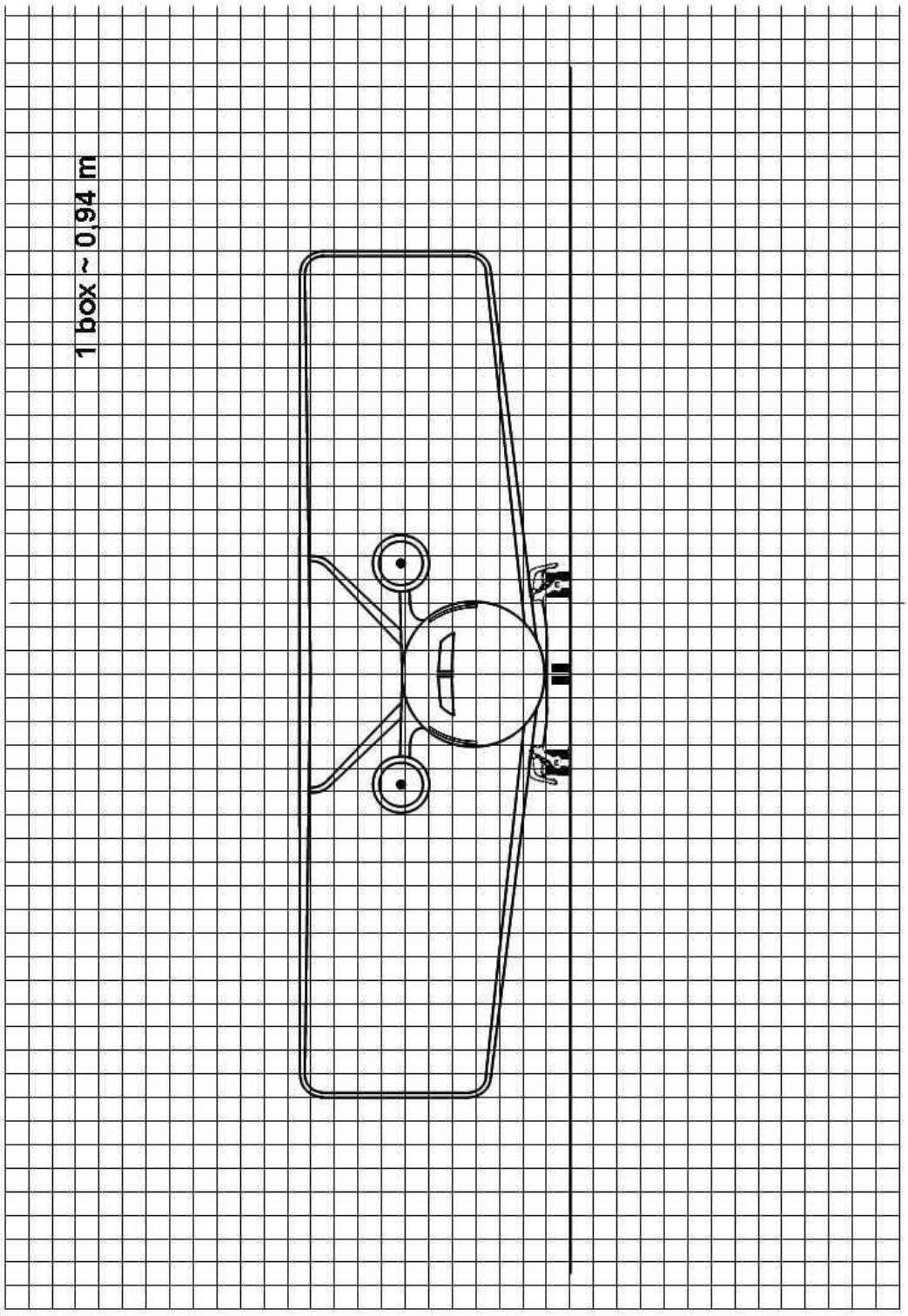

Figure D.2 Scaled front view of the final box wing configuration

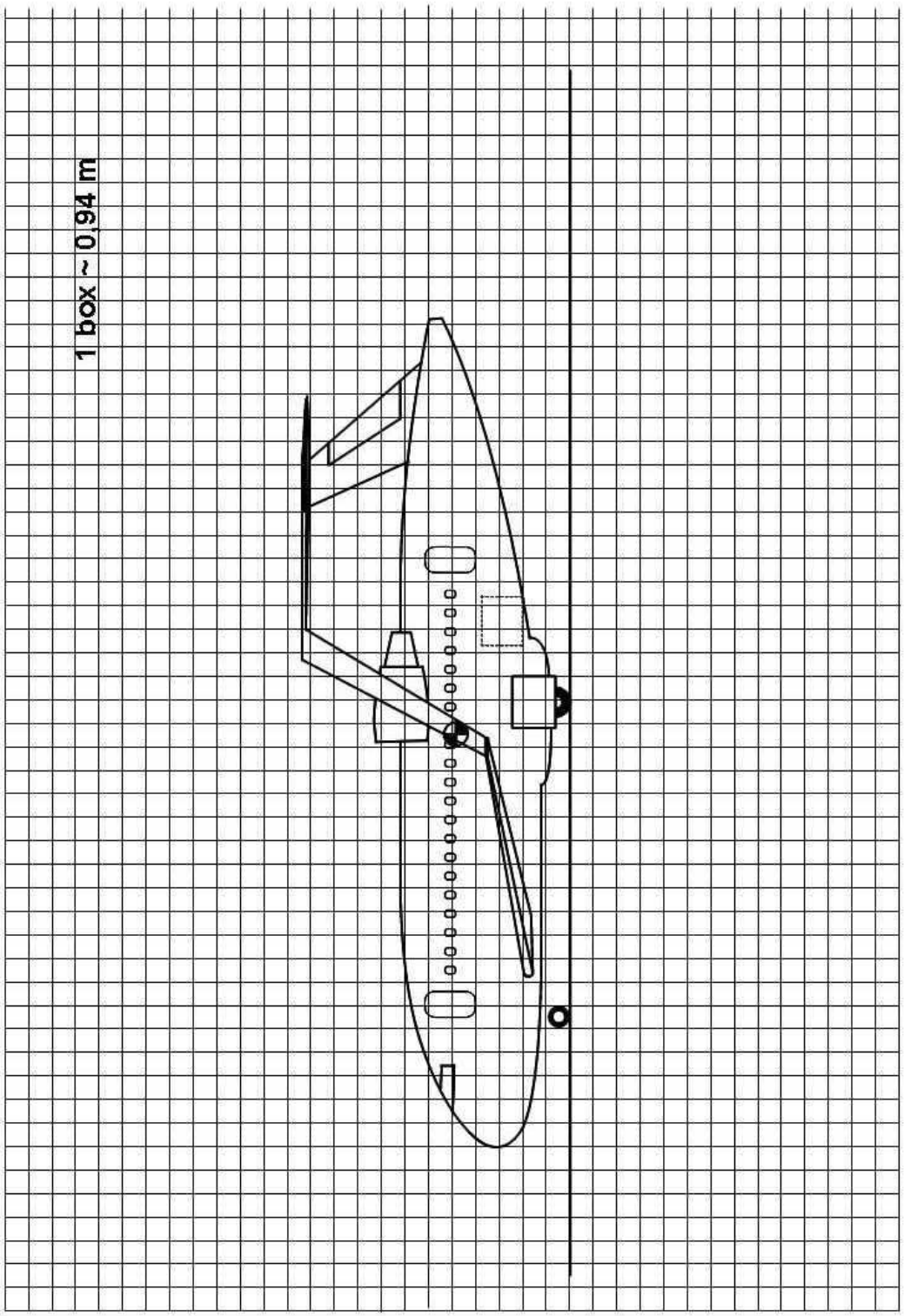

Figure D.3 Scaled side view of the final box wing configuration

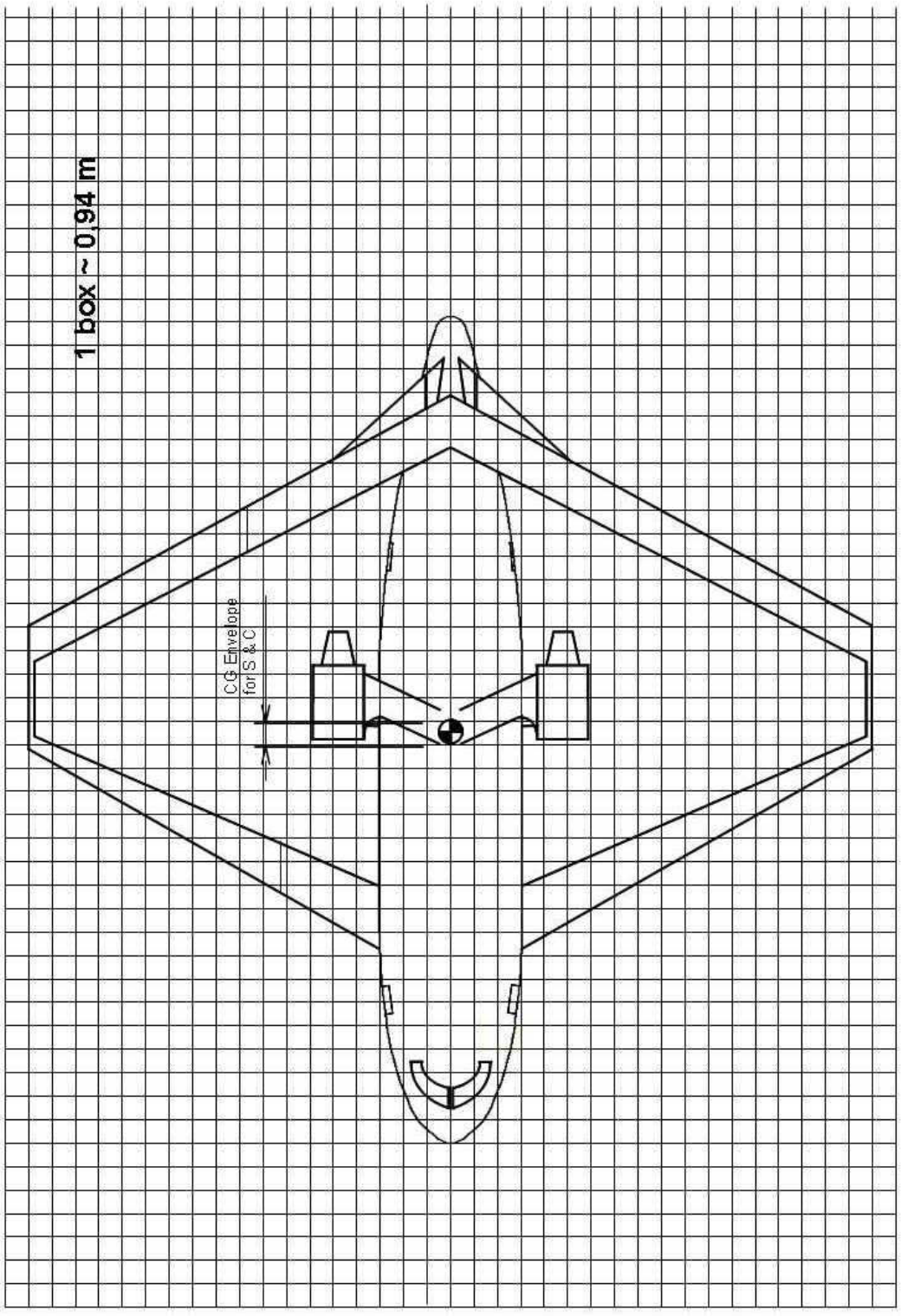

Figure D.4 Scaled top view of the final box wing configuration

D.2 Selected Intermediate Versions

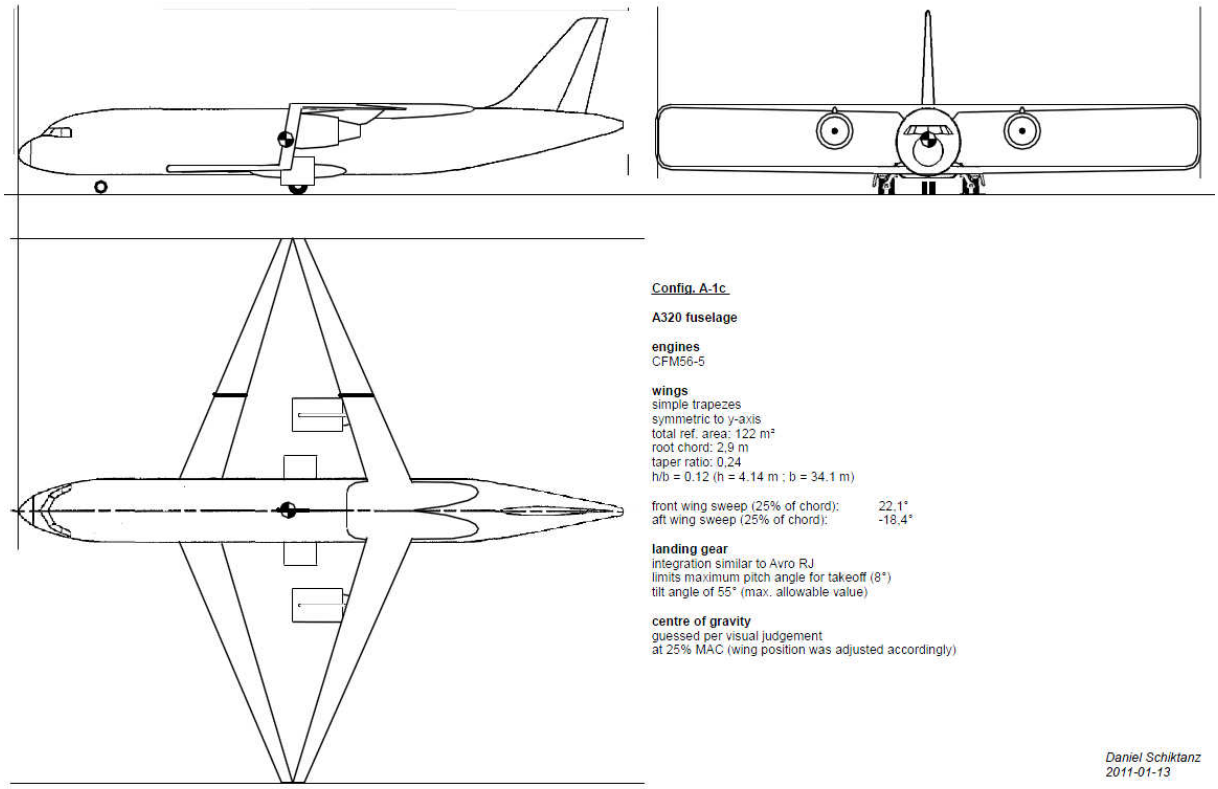

Figure D.5 Version A-1c

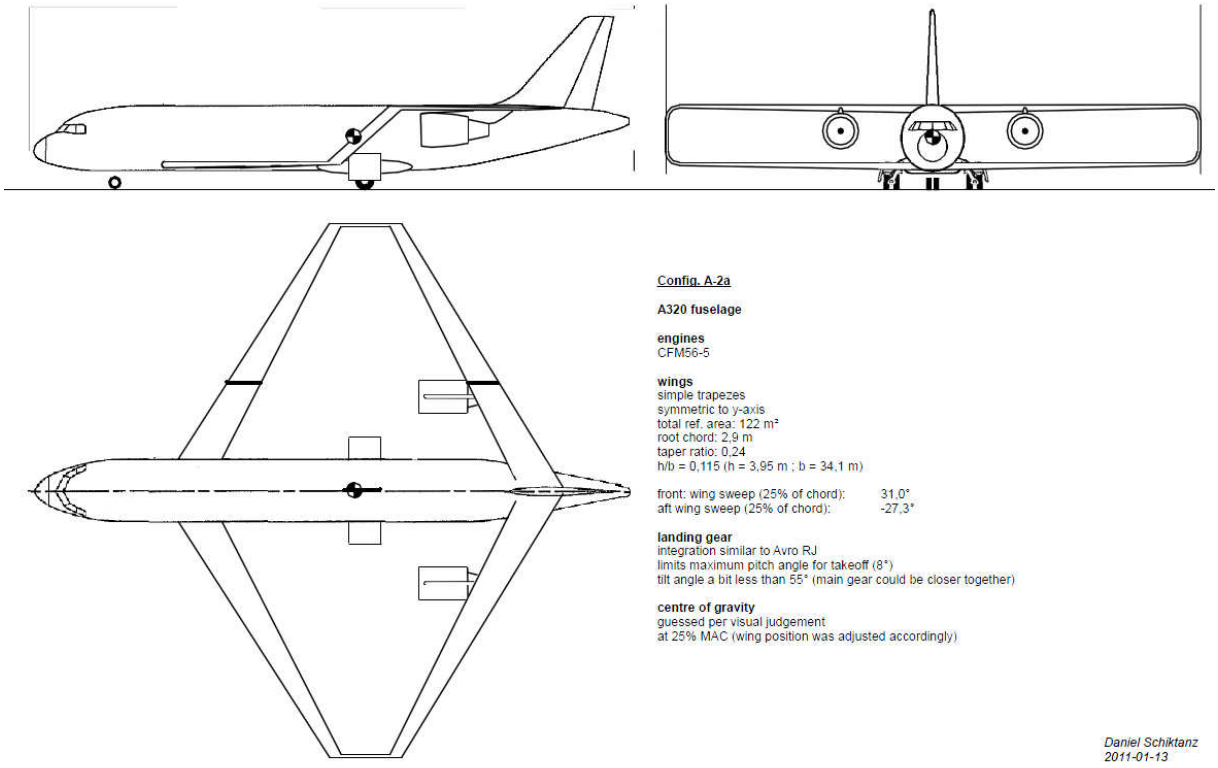

Figure D.6 Version A-2a

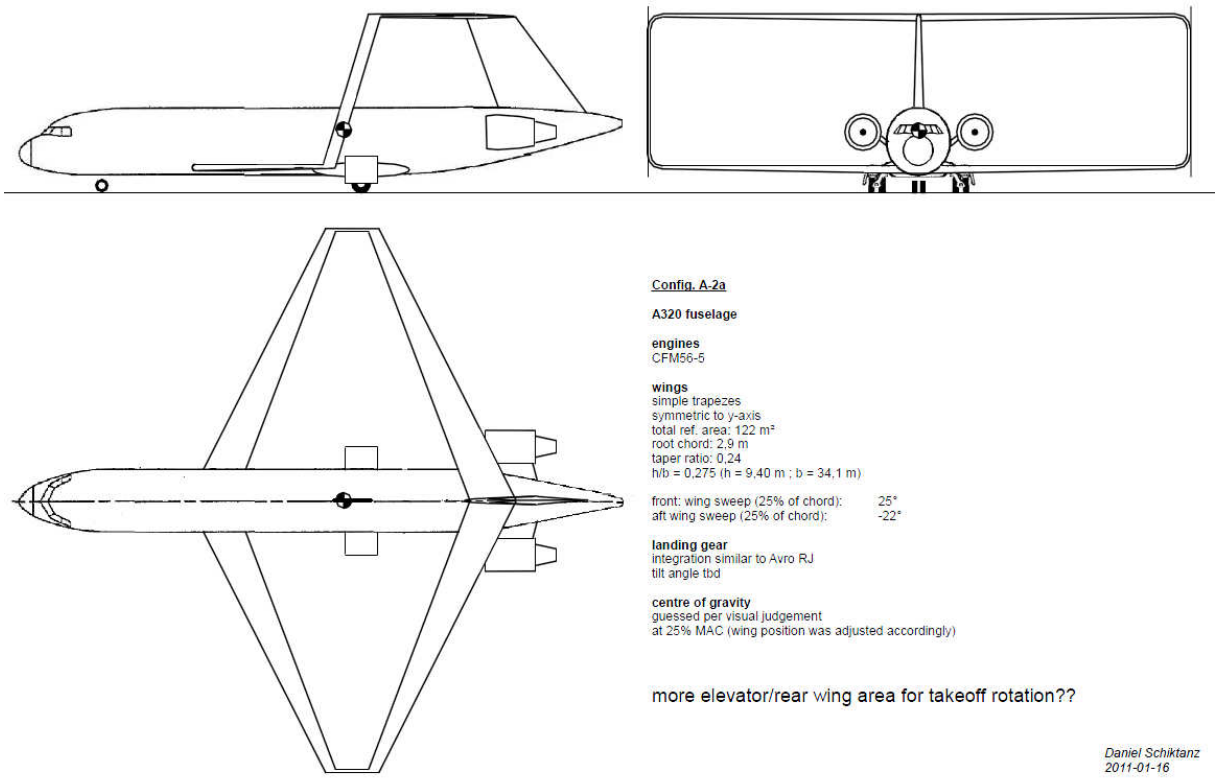

Figure D.7 Version B-2 (don't mind the wrong name in the drawing)

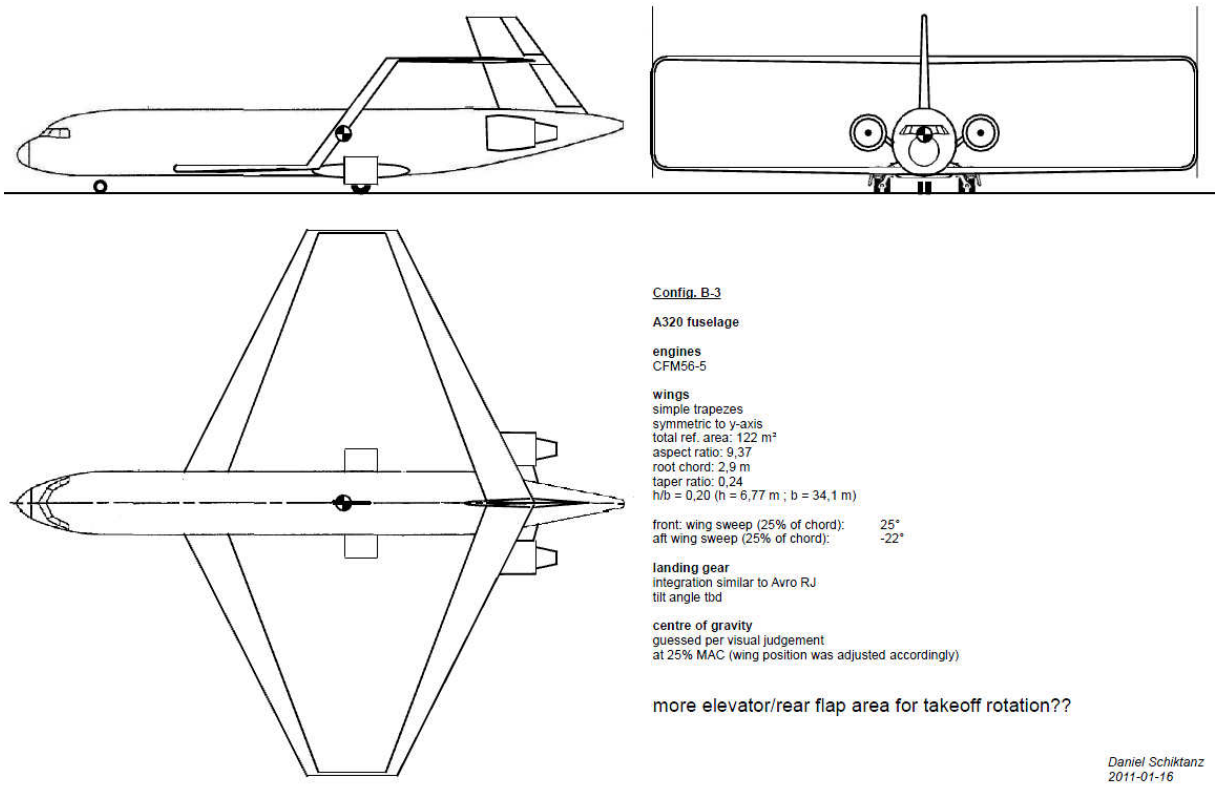

Figure D.8 Version B-3

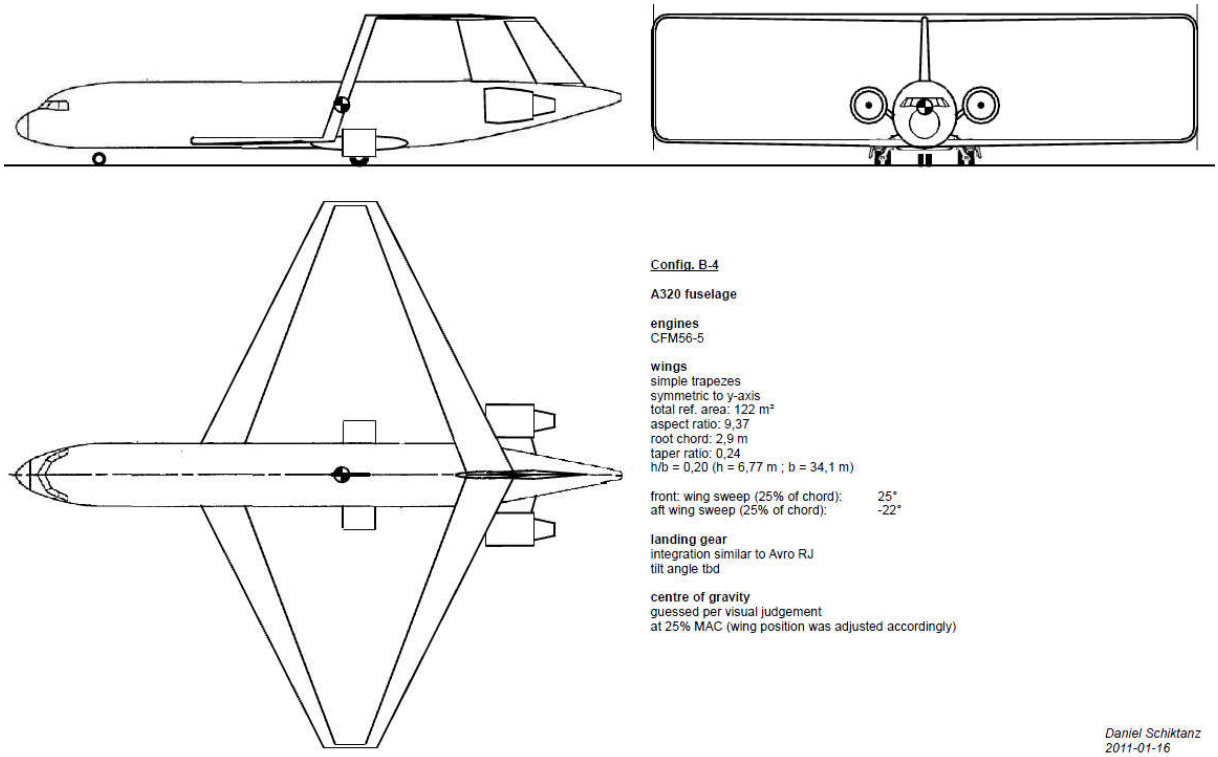

Config. B-4

A320 fuselage

engines
CFM56-5

wings
simple trapezes
symmetric to y-axis
total ref. area: 122 m²
aspect ratio: 9,37
root chord: 2,9 m
taper ratio: 0,24
h/b = 0,20 (h = 6,77 m ; b = 34,1 m)

front: wing sweep (25% of chord): 25°
aft wing sweep (25% of chord): -22°

landing gear
integration similar to Avro RJ
tilt angle tbd

centre of gravity
guessed per visual judgement
at 25% MAC (wing position was adjusted accordingly)

Daniel Schiktanz
2011-01-16

Figure D.9 Version B-4

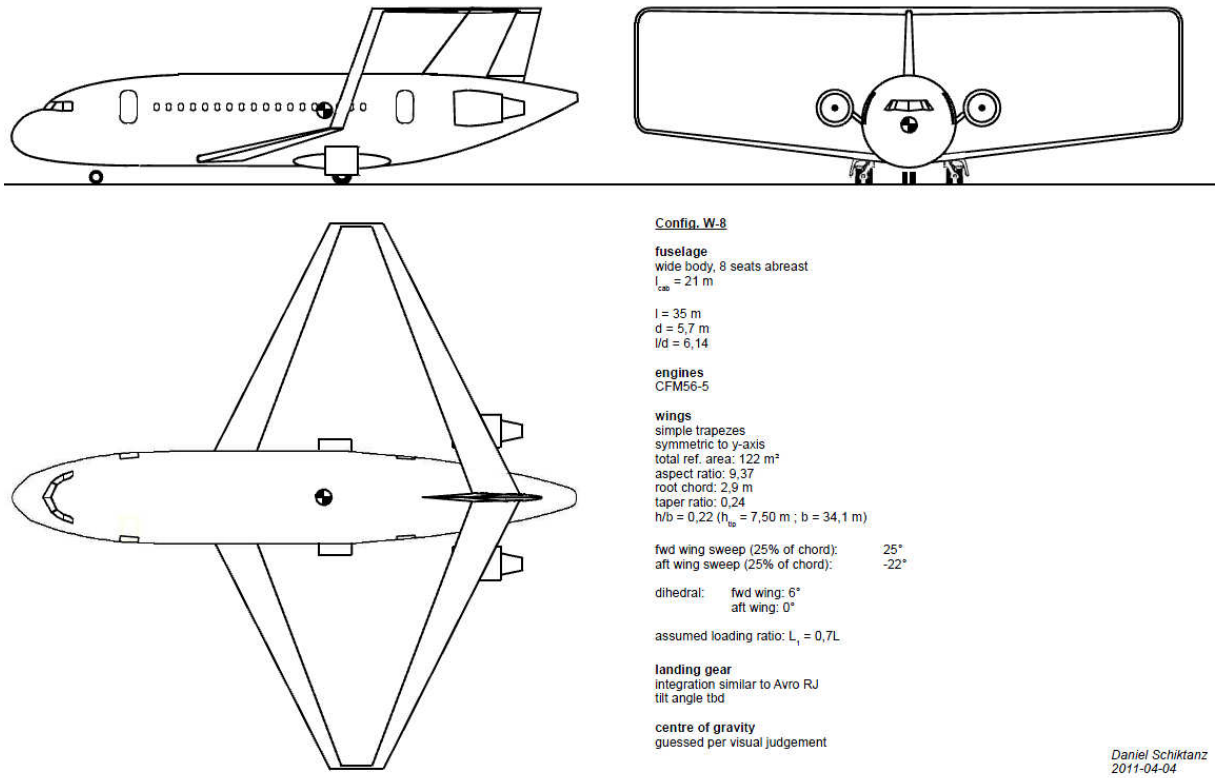

Config. W-8

fuselage
wide body, 8 seats abreast
l_{cab} = 21 m

l = 35 m
d = 5,7 m
l/d = 6,14

engines
CFM56-5

wings
simple trapezes
symmetric to y-axis
total ref. area: 122 m²
aspect ratio: 9,37
root chord: 2,9 m
taper ratio: 0,24
h/b = 0,22 (h_{bp} = 7,50 m ; b = 34,1 m)

fwd wing sweep (25% of chord): 25°
aft wing sweep (25% of chord): -22°

dihedral: fwd wing: 6°
aft wing: 0°

assumed loading ratio: L_1 = 0,7L

landing gear
integration similar to Avro RJ
tilt angle tbd

centre of gravity
guessed per visual judgement

Daniel Schiktanz
2011-04-04

Figure D.10 Version W-8

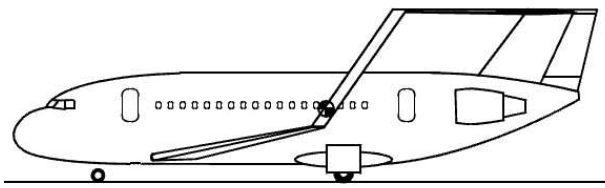

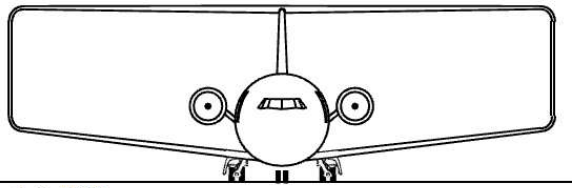

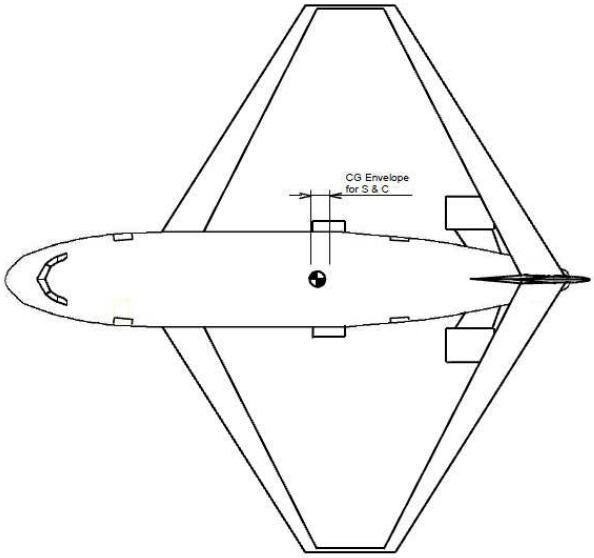

Config. W-8-30

fuselage
wide body, 8 seats abreast
l_{cab} = 21 m

l = 35 m
d = 5,7 m
l/d = 6,14

cargo: 4 x LD6 ("1 for fuel")
V_{cargo} = 26,1 m³

engines
CFM56-5

wings
simple trapezes
symmetric to y-axis

total ref. area:	122 m²
aspect ratio:	9,37
root chord:	2,9 m
taper ratio:	0,24
MAC:	2,02 m
h/b:	0,22 (h_{tip} = 7,50 m ; b = 34,1 m)
sweep (25% of chord):	fwd: 30,4°
	aft: -28,0°
dihedral:	fwd: 6°
	aft: 0°
loading ratio L_1/L_2:	1,72
lift coefficients:	C_{L1} = 1; C_{L2} = 0,58; C_L = 0,79

landing gear
integration similar to Avro RJ
tilt angle tbd

CG and static long. stability
CG guessed per visual judgement
static margin: 52 % MAC

Daniel Schiktanz
2011-04-05

Figure D.11 Version W-8-30

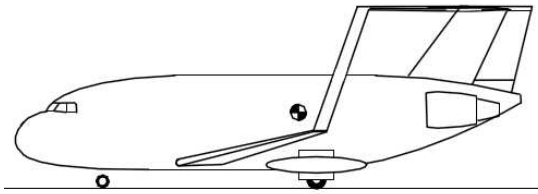

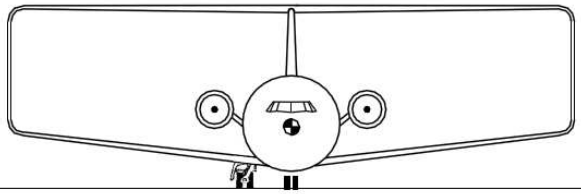

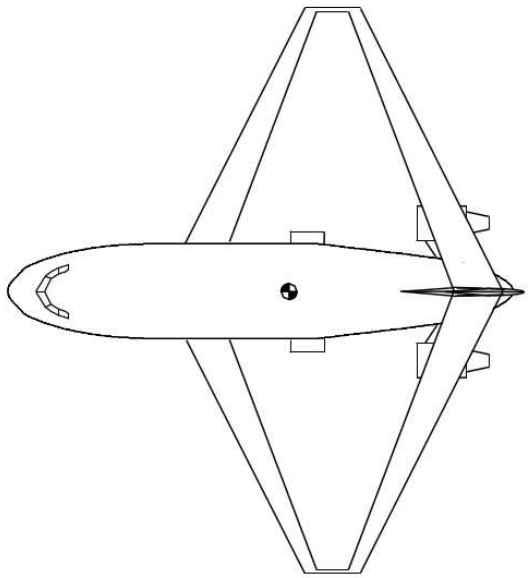

Config. W-8 short

fuselage
wide body, 8 seats abreast
l_{cab} = 21 m

very short nose and tail
l = 30 m
d = 5,7 m
l/d = 5,3

engines
CFM56-5

wings
simple trapezes
symmetric to y-axis
total ref. area: 122 m²
aspect ratio: 9,37
root chord: 2,9 m
taper ratio: 0,24
h/b = 0,22 (h_{tip} = 7,50 m ; b = 34,1 m)

fwd wing sweep (25% of chord): 25°
aft wing sweep (25% of chord): -22°

dihedral: fwd wing: 6°
aft wing: 0°

assumed loading ratio: L_1 = 0,7L

landing gear
integration similar to Avro RJ
tilt angle tbd

centre of gravity
guessed per visual judgement

Daniel Schiktanz
2011-04-04

Figure D.12 Version W-8-short

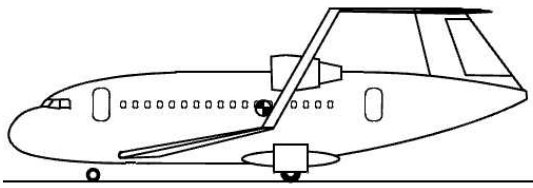

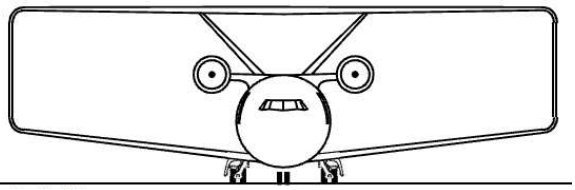

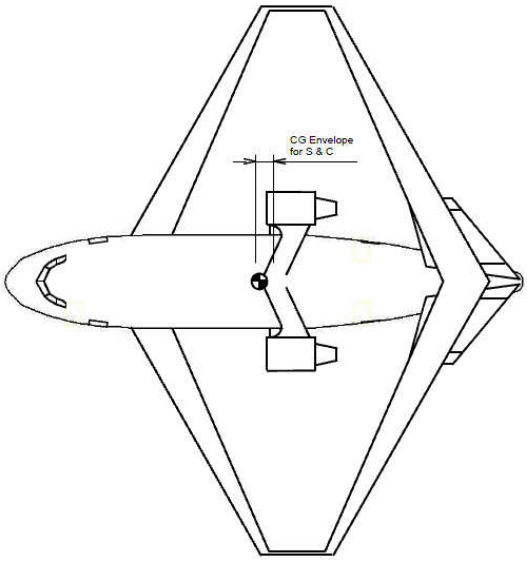

Config. W-8-x

fuselage
wide body, 8 seats abreast
l_{cab} = 21 m

l = 32 m
d = 5,7 m
l/d = 5,6

cargo: 4 x LD6 ("1 for fuel")
V_{cargo} = 26,1 m³

engines
CFM56-5

wings
simple trapezes
symmetric to y-axis

total ref. area:	122 m²
aspect ratio:	9,37
root chord:	2,9 m
taper ratio:	0,24
MAC:	2,02 m
h/b:	0,22 (h_{sp} = 7,50 m ; b = 34,1 m)
sweep (25% of chord):	fwd: 28,5° aft: -25,0°
dihedral:	fwd: 6° aft: 0°
loading ratio L_1/L_2:	1,94
lift coefficients:	$C_{L,1}$ = 0,97; $C_{L,2}$ = 0,5; C_L = 0,735

landing gear
integration similar to Avro RJ
tilt angle tbd

CG and static long. stability
CG at 15,8 m (acc. to prel. weight & balance)
static margin: 50 % MAC

Daniel Schiktanz
2011-04-11

Figure D.13 Version W-8-x

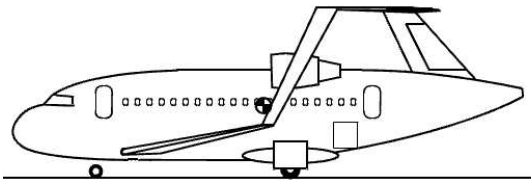

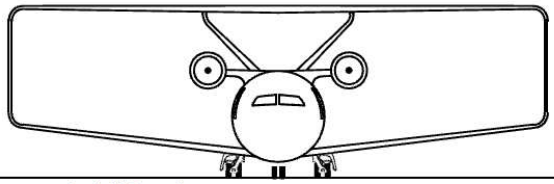

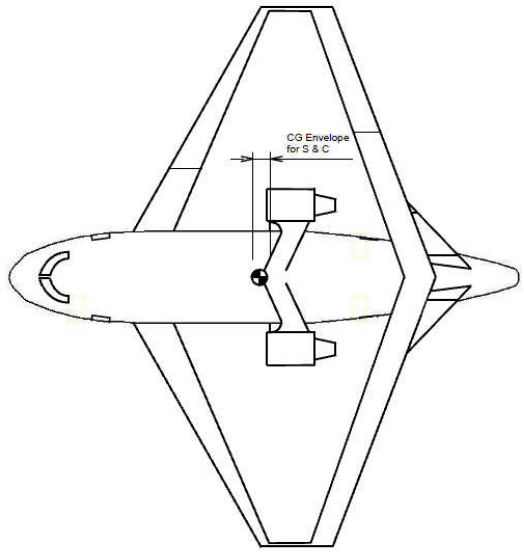

Config. W-8-x-mod

fuselage
wide body, 8 seats abreast
l_{cab} = 21 m

l = 32 m
d = 5,7 m
l/d = 5,6

cargo: 4 x LD6 ("1 for fuel")
V_{cargo} = 26,1 m³

engines
CFM56-5

wings
simple trapezes

total ref. area:	124 m²
total aspect ratio:	9,3
h/b:	0,22 (h_{sp} = 7,50 m ; b = 34,1 m)
loading ratio L_1/L_2:	1,81
total lift coefficient (cruise):	C_L = 0,715
$D/D_{L,min}$:	1,035

	fwd wing	aft wing
reference area (m²)	62	62
MAC	2,06	1,83
aspect ratio	18,6	18,6
root chord	2,95	2,03
taper ratio	0,24	0,8
sweep (25%)	28,5°	-19,5°
dihedral	6°	0°
lift coefficient (cruise)	0,92	0,51

landing gear
integration similar to Avro RJ
tilt angle tbd

CG and static long. stability
CG at 15,7 m (acc. to prel. weight & balance)
static margin: 48 % MAC

Daniel Schiktanz
2011-04-20

Figure D.14 Version W-8-x-mod

Appendix E

Calculation of the Tilting Angle

In this section it is shown how to calculate the tilting angle referred to in section 8.4.2. The calculation is based on analytical geometry and is implemented into a spreadsheet. For illustrating the method Fig. E.1 shows the geometrical relations.

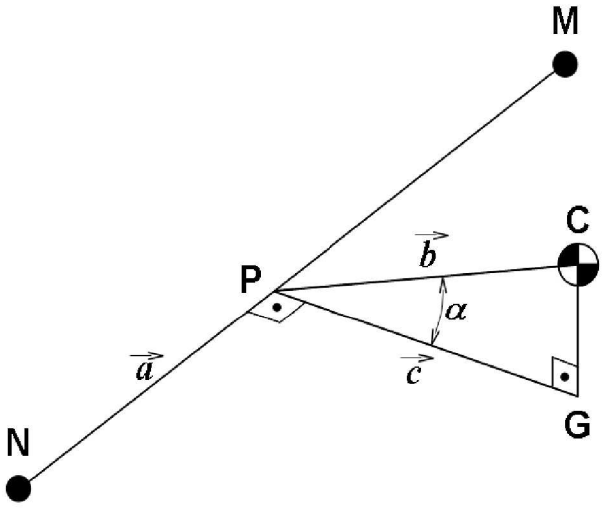

C - center of gravity
G - point on ground vertically below center of gravity
M - main landing gear (right)
N - nose landing gear
P - intersection of plane CGP and vector NM

Figure E.1 Geometry for calculating the tilting angle

All points except the point *P* are given. In order to calculate the tilting angle α the point *P* needs to be determined. This point is the intersection of the plane which is orthogonal to the vector $\vec{a}$ and which goes through the point *C*. Once the coordinates of *P* are known the vectors $\vec{b}$ and $\vec{c}$ can be determined which are needed to calculate α.

In the following each step of the calculation method is presented. For an easier understanding the coordinates of all points are given in table E.1 so that the numeric results of each step can be given. The coordinated are taken from the drawings in Appendix D.1.

Table E.1 Input parameters for the tilting angle calculation

Point	Coordinates (m)		
	x	y	z
C	16,4	0	4,7
G	16,4	0	0
M	17,7	4	0
N	5,2	0	0

1) Determination of *P*

At first the plane orthogonal to $\vec{a}$ and going through *C* has to be determined. For this the vector $\vec{a}$ is needed:

$$\vec{a} = \begin{pmatrix} x_M - x_N \\ y_M - y_N \\ z_M - z_N \end{pmatrix} \quad . \tag{E.1}$$

Now the equation for the plane orthogonal to $\vec{a}$ and going through *C* can be set up:

$$\left(x_M - x_N\right)x + \left(y_M - y_N\right)y + \left(z_M - z_N\right)z = \begin{pmatrix} x_C \\ y_C \\ z_C \end{pmatrix} \cdot \begin{pmatrix} x_M - x_N \\ y_M - y_N \\ z_M - z_N \end{pmatrix} \quad . \tag{E.2}$$

Inserting the values given in table E.1 gives the planar equation

$$12{,}5\,x + 4\mathrm{y} = 205 \quad . \tag{E.3}$$

Now the equation for the line $\overrightarrow{NM}$ has to be determined, which simply is

$$\overrightarrow{NM} = \begin{pmatrix} x_N \\ y_N \\ z_N \end{pmatrix} + r \cdot \vec{a} = \begin{pmatrix} 5{,}2 + 12{,}5\,r \\ 4\mathrm{r} \\ 0 \end{pmatrix} \tag{E.4}$$

The intersection point P can be calculated by inserting the components of the linear equation [Eq. (E.4)] into the planar equation [Eq. (E.3)]. This results in

$$12{,}5 \cdot \left(5{,}2 + 12{,}5\,r\right) + 4 \cdot 4\,r = 205 \quad . \tag{E.5}$$

The coordinates of the intersection point *P* are determined by solving Eq. (E.5) for *r*, giving $r = 0{,}813$, and inserting the result into the linear equation. This finally gives

$$P = \begin{pmatrix} 15{,}36 \\ 3{,}25 \\ 0 \end{pmatrix} \quad . \tag{E.6}$$

2) Determination of *α*

The tilting angle *α* is the angle between the vectors $\vec{b}$ and $\vec{c}$, which can easily be determined now that the coordinates of point *P* are known:

$$\vec{b} = \begin{pmatrix} x_C - x_P \\ y_C - y_P \\ z_C - z_P \end{pmatrix} = \begin{pmatrix} 1{,}04 \\ -3{,}25 \\ 4{,}7 \end{pmatrix} \tag{E.7}$$

and

$$\vec{c} = \begin{pmatrix} x_G - x_P \\ y_G - y_P \\ z_G - z_P \end{pmatrix} = \begin{pmatrix} 1{,}04 \\ -3{,}25 \\ 0 \end{pmatrix} \quad . \tag{E.8}$$

The tilting angle *α* then is

$$\alpha = \arccos\left(\frac{\vec{b}\cdot\vec{c}}{|\vec{b}|\cdot|\vec{c}|}\right) \tag{E.9}$$

with

$$\vec{b}\cdot\vec{c} = \begin{pmatrix} 1{,}04 \\ -3{,}25 \\ 4{,}7 \end{pmatrix}\cdot\begin{pmatrix} 1{,}04 \\ -3{,}25 \\ 0 \end{pmatrix} = 11{,}64 \tag{E.10}$$

and

$$|\vec{b}|\cdot|\vec{c}| = \sqrt{1{,}04^2 + (-3{,}25)^2 + 4{,}7^2}\cdot\sqrt{1{,}04^2 + (-3{,}25)^2} = 19{,}82 \tag{E.11}$$

which gives a tilting angle of 54,0°.

Appendix F

Data from Spreadsheets

F.1 Preliminary Sizing Spreadsheet

F.1.1 Final Box Wing Configuration

1.) Peliminary Sizing I
Calculations for flight phases approach, landing, tak-off, 2nd segment and missed approach

Bold blue values represent input data.
Values based on experience are light blue. Usually you should not change these values!
Results are marked **red**. Don't change these cells!
Interim values, constants, ... are in black!
"<<<<" marks special input or user action.

Author:
Prof. Dr.-Ing. Dieter Scholz, MSME
HAW Hamburg
http://www.ProfScholz.de
Example data: See Klausur SS05

Approach

Factor	k_{APP}	1,70 (m/s²) [1)]	
Conversion factor	m/s -> kt	1,944 kt / m/s	
Given: landing field length		**yes**	**<<<< Choose according to task** (ja = yes; nein = no)
Landing field length	s_{LFL}	**1700 m**	
Approach speed	V_{APP}	70,2 m/s	
Approach speed	V_{APP}	**136,4 kt**	$V_{APP} = k_{APP} \cdot \sqrt{s_{LFL}}$
Given: approach speed		**no**	
Approach speed	V_{APP}	**134,0 kt**	$V_{APP} = \left(\frac{s_{LFL}}{k_{APP}} \right)^2$
Approach speed	V_{APP}	68,9 m/s	
Landing field length	s_{LFL}	**1641 m**	

Landing

Landing field length	s_{LFL}	1700 m	
Temperature above ISA (288,15K)	ΔT_L	**0 K**	
Relative density	σ	1,000	
Factor	k_L	0,107 kg/m³	$k_L = 0{,}03694\ K_{APP}$
Max. lift coefficient, landing	$C_{L,max,L}$	**2,920**	
Mass ratio, landing - take-off	m_{ML} / m_{TO}	**0,889000**	$m_{ML} / S_W = k_L \cdot \sigma \cdot C_{L,max,L} \cdot s_{LFL}$
Wing loading at max. landing mass	m_{ML} / S_W	**531 kg/m²**	
Wing loading at max. take-off mass	m_{MTO} / S_W	**597 kg/m²**	$m_{MTO} / S_W = \frac{m_{ML} / S_W}{m_{ML} / m_{MTO}}$

Take-off

Take-off field length	s_{TOFL}	**2200**	**m**
Temperatur above ISA (288,15K)	ΔT_{TO}	**0**	**K**
Relative density	σ	1,000	
Factor	k_{TO}	2,34	m³/kg
Exprience value for $C_{L,max,TO}$	0,8 * $C_{L,max,L}$	2,336	
Max. lift coefficient, take-off	$C_{L,max,TO}$	**2,1**	
Slope	a	**0,0005065**	**kg/m³**
	T_{TO}/m_{MTO}*g at m_{MTO}/S_W calculated		
Thrust-to-weight ratio	from landing	**0,303**	

$$a = \frac{T_{TO}/(m_{MTO}\cdot g)}{m_{MTO}/S_W} = \frac{k_{TO}}{s_{TOFL}\cdot\sigma\cdot C_{L,max,TO}}$$

2nd Segment

Calculation of glide ratio

Aspect ratio	A	**9,5**	
Lift coefficient, take-off	$C_{L,TO}$	1,46	
Lift-independent drag coefficient, clean	$C_{D,0}$ (bei Berechnung: 2. Segment)	0,021	
Lift-independent drag coefficient, flaps	$\Delta C_{D,flap}$	0,018	
Lift-independent drag coefficient, slats	$\Delta C_{D,slat}$	0,000	
Profile drag coefficient	$C_{D,P}$	0,039	
Oswald efficiency factor; landing configuration	e	0,964	
Glide ratio in take-off configuration	E_{TO}	12,92	

n_E	sin(γ)
2	0,024
3	0,027
4	0,030

Calculation of thrust-to-weight ratio

Number of engines	n_E	**2**	
Climb gradient	sin(γ)	0,024	
Thrust-to-weight ratio	T_{TO}/m_{MTO}*g	**0,203**	

$$\frac{T_{TO}}{m_{MTO}\cdot g} = \left(\frac{n_E}{n_E - 1}\right)\cdot\left(\frac{1}{E_{TO}} + \sin\gamma\right)$$

Missed approach

Calculation of the glide ratio

Lift coefficient, landing	$C_{L,L}$	1,73	
Lift-independent drag coefficient, clean	$C_{D,0}$ (bei Berechnung: Durchstarten)	0,021	
Lift-independent drag coefficient, flaps	$\Delta C_{D,flap}$	0,031	
Lift-independent drag coefficient, slats	$\Delta C_{D,slat}$	0,000	
Choose: Certification basis	JAR-25 bzw. CS-25	**no**	**<<<< Choose according to task**
	FAR Part 25	**yes**	
Lift-independent drag coefficient, landing gear	$\Delta C_{D,gear}$	0,015	
Profile drag coefficient	$C_{D,P}$	0,067	
Glide ratio in landing configuration	E_L	10,10	

	JAR-25 bzw. CS-25	FAR Part 25
$\Delta C_{D,gear}$	0,000	0,015

n_E	sin(γ)
2	0,021
3	0,024
4	0,027

Calculation of thrust-to-weight ratio

Climb gradient	sin(γ)	0,021	
Thrust-to-weight ratio	T_{TO}/m_{MTO}*g	**0,213**	

$$\frac{T_{TO}}{m_{MTO}\cdot g} = \left(\frac{n_E}{n_E - 1}\right)\cdot\left(\frac{1}{E_L} + \sin\gamma\right)\cdot\frac{m_{ML}}{m_{MTO}}$$

2.) Max. Glide Ratio in Cruise

Estimation of k_E by means of 1.), 2.) or 3.)

1.) From theory

Oswald efficiency factor for k_E	e	**1,17**	
Equivalent surface friction coefficient	$C_{f,eqv}$	**0,003**	
Factor	k_E	17,5	

2.) Acc. to RAYMER

Factor	k_E	15,8	

3.) From own statistics

Factor	k_E	**14,9**	

Estimation of max. glide ratio in cruise, E_{max}

Factor	$k_{E\ chosen}$	**17,5**	**<<<< Choose according to task**
Relative wetted area	S_{wet}/S_w	**7**	S_{wet}/S_w = 6,0 ... 6,2
Aspect ratio	A	9,5	(from sheet 1)
Max. glide ratio	E_{max}	**20,39**	
	or		
Max. glide ratio	$E_{max\,chosen}$	**20,39**	**<<<< Choose according to task**

3.) Preliminary Sizing II

Calculations for cruise, matching chart, fuel mass, operating empty mass and aircraft parameters m_{MTO}, m_L, m_{OE}, S_W, T_{TO}, ...

Parameter		Value
By-pass ratio	BPR	**4,8**
Max. glide ratio, cruise	E_{max}	20,39 (aus Teil 2)
Aspect ratio	A	9,5 (aus Teil 1)
Oswald eff. factor, clean	e	1,17
Zero-lift drag coefficient	$C_{D,0}$	0,021
Lift coefficient at E_{max}	$C_{L,m}$	0,86
Mach number, cruise	M_{CR}	**0,76**

$$C_{D,0} = \frac{\pi \cdot A \cdot e}{4 \cdot E_{max}^2}$$

$$C_{L,m} = \sqrt{C_{D,0} \cdot \pi \cdot A \cdot e}$$

Parameter	Value
Estimated V/V_m	**1,00**
$C_L/C_{L,m}$	1,000
C_L	0,856
E	20,390
Density	0,269858502
Vm	225,1183557
Vcr	224,2886598
Real Vcr/Vm	0,996314402

Jet, Theory, Optimum: 1,316074013

$$C_L / C_{L,m} = 1 / (V / V_m)^2$$

$$E = E_{max} \cdot \frac{2}{\frac{1}{\left(\frac{C_l}{C_{l,m}}\right)} + \left(\frac{C_l}{C_{l,m}}\right)}$$

Constants		
Ratio of specific heats, air	γ	1,4
Earth acceleration	g	9,81 m/s²
Air pressure, ISA, standard	p_0	101325 Pa
Euler number	e	2,718282

$$\frac{T_{TO}}{m_{MTO} \cdot g} = \frac{1}{(T_{CR}/T_0) \cdot (L/D)_{max}}$$

$$\frac{m_{MTO}}{S_W} = \frac{C_L \cdot M^2}{g} \cdot \frac{\gamma}{2} \cdot p(h)$$

Altitude		Cruise				2nd Segment	Missed appr.	Take-off	Cruise
h [km]	h [ft]	T_{CR}/T_{TO}	$T_{TO}/m_{MTO}*g$	p(h) [Pa]	m_{MTO}/S_W [kg/m²]	$T_{TO}/m_{MTO}*g$	$T_{TO}/m_{MTO}*g$	$T_{TO}/m_{MTO}*g$	$T_{TO}/m_{MTO}*g$
0	0	0,593	0,083	101325	3576	0,203	0,213	1,81	0,08
1	3281	0,560	0,088	89873	3172	0,203	0,213	1,61	0,09
2	6562	0,527	0,093	79493	2805	0,203	0,213	1,42	0,09
3	9843	0,493	0,099	70105	2474	0,203	0,213	1,25	0,10
4	13124	0,460	0,107	61636	2175	0,203	0,213	1,10	0,11
5	16405	0,426	0,115	54015	1906	0,203	0,213	0,97	0,12
6	19686	0,393	0,125	47176	1665	0,203	0,213	0,84	0,12
7	22967	0,359	0,137	41056	1449	0,203	0,213	0,73	0,14
8	26248	0,326	0,151	35595	1256	0,203	0,213	0,64	0,15
9	29529	0,292	0,168	30737	1085	0,203	0,213	0,55	0,17
10	32810	0,259	0,189	26431	933	0,203	0,213	0,47	0,19
11	36091	0,225	0,218	22627	799	0,203	0,213	0,40	0,22
12	39372	0,192	0,256	19316	682	0,203	0,213	0,35	0,26
13	42653	0,158	0,309	16498	582	0,203	0,213	0,29	0,31
14	45934	0,125	0,392	14091	497	0,203	0,213	0,25	0,39
15	49215	0,092	0,536	12035	425	0,203	0,213	0,22	0,54
					597				
					598				
Remarks:	1m=3,281 ft	T_{CR}/T_{TO}= f(BPR,h)	Gl.(5.27)	Gl. (5.32/5.33)	Gl. (5.34)	from sheet 1.)	from sheet 1.)	from sheet 1.)	Repeat for plot

Wing loading	m_{MTO}/S_W	**597 kg/m²**	<<<< **Read design point from matching chart!**
Thrust-to-weight ratio	$T_{TO}/(m_{MTO}*g)$	**0,303**	<<<< Given data is correct when take-off and landing is sizing the aircraft at the same time.
Thrust ratio	$(T_{CR}/T_{TO})_{CR}$	0,162	
Conversion factor	m -> ft	0,305 m/ft	
Cruise altitude	h_{CR}	**12893 m**	
Cruise altitude	h_{CR}	**42299 ft**	
Temperature, troposphere	$T_{Troposphäre}$	204,35 K	$T_{Stratosphäre}$ 216,65 K
Temperature, h_{CR}	$T(h_{CR})$	216,65	
Speed of sound, h_{CR}	a	295 m/s	
Cruise speed	V_{CR}	**224 m/s**	
Conversion factor	NM -> m	1852 m/NM	
Design range	R	**1550 NM**	
Design range	R	2870600 m	
Distance to alternate	$s_{to\_alternate}$	200 NM	
Distance to alternate	$s_{to\_alternate}$	370400 m	
Chose: FAR Part121-Reserves?	domestic	**no**	
	international	**yes**	
Extra-fuel for long range		10%	
Extra flight distance	s_{res}	657460 m	
Spec.fuel consumption, cruise	SFC_{CR}	**1,63E-05 kg/N/s**	typical value 1,60E-05 kg/N/s
Breguet-Factor, cruise	B_s	28587497 m	
Fuel-Fraction, cruise	$M_{ff,CR}$	0,904	
Fuel-Fraction, extra flight distance	$M_{ff,RES}$	0,977	
Loiter time	t_{loiter}	1800 s	
Spec.fuel consumption, loiter	SFC_{loiter}	**1,63E-05 kg/N/s**	
Breguet-Factor, flight time	B_t	127459 s	
Fuel-Fraction, loiter	$M_{ff,loiter}$	0,986	
Fuel-Fraction, engine start	$M_{ff,engine}$	**0,999** <<<< **Copy**	
Fuel-Fraction, taxi	$M_{ff,taxi}$	**0,996** <<<< **values**	
Fuel-Fraction, take-off	$M_{ff,TO}$	**0,995** <<<< **from**	
Fuel-Fraction, climb	$M_{ff,CLB}$	**0,995** <<<< **table**	
Fuel-Fraction, descent	$M_{ff,DES}$	**0,992** <<<< **on the**	
Fuel-Fraction, landing	$M_{ff,L}$	**0,992** <<<< **right !**	

Reserve flight distance:

FAR Part 121	s_{res}
domestic	370400 m
international	657460 m

Extra time:

FAR Part 121	t_{loiter}
domestic	2700 s
international	1800 s

Phase	M_{ff} per flight phases [Roskam]	
	transport jet	business jet
engine start	0,990	0,990
taxi	0,990	**0,995**
take-off	0,995	0,995
climb	0,998	0,998
descent	0,990	0,990
landing	0,992	0,992

Fuel-Fraction, standard flight	$M_{ff,std}$	0,881	
Fuel-Fraction, all reserves	$M_{ff,res}$	0,951	
Fuel-Fraction, total	M_{ff}	0,838	
Mission fuel fraction	m_F/m_{MTO}	0,162	
Realtive operating empty mass	m_{OE}/m_{MTO}	0,545	acc. to Loftin
Realtive operating empty mass	m_{OE}/m_{MTO}	**0,573**	from statistics (if given)
Realtive operating empty mass	m_{OE}/m_{MTO}	**0,565**	<<<< **Choose according to task**
Choose: type of a/c	short / medium range	**yes**	<<<< **Choose according to task**
	long range	**no**	
Mass: Passengers, including baggage	m_{PAX}	93,0 kg	
Number of passengers	n_{PAX}	**150**	
Cargo mass	m_{cargo}	**6050 kg**	
Payload	m_{PL}	**20000 kg**	
Max. Take-off mass	m_{MTO}	**73245 kg**	
Max. landing mass	m_{ML}	**65115 kg**	
Operating empty mass	m_{OE}	**41383 kg**	
Mission fuel fraction, standard flight	m_F	**11861 kg**	
Wing area	S_w	**122,6 m²**	
Take-off thrust	T_{TO}	217437 N	**all engines together**
T-O thrust of ONE engine	T_{TO}/n_E	**108718 N**	
T-O thrust of ONE engine	T_{TO}/n_E	24440 lb	**one engine**
Fuel mass, needed	$m_{F,erf}$	12168 kg	
Fuel density	ρ_F	785 kg/m³	
Fuel volume, needed	$V_{F,erf}$	**15,5 m³**	(check with tank geometry later on)
Max. Payload	m_{MPL}	**20000 kg**	
Max. zero-fuel mass	m_{MZF}	61383 kg	
Fuel mass, all reserves	$m_{F,res}$	3584 kg	
Check of assumptions	check:	m_{ML}	> $m_{MZF} + m_{F,res}$?
		65115 kg	> 64967 kg
			yes
			Aircraft sizing finished!

in kg	Short- and Medium Range	Long Range
m_{PAX}	93,0	97,5

Matching Chart

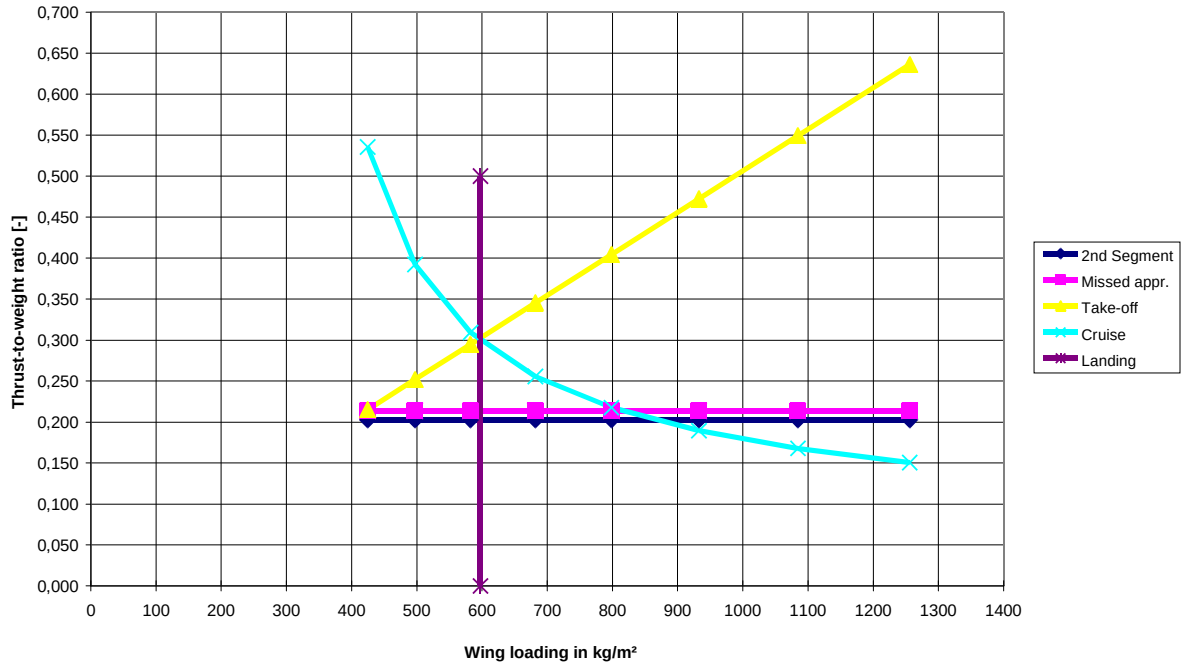

F.1.2 Reference Configuration

The following data are taken from **Pester 2010b**.

1.) Peliminary Sizing I

Calculations for flight phases approach, landing, tak-off, 2nd segment and missed approach

Bold blue values represent input data.
Values based on experience are light blue. Usually you should not change these values!
Results are marked **red**. Don't change these cells!
Interim values, constants, ... are in black!
"<<<<" marks special input or user action.

Author:
Prof. Dr.-Ing. Dieter Scholz, MSME
HAW Hamburg
http://www.ProfScholz.de
Example data: See Klausur SS05

Approach

Factor	k_{APP}	1,70 $(m/s^2)^{0,5}$	
Conversion factor	m/s -> kt	1,944 kt / m/s	
Given: landing field length		**yes**	**<<<< Choose according to task** (ja = yes; nein = no)
Landing field length	s_{LFL}	**1700 m**	
Approach speed	V_{APP}	70,2 m/s	
Approach speed	V_{APP}	**136,4 kt**	$V_{APP} = k_{APP} \cdot \sqrt{s_{LFL}}$
Given: approach speed		**no**	
Approach speed	V_{APP}	**134,0 kt**	$V_{APP} = \left(\frac{s_{LFL}}{k_{APP}} \right)^2$
Approach speed	V_{APP}	68,9 m/s	
Landing field length	s_{LFL}	**1641 m**	

Landing

Landing field length	s_{LFL}	1700 m	
Temperature above ISA (288,15K)	ΔT_L	**0 K**	
Relative density	σ	1,000	
Factor	k_L	0,107 kg/m³	$k_L = 0{,}03694 \; K_{APP}$
Max. lift coefficient, landing	$C_{L,max,L}$	**2,900**	
Mass ratio, landing - take-off	m_{ML} / m_{TO}	**0,878000**	$m_{ML} / S_W = k_L \cdot \sigma \cdot C_{L,max,L} \cdot s_{LFL}$
Wing loading at max. landing mass	m_{ML} / S_W	**528 kg/m²**	
Wing loading at max. take-off mass	m_{MTO} / S_W	**601 kg/m²**	$m_{MTO} / S_W = \frac{m_{ML} / S_W}{m_{ML} / m_{MTO}}$

Take-off

Take-off field length	s_{TOFL}	**2200 m**	
Temperatur above ISA (288,15K)	ΔT_{TO}	**0 K**	
Relative density	σ	1,000	
Factor	k_{TO}	2,34 m³/kg	
Exprience value for $C_{L,max,TO}$	0,8 * $C_{L,max,L}$	2,32	
Max. lift coefficient, take-off	$C_{L,max,TO}$	**2,07**	
Slope	a	**0,0005138 kg/m³**	$a = \frac{T_{TO} / (m_{MTO} \cdot g)}{m_{MTO} / S_W} = \frac{k_{TO}}{s_{TOFL} \cdot \sigma \cdot C_{L,max,TO}}$
Thrust-to-weight ratio	T_{TO}/m_{MTO}*g at m_{MTO}/S_W calculated from landing	**0,309**	

2nd Segment

Calculation of glide ratio

Aspect ratio	A	**9,5**	
Lift coefficient, take-off	$C_{L,TO}$	1,44	
Lift-independent drag coefficient, clean	$C_{D,0}$ (bei Berechnung: 2. Segment)	0,020	
Lift-independent drag coefficient, flaps	$\Delta C_{D,flap}$	0,017	
Lift-independent drag coefficient, slats	$\Delta C_{D,slat}$	0,000	
Profile drag coefficient	$C_{D,P}$	0,037	
Oswald efficiency factor; landing configuration	e	0,7	
Glide ratio in take-off configuration	E_{TO}	10,59	

n_E	sin(γ)
2	0,024
3	0,027
4	0,030

Calculation of thrust-to-weight ratio

Number of engines	n_E	**2**	
Climb gradient	sin(γ)	0,024	
Thrust-to-weight ratio	T_{TO} / m_{MTO}*g	**0,237**	$\frac{T_{TO}}{m_{MTO} \cdot g} = \left(\frac{n_E}{n_E - 1} \right) \cdot \left(\frac{1}{E_{TO}} + \sin\gamma \right)$

Missed approach

Calculation of the glide ratio

Lift coefficient, landing	$C_{L,L}$	1,72	
Lift-independent drag coefficient, clean	$C_{D,0}$ (bei Berechnung: Durchstarten)	0,020	
Lift-independent drag coefficient, flaps	$\Delta C_{D,flap}$	0,031	
Lift-independent drag coefficient, slats	$\Delta C_{D,slat}$	0,000	
Choose: Certification basis	JAR-25 bzw. CS-25	**no**	**<<<< Choose according to task**
	FAR Part 25	**yes**	
Lift-independent drag coefficient, landing gear	$\Delta C_{D,gear}$	0,015	
Profile drag coefficient	$C_{D,P}$	0,066	
Glide ratio in landing configuration	E_L	8,30	

	JAR-25 bzw. CS-25	FAR Part 25
$\Delta C_{D,gear}$	0,000	0,015

n_E	sin(γ)
2	0,021
3	0,024
4	0,027

Calculation of thrust-to-weight ratio

Climb gradient	sin(γ)	0,021	
Thrust-to-weight ratio	$T_{TO} / m_{MTO} * g$	**0,248**	

$$\frac{T_{TO}}{m_{MTO} \cdot g} = \left(\frac{n_E}{n_E - 1}\right) \cdot \left(\frac{1}{E_L} + \sin\gamma\right) \cdot \frac{m_{ML}}{m_{MTO}}$$

2.) Max. Glide Ratio in Cruise

Estimation of k_E by means of 1.), 2.) or 3.)

1.) From theory

Oswald efficiency factor for k_E	e	**0,85**	
Equivalent surface friction coefficient	C_{feqv}	**0,003**	
Factor	k_E	14,9	

2.) Acc. to RAYMER

Factor	k_E	15,8	

3.) From own statistics

Factor	k_E	**14,9**	

Estimation of max. glide ratio in cruise, E_{max}

Factor	$k_{E\ chosen}$	**14,9**	**<<<< Choose according to task**
Relative wetted area	S_{wet} / S_w	**6,1**	S_{wet} / S_w = 6,0 ... 6,2
Aspect ratio	A	9,5	(from sheet 1)
Max. glide ratio	E_{max}	**18,59**	
	or		
Max. glide ratio	$E_{max\,chosen}$	**17,88**	**<<<< Choose according to task**

3.) Preliminary Sizing II

Calculations for cruise, matching chart, fuel mass, operating empty mass and aircraft parameters m_{MTO}, m_L, m_{OE}, S_W, T_{TO}, ...

Parameter		Value
By-pass ratio	BPR	**4,8**
Max. glide ratio, cruise	E_{max}	17,88 (aus Teil 2)
Aspect ratio	A	9,5 (aus Teil 1)
Oswald eff. factor, clean	e	0,85
Zero-lift drag coefficient	$C_{D,0}$	0,020
Lift coefficient at E_{max}	$C_{L,m}$	0,71
Mach number, cruise	M_{CR}	**0,76**

$$C_{D,0} = \frac{\pi \cdot A \cdot e}{4 \cdot E_{max}^2} \qquad C_{L,m} = \sqrt{C_{D,0} \cdot \pi \cdot A \cdot e}$$

Parameter	Value
Estimated V/V_m	**0,99**
$C_L/C_{L,m}$	1,020
C_L	0,724
E	17,876
Density	0,29509386
Vm	237,2125915
Vcr	224,2886598
Real Vcr/Vm	0,945517514

Jet, Theory, Optimum: 1,316074013

$$C_L / C_{L,m} = 1 / (V / V_m)^2$$

$$E = E_{max} \cdot \frac{2}{\frac{1}{\left(\frac{C_l}{C_{l,m}}\right)} + \left(\frac{C_l}{C_{l,m}}\right)}$$

Constants		
Ratio of specific heats, air	γ	1,4
Earth acceleration	g	9,81 m/s²
Air pressure, ISA, standard	p_0	101325 Pa
Euler number	e	2,718282

$$\frac{T_{TO}}{m_{MTO} \cdot g} = \frac{1}{(T_{CR} / T_0) \cdot (L/D)_{max}} \qquad \frac{m_{MTO}}{S_W} = \frac{C_L \cdot M^2}{g} \cdot \frac{\gamma}{2} \cdot p(h)$$

Altitude		Cruise				2nd Segment	Missed appr.	Take-off	Cruise
h [km]	h [ft]	T_{CR}/T_{TO}	$T_{TO}/m_{MTO}*g$	p(h) [Pa]	m_{MTO}/S_W [kg/m²]	$T_{TO}/m_{MTO}*g$	$T_{TO}/m_{MTO}*g$	$T_{TO}/m_{MTO}*g$	$T_{TO}/m_{MTO}*g$
0	0	0,549	0,102	101325	3023	0,237	0,248	1,55	0,10
1	3281	0,518	0,108	89873	2681	0,237	0,248	1,38	0,11
2	6562	0,487	0,115	79493	2371	0,237	0,248	1,22	0,11
3	9843	0,456	0,123	70105	2091	0,237	0,248	1,07	0,12
4	13124	0,425	0,132	61636	1839	0,237	0,248	0,94	0,13
5	16405	0,394	0,142	54015	1611	0,237	0,248	0,83	0,14
6	19686	0,363	0,154	47176	1407	0,237	0,248	0,72	0,15
7	22967	0,332	0,168	41056	1225	0,237	0,248	0,63	0,17
8	26248	0,301	0,186	35595	1062	0,237	0,248	0,55	0,19
9	29529	0,270	0,207	30737	917	0,237	0,248	0,47	0,21
10	32810	0,239	0,234	26431	788	0,237	0,248	0,41	0,23
11	36091	0,208	0,268	22627	675	0,237	0,248	0,35	0,27
12	39372	0,178	0,315	19316	576	0,237	0,248	0,30	0,32
13	42653	0,147	0,382	16498	492	0,237	0,248	0,25	0,38
14	45934	0,116	0,484	14091	420	0,237	0,248	0,22	0,48
15	49215	0,085	0,660	12035	359	0,237	0,248	0,18	0,66
					601				
					601				
Remarks:	1m=3,281 ft	T_{CR}/T_{TO}= f(BPR,h)	Gl.(5.27)	Gl. (5.32/5.33)	Gl. (5.34)	from sheet 1.)	from sheet 1.)	from sheet 1.)	Repeat for plot

Wing loading	m_{MTO}/S_W	**601 kg/m²**	<<<< **Read design point from matching chart!**
Thrust-to-weight ratio	$T_{TO}/(m_{MTO}*g)$	**0,309**	<<<< Given data is correct when take-off and landing is sizing the aircraft at the same time.
Thrust ratio	$(T_{CR}/T_{TO})_{CR}$	0,181	
Conversion factor	m -> ft	0,305 m/ft	
Cruise altitude	h_{CR}	**12326 m**	
Cruise altitude	h_{CR}	**40439 ft**	
Temperature, troposphere	$T_{Tropopause}$	208,03 K	$T_{Stratopause}$ 216,65 K
Temperature, h_{CR}	$T(h_{CR})$	216,65	
Speed of sound, h_{CR}	a	295 m/s	
Cruise speed	V_{CR}	**224 m/s**	
Conversion factor	NM -> m	1852 m/NM	
Design range	R	**1550 NM**	
Design range	R	2870600 m	
Distance to alternate	$s_{to\_alternate}$	200 NM	
Distance to alternate	$s_{to\_alternate}$	370400 m	**Reserve flight distance:**
Chose: FAR Part121-Reserves?	domestic	**no**	
	international	**yes**	
Extra-fuel for long range		10%	
Extra flight distance	s_{res}	657460 m	
Spec.fuel consumption, cruise	SFC_{CR}	**1,63E-05 kg/N/s**	typical value 1,60E-05 kg/N/s
Breguet-Factor, cruise	B_s	25063326 m	**Extra time:**
Fuel-Fraction, cruise	$M_{ff,CR}$	0,892	
Fuel-Fraction, extra flint distance	$M_{ff,RES}$	0,974	
Loiter time	t_{loiter}	1800 s	
Spec.fuel consumption, loiter	SFC_{loiter}	**1,63E-05 kg/N/s**	
Breguet-Factor, flight time	B_t	111746 s	
Fuel-Fraction, loiter	$M_{ff,loiter}$	0,984	

FAR Part 121	s_{res}
domestic	370400 m
international	657460 m

FAR Part 121	t_{loiter}
domestic	2700 s
international	1800 s

Fuel-Fraction, engine start	$M_{ff,engine}$	**0,999**	<<<< **Copy**
Fuel-Fraction, taxi	$M_{ff,taxi}$	**0,996**	<<<< **values**
Fuel-Fraction, take-off	$M_{ff,TO}$	**0,995**	<<<< **from**
Fuel-Fraction, climb	$M_{ff,CLB}$	**0,995**	<<<< **table**
Fuel-Fraction, descent	$M_{ff,DES}$	**0,992**	<<<< **on the**
Fuel-Fraction, landing	$M_{ff,L}$	**0,992**	<<<< **right !**

Phase	M_{ff} per flight phases [Roskam]	
	transport jet	business jet
engine start	0,990	0,990
taxi	0,990	**0,995**
take-off	0,995	0,995
climb	0,998	0,998
descent	0,990	0,990
landing	0,992	0,992

Fuel-Fraction, standard flight	$M_{ff,std}$	0,869	
Fuel-Fraction, all reserves	$M_{ff,res}$	0,946	
Fuel-Fraction, total	M_{ff}	0,822	
Mission fuel fraction	m_F/m_{MTO}	0,178	
Realtive operating empty mass	m_{OE}/m_{MTO}	0,551	acc. to Loftin
Realtive operating empty mass	m_{OE}/m_{MTO}	**0,573**	from statistics (if given)
Realtive operating empty mass	m_{OE}/m_{MTO}	**0,550**	<<<< **Choose according to task**
Choose: type of a/c	short / medium range	**yes**	<<<< **Choose according to task**
	long range	**no**	
Mass: Passengers, including baggage	m_{PAX}	93,0 kg	
Number of passengers	n_{PAX}	**150**	
Cargo mass	m_{cargo}	**6050 kg**	
Payload	m_{PL}	**20000 kg**	
Max. Take-off mass	m_{MTO}	**73528 kg**	
Max. landing mass	m_{ML}	**64557 kg**	
Operating empty mass	m_{OE}	**40440 kg**	
Mission fuel fraction, standard flight	m_F	**13088 kg**	
Wing area	S_w	**122,3 m²**	
Take-off thrust	T_{TO}	222884 N	**all engines together**
T-O thrust of ONE engine	T_{TO}/n_E	**111442 N**	
T-O thrust of ONE engine	T_{TO}/n_E	25052 lb	**one engine**
Fuel mass, needed	$m_{F,erf}$	13390 kg	
Fuel density	ρ_F	785 kg/m³	
Fuel volume, needed	$V_{F,erf}$	**17,1 m³**	(check with tank geometry later on)
Max. Payload	m_{MPL}	**20000 kg**	
Max. zero-fuel mass	m_{MZF}	60440 kg	
Fuel mass, all reserves	$m_{F,res}$	3962 kg	
Check of assumptions	check:	m_{ML}	> $m_{MZF} + m_{F,res}$?
		64557 kg	> 64402 kg
			yes
			Aircraft sizing finished!

in kg	Short- and Medium Range	Long Range
m_{PAX}	93,0	97,5

Matching Chart

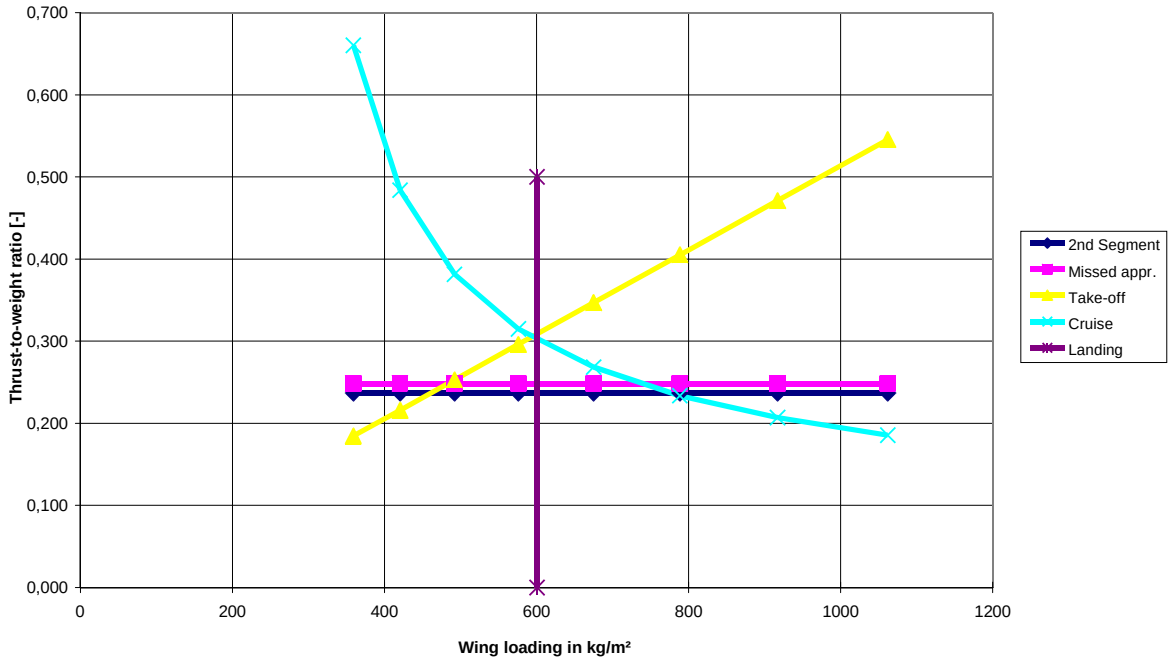

F.2 Box Wing Sizing Spreadsheet

F.2.1 Sizing According to Static Longitudinal Stability and Controllability

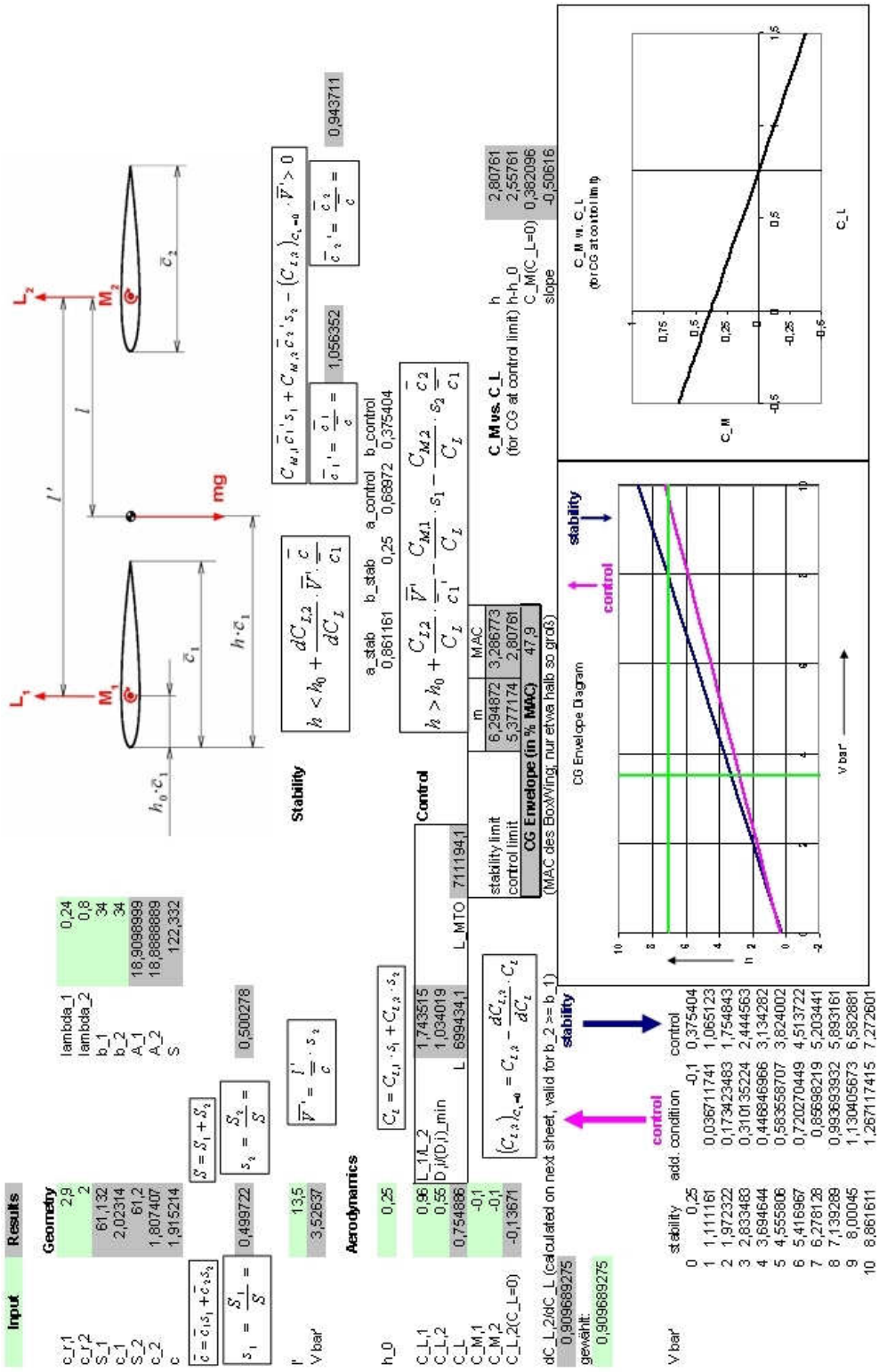

$$\frac{dC_{L,2}}{dC_L} = \frac{a_2}{a}\left(1 - \frac{\partial\varepsilon}{\partial\alpha}\right) = 0{,}90969$$

alternative (simple downwash)
0,896247

M	**0**

DATCOM 4.1.3.2 (Wing Lift Curve Slope)

$$a_2 = \frac{dC_{L,2}}{d\alpha_2} = \frac{2\pi \cdot A_2}{2 + \sqrt{A_2{}^2 \cdot (1 + \tan^2\varphi_{50,2} - M^2) + 4}}$$

b_2	34
phi_50,2 (°)	-28
phi_50,2 (rad)	-0,488692191
A_2	18,88888889
a_2	**5,053265748**

DATCOM 4.4.1 (Wing-Wing Combinations at Angle of Attack, Method 2)

$$\frac{\partial\varepsilon}{\partial\alpha} = 4{,}44 \cdot \left(k_A \cdot k_\lambda \cdot k_H \cdot \sqrt{\cos\varphi_{25,W}}\right)^{1{,}19} \cdot \frac{(C_{L,\alpha})_M}{(C_{L,\alpha})_{M=0}}$$

$$k_A = \frac{1}{A} - \frac{1}{1 + A^{1{,}7}} \qquad k_\lambda = \frac{10 - 3\lambda}{7} \qquad k_H = \frac{1 - |z_H/b|}{\sqrt[3]{2l_H/b}}$$

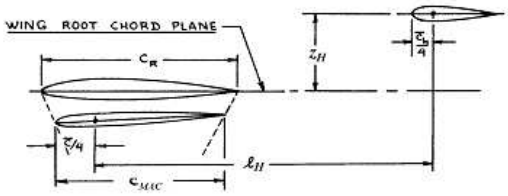

phi_25,1 (°)	28,5
b_2	34
lambda_2	0,8
z_H	8,5
phi_25,1 (rad)	0,497418837
phi_50,1 (rad)	0,492869651
(C_L,alpha)M	5,04356452
(C_L,alpha)M=0	5,04356452
A_1	18,90989989
k_A	0,046172631
k_lambda	1,085714286
k_H	0,80990295
depsilon/dalpha	**0,090814886**

acc. to DATCOM 4.5.1.1 (Wing-Body-Tail Lift Curve Slope) with adjustments and assumptions (more details: see thesis paper)

$$a = \frac{dC_L}{d\alpha} = s_1 \cdot \left(\frac{dC_L}{d\alpha}\right)_1 \cdot \frac{S_{1e}}{S_1} \cdot \left(K_N + K_{W(B)} + K_{B(W)}\right)_1 + s_2 \cdot \left(\frac{dC_L}{d\alpha}\right)_2 \cdot \left(K_{W(B)} + K_{B(W)}\right)_2 \cdot \frac{q_2}{q_\infty} \cdot \frac{S_{2e}}{S_2} + \left(\frac{dC_L}{d\alpha}\right)_{W,2(V)}$$

$$K_N = \frac{\pi d^2}{2 \cdot \left(\frac{dC_L}{d\alpha}\right)_1 \cdot S_{1,e}} \qquad K_{W(B)} + K_{B(W)} = \left(\frac{d}{b} + 1\right)^2 \qquad K_{W(B)} = 0{,}8\frac{d}{b} + 0{,}1$$

$$\left(\frac{dC_L}{d\alpha}\right)_{W,2(V)} = \frac{\left(\frac{dC_L}{d\alpha}\right)_1 \cdot \left(\frac{S_e}{S}\right)_1 \cdot \left(\frac{dC_L}{d\alpha}\right)_2 \cdot \frac{q_2}{q_\infty} \cdot K_{W(B)} \cdot I_{V,W_1(W_2)} \cdot \left(\frac{b_2}{2} - \frac{d_2}{2}\right)}{2\pi \cdot A_{2,e} \cdot \left(\frac{b_2}{2} - \frac{d_2}{2}\right)}$$

(S_e/S)_1	0,9
(S_e/S)_2	0,98
H_1	4
d_2	0,5
q_2/q_inf	0,9
I_V,W_1(W_2)	-1,33748125
(K_N)_1	0,090571418
(K_W(B)+K_B(W))_1	1,249134948
(K_W(B)+K_B(W))_2	1,029628028
(K_W(B))_1	1,094117647
A_2,e = A_2	18,88888889
(d_CL/d_alpha)_W,2(v)	-0,284239045
a	**5,050465168**
a_alternative (simple downwash)	5,126212179

F.2.2 Estimation of Mass and Center of Gravity

Aircraft Mass and Center of Gravity

	Preliminary Sizing (PreSTo)	calculated here	deviation (in %)	C/G position (m) 16,41
m_{mw}	61383	61333	-0,08	
m_{mc}	73245	73501	0,35	
m_{fc}	20000			
m_{ce}	41383	41333	-0,12	

aircraft nose : x = 0m
fuselage length: 33,1

Group		Mass (kg) calculated	Mass (kg) insert final value	remarks	Center of Gravity x (m)	Center of Gravity estimation method
aerodynamic surfaces						
fwd wing		4390,740478	6704	calculated value from Torenbeek	11,3	0,7 MAC
b_S	38,59344179			inserted value from more precise estimation		
L_1/L	0,635504109					
t_r	0,6					
aft wing		3354,147436	5009	calculated value from Torenbeek	24,8	0,7 MAC
b_S	38,50738172			inserted value from more precise estimation		
L_2/L	0,364495891					
t_r	0,4					
winglets			1000	adjustment acc. to chord proportional weight function	17,9	acc. to drawing
			1600	PreSTo		
tail surfaces		2197,35	2197	3 % ofMTOW (Torenbeek first guess)	27,7	acc. to drawing
fuselage		7799,795858		Torenbeek		
V_D (m/s EAS)	276			PreSTo		
l_H (m)	13,6			visual judgement, very conservative, hor. tail not comparable to conv. one!!		
w_F (m)	5,7			PreSTo Cabin		
h_F (m)	5,7			PreSTo Cabin		
lambda_F	5,81			PreSTo Cabin		
S_F,wet (m²)	460,6425563			Torenbeek (FE Eq. 13.8)		
factor acc. to Raymer	24	11055,42135		Raymer		
			7800	fuselage supported bytwo wings!	14,895	0,45 fuselage length
landing gear						
nose gear						
k	1	433,06	433	Torenbeek	5,2	acc. to drawing
A	9,1					
B	0,082					
C	0					
D	2,97E-06					
main gear						
k	1,08	2629,86	2450	Torenbeek	18	acc. to drawing
A	18,1			might be more compact, thus lighter. But Avro main gear very heavy		
B	0,131			because of a lot of hinges =>		
C	0,019			assume same weight as A320		
D	2,23E-05					
engines inst. (incl. nacelles)			6500	PreSTo: 5900 kg, + add. supporting beam	17,7	acc. to drawing
systems and stand. + op. items		9240,07114	9240	Torenbeek (medium range aircraft)	14,895	0,45 fuselage length
k_equip	0,11					
k_F/C	0,88					
payload						
pax						
m_pax	93	13950	13950	ROSKAM	14,6	centre ofcabin
n_pax	150					
cargo			6050	rest of payload	16	estimated acc. to drawing
fuel			12168	given acc. to Prel. Sizing		
fwd wing tank			4905	acc. to volume estimate (Torenbeek)	11,3	CG at wing CG
aft wing tank			4157	acc. to volume estimate (Torenbeek)	24,8	CG at wing CG
fuselage tank			2106	rest	12,2	estimated acc. to drawing
tail tank/trim tank			1000	guessed	27,7	

F.3 Payload-Range Calculation

Box	payload (t)	range (nm)
	20	0
	20	2870
	15,406	5247
	0	7580

A320	payload	range
	20	0
	20	2870
	14,36	5313
	0	7481

	Box	Ref
MTOW	73501	73500
MPL	20000	20000
OEW	41333	40440
Max Fuel	16762	18700
PL(max fuel)	15406	14360
ML(max fuel)	56739	54800
M1/MO (max fuel)	0,771949	0,745578
Mff,CR (max fuel)	0,832304	0,80897
TOW(ferry)	58095	59140
M1/MO (ferry)	0,711473	0,683801
Mff,CR (ferry)	0,7671	0,741941

Fuel Fractions

	Box	Ref
engine	0,999	0,999
taxi	0,996	0,996
take off	0,995	0,995
climb	0,995	0,995
descent	0,992	0,992
landing	0,992	0,992
res	0,952	0,946

	Box
B_R	2,86E+07
B_t	1,27E+05

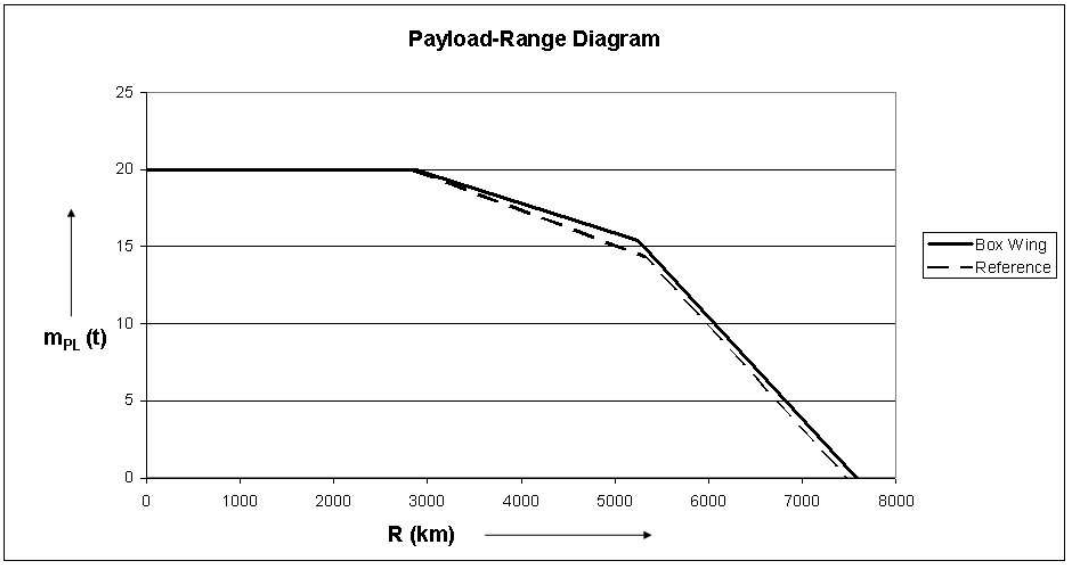

Appendix G

CD-ROM

The attached CD-ROM contains the text of this thesis as PDF-file and as ODT-file, the poster presentation as well as the following spreadsheets:

- Preliminary sizing of the reference aircraft
  A-C_Preliminary_SizingA320.xls
- Preliminary sizing of the box wing aircraft
  A-C_Preliminary_Sizing_BoxWing.xls
- Calculations regarding the span efficiency factor and the glide ratio
  Glide_Ratio_and_Oswald_Factor_Calculations.xlsds11
- Wing mass estimation for flexible connections
  Internal_Loads_Wing_Mass_hinged_edges.xls
- Wing mass estimation for rigid connections
  Internal_Loads_Wing_Mass_rigid_edges.xls
- Calculation of MAC, wing tank volume and max. allowed t/c ratio
  MAC_Fuel_t_c.xls
- Payload-range calculation
  payload_range.xls
- Sizing sheet of the box wing aircraft
  Sizing_Sheet_A320.xls
- Sizing sheet of the reference aircraft
  Sizing_Sheet_Box_Wing.xls
- Tilting angle calculation
  tip_over_stability.xls
- Wing mass overview
  Wing_Mass_Overview.xls